



PERFORMANCE ENHANCEMENT OF PHOTOVOLTAIC PANEL USING SINGLE AXIS TRACKING AND WATER SPRAY SYSTEMS

A Dissertation

Submitted to the Council of the Erbil Technical Engineering
College at Erbil Polytechnic University in Partial Fulfillment
of the Requirements for the Degree of Doctor of Philosophy
(Ph.D.) of Science in Mechanical and Energy Engineering

By

Sally Afram Polus

B.Sc. in Refrigeration and Air-Conditioning Engineering

M.Sc. in Mechanical and Energy Engineering

Supervised by

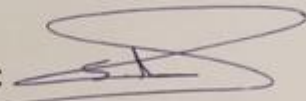
Asst. Prof. Dr. Ranj Sirwan Abdullah

Erbil KURDISTAN

October 2023

DECLARATION

I declare that the Ph.D. dissertation entitled "**Performance Enhancement of Photovoltaic Panel Using Single Axis Tracking and Water Spray Systems**" is my own original work, and hereby I certify that unless stated, all work contained within this dissertation is my independent research and has not been submitted for the award of any other degree at any institution, except where due acknowledgment is made in the text.

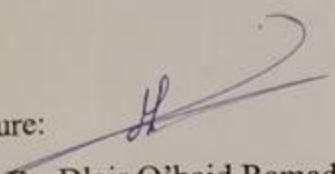
Signature: 

Student Name: Sally Afram Polus

Date: 12/9/2023

LINGUISTIC REVIEW

I confirm that I have reviewed Ph.D. dissertation **Performance Enhancement of Photovoltaic Panel Using Single Axis Tracking and Water Spray Systems** from the English linguistic point of view, and I can confirm that it is free of grammatical and spelling errors.

Signature: 

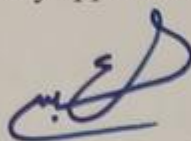
Name: Dr. Dlair O'baid Ramadan

Date: 4/9/2023

SUPERVISOR CERTIFICATE

This dissertation has been written under my supervision and has been submitted for the award of the degree of Ph.D. of Science in Mechanical and Energy Engineering with my approval as supervisor

Signature:

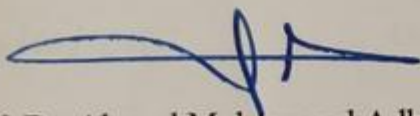


Name: Assistant Prof. Dr. Ranj Sirwan Abdullah

Date: 14-9-2023

I confirm that all requirements have been fulfilled.

Signature:



Name: Prof. Dr. Ahmed Mohammed Adham

Head of the Department of Technical Mechanical and Energy Engineering

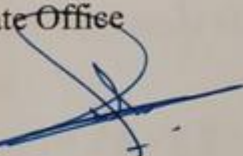
Date: 14/9/2023



I confirm that all requirements have been fulfilled.

Postgraduate Office

Signature:



Name: Mr. Bayad Abdulqader Ahmed

Date: 14-11-2023

EXAMINING COMMITTEE CERTIFICATION

We certify that we have read this dissertation:

Performance Enhancement of Photovoltaic Panel Using Single Axis Tracking and Water Spray Systems

As an examining committee examined the student (Sally Afram Polus) in its content and what is related to it. We approve that it meets the standards of a dissertation for the degree of Ph.D. in Mechanical Engineering.

Signature

Name: Assist. Prof. Dr. Ayad Y. Abdulla

Member

Date 30/10/2023

Signature

Name: Assist. Prof. Dr. Omar M. Hamdoon

Member

Date 30/10/2023

Signature

Name: Assist. Prof. Dr. Banipal N. Yaqob

Member

Date 30/10/2023

Signature

Name: Assist. Prof. Dr. Azhar K. Mohammed

Member

Date 30/10/2023

Signature

Name: Prof. Dr. Ahmed M. Adham

Chairman

Date 30/10/2023

Signature

Name: Assist. Prof. Dr. Ranj Sirwan Abdullah

Supervisor

Date 30/10/2023

Signature

Name: Prof. Dr. Ayad Zaki Saber

Dean of Erbil Technical Engineering College

Date: 14.11.2023

DEDICATION

I would like to dedicate this dissertation to the unwavering support and love of my husband, Atheer, who has been my rock throughout this entire journey.

To my precious sons, Eleanor and Aniello, thank you for your patience and understanding during the countless nights I spent buried in books and research. Your smiles and laughter provided the motivation I needed to keep going.

A heartfelt thank you goes out to my parents, who have always been my biggest cheerleaders. Your constant encouragement and belief in my abilities have been the driving force behind my success.

I cannot forget to mention my beloved Aunt Suaad, who has been a second mother to me. Your guidance, love, and unwavering support are the reasons I stand here today.

To my siblings (Armen, Salvia and Swain), thank you for always believing in me and for being a constant source of inspiration. Your support, both emotionally and intellectually, has been priceless.

My friends specially Renas. Your friendship and constant encouragement have been instrumental in overcoming the many challenges I faced during this research journey.

I am deeply grateful to each and every one of you for your love, support, and encouragement. This dissertation would not have been possible without your unwavering belief in me. From the bottom of my heart, thank you all for being a part of this incredible journey.

ACKNOWLEDGMENT

I would like to begin this acknowledgment by expressing my utmost gratitude to God for providing me with the strength, guidance, and inspiration throughout my whole life and to finish this dissertation journey.

I extend my heartfelt thanks to my supervisor, Assist. Prof. Dr. Ranj Sirwan Abdullah, for their continuous support and invaluable guidance. Their expertise, patience, and commitment to excellence have shaped my research and enriched my understanding of the subject matter. I am truly grateful for their mentorship and for pushing me to explore new avenues of knowledge.

A special mention goes to my dear Dr. Abdulrahman for having encouraged me to start this journey and for his continued assistance.

I would like to extend a special thank you to Mr. Bashir for his unwavering support and assistance.

Dr. Dlair, thank you for your support and encouragement.

Lastly, I would like to express my gratitude to Dr. Hemn Kakakhan for his support at the research center. Their assistance and guidance have been crucial to the successful completion of this dissertation.

In conclusion, I am truly grateful to all those mentioned above and to countless others who have supported me in various ways throughout this dissertation journey. Without their unwavering support and encouragement, this achievement would not have been possible.

ABSTRACT

A solar tracking system with an effective cooling technique is developed and implemented in this study, because the solar irradiance, temperature and dusty climate condition affected on the output of photovoltaic panel. A single east-west solar tracking system incorporating a monocrystalline panel and a front surface spray water cooling system was conducted and compared to a fixed reference panel with an inclination angle 36° facing south. An appropriate cooling system was developed with six nozzles placed on top, left and right side of the panel, to ensure that the panel's front surface is covered with water from all orientations. Two different types of spray water cooling were performed; first by adjusting the panel surface temperature (35°C , 40°C and 45°C), through adjustable water flow rate, and the second was fixing the water volume flow rate at (2 l/min, 3 l/min, 4 l/min and 5 l/min). This experiment was conducted during the summer season of the year 2022 in Erbil, Iraq (latitude 36.191° and longitude 44.009°).

A simulation study was also conducted using ANSYS Fluent R19.2. The experimental study demonstrated a maximum electrical efficiency improvement reaching 9.9% which was recorded as an enhancement compared to the fixed reference panel by using the solar east-west tracking system. While tracking with a cooling system at 35°C set point temperature has resulted in an improvement in efficiency up to 25.11%. Another parameter that has been optimized is the cooling water consumption. The optimal cooling setting temperature was determined at a surface temperature of 40°C . Alternatively, upon the incorporation of a cooling system to the PV panel at setpoint temperatures of 45°C , 40°C , and 35°C , without the integration of a solar tracking system, improvements of 18.25%, 19.94%, and 22.82% were achieved in electrical efficiency, respectively. When the solar radiation exceeds the power at standard operating conditions, even if the panel temperature is higher

than that of the standard test, the PV panel is able to produce the same power as the standard test of 210 W. Additionally, integrating a solar tracking system with cooling at a water volume flow rate of 2 L/min resulted in double the power production compared to a fixed panel cooled at the same flow rate. This model demonstrates that the performance of a photovoltaic panel decreased by only 0.2-0.3% when the surface temperature increased by 5 °C within a range of 25 to 40 °C.

The simulation results indicated that the impact of the different variables on both panel performance as well as temperature could be accurately predicted and the temperature of the photovoltaic panel reduced significantly, leading to an increase in power production. The contribution from the ANSYS fluent simulation was that solar radiation intensity is the most influential factor on cooled PV module power production, as by maximizing solar irradiance by 100 W/m², the power production will be increased by 16.6%. While increasing the water flow rate at a lower water inlet temperature improved the performance of the photovoltaic panel. This study provides insights essential for design and implementation of efficient photovoltaic with front surface cooling.

LIST OF CONTENTS

DECLARATION	I
LINGUISTIC REVIEW	II
SUPERVISOR CERTIFICATE	III
EXAMINING COMMITTEE CERTIFICATION	IV
DEDICATION	V
ACKNOWLEDGMENT	VI
ABSTRACT	VII
LIST OF CONTENTS	IX
LIST OF FIGURES	XV
LIST OF TABLES	XXII
LIST OF ABBREVIATIONS.....	XXIII
LIST OF SYMBOLS.....	XXIV
GREEK LETTERS	XXVI
CHAPTER ONE.....	1
(INTRODUCTION)	1
1.1 OVERVIEW	1
1.2 SOLAR ENERGY TRANSFORMATIONS TECHNIQUE.....	3
1.2.1 Thermal Solar Collector	4
1.2.2 Solar Photovoltaic Technology	5
1.2.3 Solar Photovoltaic Thermal (PV/T) Technology	8
1.3 SOLAR TRACKING SYSTEMS	9
1.3.1 Single Axis Solar Tracker	10
1.3.2 Dual Axis Solar Tracker.....	10
1.4 PROBLEM STATEMENT	10
1.5 PURPOSE AND OBJECTIVES	11

1.6 RESEARCH METHODOLOGY	12
1.7 THESIS STRUCTURE	13
CHAPTER TWO.....	15
(LITERATURE REVIEW)	15
2.1 INTRODUCTION	15
2.2 PV SOLAR CELL	16
2.3 SOLAR TRACKING SYSTEM.....	17
2.4 ENVIRONMENTAL ELEMENT INFLUENCE ON PANEL PERFORMANCE.....	19
2.4.1 Influence of Solar Intensity	19
2.4.2 Influence of Dust	20
2.4.3 Influence of Ambient Temperature	22
2.5 PHOTOVOLTAIC PANEL COOLING TECHNIQUE	23
2.5.1 Water Cooling Strategy	25
2.5.1.a Front Surface Cooling.....	25
2.5.1.b Back Surface Cooling	34
2.5.1.c Front and Back Surface Cooling.....	38
2.5.2 Air Cooling Strategy	40
2.5.2.a Forced Air Cooling	40
2.5.2.b Natural Air Cooling	43
2.5.3 PCM Cooling Strategy	45
2.5.4 Nano Fluid Cooling Strategy.....	48
2.6 SUMMARY.....	50
CHAPTER THREE	52
(THEORETICAL ANALYSIS)	52
3.1 INTRODUCTION	52

3.2	CFD ANALYSIS FOR PV FRONT SURFACE COOLING	52
3.3	CFD PROCEDURES	53
3.3.1	Geometry	55
3.3.2	Meshing	56
3.3.3	Setup	59
3.3.3.a	Energy Model.....	59
3.3.3.b	Radiation Model.....	60
3.3.3.c	Materials.....	62
3.3.3.d	Cell Zone Condition.....	63
3.3.3.e	Boundary Conditions	64
3.3.4	Governing Equations.....	67
3.3.5	Solution Method	69
3.4	SOLAR ANGLES	70
3.5	ELECTRICAL MODELING	70
CHAPTER FOUR.....		73
(EXPERIMENTAL WORK)		73
4.1	INTRODUCTION	73
4.2	EXPERIMENTAL SETUP	73
4.2.1	Photovoltaic Panel.....	76
4.2.2	Solar Tracking System	77
4.2.2.a	Frame with Rotating Shaft.....	77
4.2.2.b	Light Intensity Sensor	78
4.2.2.c	Arduino	79
4.2.2.d	Stepper Motor and Gearbox.....	80
4.2.2.e	Working Principle	81
4.2.3	Spray Water Cooling System.....	82

4.2.3.a	Nozzles.....	83
4.2.3.b	Supply Water Pump	84
4.2.3.c	Motorized Valve	84
4.2.3.d	Return water pump.....	85
4.2.3.e	Primary Water Tank.....	86
4.2.3.f	Water Softener	86
4.2.3.g	Secondary Water Tank.....	87
4.2.3.h	MPPT Solar Charge Controller.....	88
4.2.3.i	Batteries	89
4.2.4	Sensors and Measuring Devices.....	90
4.2.4.a	Water Flow Sensor.....	90
4.2.4.b	Ambient Temperature Sensor	91
4.2.4.c	PV Temperature Sensor	92
4.2.4.d	Current Sensor	93
4.2.4.e	Voltage Sensor	93
4.2.4.f	Solar Power Meter	94
4.3	EXPERIMENTAL PROCEDURE.....	96
4.3.1	Comparison between Reference and Tracking Panel	96
4.3.2	Comparison between Reference and Tracking with Cooling at Various Setpoint Temperature Panels.....	96
4.3.3	Comparison between Reference and Fixed with Cooling at Various Setpoint Temperature Panels.....	97
4.3.4	Comparison between Reference and Tracking with Cooling at Different Volume Flow Rates Panels.....	97
4.3.5	Comparison between Reference and Fixed with Cooling at Different Volume Flow Rates Panels	98
4.3.6	PV Performance at Different Surface Temperature and Solar Irradiance	98

4.4	EQUIPMENT'S CALIBRATIONS	99
4.4.1	Calibration of Water Flow Sensor.....	99
4.4.2	Calibration of K-Type Thermocouple.....	100
4.4.3	Calibration of Solar Power Meter	101
4.5	UNCERTAINTY	102
CHAPTER FIVE.....		104
(RESULT AND DISCUSSION).....		104
5.1	INTRODUCTION	104
5.2	TILT ANGLE	104
5.3	EXPERIMENTAL RESULTS	105
5.3.1	Comparison between Reference, Tracking and Tracking with Cooling PV Panel at Various Setpoint Temperature	107
5.3.2	Comparison between Reference and Fixed Equipped with Cooling at Various Setpoint Temperature PV Panel	115
5.3.3	Comparison between Reference and Tracking PV Panel Equipped with Cooling at Different Volume Flow Rate.....	121
5.3.4	Comparison between Reference and Fixed PV Panel Equipped with Cooling at Different Volume Flow Rate	126
5.3.5	PV Performance at Different Surface Temperature and Solar Intensity 132	
5.3.6	Comparative Study with Previous Literature	134
5.4	VALIDATION RESULTS	135
5.5	ANSYS FLUENT RESULTS	138
5.5.1	Influence of Variation in Ambient Temperature.....	138
5.5.2	Influence of Variation in Solar Irradiance	144
5.5.3	Influence of Variation in Water Inlet Temperature.....	149
CHAPTER SIX.....		157
(CONCLUSIONS AND RECOMMENDATIONS)		157

6.1	INTRODUCTION	157
6.2	CONCLUSIONS	157
6.3	RECOMMENDATIONS.....	161
	REFERENCES	R1
	APPENDIX A	A1
	UNCERTAINTY ANALYSIS.....	A1
	APPENDIX B.....	A3
	VARIATION BETWEEN FIXED AND TRACKING SOLAR IRRADIANCE.....	A3
	LIST OF PUBLICATIONS.....	

LIST OF FIGURES

Fig. 1-1 The difference between need and available energy in Iraq (Al-Saffa, F. Salim, S. Sallam, S. Jamal, 2021)	2
Fig. 1-2 Various types of solar energy conversion technology	4
Fig. 1-3 Solar flat plate collector (Dobriyal et al., 2020).....	5
Fig. 1-4 Photovoltaic cell working principle (Husain et al., 2018)	6
Fig. 1-5 Solar PV system	7
Fig. 1-6 Three main technical silicon-based PV cells.....	8
Fig. 1-7 Typical solar photovoltaic thermal technology (Joshi et al., 2009)	9
Fig. 2-1 Block diagram of tracking system (Baouche et al., 2022)	18
Fig. 2-2 Effect of irradiance on characteristic of the panel (Mohsin and Abdulbaqi, 2018).....	19
Fig. 2-3 Monthly average dust accumulated and visibility in Kuwait 2013 (Aldihani, 2017)	20
Fig. 2-4 Effect of dust density on PV power production (Chaichan and Kazem, 2020)	21
Fig. 2-5 Dust storm effect on solar radiation intensity (Chaichan et al., 2023)	22
Fig. 2-6 Variation of PV efficiency and power production with ambient temperature (Bonkaney, Madougou and Adamou, 2017).....	23
Fig. 2-7 Cooling strategies	24
Fig. 2-8 Creation of film cooling technique (Krauter, 2004).....	28
Fig. 2-9 Experimental rig 1 – PV module, 2 – tank, 3 – pump, 4 – filter, 5 – nozzle and 6 – drain pipe (Moharram et al., 2013).	29
Fig. 2-10 Experimental system 1&2- cells with air cooling, 3&4- cells	30
Fig. 2-11 Schematic diagram of experimental rig (Govardhanan et al., 2020)	32
Fig. 2-12 Spray water cooling system with three nozzles (Benato et al., 2021)	33
Fig. 2-13 Experimental system layout (Nateqi, Zargarabadi and Rafee, 2021)	34
Fig. 2-14 Absorber designs used for cooling PV (Ibrahim et al., 2010).....	35

Fig. 2-15 Experimental module (Muslim, Ghadhbhan and Hilal, 2020)	36
Fig. 2-16 Experimental rig of different cooling system implemented to the back surface of the panel (Bevilacqua et al., 2021)	37
Fig. 2-17 Front and back cooling chamber (Mohammed, Mohammed and Sanad, 2019).....	38
Fig. 2-18 Experimental setup back and front PV cooling system (Sainthiya and Beniwal, 2019)	39
Fig. 2-19 front and rear spray water cooling system(Khalil, Abdelgaied and Hamdy, 2019).....	40
Fig. 2-20 Cross section of the system (Tripanagnostopoulos, Y. Nousia, 2001).....	41
Fig. 2-21 Double air pass cooling PV (Kumar and Rosen, 2011)	41
Fig. 2-22 Experimental rig (a) Natural air cooling. (b) Forced air cooling (Mazón-Hernández et al., 2013).....	42
Fig. 2-23 schematic diagram of experimental system (Sajjad et al., 2019)...	43
Fig. 2-24 Experimental rig of air natural cooling (Tripanagnostopoulos and Themelis, 2010).....	44
Fig. 2-25 Heat sink a- inclined segment b- straight fins (Hernandez-Perez et al., 2020).....	45
Fig. 3-1 CFD flow chart procedure	54
Fig. 3-2 Geometry of the panel's layers with water cooling system	55
Fig. 3-3 Meshing types in ANSYS	57
Fig. 3-4 Mesh generated for photovoltaic water-cooling system	57
Fig. 3-5 Grid independence test	58
Fig. 3-6 Naming of PV layers and faces	59
Fig. 3-7 Viscous model	60
Fig. 3-8 Radiation model.....	61
Fig. 3-9 Solar calculator specifications	61
Fig. 3-10 Fluid material (water-liquid) properties	62
Fig. 3-11 Solid material (EVA-1) properties	63
Fig. 3-12 Cell zone condition of glass	63
Fig. 3-13 Boundary conditions list of PV front surface cooling.....	64
Fig. 3-14 Water mass flow inlet boundary condition	65

Fig. 3-15 Water pressure outlet boundary condition	65
Fig. 3-16 Interface boundary condition.....	65
Fig. 3-17 Wall boundary condition	66
Fig. 4-1 Schematic diagram of the experimental setup.....	74
Fig. 4-2 Experimental system connection and description	75
Fig. 4-3 Experimental rig	76
Fig. 4-4 PV framework and rotating shaft	78
Fig. 4-5 TEMT6000X01 sensor	78
Fig. 4-6 Two light intensity sensors with a separating plate.....	79
Fig. 4-7 Arduino	80
Fig. 4-8 Stepper motor and gearbox.....	80
Fig. 4-9 Block diagram of solar tracking system for one iteration	81
Fig. 4-10 PV module with tracking system.....	82
Fig. 4-11 Water spray nozzle	83
Fig. 4-12 Nozzles over the front surface.....	83
Fig. 4-13 Supply water pump.....	84
Fig. 4-14 Motorized valve	85
Fig. 4-15 Return water pump	85
Fig. 4-16 Primary water tank	86
Fig. 4-17 water softener	87
Fig. 4-18 secondary water tank	88
Fig. 4-19 MPPT solar charge controller.....	89
Fig. 4-20 Batteries, PV and load connection with MPPT	90
Fig. 4-21 Water flow sensor YF-S401	91
Fig. 4-22 DHT11 ambient temperature sensor.....	91
Fig. 4-23 K type thermocouple and MAX6675 Amplifier	92
Fig. 4-24 Connection of K type thermocouple with MAX6675 and Arduino	92
Fig. 4-25 Current sensor ACS712.....	93
Fig. 4-26 SEN32 REV1.1 voltage sensor	94
Fig. 4-27 GENERAL DBTU1300 solar power meter	94

Fig. 4-28 Data logger board	95
Fig. 4-29 Calibration of flowmeter using stop watch and glass beaker.....	99
Fig. 4-30 Calibration curve between flowmeter reading and actual flow rate	100
Fig. 4-31 Calibration of K-type thermocouple with VOLTCRAFT thermometer.....	100
Fig. 4-32 Calibration curve of K-type thermocouple and thermometer	101
Fig. 4-33 Calibration of solar power meter.....	101
Fig. 5-1 Average daily ambient temperature during July and August.....	106
Fig. 5-2 Average daily solar intensity over fixed and tracking panel during July and August.....	107
Fig. 5-3 Solar radiation intensity difference between fixed and tracking panel 2 nd August.....	108
Fig. 5-4 surface temperature difference between fixed and solar tracking panel on 2 nd August.....	110
Fig. 5-5 Variation of water flow rate supply at different panel surface temperature.....	111
Fig. 5-6 Variation of PV power production with time using tracking and setpoint temperature	112
Fig. 5-7 Variation of PV electrical efficiency with time using tracking and setpoint temperature	113
Fig. 5-8 Variation of fill factor with time using tracking and setpoint temperature.....	113
Fig. 5-9 Maximum electrical efficiency improvement at different modifications	114
Fig. 5-10 Water consumption rate and average electrical efficiency at different PV set temperature	115
Fig. 5-11 Variation of water volume flow rate at various panel setpoint temperature.....	117
Fig. 5-12 Variation of power with time at various panel set point temperature	118
Fig. 5-13 Variation of electrical efficiency with time at various panel set point temperature.....	119

Fig. 5-14 Variation of fill factor with time at various panel set point temperature	119
Fig. 5-15 Maximum electrical efficiency enhancement at different set point temperature	120
Fig. 5-16 Water consumption rate and average electrical efficiency at different PV set temperature	121
Fig. 5-17 Variation of fixed and tracking solar irradiance with time on 26 th July	123
Fig. 5-18 Variation in panel surface temperature at different volume flow rate	123
Fig. 5-19 PV power production at various water flow with solar tracking system	124
Fig. 5-20 Variation in fill factor of the panel at various water flow	125
Fig. 5-21 Variation in electrical efficiency of the panel at various water flow	126
Fig. 5-22 Average daily efficiency and power production at different water flow rate with a tracking system	126
Fig. 5-23 Variation in fixed panel surface temperature at various flow	129
Fig. 5-24 Variation in fixed panel Power production at various flow	130
Fig. 5-25 Variation in fixed panel fill factor at various flow	130
Fig. 5-26 Variation in fixed panel electrical efficiency at various flow	131
Fig. 5-27 Average daily power and electrical efficiency of fixed panel at various flow	132
Fig. 5-28 Variation of output power and electrical efficiency with panel temperature at 1000 w/m ² solar radiation	133
Fig. 5-29 Variation of output power with solar irradiance at different set point temperature	134
Fig. 5-30 Comparative study of maximum electrical efficiency improvement	134
Fig. 5-31 Verification of experimental and ANSYS Fluent PV surface Temperature at various water flow rate	137
Fig. 5-32 Verification of experimental and ANSYS Fluent PV water outlet temperature at various water flow rate	137
Fig. 5-33 Variation of PV temperature with flow rate at various ambient temperature	139

Fig. 5-34 Variation in PV power with flow rate at various ambient temperature	140
Fig. 5-35 Variation of PV efficiency with flow rate at various ambient temperature	141
Fig. 5-36 Variation in water temperature distribution at 35 °C ambient temperature at various flow rates	142
Fig. 5-37 Variation in surface temperature of uncooled PV with ambient temperature at 1000 W/m ²	143
Fig. 5-38 Variation in power and electrical efficiency of uncooled PV with ambient temperature at 1000 W/m ²	143
Fig. 5-39 Variation in PV temperature with flow at different solar irradiance	144
Fig. 5-40 Variation in PV power production with flow at various solar irradiance	145
Fig. 5-41 variation in PV electrical efficiency with flow at various solar irradiance	146
Fig. 5-42 Variation in water temperature distribution at 800 W/m ² solar irradiance at various flow rates	147
Fig. 5-43 Variation in PV surface Temperature at various solar irradiance .	148
Fig. 5-44 Variation in PV power production and electrical efficiency at various solar irradiance	148
Fig. 5-45 Variation in PV temperature with flow at various water inlet temperature &1000 W/m ²	149
Fig. 5-46 Variation in PV temperature with flow at various water inlet temperature &800 W/m ²	150
Fig. 5-47 Variation in PV temperature with flow at various water inlet temperature &600 W/m ²	150
Fig. 5-48 Variation in PV power with flow at various water inlet temperature &1000 W/m ²	151
Fig. 5-49 Variation in PV power with flow at various water inlet temperature &800 W/m ²	151
Fig. 5-50 Variation in PV power with flow at various water inlet temperature &600 W/m ²	151
Fig. 5-51 Variation in PV efficiency with flow at various water inlet temperature &1000 W/m ²	153

Fig. 5-52 Variation in PV efficiency with flow at various water inlet temperature & 800 W/m ²	153
Fig. 5-53 Variation in PV efficiency with flow at various water inlet temperature & 600 W/m ²	153
Fig. 5-54 Variation in water distribution temperature at various flow and 20 °C water inlet temperature & 1000 W/m ² solar irradiance	155
Fig. B-1 Variation between fixed and tracking panel solar irradiance 7 th July	A3
Fig. B-2 Variation between fixed and tracking panel solar irradiance 17 th July	A3
Fig. B-3 Variation between fixed and tracking panel solar irradiance 18 th July	A4
Fig. B-4 Variation between fixed and tracking panel solar irradiance 27 th July	A4
Fig. B-5 Variation between fixed and tracking panel solar irradiance 28 th July	A5
Fig. B-6 Variation between fixed and tracking panel solar irradiance 31 st July	A5

LIST OF TABLES

Table 2-1 Front surface cooling researches	25
Table 2-2 PV cooling by utilizing PCM	46
Table 3-1 Photovoltaic panel layers thickness	55
Table 3-2 Materials specifications (Syafiqah et al., 2017)	62
Table 4-1 Technical features of PV at nominal operating condition (25 °C, 1000 W/m ² , 1.5 m/s)	77
Table 4-2 Calibration of solar power meter DBTU1300 with SM206-SOLAR	102
Table 4-3 Uncertainty of the equipment	103
Table 5-1 Tilt angle for the average day of the month for Erbil.....	105
Table 5-2 Recorded ambient temperature on 7 th , 17 th & 18 th July and 2 nd August at Erbil City.....	109
Table 5-3 Ambient temperature and solar irradiance on 19 th , 21 st and 24 th of July	116
Table 5-4 Variation in ambient temperature with time on 26 th , 27 th , 28 th and 31 st of July	122
Table 5-5 Variation in ambient temperature and solar irradiance on 7 th , 9 th , 10 th and 11 th August.....	128
Table A-1 Flowmeter uncertainty calculation sample	A1

LIST OF ABBREVIATIONS

CFD	Computational Fluid Dynamics
DC	Direct Current
DEE	discrete energy equation
DO	Discrete Ordinates
DORM	Discrete Ordinary radiation model
EVA	Ethylene Vinyl Acetate
FEA	Finite Element Analysis
H.E	Heat Exchanger
IDE	integrated development environment
LCD	Liquid Crystal Display
LDR	Light Dependent Resister
MPPT	Maximum Power Point Tracking
PCM	Phase change material
PV	Photovoltaic
PV/T	Photovoltaic Thermal
SATs	Single-axis trackers
SD	Secure Digital
ST	Solar Thermal
STC	Standard Test Condition
wt	weight
PM	particulate matters

LIST OF SYMBOLS

Symbol	Definition	Unit
A	Area of the panel	m^2
FF	Fill factor	-
G	Incident solar radiation	W/m^2
$I_{b\lambda}$	Black body intensity	W/m^2
I_m	Maximum current	A
I_{sc}	Short-circuit current	A
I_{mpp}	Maximum power point Voltage	A
K	Coefficient of absorption	-
k	Thermal conductivity of solid	$W/m.k$
L	Characteristic length	m
N	Number of readings	-
n_d	Day of the year	-
n	Refractive index	-
P_{PV}	PV power output	W
$P_{enh.}$	Enhanced power of PV	%
P_m	Maximum power	W
P_{ref}	Reference PV power output	W
Re	Reynolds numbers	-
\vec{r}	Position vector	-
\vec{s}	Direction vector	-
\vec{s}'	Scattering direction vector	-
T	Temperature	$^{\circ}C$
T_c	Cell temperature	$^{\circ}C$
t	Recorded time	min
V_f	Recorded volume	L

V_{in}	Inlet water velocity	m/s
V_m	Maximum voltage	V
V_{mpp}	Maximum power point voltage	V
V_{oc}	Open circuit voltage	V
V_w	Water volume flow rate	
u	Velocity component in the x-direction	
\mathbf{u}	Velocity vector	m/s
g_x	Acceleration due to gravity in the x-direction	m/s ²
V_{wa}	Water velocity	m/s
V_{wi}	Wind speed	m/s
\bar{x}	The average value of all of the readings taken for the X variable	-
x_i	i th measurement value	-
Q	internal heat generation	-

GREEK LETTERS

$\eta_{T_{ref}}$	Panel's electrical efficiency at the reference temperature	-
$\eta_{elec.}$	Electrical efficiency	-
η_{PV}	Electrical efficiency for CFD	-
$\eta_{enh.}$	Electrical efficiency enhancement	-
μ	Dynamic viscosity	kg/m.s
ρ	Density of fluid	kg/m ³
C_p	specific heat	J/(kg °C)
τ_{pv}	PV transmittance	-
ν_f	Kinematic viscosity	m ² /s
\emptyset	Latitude	Degree
Φ	Phase function	-
α	Absorption coefficient	-
β	Temperature coefficient of PV efficiency	%/°C
β	Tilt angle	Degree
δ	Declination angle	Degree
λ	Wave length	m
Ω'	Phase angle	Degree
σ	Stefan-Boltzmann constant	W/m ² -K ⁴

CHAPTER ONE

(INTRODUCTION)

1.1 OVERVIEW

Energy is a fundamental necessity for human progress and plays a pivotal role in determining the economic growth of nations. Fossil fuels, including petroleum, gas and coal, remain the primary energy sources. The rising demand for energy and its associated environmental impacts are an area of legitimate concern (Kumar, M.S. and Annappa, 2013). The energy demand is increasing on a daily basis due to an increasing population and industrial activities, which are also notable agents of the economic development of any country. Fossil fuels such as natural gas and oil are the main sources of energy. It is predicted that in 2035, in some developed countries, fossil fuels will be used to produce about 80% of energy (Fumo, Bortone and Zambrano, 2013). The byproducts of these sources have been largely responsible for a high percentage of environmental contamination, leading to acid rain, the depletion of the ozone layer, and global warming. Despite the negative impact, energy sources have greatly helped to bridge the difference between energy need and energy availability (Hannah, E. Murdock, D. and Gibb, 2019)(Sorrell, 2015). Fig. 1-1 Presents the difference between the need for and availability of energy in Iraq. To address these issues, it is essential to implement long-term strategies for sustainable development. It is projected that the demand for energy worldwide will grow, and fossil fuels will likely not be able to keep up with this surge, largely because of decreasing production of oil and ecological concerns (such as air pollution, the greenhouse effect, and climate change). As the cost of these fuels continues to climb, using sustainable energy resources, including solar energy, geothermal energy, as well as wind energy, instead of the conventional way is essential (Eicker et al., 2014). Renewable energy sources appear to be

one of the most viable solutions (Kasim and Atwan, 2017). Renewable energy sources have gained significant traction in recent years and now play an integral role in sustainable development. They also offer an environmentally friendly alternative (Stambouli and Koinuma, 2012). Using these types of energy sources instead of the conventional sources are crucial (Al-Saffa, F. Salim, S. Sallam, S. Jamal, 2021). So that researchers and engineers are putting a huge focus on renewable energy.

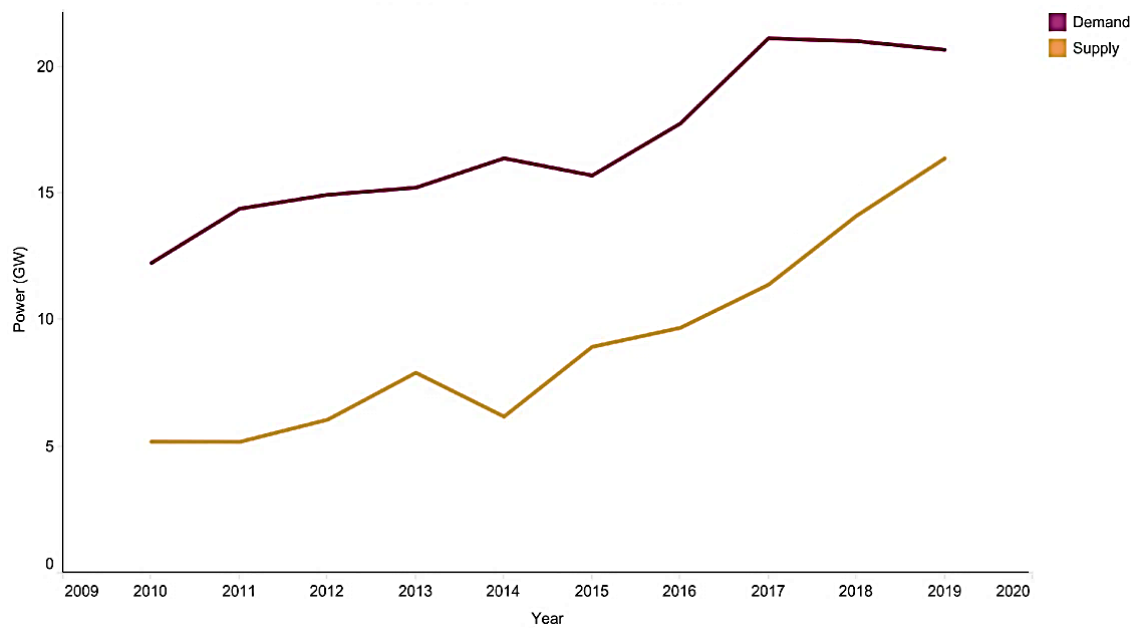


Fig. 1-1 The difference between need and available energy in Iraq (Al-Saffa, F. Salim, S. Sallam, S. Jamal, 2021)

The use of solar energy has become an attractive most available and clean as compared to the conventional source of energy. The sun is 109 times wider than the earth and is located 150 million kilometers away. Its diameter is 1.392 million kilometers, and the average surface temperature is 5,778 K, with the core temperature reaching 15.7 million Kelvin. Its huge potential for supplying energy to our planet is undeniable (Kumar, 2018).

Solar energy is the energy that the sun gives off as radiation. Mainly, solar thermal system counts upon the energy that is heating up the fluid by the radiation received, while photovoltaic is used to produce electricity from the received radiation. There are also some specific ways for accumulating thermal

energy by using a concentrating solar collector which is done by a reflector that will concentrate solar radiation to the collector, so that the production of thermal energy will be maximized (John and Beckman, 1982).

Investigations into hybrid solar panels have increased significantly in recent years as their capacity for efficiently producing both thermal and electrical energy has become more apparent. By combining these two energy sources, hybrid solar panels provide an effective alternative to the traditional methods of separately harvesting thermal and electrical energy. As such, these panels have become increasingly attractive to researchers and engineers, offering a more efficient means of energy production (Xu *et al.*, 2021).

1.2 SOLAR ENERGY TRANSFORMATIONS TECHNIQUE

Traditionally, the conversion of solar energy has been done through two distinct methods: the production of electricity via photovoltaic modules or the generation of heat through thermal collectors. However, a new area of research has emerged that combines both of these methods together in a process known as photo thermo conversion (Grant *et al.*, 2002). This dual energy conversion process is referred to as a photovoltaic-thermal collector (PV/T) with hybrid functionality, which is capable of producing both electricity and heat simultaneously. Such a device offers an attractive solution to the problem of satisfying both energy demands, making it a logical development path. Fig. 1-2 presents the various types of solar energy transformation techniques.

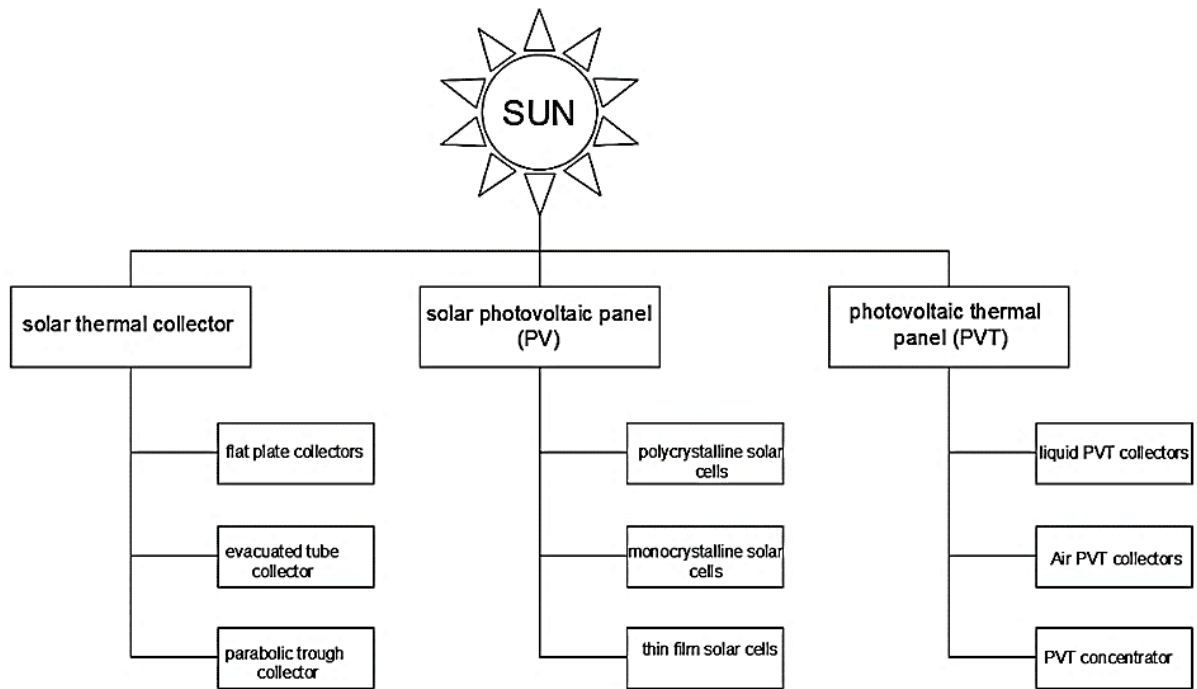


Fig. 1-2 Various types of solar energy conversion technology

1.2.1 Thermal Solar Collector

Solar thermal collectors are a particular kind of heat exchanger, which transform solar radiation energy into the thermal energy of the working fluid. This thermal energy can then be used to provide heat, hot water, and other energy services. The two main types of solar collectors are flat-plate collectors and evacuated tube collectors. Flat-plate collectors are the most commonly used type of collector and consist of a flat absorber plate, a transparent cover, and an insulated back plate. They are typically used for residential and commercial applications, such as heating swimming pools, hot water, and space heating. Evacuated tube collectors are a more efficient type of collector, consisting of a series of glass tubes with a vacuum space between the layers that reduces heat loss. These collectors are typically used in high-temperature applications, such as industrial processes. Fig. 1-3 illustrates a typical flat plate collector.

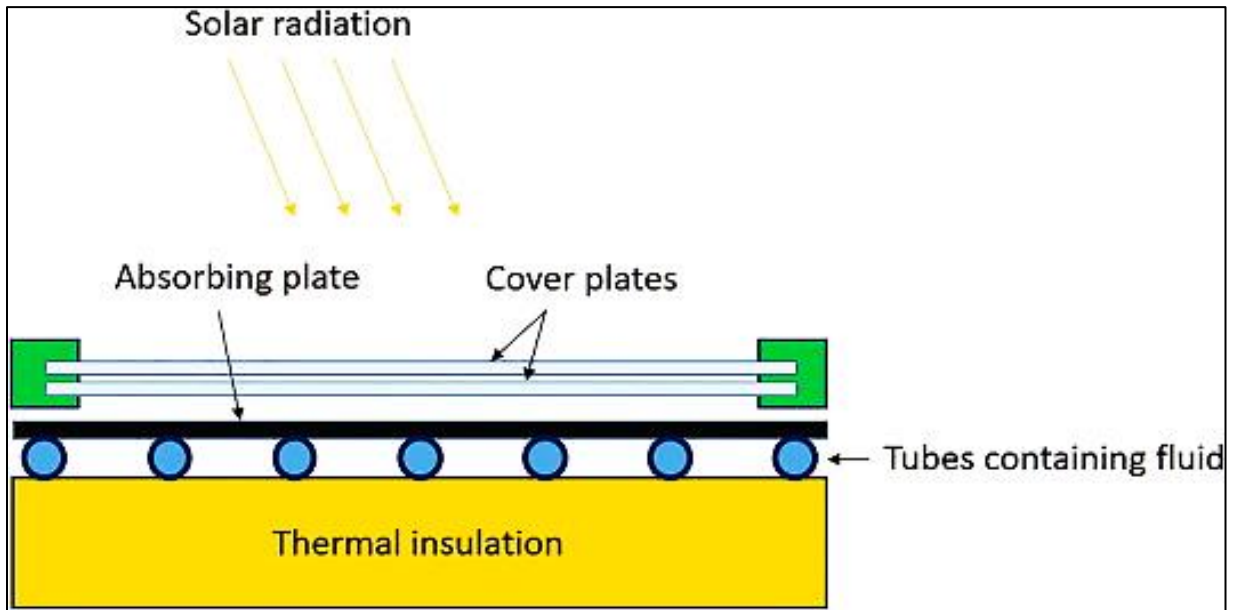


Fig. 1-3 Solar flat plate collector (Dobriyal et al., 2020)

1.2.2 Solar Photovoltaic Technology

Photovoltaics utilize solar radiation to directly generate electricity from the absorbed radiation. The term "photovoltaic" is derived from the Greek words for light and voltage, respectively. Solar cells, also referred to as photovoltaic modules, generate electricity when exposed to sunlight. When solar radiation strikes a PV cell, the photons of the absorbed radiation shift the electrons from the atoms of the cell. The free electrons then move towards the cell, creating and filling in holes in the cell. This movement of electrons and holes generates electricity. This physical process of converting solar radiation into electricity is known as the photovoltaic effect. Photovoltaic systems are composed of solar cells and other components. In 1954, Bell Telephone Laboratories successfully demonstrated the first practical conversion of solar radiation into electric energy using a p–n junction type solar cell with 6% efficiency. A solar cell must have a junction between two different semiconductors. The electrical conductivity of semiconductors is lower than that of conductors and higher than that of insulators. The working principle of the photovoltaic effect is shown in Fig. 1-4.

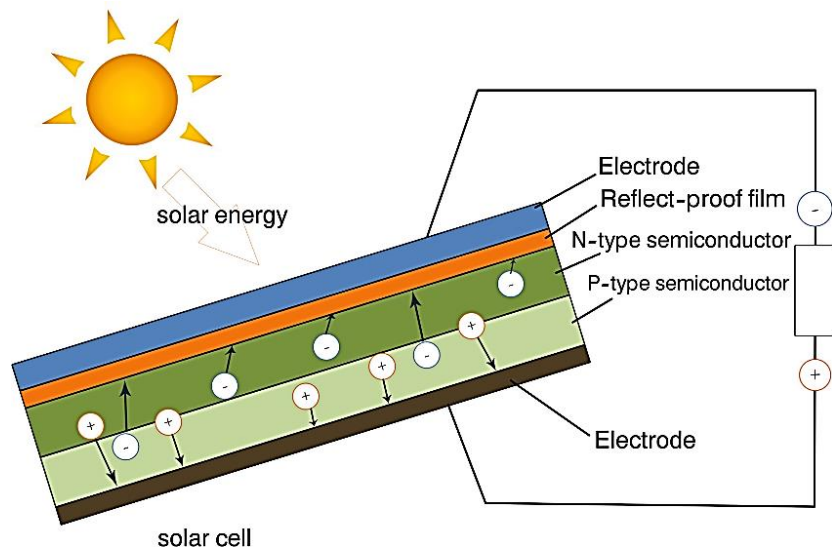


Fig. 1-4 Photovoltaic cell working principle (Husain et al., 2018)

The most common solar cells are made of crystalline and amorphous silicon materials. When solar radiation strikes the solar cell, some of the radiation's spectrum imparts enough energy to produce electron-hole pairs in the semiconductor material. The formation of a junction between two dissimilarly doped semiconductor layers creates a potential barrier that separates the electrons and holes, inducing a voltage. The current available is a function of the PV cell area and solar radiation intensity. The electricity is collected and transmitted by metallic contacts placed on both sides of the cell (Solanki, 2011) .

Photovoltaic cells are organized into modules by connecting them in parallel and series orientations to increase the voltage and current output. For higher power ratings, PV modules can be linked in groups to form arrays. Fig. 1-5 illustrates a basic PV system. Solar panels are composed of an array of photovoltaic modules that convert solar energy into electricity. Charge controllers are used to optimize the power output from the solar panels, supply charge to batteries, control charge current and charge level. Batteries store the energy provided to them and are employed when solar energy is not available. Inverters are utilized to convert DC power into AC power for use in AC applications.

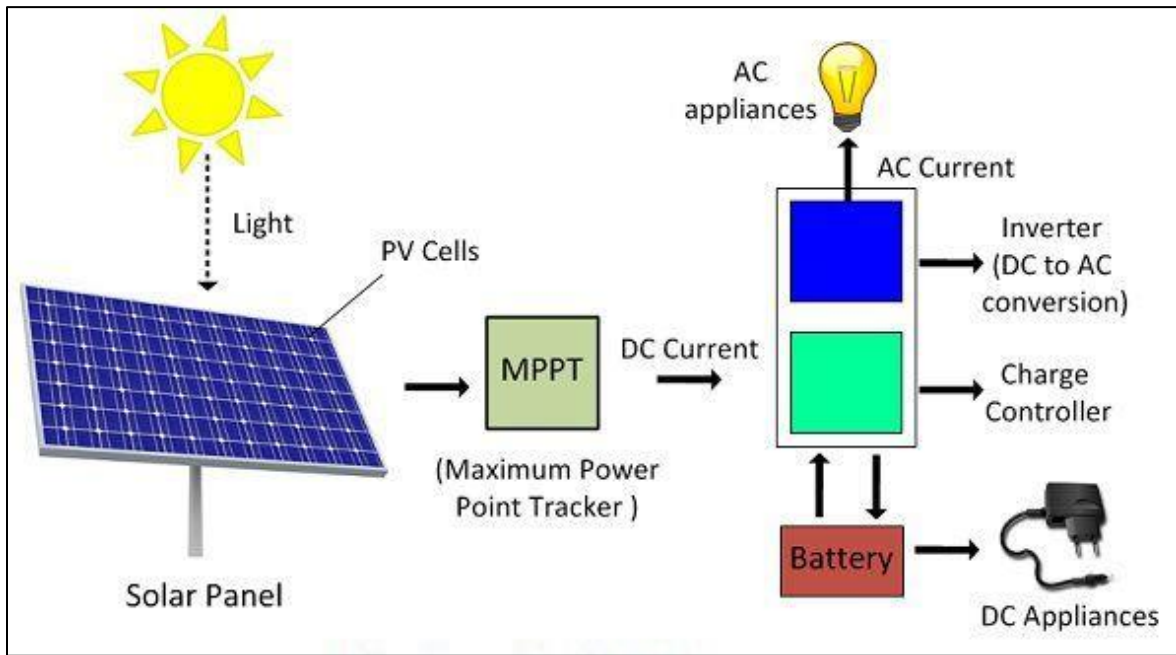


Fig. 1-5 Solar PV system

Commercially available PV modules have the capability to convert solar radiation into electricity with efficiencies ranging from 5-25%, becoming increasingly cost-effective and competitive with other technologies. This is largely attributed to the advancements made in the space program, which have seen photovoltaic cells made from semiconductor-grade silicon become the primary source of power for satellites (Li *et al.*, 2006).

Mainly, there are three technical types of silicon-based PV cells: mono-crystalline, polycrystalline, and thin-film cells, as presented in Fig. 1-6. Mono-crystalline cells are made from a single, large crystal of silicon and are the most efficient type of cell, with efficiencies of up to 23%. Polycrystalline cells are made from multiple, smaller crystals of silicon and are slightly less efficient than mono-crystalline cells, with efficiencies of up to 18%. Amorphous silicon cells are made from a thin film of amorphous silicon, which is a non-crystalline form of silicon. Thin film cells are the least efficient sort of cell, with efficiencies of up to 14%. Additionally, thin film cells are the least expensive type of cell, making them ideal for large-scale solar installations (Sugianto, 2020).



Fig. 1-6 Three main technical silicon-based PV cells

Mainly PV panel consist of five different layers (glass, EVA1, silicon, EVA2 and tedlar). Whereas the glass layer serves as a protective shield for the solar cells, it allows sunlight to pass through while protecting the cells from environmental factors. While EVA serves as a protective, adhesive, and insulating layer in PV panels, contributing to their overall performance, durability, and efficiency in converting sunlight into electricity. The silicon solar cells are core of the PV panel, solar cells are responsible for converting sunlight into electrical energy through the photovoltaic effect. On the other hand, tedlar layer in a PV panel functions as a protective barrier against moisture and chemicals, provides UV resistance, offers electrical insulation, and contributes to the mechanical strength of the solar panel, enhancing its performance and lifespan (Benda and Černá, 2020).

1.2.3 Solar Photovoltaic Thermal (PV/T) Technology

Solar Photovoltaic Thermal (PV/T) Technology combines the two most commonly used solar technologies, photovoltaic (PV) and solar thermal, into one system. It is an innovative technology that can be used to generate both electricity and heat from the same system. It appears to be a wise decision to develop a device that can not only meet the demand for solar heat and electricity, but also maximize the efficiency of the module. This could be

accomplished by integrating PV cells with a thermal solar collector to create a device that can convert the solar radiation into both electricity and heat simultaneously. The electricity generated can then be used for immediate consumption, while the heat can be stored for future use. By utilizing this approach, we can not only meet the dual demand for electricity and heat, but also maximize the efficiency of the panel by reducing the panel's temperature, which will increase the lifespan of the PV panel. A sample model of solar photovoltaic thermal (PV/T) technology is shown in Fig. 1-7.

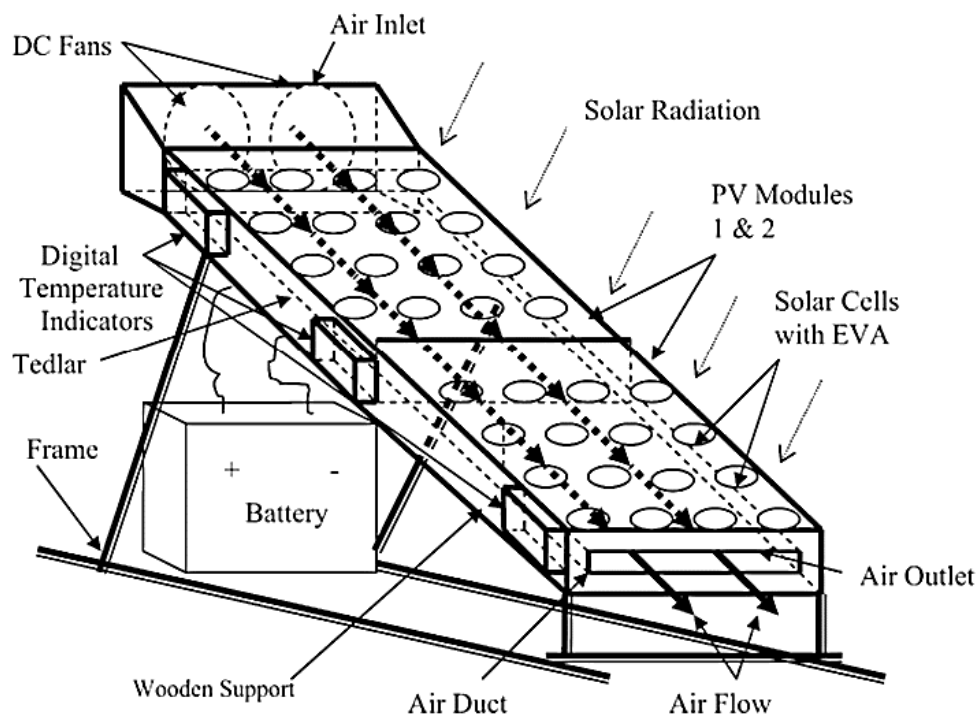


Fig. 1-7 Typical solar photovoltaic thermal technology (Joshi et al., 2009)

1.3 SOLAR TRACKING SYSTEMS

Solar tracking systems are an advanced technology for photovoltaic (PV) installations that helps to maximize energy production. They are designed to move the PV surface to the optimal angle and orientation to capture the most sunlight throughout the day. Single-axis and dual-axis solar tracking mechanisms are the two main types of tracking systems available.

1.3.1 Single Axis Solar Tracker

Single-axis trackers (SATs) allow solar PV panels to rotate around a single axis, typically parallel to the north meridian. They provide a good balance between flexibility, efficiency, and simplicity. A single-axis solar tracker can be configured in a variety of ways, depending on the orientation of the axis with respect to the ground, including tilted single-axis trackers, which track between the axes of horizontal and vertical, horizontal single-axis trackers, which are horizontally positioned with respect to the ground, and vertical single-axis trackers, which are vertically positioned with respect to the ground. These trackers enable the solar modules to orient themselves east-west according to the sun's position (Racharla and Rajan, 2017).

1.3.2 Dual Axis Solar Tracker

Dual-axis trackers have two axes of rotation that are perpendicular to each other. The axis that is fixed in place is the primary axis. The module's orientation relative to the tracker axis is important to measure power production or performance. These trackers are highly beneficial for solar energy production since they can be adjusted to follow the sun, regardless of its position in the sky. This allows them to always remain in direct contact with the sun (Racharla and Rajan, 2017).

1.4 PROBLEM STATEMENT

The efficacy of photovoltaic (PV) panels is contingent upon cell temperature, with the PV module attaining the highest efficiency at 25 °C and 1000 W/m² nominal operating conditions. As cell temperature rises, the module efficiency declines, thereby reducing the panel's electrical power production and the proportion of solar radiation converted to electrical energy, which ranges from 5-25%. When panel operates at high ambient temperatures, a significant portion of the solar radiation captured by the cell is transformed into undesirable heat, which results in further increase in the cell temperature and

decreases efficiency. The ambient temperature in Iraq generally, started to increase above 25 °C during the months from April until the end of October, this makes a crucial factor to think about the water-cooling technology for PV panels. The accumulation of dust on the panel surface creates a barrier that reduces the efficiency of the photovoltaic cells in converting sunlight into electricity. Many researches have been carried out to enhance the efficiency of photovoltaic panel experimentally as well as numerically by utilizing different cooling strategies to lower the panel's temperature, most efficient way was by using water. Finally, this research will answer the following equations:

- What is the most effective way of cooling PV cells? How should the rate of water be controlled in accordance with the panel surface temperature?
- How will the combination of a solar tracking system with a water cooling technique influence the increase in power production from photovoltaic panels?
- Which parameter has the highest impact on the efficiency and power production of the photovoltaic panel?

1.5 PURPOSE AND OBJECTIVES

The objectives of this research are as follow:

1. Improving the photovoltaic panel's performance by implementing a spray water cooling system on top, left and right side of the front surface of the panel, where the proposed system performs to:
 - a- Minimize the operating temperature of PV panel which will result in higher electric power production.
 - b- Self-cleaning of the photovoltaic panel, which has a significant influence on increasing the power production as a result of optimizing sun light absorption, especially in countries with dusty weather.

2. To demonstrate the effect of implementing a single east-west solar tracking system on getting optimum solar radiation, by comparing it with a fixed reference panel.
3. To investigate the effect of adjusting and optimizing the water flow rate automatically in accordance with the panel surface temperature.
4. The developed panel with the tracking system and spray water cooling system will be compared against the fixed panel as a benchmark.
5. To optimize the influence of panel operating temperature over electric power production.
6. Establish and develop a 3D numerical model by using (ANSYS Fluent R19.2) and validate the model against experimental results.
7. To study the impact of ambient temperature, solar irradiance and water inlet temperature on the efficiency and power production of a cooled photovoltaic panel.

1.6 RESEARCH METHODOLOGY

1. Conducting a comprehensive review of previous research on photovoltaic panels with cooling is needed in order to identify areas of research that are yet to be explored. This review will help in narrowing down the scope and highlighting the issues that require further investigation.
2. Identify the primary factors influencing the cell's temperature and the quantity of electric power generated by the photovoltaic (PV) panel, and determine the optimal methods to maximize the PV panel's performance.
3. A photovoltaic panel spray water cooling system with a tracking system was developed and installed at the research center of Erbil Polytechnic University. A comprehensive set of experiments was carried out to assess the system's performance, and the collected data was used to assess its overall effectiveness and efficiency.

4. Developing a numerical 3D model using ANSYS (Fluent R19.2) to evaluate the performance of a photovoltaic panel and validate the model against experimental results.
5. Calculating the system's electrical performance for the experimental as well as ANSYS results.
6. Numerical and experimental results are compared and discussed.

1.7 THESIS STRUCTURE

The dissertation consists of six chapters.

Chapter one provides an overview of the research topic and its context. It outlines the research objectives, research questions, and research methodology used. The chapter concludes with a summary of the thesis structure.

Chapter two provides a comprehensive review of the existing literature pertaining to the research topic of solar photovoltaic cooling systems and their electrical and thermal energy performance. It will also provide an overview of solar tracking system, and how their use affects the overall performance of a system. The aim of this review is to offer an understanding of the definition and classification of PV cooling systems. The research gap of the dissertation is then established in light of the literature review.

Chapter three outlined the mathematical modeling that encompasses calculations for electrical efficiency, power production and PV angles. Furthermore, the simulation process was elucidated with the aid of the ANSYS Fluent software, providing a comprehensive understanding of the fundamentals.

Chapter four describes the design and fabrication of a PV spray water cooling technique test apparatus, along with an examination of the

measurement equipment's uncertainty. The instruments used to measure parameters such as inlet and outlet water temperature, PV surface temperature, water volume flow rate, voltage and current are discussed, followed by a description of the experimental procedure. The numerical model is then validated, and the effects of the tracking system and adjusting the water flow rate due to the surface set point temperature on the system's performance are investigated experimentally.

In **Chapter Five**, the outcomes derived from the experimental and computational results for the present photovoltaic cooling system with tracking system are discussed. Results from both the water cooling and tracking systems at different operation adjustments were presented. The performance of the spray water cooling at different set point temperatures, different flow rate with and without tracking were reported. Additional information, like the water flow temperature and the CFD temperature contour on different layers of PV/T systems was also reported. The outcomes from the CFD were compared with the corresponding experimental values and the degree of agreement was presented.

Chapter Six summarizes the study's main results and conclusions with suggestions for further research.

CHAPTER TWO

(LITERATURE REVIEW)

2.1 INTRODUCTION

As the need for energy continues to increase, the utilization of solar power has emerged as a reliable and sustainable alternative to conventional fossil fuels. Solar energy is a renewable source that is free to use as well as poses minimal environmental hazards. Additionally, the supply of this energy resource is abundant and thus can help to ensure a steady flow of energy. Hence, solar energy is deemed to be a promising and sustainable resource that can fulfill the energy needs of today without compromising the environment. It can also help to maintain ecological balance and reduce dependence on conventional energy sources.

Especially solar photovoltaic thermal panels (PVT) play a major role in meeting the energy demand, as it supplies thermal and electrical energy simultaneously. The performance of photovoltaic systems can be improved throughout cooling the panel, concentrating solar radiation and/or providing a solar tracking system. In this chapter, a comprehensive literature review explores up to date researches and techniques regarding the enhancement of the PV panels performance through cooling the panel to enhance the electrical performance of the module as high operating temperatures will negatively affect the PV efficiency. Also, reviewing tracking systems for the PV panels which leads the panel to increase the solar energy received by the panel throughout the day. Finally, the research will conclude with a discussion of the potential benefits and drawbacks of the cooling and tracking systems, as well as the potential applications of these enhanced performance PV systems.

The purpose of this review is to identify areas in need of improvement to optimize the performance of a photovoltaic system, as well as to determine the most effective form of cooling for regions with dusty weather.

2.2 PV SOLAR CELL

Alexander-Edmond Becquerel's discovery of the photovoltaic effect in 1839 was a groundbreaking moment in history (Yadav, A. and Kumar, 2015).

In 1946, the pioneering solar cell composed of silicon was developed by Russel Ohl (Robert, 2010; Yadav, A. and Kumar, 2015).

(Chapin, D. N., Fuller, C. S. and Pearson, 1954) were the first to publish research on generating power via photovoltaic phenomena utilizing crystalline silicon, notwithstanding the fact that this phenomenon had been known for some time beforehand. This research ushered in a new era of exploration in the energy field.

The original photovoltaic cells are comprised of feeble silicon wafers that can convert the energy of the sun into electrical energy. The utilization of silicon wafers for the fabrication of the earliest solar cells proved to be remarkably successful, due to their high-power efficiency, and continues to remain the most popular option today (Sharma, Jain and Sharma, 2015).

The first generation of solar technologies can be sectioned into two divisions (Choubey, Oudhia and Dewangan, 2012; Bagher, Mahmoud and Mirhabibi Mohsen, 2015):

- multi or poly-crystalline silicon solar cells.
- single or mono-crystalline silicon solar cells

Polycrystalline solar cells are generated out from extensive blocks of silicon through the application of special crucibles that progressively cool down the liquefied silicon, thus enabling large-grained polycrystalline structures to be formed. Subsequently, the blocks are sawed into wafer segments. Polycrystalline cells, though not as effective as monocrystalline ones

(Jumrusprasert, Smith and Kirkup, 2007; Ayadi *et al.*, 2022), are relatively less expensive to manufacture due to the absence of energy-consuming processes involved in crafting single crystals (Parida, Iniyan and Goic, 2011).

Monocrystalline solar cells are considered to possess the maximum conversion efficacy among silicon solar cells. Research in the laboratory indicates that a single photovoltaic unit's efficiency can ascend to 24%, while cells generated in mass scale production have a productivity of around 17% (Parida, Iniyan and Goic, 2011).

2.3 SOLAR TRACKING SYSTEM

Exploring the problem of getting maximum output from photovoltaic panels necessitated looking into the issue of their orientation, meaning that a solar tracker must be connected to the PV system. This mechanism follows the sun's position over the duration of the day, in order to make sure that the solar panel is kept in a position where the sun is continually at a normal angle. Gaining the maximum output of the system required two strategies: improving the transformation and absorption percentages and increasing the incident rays by having a solar tracking system.

A solar tracker is an apparatus that contains a motor-operated mechanism, allowing it to be situated such that photovoltaic panels are directed to follow the sun's movement across the sky. There are two types of these trackers, with differences derived from the level of automation present in their designs, as well as the sensitivity of the sensors employed or the system by which they position their panels (Chong and Wong, 2009; Hua *et al.*, 2019; Gómez-Uceda *et al.*, 2020).

A multitude of studies have been conducted to enhance and expand the delivery of electricity by utilizing the sun's rays. Among the many studies done in this field, one can point to the work of Corio (2008), which investigated for the first time the potential benefit of implementing a simple solar tracking

system, making use of a stepper motor and a light sensor. Through design, implementation, and experimentation, they were able to prove the system's efficiency with positive intermediate results.

Barsoum and Vasant (2010) demonstrated that a single-axis solar tracking system can augment energy output by around 20%.

Tudorache, T., Oancea, C.D. and Kreindler (2012) investigated the effectiveness of a single east-west tracking system by implementing a DC motor under the control of a smart driving system that receives signals from suitable light intensity sensors. The results indicated that the system is able to produce 57.55% more electric power than the fixed panel.

The studies surveyed in the articles (Alexandru and Pozna, 2008; Natarajan *et al.*, 2019; AL-Rousan, Mat Isa and Mat Desa, 2021) illustrate that the alignment of solar cells can boost their transformation performance by a range of 20 to 50%, which means a substantial rise in electrical wattage.

Baouche *et al.* (2022) designed their own solar tracking system by using an Arduino board and a control program and light dependent resister LDR, the block diagram of their system is presented in Fig. 2-1, they conclude that their system was cost less than regular commercial systems while giving a better efficiency rate than a stationary one.

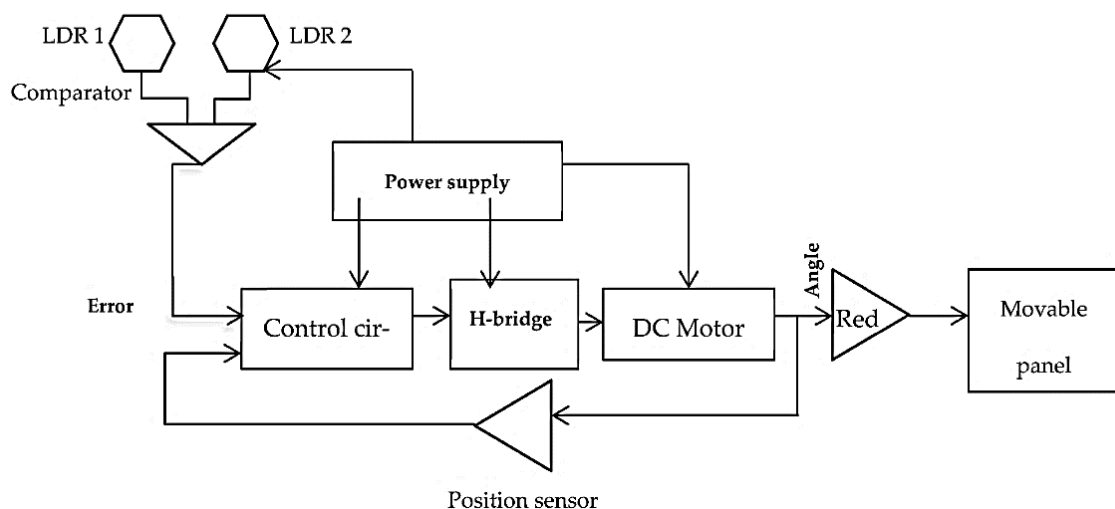


Fig. 2-1 Block diagram of tracking system (Baouche *et al.*, 2022)

2.4 ENVIRONMENTAL ELEMENT INFLUENCE ON PANEL PERFORMANCE

Various environmental conditions affect the performance of solar modules, such as ambient temperature, solar radiation intensity, and dust. These factors demonstrate how much energy can be extracted from the PV cells.

2.4.1 Influence of Solar Intensity

The level of current which passes through a short circuit (I_{SC}) is responsive to the number of photons taken up by the semiconducting material, therefore it is relevant to the light strength (Luo *et al.*, 2017). The power output related to the irradiance usually remains stable due to the constant energy conversion efficiency. This current output can be detrimentally affected when the irradiance increases as displayed in Fig. 2-2. While the light intensity may affect the module voltage to some extent, the degree of this influence is negligible in most cases (Mohsin and Abdulbaqi, 2018).

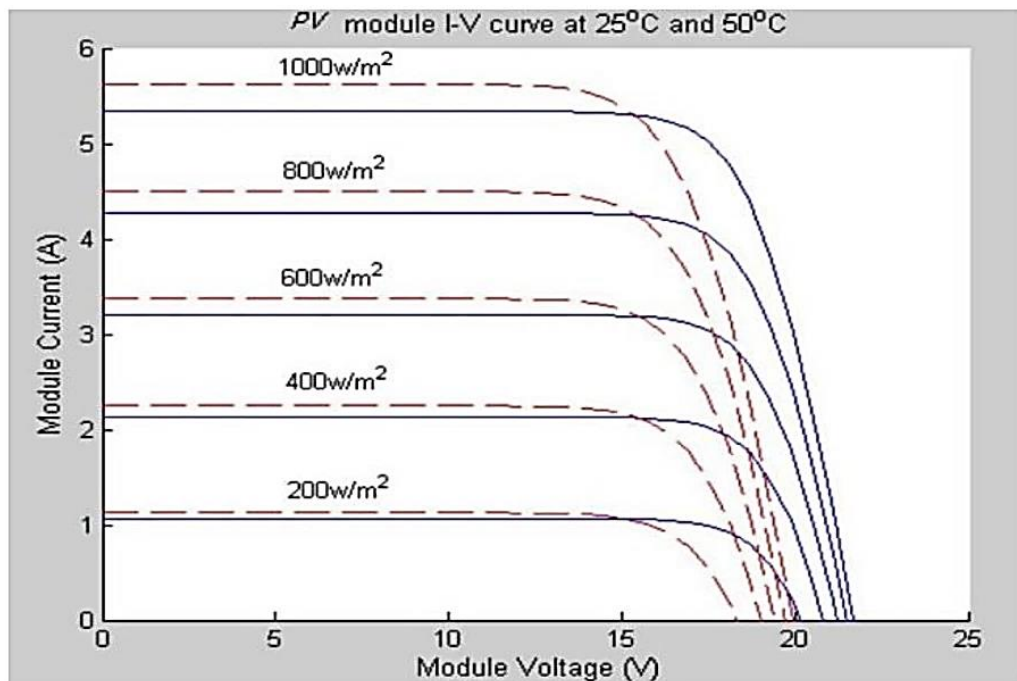


Fig. 2-2 Effect of irradiance on characteristic of the panel (Mohsin and Abdulbaqi, 2018)

2.4.2 Influence of Dust

In regions surrounded by desert, sand dust can be a real problem for the implementation of PV technology. Due to its ability to scatter, reflect and absorb sunlight, it can obstruct the illumination of PV panels, drastically reducing their efficiency. The degree to which the dust settles can be determined by four major factors: size, kind, concentration and the interval for which it comprises (Al-Hasan, 1998). The weight of particles, along with electrostatic and mechanical forces (rain droplets or air-current), causes them to settle on the surface below. Subsequently, the particles are adhered to the surface due to variations in electrical field potential, cohesive energy effects, along with gravity and electrostatic forces. Dust in the atmosphere is omnipresent, but the size and composition of the particles vary according to where it is released. In some parts of the planet, such as Kuwait between May and August, dust may be present for up to 27% of the daylight hours, reducing visibility significantly as shown in Fig. 2-3 (Aldihani, 2017).

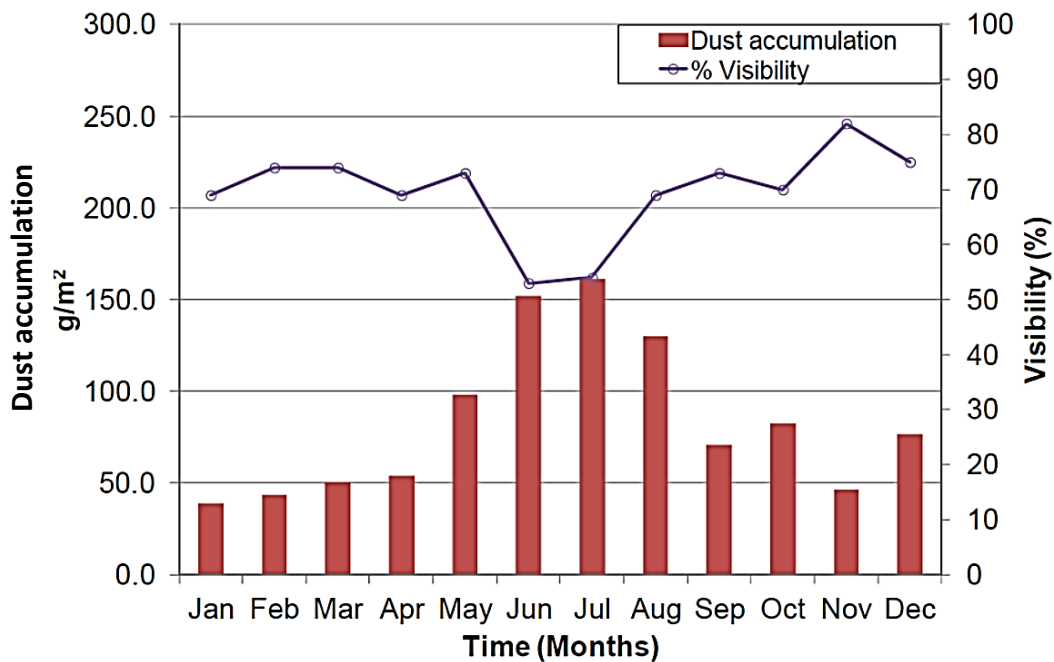


Fig. 2-3 Monthly average dust accumulated and visibility in Kuwait 2013 (Aldihani, 2017)

The scientist Abdulazeez (2018) conducted an experiment on two identical PV modules with a dual-axis sun tracker and monitored the results in real-time to evaluate the impact of dust accumulation on the efficiency and energy losses of photovoltaic systems at Kirkuk, Iraq. The findings showed that dust deposition led to considerable losses of energy in both fixed and sun-tracker modules although the effect was less pronounced in the tracking system.

The effect of dust on PV power production in Iraq was studied by Chaichan and Kazem (2020) the result indicated that when the accumulated dust over the panel surface is increased the PV surface temperature is boosted as well, resulting in decreased power output, as presented in Fig. 2-4.

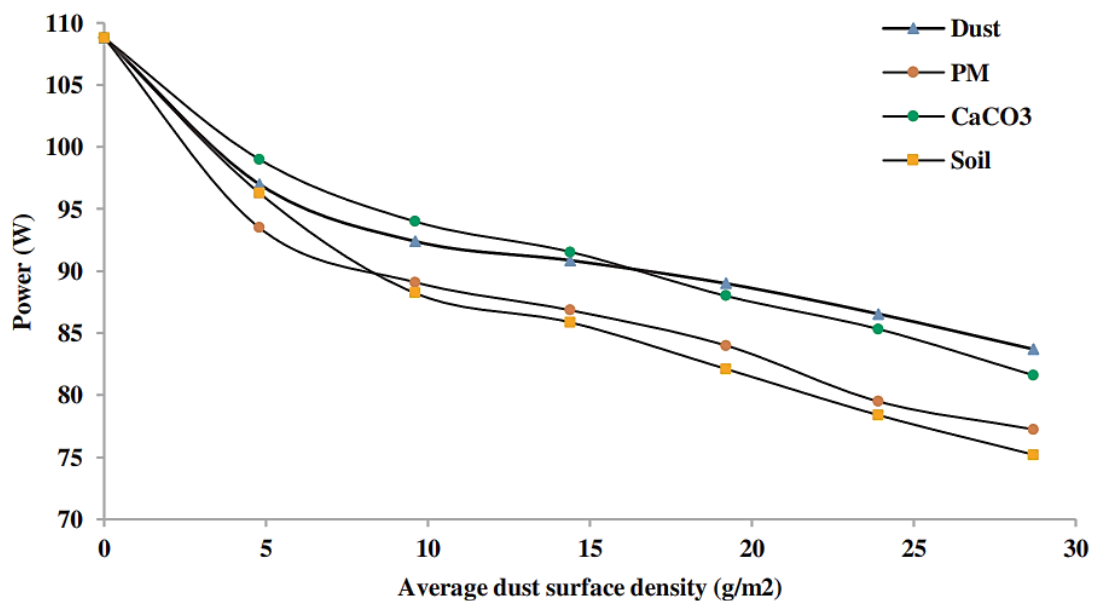


Fig. 2-4 Effect of dust density on PV power production (Chaichan and Kazem, 2020)

Chaichan *et al.* (2023) experimentally investigated the effect of a dust storm on solar radiation absorptance by the panel; the findings proved that prior to the storm, the solar radiation strength was powerful at around 720 W/m². During the storm, however, the radiation plummeted, slipping by 50.54%, as shown in Fig. 2-5.

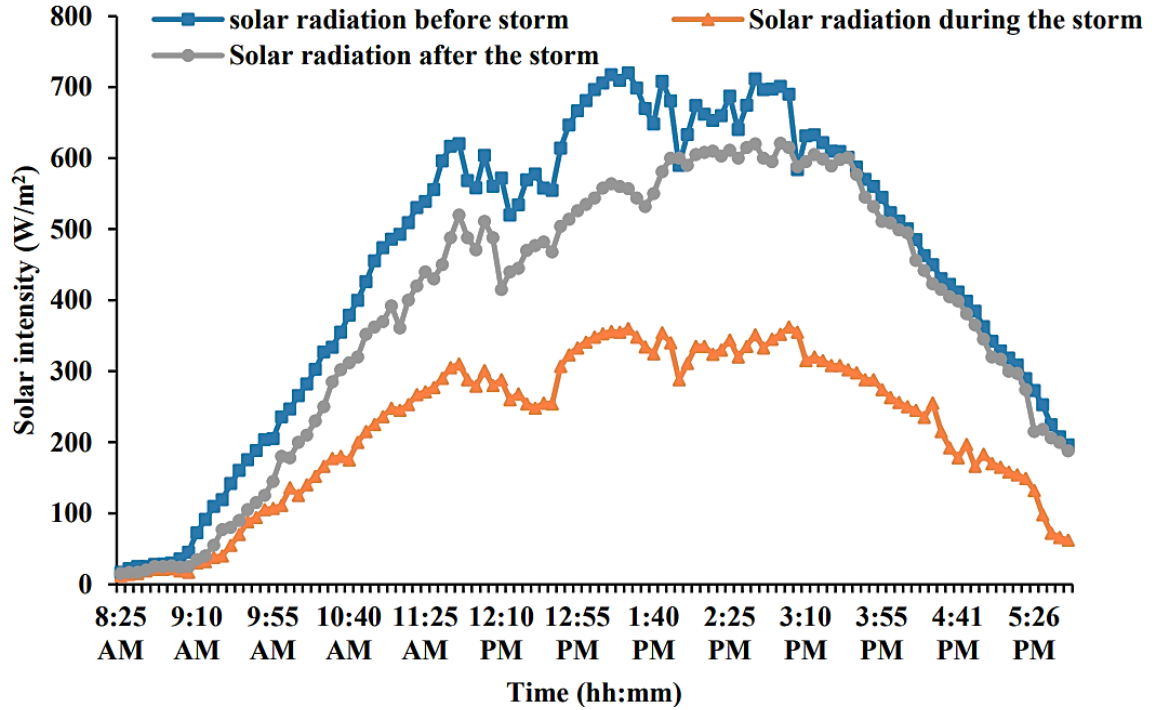


Fig. 2-5 Dust storm effect on solar radiation intensity (Chaichan *et al.*, 2023)

2.4.3 Influence of Ambient Temperature

Previously, researchers found that solar cells differed in output depending on temperature changes. (Skoplaki and Palyvos, 2008) stated that the power output of PV modules was seen to lessen by 0.4 - 0.5% for each degree Celsius increase in temperature beyond the predetermined operational temperature, depending on the temperature coefficient of the power of the module. It was also discovered that the desired efficiency of a PV module could be influenced by varying the temperature around it (Al-Waeli *et al.*, 2016).

(Bonkaney, Madougou and Adamou, 2017) Studied the influence of ambient temperature over PV efficiency and power production, the study showed that when PV temperature raises by one degree Celsius the electrical performance and power output will reduce by 0.49% and 2.6 W respectively, as presented in Fig. 2-6.

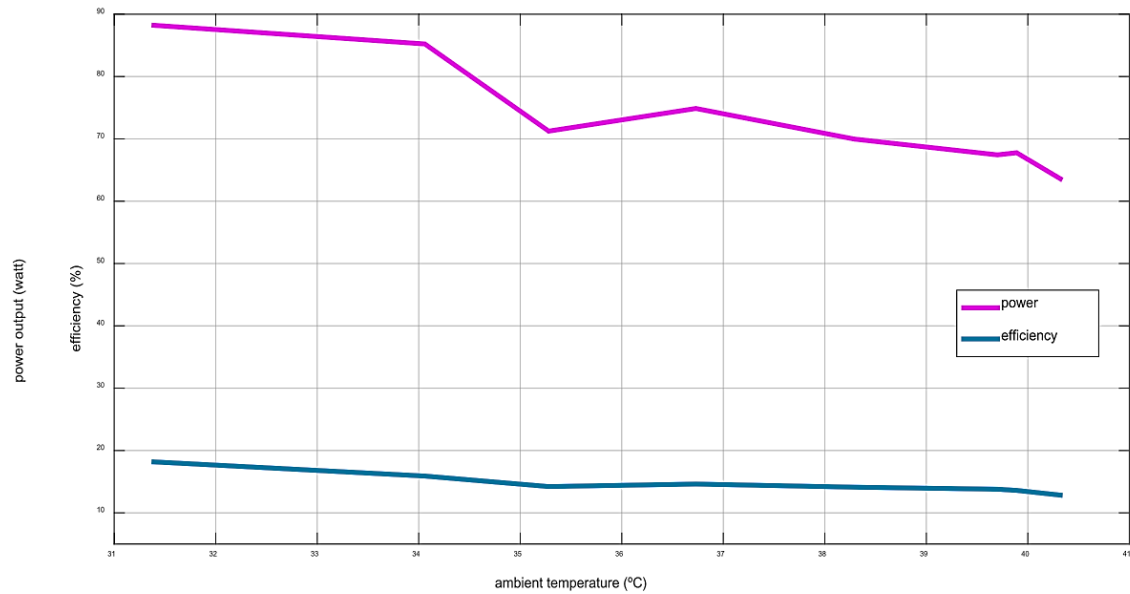


Fig. 2-6 Variation of PV efficiency and power production with ambient temperature
(Bonkaney, Madougou and Adamou, 2017)

(Al-Damook *et al.*, 2022) Studied the photovoltaic performance in Iraq under hazardous weather, and the results showed that with the lower ambient temperature would lead to higher power production.

While another experimental was conducted in Baghdad, Iraq, by (Al-Ghezi, Ahmed and Chaichan, 2022), they concluded that the PV panels are strongly affected by fluctuation in ambient temperature, by increasing the power by 1 degree Celsius the power and efficiency will decrease by 0.489% and 0.586% respectively.

2.5 PHOTOVOLTAIC PANEL COOLING TECHNIQUE

In order to preserve the performance of photovoltaic panels in outdoor environments, it is essential to utilize cooling methods that minimize the effects of environmental elements on the surface temperature of the panel. An effective way to do this is by implementing suitable cooling measures to reduce the operational temperature of photovoltaic panels and thus protect their performance.

Researchers are actively developing cooling systems that are specifically designed to decrease solar cell operational temperatures, including active and passive approaches. Such minimization of the temperature of the photovoltaic array assists in the reduction of power losses and augments the dependability of the PV module. To optimize the effectiveness of photovoltaic modules, passive and active cooling techniques are being employed.

Active cooling necessitates an agent of cooling, such as air or water, which usually necessitates the use of a fan or pump. In contrast, passive cooling does not need supplemental energy to decrease the PV cell temperature (Teo, Lee and Hawlader, 2012; Sharaf, Yousef and Huzayyin, 2022). Fig. 2-7 shows the cooling mechanisms used to minimize the panel's operating temperature.

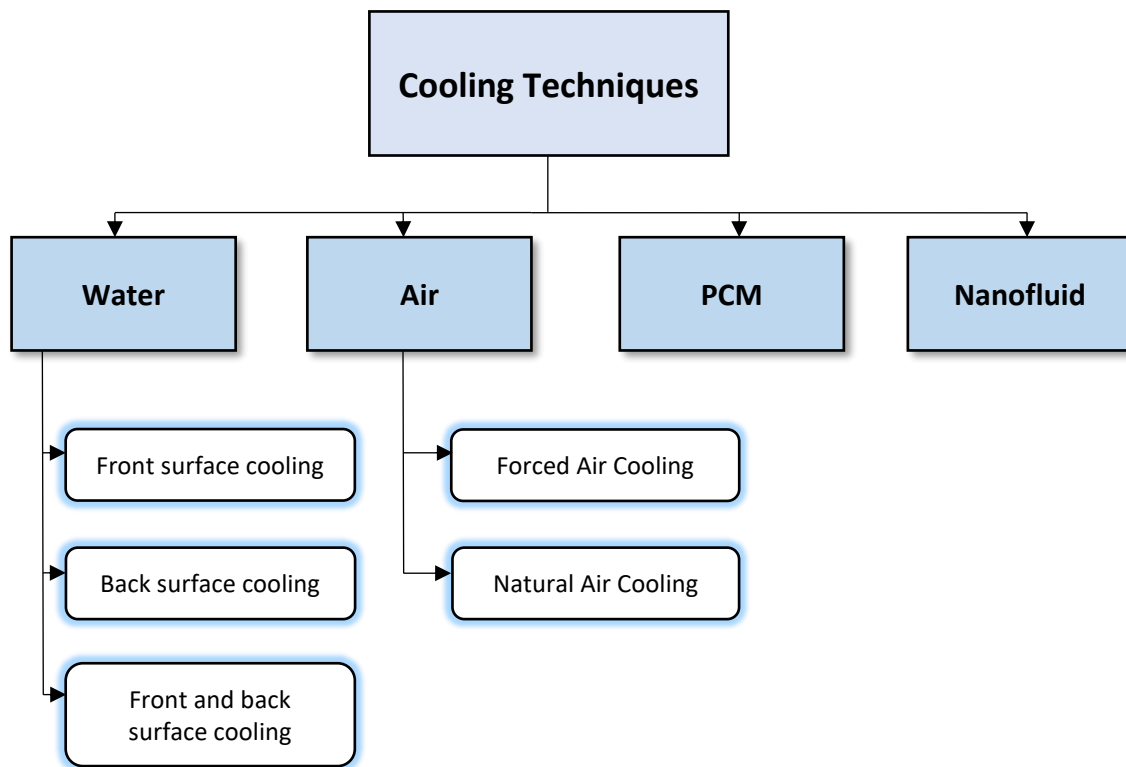


Fig. 2-7 Cooling strategies

2.5.1 Water Cooling Strategy

2.5.1.a Front Surface Cooling

Front surface water cooling of photovoltaic (PV) panels is a relatively new technology that has been gaining increasing attention in recent years. This innovative method is seen as a potential solution to address the thermal issues that have been hampering the efficiency of PV cells in many countries around the world. In this literature, the current state of research and development in the field of front surface water cooling of PV panels is explored. Table 2-1 presents studies and their improvement in electrical efficiency using front surface cooling technique.

Table 2-1 Front surface cooling researches

Researcher	Type of study	Cooling Mechanism	Temperature reduction (°C)	Efficiency improvement %	Country
(Krauter, 2004)	Experimental	Twelve nozzles along top of module, constant flow, continuous cooling	22	10.3	Brazil
(Abdolzadeh and Ameri, 2009)	Experimental	Tube with small holes, constant flow, continuous cooling	23	12.5	Iran
(Wu and Xiong, 2014)	Experimental	Rainwater distribution tube on the top of the panel, constant flow, continuous cooling	19	8.3	UK
(Nižetić <i>et al.</i> , 2016)	Experimental	10 nozzles on the front side, 3 up, 3 down and 2 on each side, three different flow rates were tested	26.4	10.77	India

		144, 189, 225 L/h.			
(Jailany, Abd El-Al and Rashwan, 2016)	Experimental	Water distributing hose with on/off timer	9.07	7.87	Egypt
(Matias <i>et al.</i> , 2017)	Laboratory Experiment	perforated metallic profile, four constant flow rates were tested 1, 2, 3, 4 L/min for cooling the panel	18	22.69	Brazil
(Arefin, 2019)	Experimental and Numerical (ANSYS)	Pipe with 20 holes on the top of PV, different flow rate tested 0.5, 1, 1.25, 1.5, 1.75 and 2 L/min. continuous cooling.	14	1.5	Bangladesh
(Khalil, Abdelgaied and Hamdy, 2019)	Experimental	Spray water with 6 nozzles, 2 on topside and two at each left and right side of the panel exactly facing each other. 225 L/h constant flow continuously.	18	18.8	Egypt
(Govardhanan <i>et al.</i> , 2020)	Experimental	Immersing front surface with uniform flow, by testing three different mass flow rate 2.3, 3.8, 5.3 kg/min	20	14	India
(Benato <i>et al.</i> , 2021)	Laboratory Experiment	Three nozzles on the top of the	24	2.09	Italy

		module, five different on/off spray cycle were used.			
(Nateqi, Zargarabadi and Rafee, 2021)	Experimental	Pipe with 9 nozzles, three different on/off spray water were tested 10 s On-10 s Off), (5 s On-5 s Off) and (3 s On-3 s Off)	40	25.86	Iran
(Sultan, Farhan and Salim Alrikabi, 2021)	Experimental	Copper tube placed over the panel to sprinkle water	21	11.89	Iraq

(Krauter, 2004) studied the effect of using water film to act as an anti-reflection coating to minimize the incidence of sunlight reflection, to clean the front surface of the panel, and to cool the surface to enhance the efficiency of PV panels. The water film cooling system is presented in Fig. 2–8, and the results indicated that water with a reflecting index of 1.3 is a durable contrivance between the air and glass cover of the panel by decreasing panel reflection by up to 3.6%, reducing the panel temperature by about 22 °C, as well as boosting the efficiency of solar cells by up to 10.3%.

(Abdolzadeh and Ameri, 2009) investigated experimentally the potential of enhancing the competency of a PV water pumping system. This was achieved through water spraying on top of the PV module. Experimental findings showed that the power of the cells is augmented with water spray, so the electrical efficiency increased by 12.5% when compared to the panel without spray water cooling.



Fig. 2-8 Creation of film cooling technique (Krauter, 2004)

Research Moharram *et al.* (2013) aimed to minimize the amount of water and electricity needed to cool solar panels in hot, dry areas, like deserts in Egypt. So, they developed a cooling system which involved water spraying over solar panels by utilizing a pipe with 120 nozzles on the top of the panel as shown in Fig. 2-9, as well as a mathematical model was developed to predict the optimal time to start cooling. By analyzing results, they conclude that the system should work for 5 minutes to minimize the temperature by 10 °C, they also calculated the output energy at 40, 45, 55, 65 °C determined that the maximum allowable temperature (MAT) should be set at 45 °C, which is a compromise between the energy produced and the energy needed for cooling.

(Wu and Xiong, 2014) presented an innovative passive cooling system by utilizing collected rainwater that not only lowered the temperature of the cells but also boosted the electrical efficiency of the PV panel by a promising 8.3%.

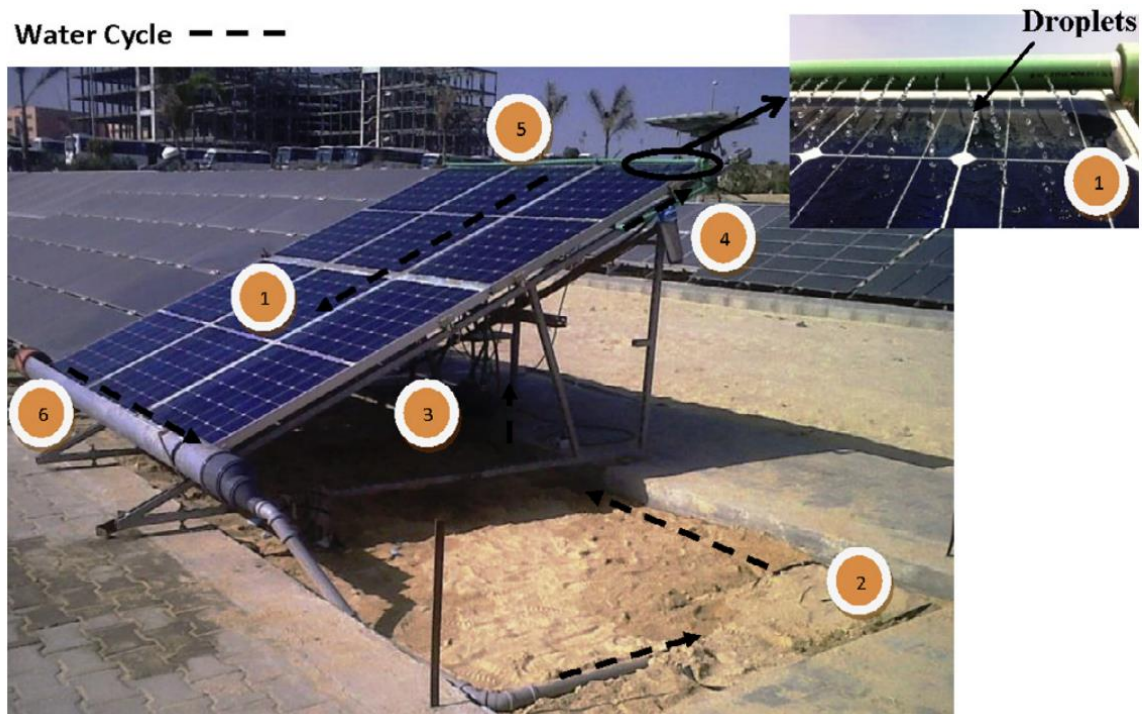


Fig. 2-9 Experimental rig 1 – PV module, 2 – tank, 3 – pump, 4 – filter, 5 – nozzle and 6 – drain pipe (Moharram *et al.*, 2013).

(Nižetić *et al.*, 2016) studied the effect of front surface cooling PV panels for Mediterranean weather by spraying water with 10 nozzles placed at an angle of 40° to ensure that the spray will cover a larger surface of the panel and to prevent shadows over the module. As the results indicated that front surface cooling will lead to increase in power production from 35 to 40.1 W. also, they indicate that the highest power production was at a 225 l/h flow rate.

(Jailany, Abd El-Al and Rashwan, 2016) used the forced water spraying technique to distribute water over the surface of the panel through a distribution hose. As presented in Fig. 2-10, it was possible to minimize the temperature of the PV up to 9.07°C over a period of 10 hours. This was accompanied by a 0.71% and 9.27% increase in efficiency and power generated by the system respectively. Thus, it was recognized that cooling the panel was effective in improving its efficiency and conserving water.

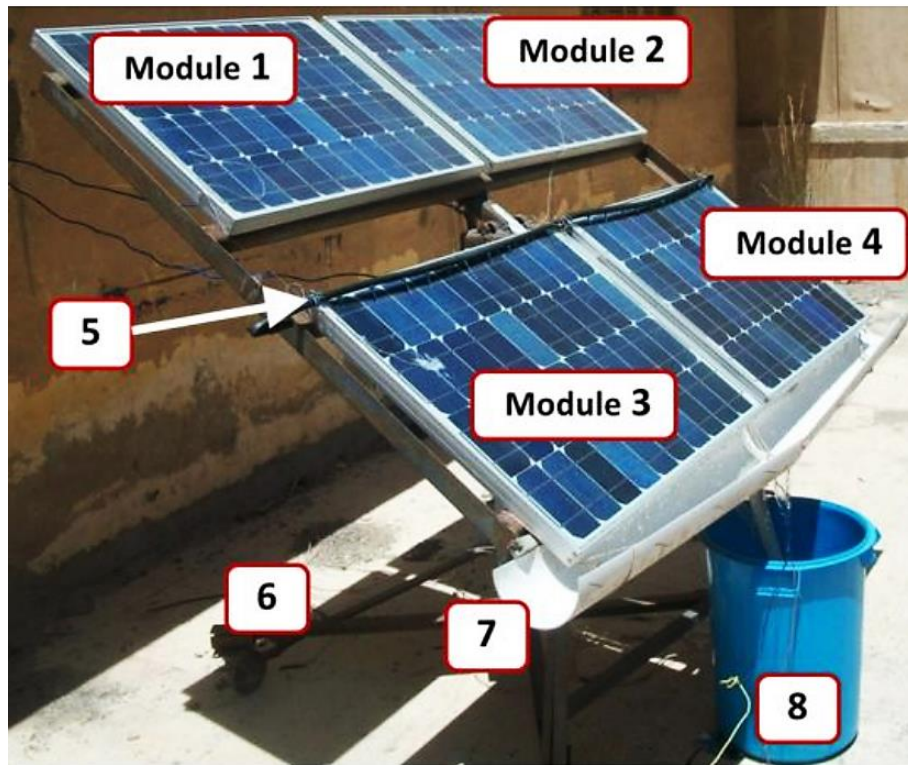


Fig. 2-10 Experimental system 1&2- cells with air cooling, 3&4- cells with water cooling, 5- Water distribution hose, 6- Frame 7- Ducts of water collection, 8- Water tank and solar pump (Jailany, Abd El-Al and Rashwan, 2016).

Matias *et al.* (2017) tried to increase the power generated from a commercial PV by providing water for coolant of the front panel surface which was done through a perforated metallic profile for the dissemination of water over the module. The result showed that the panel without using cooling was able to produce 63 watt-hours with a surface temperature of 70 °C and then by testing different flow ratio of water for cooling they came out with the conclusion that the most effective ratio was 0.6 l/min and net energy 77.41 watt-hours, compared to the panel without cooling the gain was 22.69%.

The study by Syafiqah *et al.* (2017) utilized ANSYS Fluent to explain the impact of five distinct water flow rates within the range of 0.01 to 0.05 kg/s on panel cooling and their effect on convection heat transfer rate. The results indicated that the convection heat transfer rate will be considerably reduced by increasing the flow rate to 235 watts at 0.05 kilograms per second.

Another study by Zhe *et al.* (2019) using ANSYS CFX to determine the distribution of temperature of a photovoltaic module by using front surface cooling at different water inlet temperatures showed that the panel mean temperature for the uncooled one was about 50.68 °C, while it was 45.34 °C and 29.71 °C for water inlet temperatures 45 °C and 20 °C respectively.

(Arefin, 2019) Experimentally and theoretically analyzed the performance of an integrated photovoltaic water heating system where the panel was cooled by a header pipe placed on the top of front surface and the collector was placed outside the panel and connected by integration the water out from the PV panel to the collector. The proposed system leads to increase in electrical efficiency by 1.5% at highest flow rate.

(Khalil, Abdelgaied and Hamdy, 2019) studied the front surface cooling by applying six nozzles two from top, and two at each left and right side of the panel exactly facing each other, there outcome indicated that the maximum power output improvement rate using the proposed method was 15.5%, by reducing the PV temperature from 55 °C for uncooled panel to 27 °C for front surface cooling.

In a separate study by Govardhanan *et al.* (2020) the photovoltaic panel surface was cooled by having three distinct flows of uniform water go over the top surface of the panel. The water was supplied from the tank, which was mounted on the top of the panel, as shown in Fig. 2-11. The outcomes revealed that cooling the photovoltaic panel reduced the panel temperature by 30%, resulting in increased power production from 19 watts to 23 watts. Additionally, it was concluded that the front surface water cooling system was advantageous for clearing the panel surface of dust, resulting in an enhanced visual appearance.

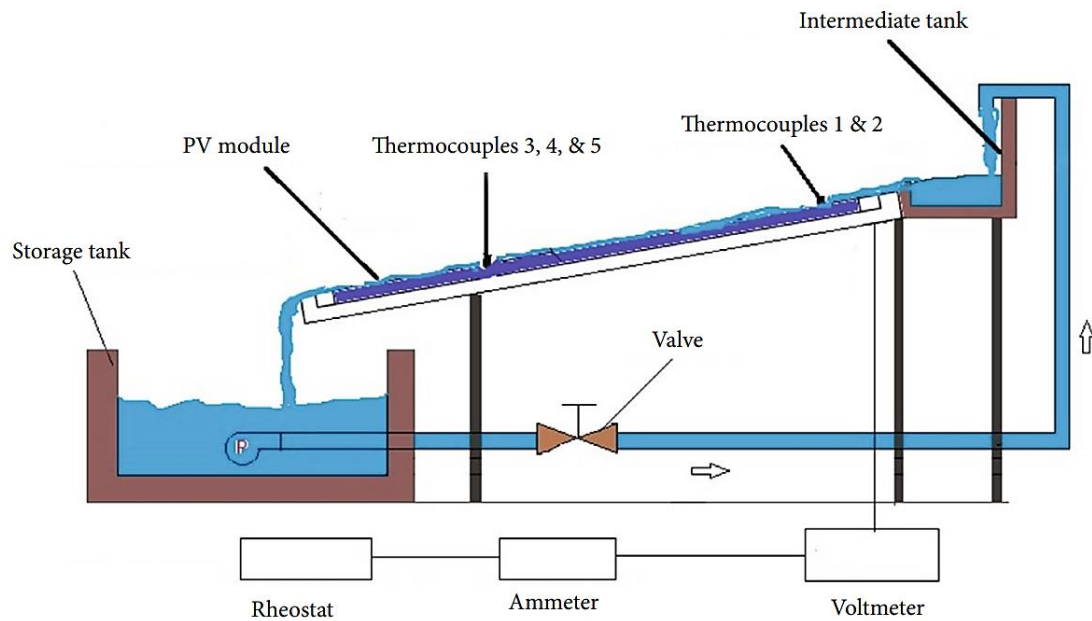


Fig. 2-11 Schematic diagram of experimental rig (Govardhanan *et al.*, 2020)

(Benato *et al.*, 2021) installed a cooling system on a PV panel that would dramatically affect the module surface temperature by spraying water with three nozzles of 90° spray angle placed on the top of the front surface of the panel, as shown in Fig. 2-12. The panel was evaluated in accordance with the panel without cooling system. The result revealed that the cooling system with an on/off controller by providing 30 seconds of running with 180 seconds of halting, the setup was capable of maximizing the efficiency from 11.18% to 13.27% and minimizing panel temperature to 24°C , so they achieved effective cooling with minimum water consumption.



Fig. 2-12 Spray water cooling system with three nozzles (Benato et al., 2021)

Nateqi, Zargarabadi and Rafee (2021) investigated the efficiency of the PV module by examining the impact of water spray angle, as well as the distance between nozzles and PV, also implementing a timer for on-off water spray system. The layout of the system is presented in Fig. 2-13, quantity of nozzles and oscillating water spray they conclude that the efficiency increase to 19.78% with decreasing spray angle to 15° which leads to a decrease in the panels temperature from 64°C to 24°C . By decreasing the space between nozzles and PV panel to the smallest distance which was 10 cm the power output was increased to 25.86% by implementing a continuous water spraying strategy. The on-off spray water cooling system leads to minimizing the water consumption but has the lowest electrical performance.

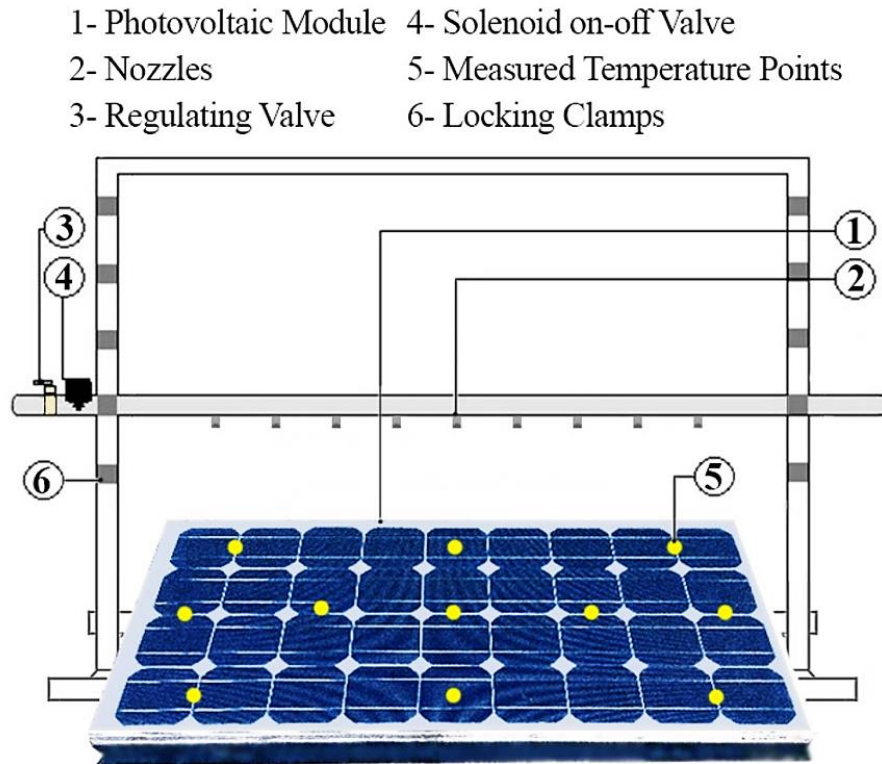


Fig. 2-13 Experimental system layout (Nateqi, Zargarabadi and Rafee, 2021)

Sultan, Farhan and Salim Alrikabi (2021) explored how cooling a photovoltaic panel with a copper cribriform pipe that sprays water onto the module affects the panel's performance in a hot region, such as south Iraq. The result indicated that spray water cooling will lead to a clean surface panel as well as a 34.32% decrease of panel temperature and a huge enhancement in electrical performance at 11.89%.

2.5.1.b Back Surface Cooling

A study conducted by the researchers (Ibrahim *et al.*, 2010) showed theoretically the impact of different volume flow rates over three different absorber shape configurations used to cool down PV panel, the absorber configurations are shown in Fig. 2-14. The result indicated that the water flow in spiral configuration is most efficient design for cooling PV back surface which results in higher performance as well as maximum reduction in PV

operating temperature, with thermal and electrical efficiency of 64% and 11% respectively.

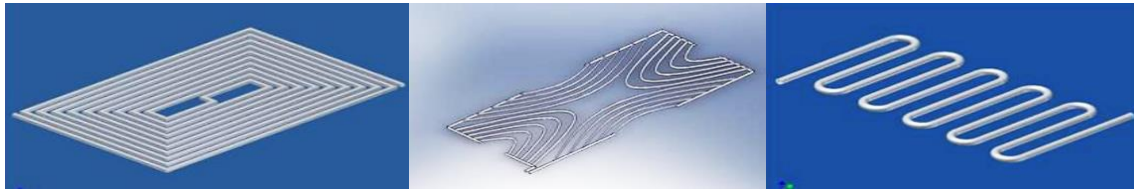


Fig. 2-14 Absorber designs used for cooling PV (Ibrahim et al., 2010)

Buonomano, Calise and Vicidomini (2016) investigated the performance differences between PV and PVT systems in an identical solar system. The authors used four polycrystalline silicon PV panels and four unglazed polycrystalline silicon PVT collectors with a total area of 13 m² and 2 kW of electrical power. The liquid used for cooling was water with the addition of glycol to avoid corrosion. TRNSYS software was utilized for simulating the system theoretically. The results indicated that the PVT system temperature is 10 °C lower than the PV panels. The electrical performance for both systems was around 15%, with PV producing greater electrical energy than PVT. However, PVT was beneficial due to the thermal energy it produced.

Researchers (Peng, Z., Herfatmanesh, M.R. and Liu, 2017) aimed to determine the effects of cooling the panel's surface temperature on its performance. To do this, they exposed the panel to various levels of radiation in a laboratory setting and spread ice to cool the panel. Results indicated that with an increase in radiation, the panel's temperature also increased. Additionally, panel efficiency for power production decreased. Cooling the panel using ice demonstrated an efficiency 47% greater than the un-cooled panel. Researchers concluded that using a cooling system on panels for residential houses could minimize cost pay-back time from 15 years to 12.1 years.

The investigators (Abdullah, 2019) conducted thermodynamic modelling to compare the thermal and electrical efficiency of the (PV) panel

within double oscillating absorbers , and one without cooling. MATLAB Simulink was used to generate theoretical data, and solar radiation levels were set to range from 300 W/m² to 1000 W/m², while mass flow rate ranged from 0.01 to 0.049 kg/s. The results suggested that cell efficiency decreased along with increased cell temperature and solar radiation. Moreover, the temperature of the panel increased with increasing levels of solar radiation. When setting the mass flow rate at higher levels, however, the temperature of the cell will decrease at any radiation level.

Muslim, Ghadhban and Hilal (2020) experimentally investigated, a cooling chamber with three separate sheet flow orientations of 60°, 30°, and 0° were mounted to the rear face of the photovoltaic module through two different flow pathways, up flow and downflow, as indicated in Fig. 2-15. Module 0 was unaltered, while Modules 1, 2, and 3 were given an upward flow and 4, 5, and 6 received a downflow. The panel was installed with a southward facing 33° tilt angle, and four varying flow rates (1, 2, 3 and 4) in liters per minute were tested. The findings showed that Module 1 achieved the highest efficiency at 80% with a flow rate of 4 liters per minute in regards to electrical efficiency, along with the 60° panel orientation.

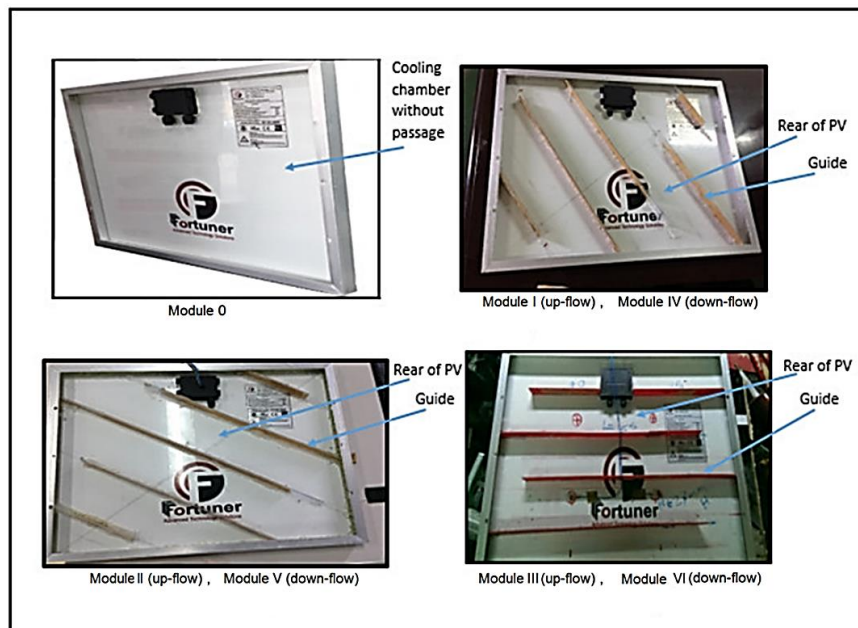


Fig. 2-15 Experimental module (Muslim, Ghadhban and Hilal, 2020)

In a recent study conducted by (Bevilacqua *et al.*, 2021) many approaches were examined with the aim of reducing the temperature of the rear surface of the modules, as seen in Fig. 2-16. They suggested that the most effective and most cost-efficient way to cool these panels was spray cooling, as water can be used to overcome the heat. The study further showed that the spray cooling method was preferable during hot periods compared to the forced convection system, as the latter was unable to cope with the higher temperatures. The electrical efficiency for reference one was 14.9% while for the cooled panel with back surface spray water was 16%.

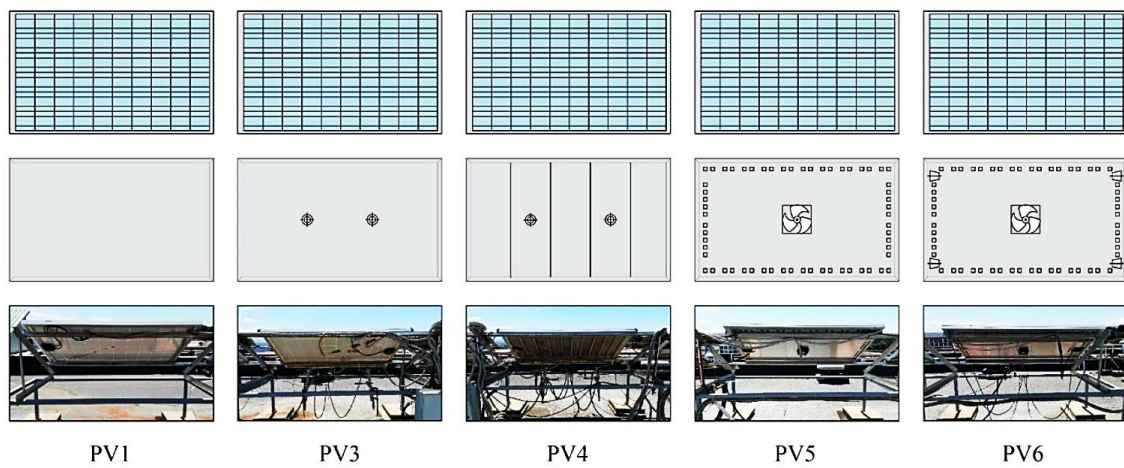


Fig. 2-16 Experimental rig of different cooling system implemented to the back surface of the panel (Bevilacqua *et al.*, 2021)

Gomaa, Ahmed and Rezk (2022) studied the effect of back side cooling panel by implementing two different chamber thicknesses 3 mm and 15 mm, with crossed channel fins. At various solar radiation and water flow rates, by using ANSYS 19.2 software. The result indicated that at both thicknesses when solar radiation was 1000 W/m^2 , the PV module temperature was 30.7 and 30.8 $^{\circ}\text{C}$ for 3 mm and 15 mm box thickness, respectively. Also, they found that the optimum flow rate at 1000 W/m^2 solar irradiance was 3 l/min.

Rosli *et al.* (2022) used ANSYS software to validate an experimental result of back cooling by using a spiral absorber to study the effect of water volume flow, water inlet temperature and solar irradiance level over the

temperature stability. They conclude that at flow rate of 40 kg/h and a solar irradiance range of 800 to 1000 W/m², is the most suitable operating condition to maintain temperature stability and high performance.

2.5.1.c Front and Back Surface Cooling

Nižetić *et al.* (2016) examined a photovoltaic panel with different arrangements of a spray-cooling system. Relying on whether the PV was cooled from the front, the back, or both sides simultaneously, the peak electrical performance of the module was 14%, with a module temperature of 54 °C. When the front-side was employed on its own, the efficiency improved by 15.65%. For rear cooling, the enhancement was 15.4%, while the all-around cooling produced a rise in efficiency by 15.9%.

An experimental analysis was conducted by Mohammed, Mohammed and Sanad (2019) to assess the effectiveness of a photovoltaic panel combined with a double-side water acrylic glass cooling mechanism, as presented in Fig. 2-17. Results demonstrated an average reduction in temperature of 45.56%, 40.12%, and 50.06% for the top, back, and double-side techniques employed, respectively. Moreover, implementing the cooling process in both sized reinforced the PV's electrical production and efficiency percentages, by 12.69% and 14.20%, respectively.

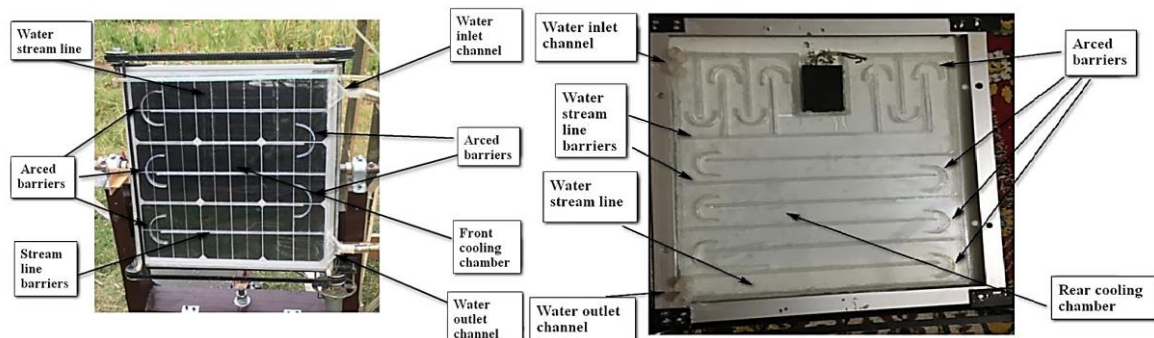


Fig. 2-17 Front and back cooling chamber (Mohammed, Mohammed and Sanad, 2019)

Sainthiya and Beniwal (2019) tried to cool down the PV panel by implementing water cooling techniques from both front and back surfaces of

the PV at four different volume flows (1, 1.5, 2, 2.5) L/min, and comparing the performance with the uncooled panel. The experimental setup front view is presented in Fig. 2-18. There outcome revealed that two sides cooling is more efficient than one side cooling, and the most effective volume flow was 1.5 l/min. Lastly, it was found that the average front surface temperature decrease of the panel during winter and summer seasons was 29.63% and 29.57% respectively.



Fig. 2-18 Experimental setup back and front PV cooling system (Sainthiya and Beniwal, 2019)

Khalil, Abdelgaied and Hamdy (2019) studied the effect of spray water cooling from the front and back surfaces of the PV panels by using nozzles 6 from front surface and 6 on the back surface, as presented in Fig. 2-19. The result showed that the two-side spray cooling system increased the power output by 17.4%, and reduced the panel temperature from 55 °C to 24 °C.



Fig. 2-19 front and rear spray water cooling system(Khalil, Abdelgaied and Hamdy, 2019)

2.5.2 Air Cooling Strategy

2.5.2.a Forced Air Cooling

Tripanagnostopoulos, Y. Nousia, T. and Souliotis M. (2001) tested experimentally, different methods of enhancing the photovoltaic performance by cooling it with forced air convection. They employed three photovoltaic cells in the experiment-reference, which was modified with an air channel at the back surface and the third model, which was the same as the second, but additionally modified with a thin sheet of metal at the center of the channel (as indicated on Fig. 2-20). Results showed that with maximizing air flow rate the panel efficiency was maximized as well and the temperature was reduced more, with the greatest temperature drops of 7.8% and 9.5% observed in the cells that had just air channels and the ones with air channel in addition to thin sheets, respectively.

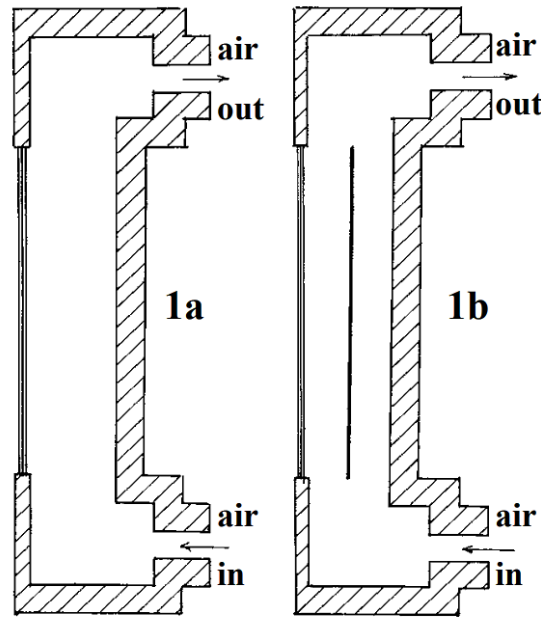


Fig. 2-20 Cross section of the system (Tripanagnostopoulos, Y. Nousia, 2001)

A system was designed and illustrated in Fig. 2-21, for cooling a photovoltaic panel with air circulation by Kumar and Rosen (2011), the influence of varying the volume flow rate of the air and solar irradiation on the system's thermal and electrical efficiency were studied. Additionally, the impact of introducing fins on the system's performance was also assessed. It was found that adding fins to the panel improved both its electrical and thermal efficiency by 10.5% and 15%, respectively. An increment in the air volume flow rate from 0.03 kg/s to 0.15 kg/s led to a substantial growth in the electrical efficiency. Also, they come out with the conclusion that an increase in solar irradiance reduced the performance of the cell, largely due to its temperature increase.

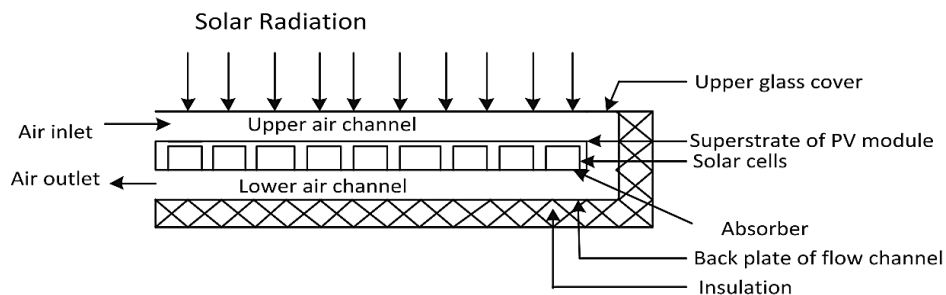


Fig. 2-21 Double air pass cooling PV (Kumar and Rosen, 2011)

Mazón-Hernández *et al.* (2013) carried out an experiment to compare the effects of natural and forced air cooling on photovoltaic performance. By utilizing two photovoltaic panels; one as the reference, while the other had a steel plate underneath it to create a channel as shown in Fig. 2-22. In the first study, natural air circulation was used to cool the photovoltaic through natural convection. The second study then utilized a centrifugal fan to drive air into the channel in order to cool the photovoltaic through forced convection (illustrated in Fig. 4). The results showed that fusing a fan leads to a decrease in panel temperature by 15 °C and an increase of 15% in electrical efficiency as compared to the natural air circulation.



Fig. 2-22 Experimental rig (a) Natural air cooling. (b) Forced air cooling (Mazón-Hernández *et al.*, 2013)

A study published by Sajjad *et al.* (2019) demonstrated the use of forcing air cooling by using the air of an air-conditioner as a method for increasing the efficiency of panel that will pass through a duct that PV is installed on. As presented in Fig. 2-23. In comparison with those without cooling, the study found that PV modules subjected to forced air cooling experienced increases of 7.2% in electric efficiency and 6% in power ratio.

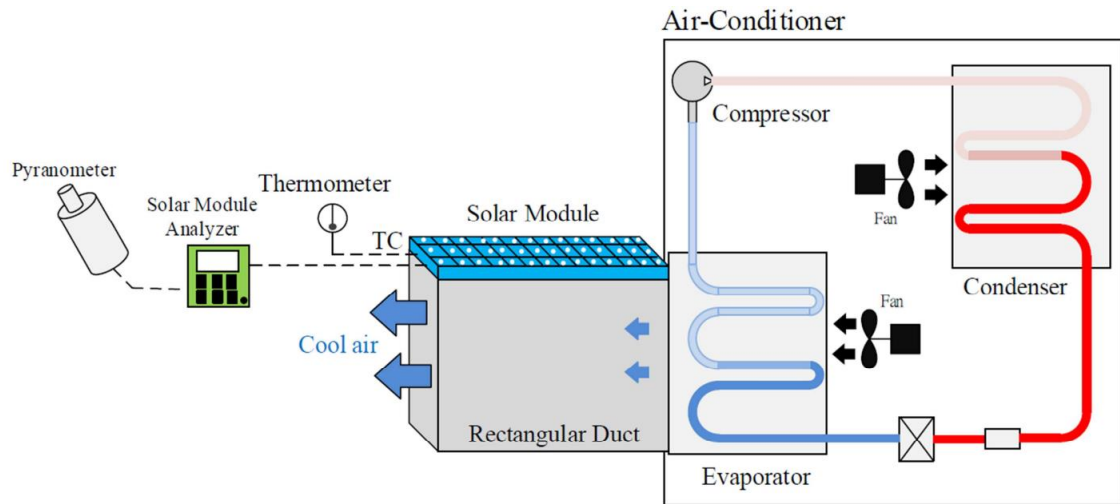


Fig. 2-23 Schematic diagram of experimental system (Sajjad *et al.*, 2019)

2.5.2.b Natural Air Cooling

Tripanagnostopoulos and Themelis (2010) conducted a three-part study to explore the cooling of PV solar cells through natural air, as presented Fig. 2-24. The first method involved placing an air duct behind the module, the second involved the same idea but with the insertion of a thin sheet of metal positioned at the air duct to increase efficiency, and the third had the same features but included metal fins at the back, further exposing the cell to a greater amount of air. Investigating the results obtained through experimentation, it was found that the module with fins was most effective, followed by the second one, and then the module with air duct only.

El Mays *et al.* (2017) conducted an experiment in which a photovoltaic panel was outfitted with a heat sink in the form of aluminum plate with parallel-fin to cool down the panel with natural convection. The merged design caused a drop in the surface temperature of approximately $6.1\text{ }^{\circ}\text{C}$, which in turn ultimate yielded performance upgrades of 1.75% in the panel's efficiency and 1.8 W in output power, as compared to the panel configuration with no finned plate.

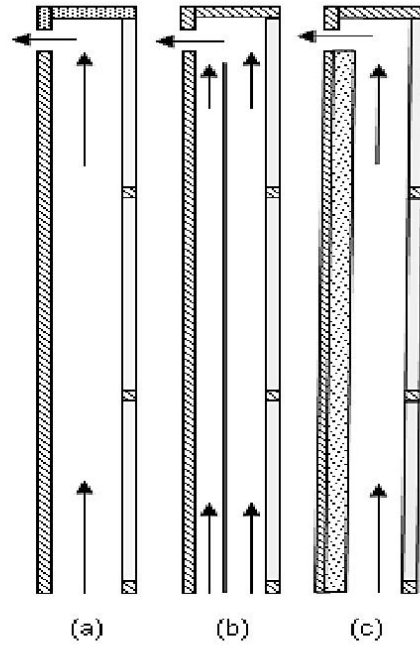


Fig. 2-24 Experimental rig of air natural cooling (Tripanagnostopoulos and Themelis, 2010)

Grubišić-Čabo *et al.* (2018) conducted an experiment to investigate a new method to cool down the PV solar cell by using fins. The first module was created with the fins affixed in a longitudinal and uniform manner on the back of the module. The second module integrated fins attached haphazardly and arbitrarily to the rear side of the panel. Outcomes revealed that the second module had more success than the first, raising the cell's efficiency by 2%.

Bayrak, Oztop and Selimefendigil (2019) put a practical experiment into action to chill the PV with natural air, utilizing fins and deploying ten distinct geometries for the fins. The largest temperature deviation that they achieved was 3.39 °C when exposed to radiation of 772 W/m². This led to a rise of 6.84 W in the generated energy. Consequently, the electrical efficiency value turned out to be 11.55%.

An investigation of two types of aluminum heat sinks, one with straight fins and another with inclined segments, as indicated in Fig. 2-25, was conducted by Hernandez-Perez *et al.* (2020). Through a combination of

computational fluid dynamics (CFD) analysis and experimentation, they observed superior performance of the segmented heat sink, which resulted in lower pressure losses as well as enhanced convective heat transfer due to greater turbulence. The maximum temperature decrease they achieved was 9.4 °C and 10 °C through numerical simulation and experimental testing, respectively, with a 4% conversion efficiency enhancement at peak solar intensity of 800 W/m² to 1000 W/m². This, therefore, provided an additional 6 W/m² capacity.

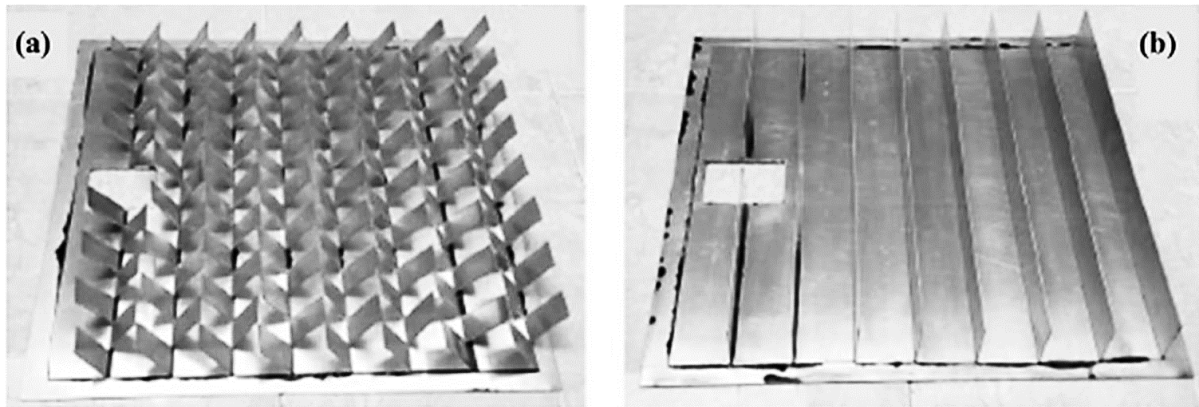


Fig. 2-25 Heat sink a- inclined segment b- straight fins (Hernandez-Perez et al., 2020)

2.5.3 PCM Cooling Strategy

Phase change materials (PCMs) can be applied to manage the heat produced by PV solar cells during the day. The process begins with PCMs absorbing sensible heat until they reach their melting point. Then, transferring from a solid to a liquid state (latent heat). This decreases the temperature of the cells, boosting the power produced of the cells. Previous studies about PCMs used for cooling PV cells are presented in Table 2-2.

Table 2-2 PV cooling by utilizing PCM

Author	PCM Employed	Test methodology	Electrical efficiency enhancement (%)	Outcome
(A. Hasan <i>et al.</i> , 2017)	Paraffin RT-42	Experiment, Attached to the back side of the PV	5.9	The thermal performance of the PCM varies throughout the different months of the year, with the PCM achieving the greatest temperature decline of 13 °C in April, and a lesser decrease of 8 °C in June.
(Waqas, Jie and Xu, 2017)	Paraffin RT-24	Experiment, copper pipe for PCM encapsulation is to create a fin effect at the back of the PV panel	3	The PV temperature reduction was from 62 °C for unaltered panel to 56 °C for PCM cooled one, the results also indicated that everyone kg of PCM was able to minimize PV temperature by 1.8 °C for each unit area of the PV.
(Savvakis, Dialyna and Tsoutsos, 2020)	Paraffins RT-27 & RT-31	Experiment, Pipe shape enclosure	4.19 & 4.24	The highest temperature point of the reference PV was 61 °C, and the performance of RT 27 and RT-31 as a comparison was indicated by a reduction of 6.4 °C and 7.5 °C respectively.

(Wongwuttanasatian, Sarikarin and Suksri, 2020)	Palm Wax	Experiment, Container with finned PCM attached at down face of the panel	5.3	showed an excellent cooling performance and caused the solar cell to drop in temperature by 6.1 °C,
(Ahmad <i>et al.</i>, 2021)	Paraffin RT-42, RT-31 and RT-25	Numerical analysis, Trapezoidal shape container place at the lower surface of the panel	10, 13 and 17	In comparison to the PCM container in a rectangular shape, the trapezoid design demonstrated notably enhanced cooling efficiency with almost no alteration in PV temperature, even if the melting point of the PCM is lower than the mean ambient temperature.
(Yousef, Sharaf and Huzayyin, 2022)	Paraffin RT-42	Experiment, Attached to the back side of the PV	9 in summer 3.7 in winter	The temperature reduction during cold months was 6.5%, while for the hot one was 7.3%.
(Metwally, 2022)	Paraffin RT-25	Numerical analysis, Container of different geometry attached to the rear surface of PV.	Up to 3	Phase change material encapsules has demonstrably increased the thermal system management, photovoltaic efficiency, and overall output power.

2.5.4 Nano Fluid Cooling Strategy

The capability of nanofluids to absorb and dissipate heat is known to substantially boost the electrical output of photovoltaic (PV) applications. These materials have a higher thermal conductivity than their simpler counterparts, allowing for greater heat abstraction. This means that by using them on a PV surface, the temperature can be reduced to optimize its performance. Researchers have also found that nanofluids possess the unique ability to be an effective coolant for the PV device and are capable of consuming and eliminating an excessive amount of heat.

Xu and Kleinstreuer (2014) explored the impact of Al_2O_3 -water nanofluid on concentration photovoltaic cells through numerical means. Variations in channel heights, nanoparticle volume fractions, and inlet fluid temperature were taken into account in the calculations. It was observed that increasing the concentration of nanoparticles and decreasing the inlet temperature of nanofluid increased the electrical efficiency of the photovoltaic cell.

Radwan, Ahmed and Ookawara (2016) devised a cooling method for photovoltaic systems which employs a microchannel heat sink in combination with different volume fractions of aluminum-oxide-to-water and silicon carbide-to-water nanofluids. It has been found that, during high levels of solar radiation, the above nanofluids are effective in lowering the temperature of solar cells to 38 °C, which yields an enhancement of 19% in electrical performance.

The effect of incorporating 3 wt% of SiC nanoparticles into water as a coolant was explored in a photovoltaic thermal system by Al-Waeli *et al.* (2017), and the thermophysical properties of the nanofluid were analyzed. The presence of the nanoparticles resulted in an 8.2% boost in thermal conductivity could be seen in the examined temperature range from 25 to 60 °C, with an

enhancement in electrical efficiency of 24.1% when compared to an uncooled panel.

Another study to increase the performance of photovoltaic panels using water and nanofluid was experimented at different flow rates by (Hussein, Numan and Abdulmunem, 2017). It has been observed that as the surface temperature of the panel rises, its efficiency decreases, yielding a maximum rate of 8% without cooling. In contrast, when the panel is cooled using water at an optimum rate of 0.2 l/s, the efficiency reaches 9.6%. Furthermore, when using nanofluid with an optimal concentration ratio of 0.3 and a volume flow rate of 0.2 l/s, the efficiency can reach a value of 12.1%.

H. A. Hasan *et al.* (2017) examined the effectiveness of three different nanoparticles, SiO₂, TiO₂, and SiC, when used in conjunction with a water-based fluid. Laboratory tests were done at various mass flow rates ranging from 0 to 0.1666 kg/s and different levels of solar irradiance. The findings indicated that the nanofluid incorporating SiC nanoparticles was the most effective, whereas the lowest efficiency was observed in the nanofluid with SiO₂ nanoparticles.

A study was conducted by Qi *et al.* (2019) to assess the performance of nanofluid mass fraction on both corrugated and smooth double-pipe heat exchangers which was placed at the back side of PV panel. The results indicated that corrugated double-tube heat exchangers performed better in terms of thermal performance than smooth double-tube heat exchangers of the same size. Further, the heat transfer rate was more durable with the addition of TiO₂-H₂O nanofluids with 0.1%, 0.3% and 0.5% wt, ultimately achieving an increase of 10.8%, 13.4% and 14.8%, respectively.

The performance of the PV was assessed by employing aluminum oxide nanoparticles with water (Ibrahim *et al.*, 2023). Results indicated a 15.5% boost in PVT efficiency. With a 0.05% volume concentration of Al₂O₃ and a flow rate of 0.07 kg/s, a temperature increases of 22.83% was obtained from the

uncooled panel. For the reference PVT system, the highest temperature and electrical performance at noontime were 75.5 °C and 12.15%, respectively. 10 °C and 20 °C temperatures fell were recorded at high temperature intervals by utilizing water or nanofluid, respectively.

Jose *et al.* (2023) conducted a survey to analyze the effect of nanofluid within serpentine copper tube H.E. over 100 W PV/T. Distilled water, as well as Al₂O₃ 0.1% and Al₂O₃ 0.2% nanofluids were tested in the respective hot seasons in India in 2018 at different mass flows. Later, CFD was applied to a study to identify outside and exit temperatures, as well as cooling effectiveness. They determined that the thermal efficiency of a water-based cooling system proved to be 53.61%, with Al₂O₃ 0.1% and Al₂O₃ 0.2% based coolants providing 69.45% and 71.02%, respectively.

2.6 SUMMARY

The exploration of photovoltaic and photovoltaic thermal systems has become an extensively studied topic, especially with the large-scale implementation of PV structures for energy production worldwide. Therefore, an investigation of possible methods that can enhance the area of photovoltaic and PV thermal analysis has been conducted during the last few years.

In this literature, extensive studies have been described through a thorough analysis of different aspects that are essential to optimizing the performance of a photovoltaic system. In this chapter, the three key elements that have influenced the photovoltaic system's power productivity are explained. Those elements are the orientation, the environmental conditions, and the cooling technique implemented on the cells. Furthermore, extensive researches were done to discuss solar tracking systems, and their positive effect on energy output. Following this, it has examined the influence of radiation intensity, dust, and ambient temperature on panel efficiency. Subsequently, multiple cooling techniques such as water, air, PCM and nanofluids were discussed in

detail, with the respective research studies exemplifying their implementation and benefits in improving photovoltaic cell performance.

The contributions from the previous studies reviles that:

- Water cooling is a promising option, and its benefits have been demonstrated in the literature by multiple studies.
- Front surface water cooling is able to reduce the reflection of sunlight and reduce the panel temperature, leading to increased efficiency.
- System designs using water spray have been tested in hot climates such as Iraq and Egypt, resulting in a decrease in panel temperature of up to 34.32% and a corresponding increase in efficiency as well as dust filtering capabilities.
- Single axis solar tracking system has a huge effect on increasing PV power production.

While the gaps of the research are:

- controlling the water volume flow rate due to the operating temperature of the photovoltaic panel.
- Implementation of cooling system with solar tracking to the PV panel simultaneously.

In this study, spray water cooling of photovoltaic panels was placed on top, left and right side of the panel, which will control the water volume flow rate due to various panel set point temperatures, is developed in addition to a single east-west tracking system. Also, cooling PV panels with various volume flow rates at different environmental conditions, with different ambient temperatures, solar intensity and water inlet temperatures, effect on PV performance, has been extensively studied using computational fluid dynamics (CFD).

CHAPTER THREE

(THEORETICAL ANALYSIS)

3.1 INTRODUCTION

The methodology of this research is discussed in detail throughout this chapter. In accordance with chapter two. And due to the literature being discussed the most efficient way for PV cooling with the cheapest method way that will lead to clean PV surface from dust, and minimize solar radiation reflection, is by implementing the front surface cooling technique, which is the most efficient mechanism for a hot region like Iraq. The current research aims to design, construct, and develop a front surface cooling system for photovoltaic panel. This study enhances PV power production by implementing front surface cooling by adding water from the top, left, and right sides of the PV panel at different flow rates, and comparing the temperature distribution, power and electrical efficiency of the cooled panel with the one without cooling, at different operating conditions (ambient temperature, solar radiation and water inlet temperature). Also optimizing which factors will mostly affect the performance of the cooled PV. So, suggesting in which region could this system could work more efficiently.

3.2 CFD ANALYSIS FOR PV FRONT SURFACE COOLING

ANSYS is an engineering simulation software that enables engineers to accurately simulate and predict the behavior of products and systems, which was developed by John Swanson in 1970. With the help of ANSYS, engineers can build virtual prototypes and optimize designs for performance, reliability, and cost-effectiveness. ANSYS has a vast array of tools and capabilities that enable engineers to find accurate and reliable solutions to difficult design and engineering challenges. The software provides a comprehensive suite of

analysis, design and optimization tools that can be used in multiple engineering domains including structural, thermal, fluid, and electromagnetic domains, among others. ANSYS Fluent is a powerful computational fluid dynamic (CFD) software package used by engineers and scientists to simulate fluid flow, heat transfer, and other related phenomena (T. D. Canonsburg, 2013).

In this descriptive research, a 3D CFD model of a photovoltaic (PV) system featuring a cooling system was assessed, numerical simulations on a commercial CFD package (ANSYS-FLUENT R19.2) introduced how the cooling module impacts the solar cell. The model is validated due to experimental results, and presented in Chapter five. Simulations have been done using a personal computer with an Intel(R) Core (TM) i7-10750H with a Radeon Graphics processor having a frequency of 2.6 GHz and 16 GB of RAM.

3.3 CFD PROCEDURES

The application of CFD to tackle flow and heat transition issues has seen a drastic escalation in recent years (Doulati *et al.*, 2011). This technique has many rewards, which include a first-rate opportunity to analyze the variables in the underlying equations more intricately and reveal flow patterns that are difficult and expensive to study through experimentation (Jiyuan, T., Guan-Heng, Y. and Chaoqun, 2018). In addition, CFD provides practical, accessible options for modelling fluid flow through the supply of precise data and illustration in a way that outperforms both analytical and experimental results. A numerical analysis is done in the three steps displayed in Fig. 3-1 for any CFD simulation.

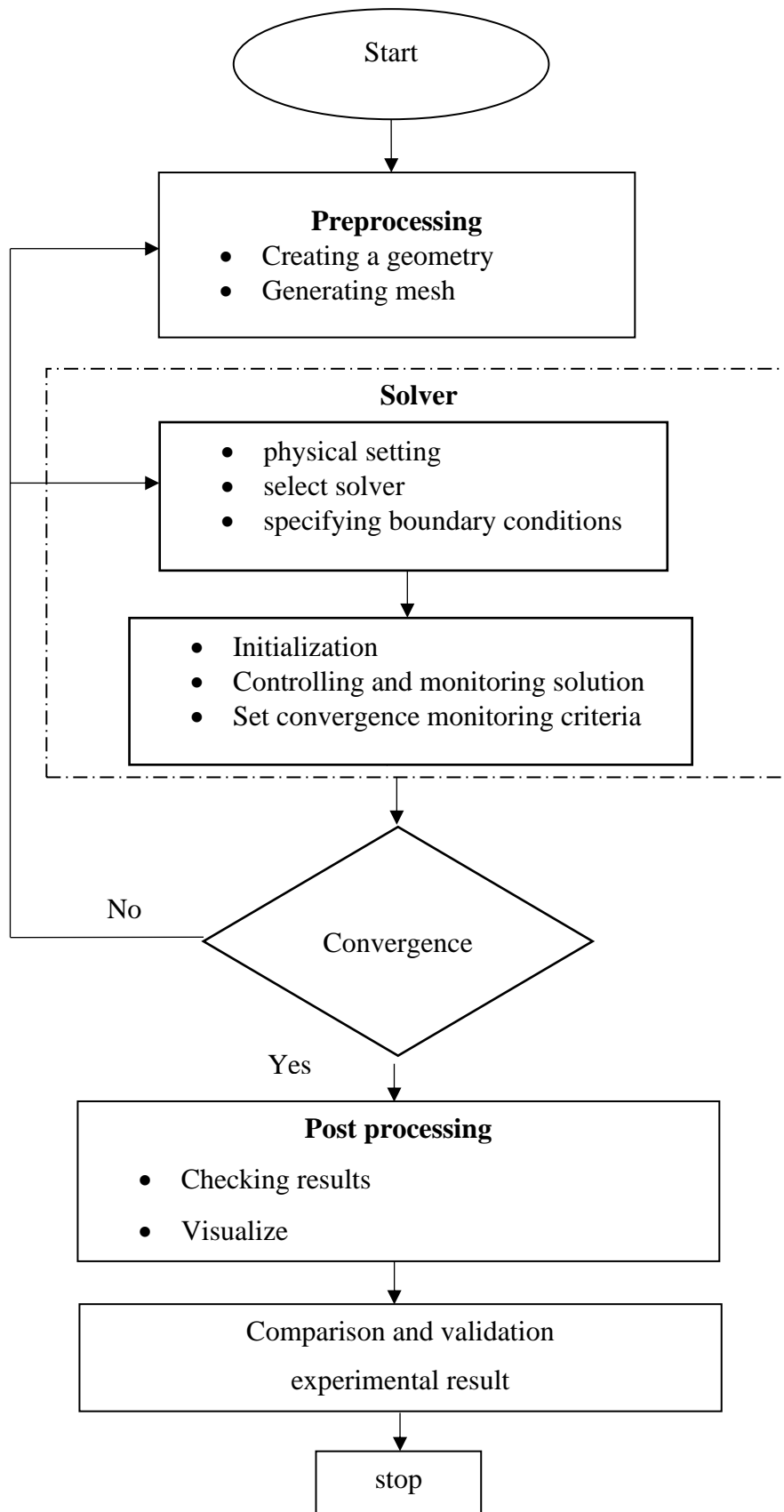


Fig. 3-1 CFD flow chart procedure (Muiruri and Motsamai, 2018)

3.3.1 Geometry

The three-dimensional model geometry of the photovoltaic module with front surface water cooling was modeled using ANSYS R19.2 geometry tool, where the PV panel consists of five solid layers (glass, Ethylene Vinyl Acetate (EVA-1), silicon, ethylene vinyl acetate (EVA-2), tedlar), and a fluid layer (water domain), the thickness of each layer is presented in Table 3-1.

Table 3-1 Photovoltaic panel layers thickness

PV Layer	Layer Thickness (mm)
Water	4.5
Glass	3
EVA-1	3
Silicon	4
EVA-2	3
Tedlar	0.1

The modelled geometry of a PV module with front surface water cooling is presented in Fig. 3-2. The dimensions of the PV panel were exactly the same as in the experimental model. A thin layer of water is adhered to the topography of the photovoltaic module, serving as a cooling system across the entirety of the module.

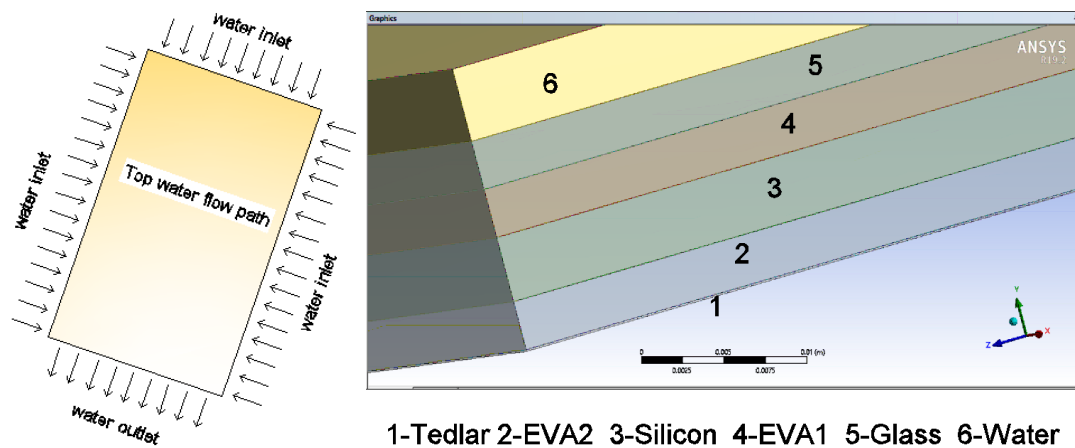


Fig. 3-2 Geometry of the panel's layers with water cooling system

A connection between the fluid and solid domains is formed through the conjugation of the two domains. This brings in the two-way exchange between the two domains with thermal energy exchange across the interface. The water flow of the photovoltaic considered as the water-cooling system model (fluid domain), while the individual layers of the PV module are designed and represented as the solid domain.

3.3.2 Meshing

Meshing is a key component of the simulation process used in ANSYS. This process produces an interconnected network of elements (usually triangles or quadrilaterals) in two or three dimensions to represent structural geometry. The mesh is used by finite element analysis (FEA) software for an accurate and efficient analysis of the problem. Mesh generation can be one of the most time-consuming steps depending on the complexity of the geometry. ANSYS, a leader in the engineering simulation software industry, provides some of the most cutting-edge automated tools available for mesh generation, the meshing types available in ANSYS are presented in Fig. 3-3. ANSYS also offers users the ability to create meshes with specified sizes through remeshing and quality control techniques. These tools enable users to create meshes that satisfy the required mesh size and aspect ratio from an existing mesh, or that can improve the meshes generated by the automatic techniques. This allows users to ensure that the analysis is reliable and accurate.

In the current simulation an automatic mesh with an element size 4 mm has been applied to the photovoltaic geometry (solid domains), while for the water layer (fluid domain), an inflation mesh was used to give precise temperature distribution and ensure that the design of the cooling system is optimized to achieve the highest possible performance. The inflation meshing technique allows high-resolution modeling and boundary layer distortion control which enable accurate and efficient geometrical representation of the

cooling system. The generated mesh is shown in Fig. 3-4, which has 1299696 elements and 753609 nodes, with 0.18 skewness.

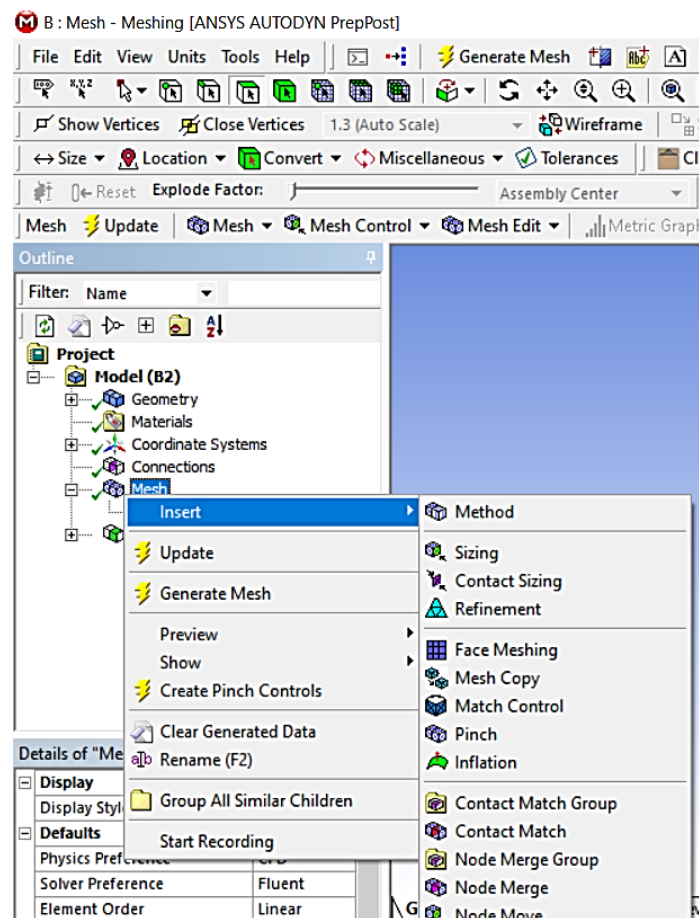


Fig. 3-3 Meshing types in ANSYS

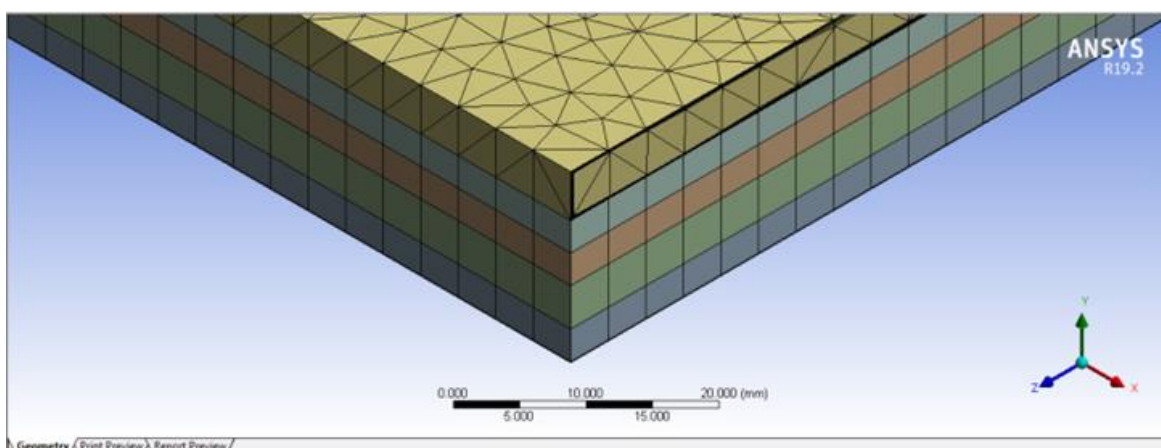


Fig. 3-4 Mesh generated for photovoltaic water-cooling system

For the grid independence test, the number of elements varies from 0.6 to 1.4 in million. It was discovered that when number of elements exceeds 1

million, a further increase in cells has less than 0.07 % variation in cell temperature value which is taken as a criterion for grid independence and the corresponding grid independence test plot is shown in Fig. 3-5.

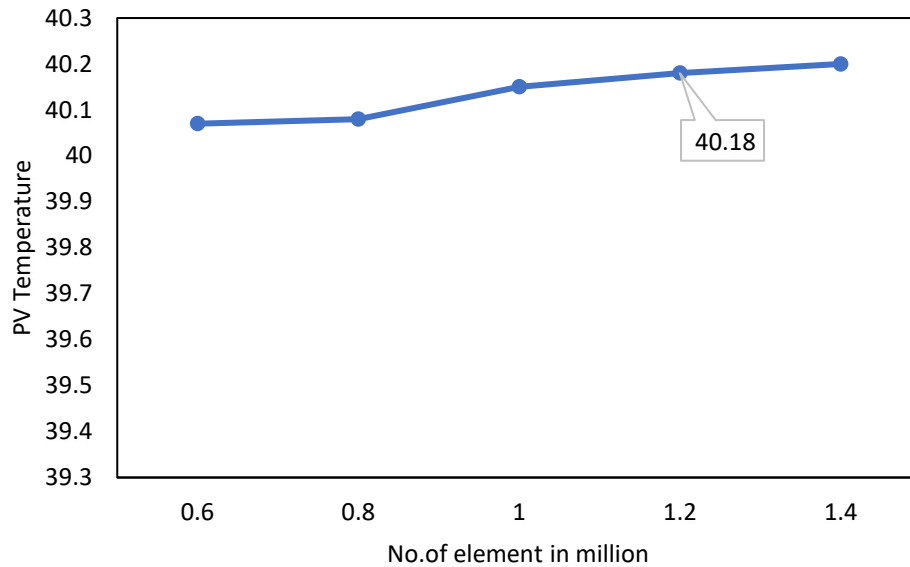


Fig. 3-5 Grid independence test

Using the named selection feature, all the layers body, interfaced surface, the inlet faces and outlet face of water was defined and named, so that it will be included in setup of boundary conditions. Interfaces allow the user to control and connect parts of the simulation, making the process easier and more efficient. They remove ambiguity and provide clarity of expectations, as well as efficient connection between components. The named selections menu of the layers and faces of this simulation is presented in Fig. 3-6, the water inlet was from three faces of the water layer top, left and right, while the outlet water was from down face.

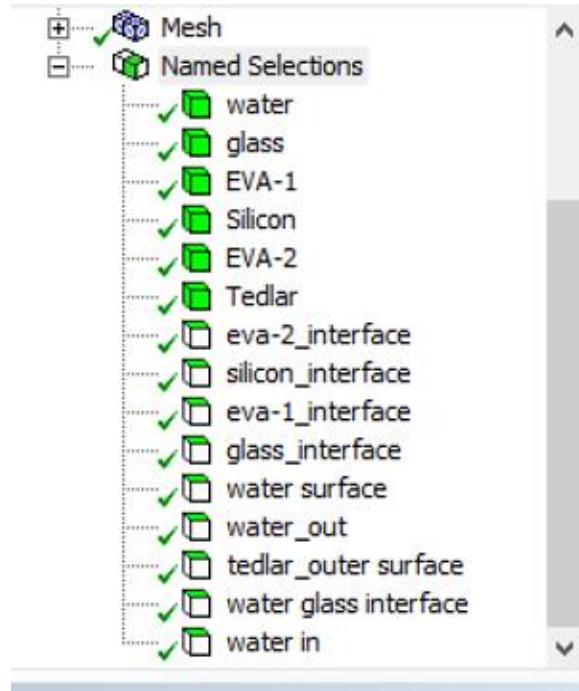


Fig. 3-6 Naming of PV layers and faces

3.3.3 Setup

ANSYS Fluent setup was used for this simulation, with double precision options and parallel processor processing options. The setup section in ANSYS Fluent allows the user to configure various settings for the simulation, such as material properties, boundary conditions, and discretization methods. In this section, the user can also define the flow physics to be solved. Additionally, the user can also configure the numerical solver size, preconditioning schemes, and convergence criteria parameters.

3.3.3.a Energy Model

Throughout the setup section activate the energy model, which involves defining the system of equations for energy balance and the governing equations for energy transfer. Then select the viscous model as laminar flow as presented in Fig. 3-7, due to the calculated Reynolds numbers (147) from the equation (3.1) (Holman, 1986):

$$Re = \frac{V_{in} \rho_f L}{\mu_f} = \frac{V_{in} L}{\nu_f} \quad (3.1)$$

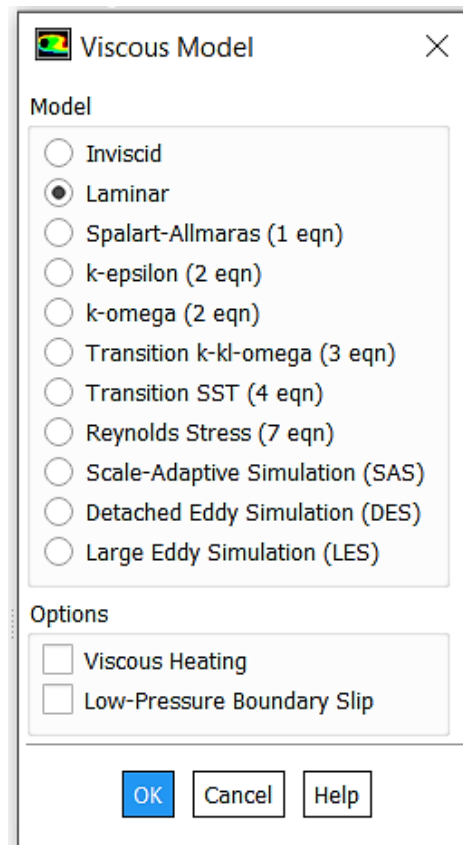
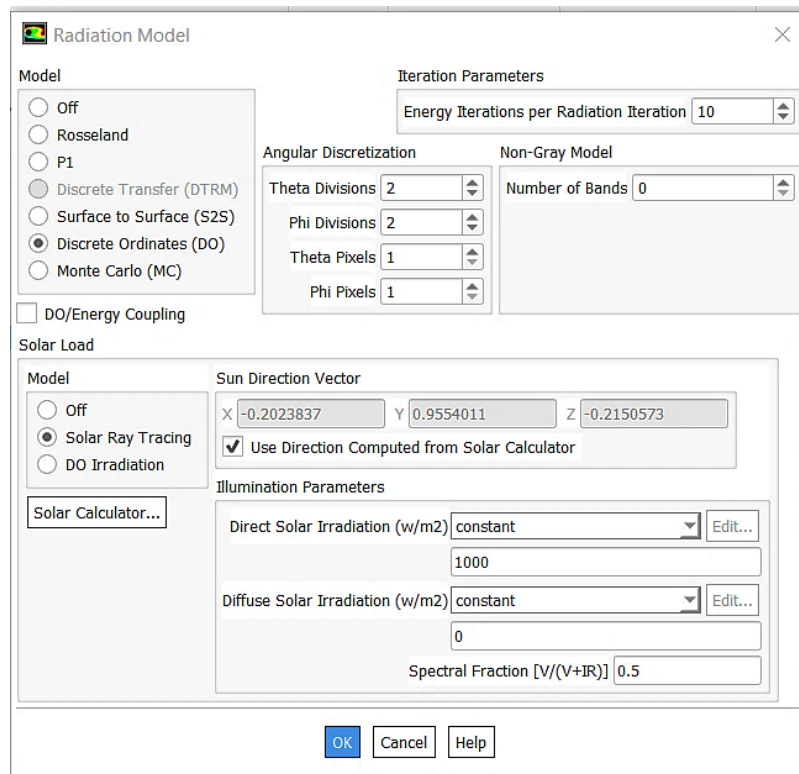


Fig. 3-7 Viscous model

3.3.3.b Radiation Model

The radiation model used for this simulation was Discrete Ordinates (DO) model as indicated in Fig. 3-8. The Discrete Ordinates (DO) is a numerical approach for solving the radiation transport equation. This model is useful for solving radiative transfer problems that involve multiple surfaces or participating media. The DORM represents the radiation exchange between the finite volumes of the domain through finite area and finite-size heat sources (or sinks) couples to the other surfaces. This model is especially useful for PV front surface cooling applications, since these tend to involve multiple finite surfaces, which can be difficult to model accurately using other radiation models. This model is also useful in predicting the thermal response of PV panels under different environmental conditions.



Radiation Model

Model

- ☐ Off
- ☐ Rosseland
- ☐ P1
- ☐ Discrete Transfer (DTRM)
- ☐ Surface to Surface (S2S)
- ☒ Discrete Ordinates (DO)
- ☐ Monte Carlo (MC)

☐ DO/Energy Coupling

Iteration Parameters

Energy Iterations per Radiation Iteration: 10

Angular Discretization

Theta Divisions: 2
Phi Divisions: 2
Theta Pixels: 1
Phi Pixels: 1

Non-Gray Model

Number of Bands: 0

Solar Load

Model

- ☐ Off
- ☒ Solar Ray Tracing
- ☐ DO Irradiation

Sun Direction Vector

X: -0.2023837 Y: 0.9554011 Z: -0.2150573

☒ Use Direction Computed from Solar Calculator

Illumination Parameters

Direct Solar Irradiation (w/m2): constant
1000

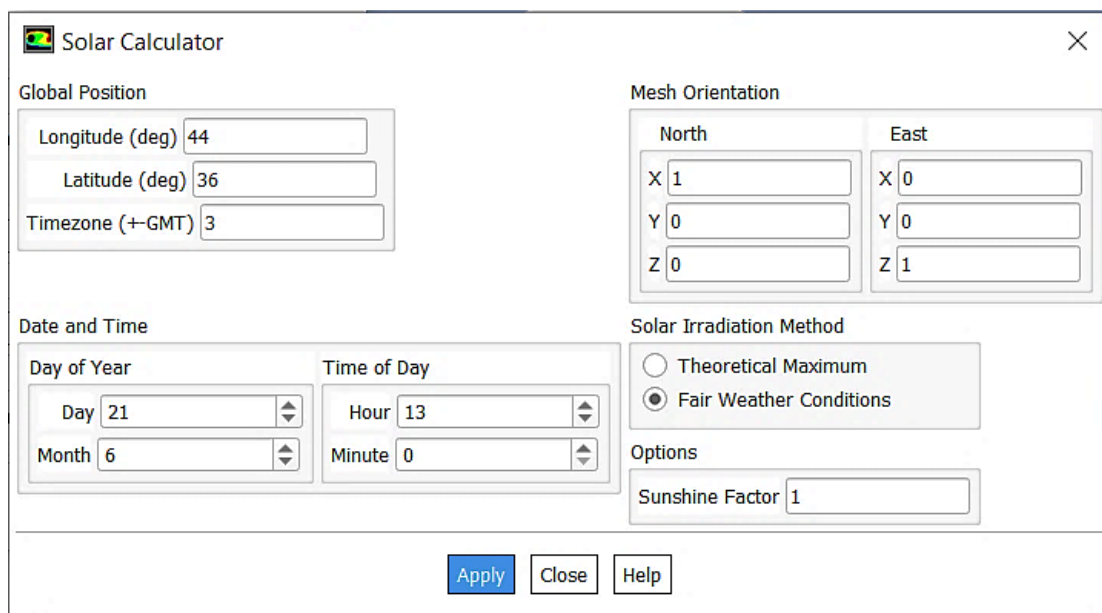
Diffuse Solar Irradiation (w/m2): constant
0

Spectral Fraction [V/(V+IR)]: 0.5

OK Cancel Help

Fig. 3-8 Radiation model

The solar load model used in this study, was the solar ray tracing, with constant solar radiation at different intensities or through the solar calculator mode which adjusted due to the Erbil longitude and latitude for a specific day as presented in Fig. 3-9.



Solar Calculator

Global Position

Longitude (deg): 44
Latitude (deg): 36
Timezone (+GMT): 3

Mesh Orientation

North		East	
X	1	X	0
Y	0	Y	0
Z	0	Z	1

Date and Time

Day of Year: Day: 21, Month: 6
Time of Day: Hour: 13, Minute: 0

Solar Irradiation Method

- ☐ Theoretical Maximum
- ☒ Fair Weather Conditions

Options

Sunshine Factor: 1

Apply Close Help

Fig. 3-9 Solar calculator specifications

3.3.3.c Materials

The Materials section of the ANSYS Fluent setup defines the properties of the fluid and solid materials used in the simulation. This includes specifying the density, specific heat and thermal conductivity which will affect the simulation results, the properties of the different solar layers of the PV and water layer used for cooling PV are shown in Table 3-2 (Syafiqah *et al.*, 2017).

Table 3-2 Materials specifications (Syafiqah *et al.*, 2017)

Materials	Density (kg/m³)	Specific heat capacity (J/kg. °C)	Thermal conductivity (W/m. K)
<i>Water</i>	997	4180	0.59
<i>Glass</i>	3000	500	0.98
<i>EVA-1</i>	960	2090	0.23
<i>Silicon</i>	2329	712	148
<i>EVA-2</i>	960	2090	0.23
<i>Tedlar</i>	1200	1250	0.36

The material section in ANSYS Fluent setup consists of two subsections fluid and solid. Due to the current simulation, the fluid is liquid water as the properties of liquid water entered are presented in Fig. 3-10, while the solid materials are glass, EVA-1, silicon, EVA-2 and tedlar, Fig. 3-11 shows the solid material properties of (EVA-1).

The screenshot shows the 'Create/Edit Materials' dialog box in ANSYS Fluent. The 'Name' field is 'water-liquid', 'Material Type' is 'fluid', 'Chemical Formula' is 'h2o<|>', and 'Mixture' is 'none'. The 'Order Materials by' section has 'Name' selected. The 'Properties' section is expanded, showing the following values: Density (kg/m3) is 998.2, Cp (Specific Heat) (J/kg-k) is 4182, Thermal Conductivity (W/m-k) is 0.59, and Viscosity (kg/m-s) is 0.001003. At the bottom are buttons for 'Change/Create', 'Delete', 'Close', and 'Help'.

Fig. 3-10 Fluid material (water-liquid) properties

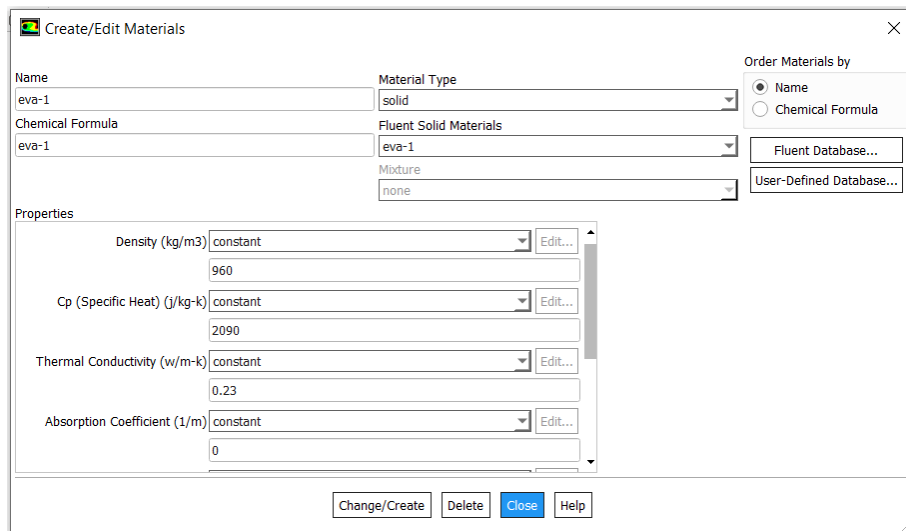


Fig. 3-11 Solid material (EVA-1) properties

3.3.3.d Cell Zone Condition

It is essential to correctly identify the type of material (solid or liquid) and to ensure that the name of the material is consistent with the name of the zone in this section. By right click on the zone name it could simply specify if the zone is fluid or solid. Fig. 3-12 indicates the cell zone condition of glass as a solid domain.

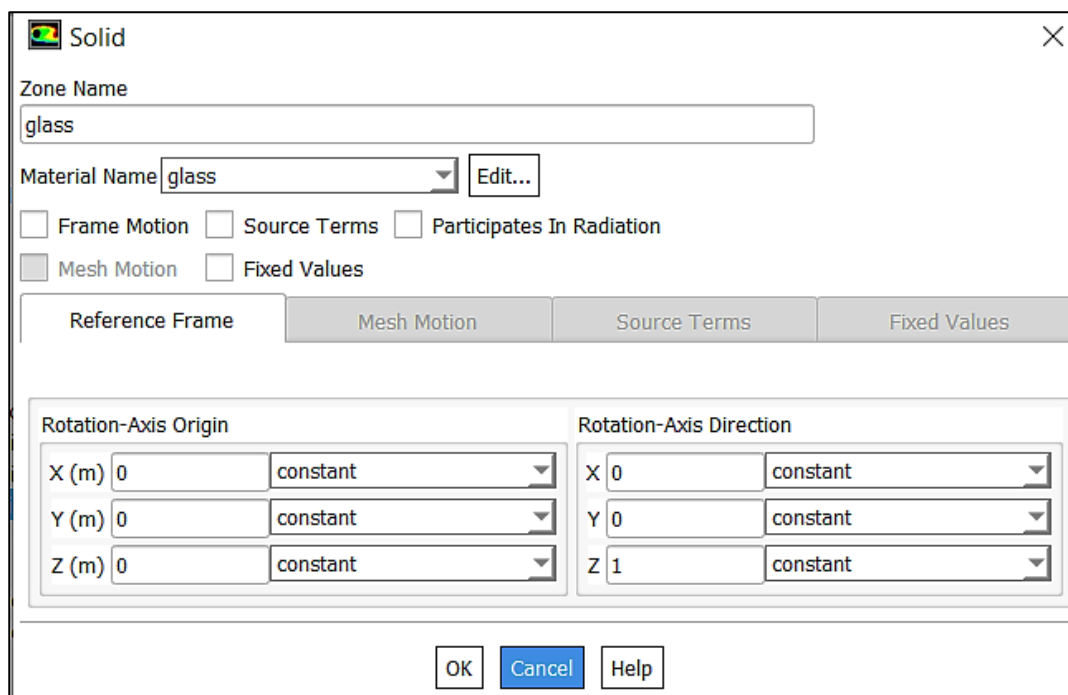


Fig. 3-12 Cell zone condition of glass

3.3.3.e Boundary Conditions

Boundary Conditions in ANSYS Fluent are the settings which define the environment surrounding the case. In a flow simulation, this is typically the inlet and outlet, walls, or other parts of the domain. The most common boundary conditions are mass flow rate, pressure, and temperature. The boundary conditions list of this study is shown in Fig. 3-13. The water inlet in this study was defined by mass flow inlet as presented in Fig. 3-14, while the boundary condition type for water outlet was outlet pressure at atmospheric pressure as indicated in Fig. 3-15.

The interfaces are the connections between two adjacent layers, in which the thermal condition is selected as coupled. By identifying zone name and adjacent zone name, also identifying the material name used, as indicated in Fig. 3-16. Interiors are the bodies of the layers used in the current simulation.

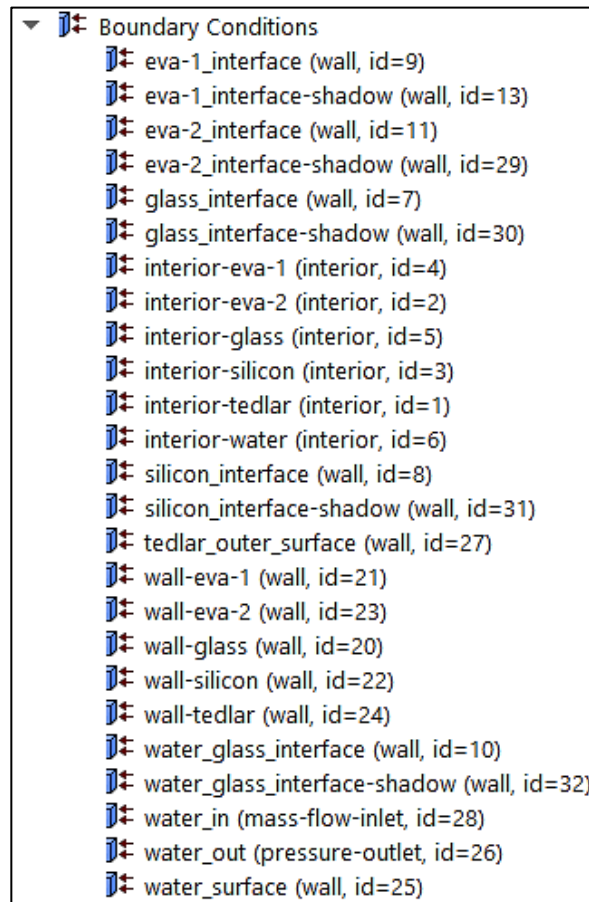
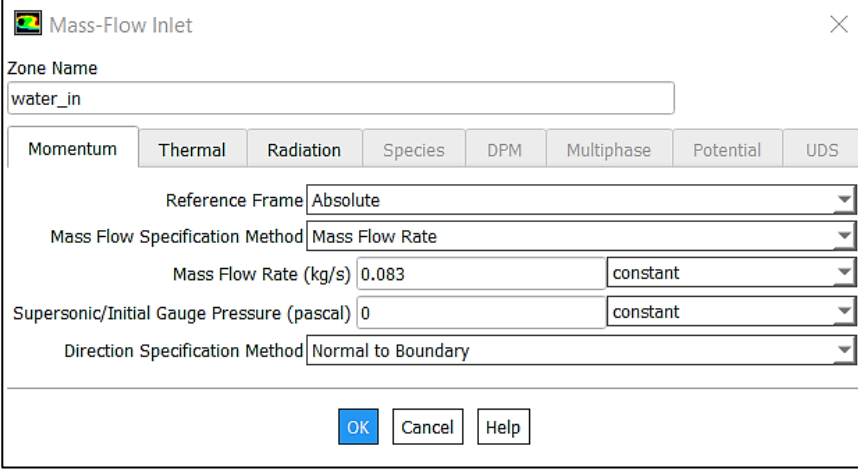


Fig. 3-13 Boundary conditions list of PV front surface cooling



Mass-Flow Inlet

Zone Name: water_in

☐ Momentum
 ☐ Thermal
 ☐ Radiation
 ☐ Species
 ☐ DPM
 ☐ Multiphase
 ☐ Potential
 ☐ UDS

Reference Frame: Absolute

Mass Flow Specification Method: Mass Flow Rate

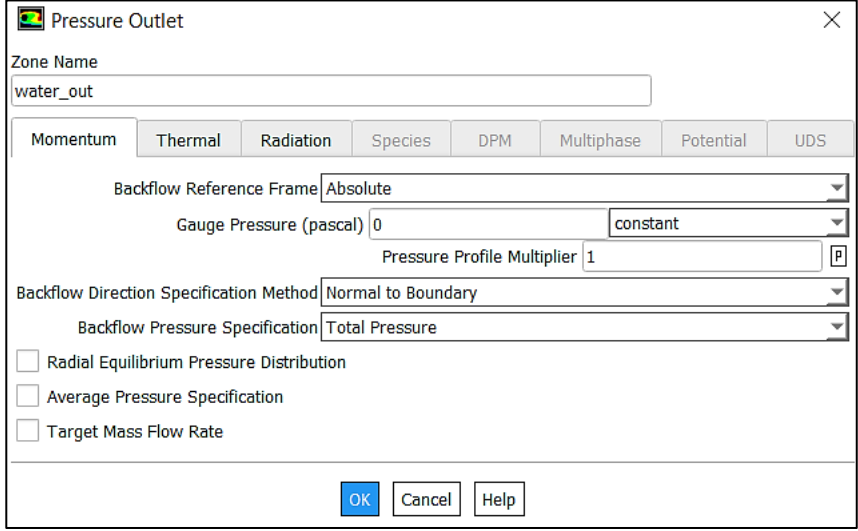
Mass Flow Rate (kg/s): 0.083 constant

Supersonic/Initial Gauge Pressure (pascal): 0 constant

Direction Specification Method: Normal to Boundary

OK Cancel Help

Fig. 3-14 Water mass flow inlet boundary condition



Pressure Outlet

Zone Name: water_out

☐ Momentum
 ☐ Thermal
 ☐ Radiation
 ☐ Species
 ☐ DPM
 ☐ Multiphase
 ☐ Potential
 ☐ UDS

Backflow Reference Frame: Absolute

Gauge Pressure (pascal): 0 constant

Pressure Profile Multiplier: 1 P

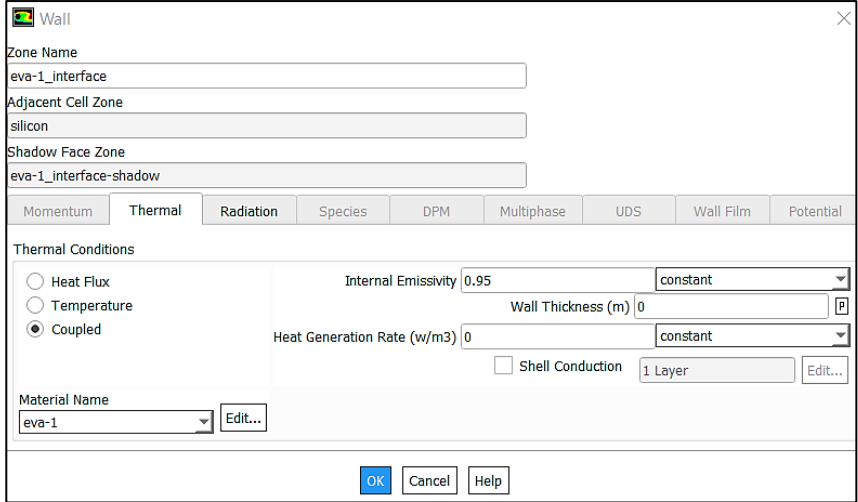
Backflow Direction Specification Method: Normal to Boundary

Backflow Pressure Specification: Total Pressure

☐ Radial Equilibrium Pressure Distribution
☐ Average Pressure Specification
☐ Target Mass Flow Rate

OK Cancel Help

Fig. 3-15 Water pressure outlet boundary condition



Wall

Zone Name: eva-1_interface

Adjacent Cell Zone: silicon

Shadow Face Zone: eva-1_interface-shadow

☐ Momentum
 ☐ Thermal
 ☐ Radiation
 ☐ Species
 ☐ DPM
 ☐ Multiphase
 ☐ UDS
 ☐ Wall Film
 ☐ Potential

Thermal Conditions

☐ Heat Flux
 ☐ Temperature
 ☒ Coupled

Internal Emissivity: 0.95 constant

Wall Thickness (m): 0 P

Heat Generation Rate (w/m3): 0 constant

☐ Shell Conduction
 1 Layer
 Edit...

Material Name: eva-1 Edit...

OK Cancel Help

Fig. 3-16 Interface boundary condition

The walls are used to define the interaction between the wall of a computational domain and the flow field. The glass wall thermal condition selected was mixed as it is a thermal condition that combines the convection and radiation boundary conditions as presented in Fig. 3-17.

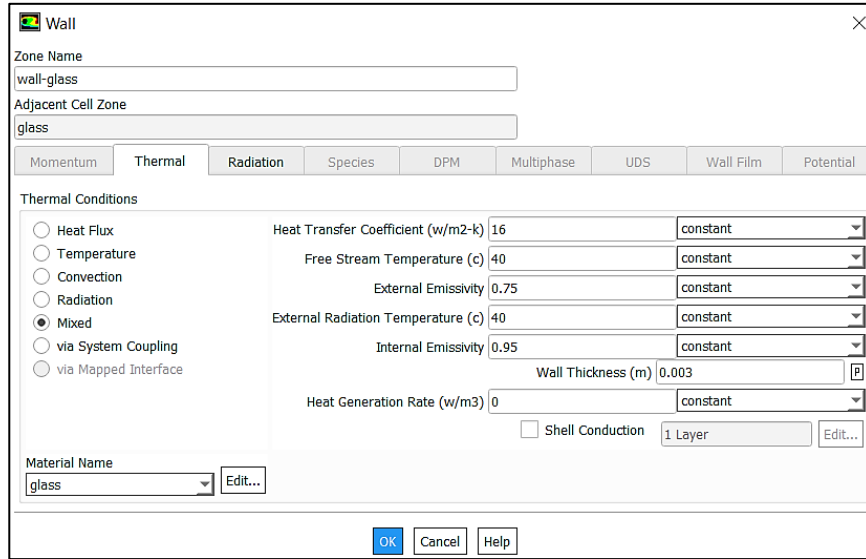


Fig. 3-17 Wall boundary condition

On the other hand, the other walls thermal condition selection was via system coupling as the transfer the thermal information between coupled domains, except for the tedlar outer surface which was exposed to the ambient its thermal condition was convection and water surface was selected as mixed as it had both convection and radiation effect. Water surface and glass were the layers that participated in solar ray tracing. The equation (3.2) was used to calculate the convection heat transfer coefficient for front surface of the panel where (V_w) indicated fluid velocity in (m/s) (Abed, Hachim, and Najim, 2021):

$$h = 5.7 + 3.8 V_w \quad (3.2)$$

while the back surface convection heat transfer coefficient for back surface of the panel was calculated using equation (3.3), as (V_w) is wind speed in (m/s) (Syafiqah *et al.*, 2017):

$$h = 2.8 + 3.8 V_w \quad (3.3)$$

In the present simulation, the influence of various factors including ambient temperature, solar radiation in addition to water inlet temperature on the cooled module was examined by evaluating their performance at different volume flow rates. The ambient temperatures tested were (35, 40, 45 and 50 °C), while the solar radiation examined were (600, 800 and 1000 W/m²). On the other hand, the water inlet temperature tested with in the current simulation were (20, 25, 30. 35 and 40 °C), at different volume flow rates (0, 2, 3, 4 and 5) l/min. Whereas the simulation was repeated 95 times.

3.3.4 Governing Equations

Computational fluid dynamics (CFD) is a field of study related to fluid mechanics. Its main purpose is to use numerical methods along with data structures to solve and analyze the fundamental equations that define the laws of fluid motion. These equations usually represent mathematical models of physical conservation laws. The simulation was done and validated by the experimental findings. The 3D model applies ANSYS (FLUENT R19.2) for CFD analysis, the process of energy transfer in the current PV water cooling system includes two main stages: a fluid domain and multiple solid domains. The fluid domain is attributed to the water employed for cooling the PV, while the solid domain is attributed to the five distinct layers of the PV. The equations (3.4) and (3.5) present the heat transfer equation for solid and fluid domains respectively (ANSYS Inc., 1999).

$$-\nabla \cdot (k \nabla T) + Q = \rho C_p \frac{\partial T}{\partial t} \quad (3.4)$$

$$\rho C_p \left(\frac{\partial T}{\partial t} + u \cdot \nabla T \right) \quad (3.5)$$

where;

$$q = k_{cond} \nabla T \quad (3.6)$$

While the momentum and continuity equations of fluid flow are indicated by equations (3.7) and (3.8), respectively. The momentum equations

for three-dimensional fluid flow consist of three equations, one for each direction (x, y, and z). Here's the general form of the equation in the x-direction:

$$\frac{\partial(\rho u)}{\partial t} + \nabla \cdot (\rho u u) = -\frac{\partial p}{\partial x} + \nabla \cdot (\mu \nabla u) + \rho g_x \quad (3.7)$$

$$\nabla \cdot (\rho u) = 0 \quad (3.8)$$

The discrete ordinates (DO) radiation model is used to apply the incoming solar radiation into the computational domain. The DO radiative transfer equation in the direction \vec{s} as a field equation and the radiative transfer equation for spectral intensity $I_\lambda(\vec{r}, \vec{s})$ are given by Equations (3.9) and (3.10), respectively.

$$\nabla \cdot (I(\vec{r}, \vec{s})\vec{s}) + (a + \sigma_s)I(\vec{r}, \vec{s}) = an^2 \frac{\sigma T^4}{\pi} + \frac{\sigma_s}{4\pi} \int_0^{4\pi} I(\vec{r}, \vec{s}') \phi(\vec{s}, \vec{s}') d\Omega' \quad (3.9)$$

$$\nabla \cdot (I_\lambda(\vec{r}, \vec{s})\vec{s}) + (a_\lambda + \sigma_s)I_\lambda(\vec{r}, \vec{s}) = a_\lambda n^2 I_{b\lambda} + \frac{\sigma_s}{4\pi} \int_0^{4\pi} I_\lambda(\vec{r}, \vec{s}') \phi(\vec{s}, \vec{s}') d\Omega' \quad (3.10)$$

where λ is the wave length, a_λ is the co-efficient of spectral absorption, and $I_{b\lambda}$ is the intensity of black body given by the Planck function. The other parameters such as scattering phase function, scattering coefficient and the refractive index (n) are assumed to be independent of wavelength.

The association of energy with radiation intensity within a cell (known as COMET) accelerates the convergence of the finite volume scheme for radiative heat transfer. The discrete energy equation (DEE) for correlated system when integrated over a controlling volume (i) is stated herein equations (3.11)-(3.14) (ANSYS Inc., 1999).

$$\sum_{j=1}^N \mu_{ij}^T T_j - \beta_i^T T_i = \alpha_i^T \sum_{k=1}^L l_{ij}^k \omega_k - S_i^T + S_i^h \quad (3.11)$$

Where;

$$\alpha_i^T = k\Delta V_i \quad (3.12)$$

$$\beta_i^T = 16k\sigma T_i^{*3} \Delta V_i \quad (3.13)$$

$$S_i^T = 12k\sigma T_i^{*4} \Delta V_i \quad (3.14)$$

Where K and ΔV are the coefficient of absorption and control volume, respectively. The coefficient μ_{ij}^T and the source term S_i^h are owing to the discretization of the diffusion and convection terms as well as the nonradiative source terms, respectively.

3.3.5 Solution Method

In this simulation, the flow regime is analyzed using a segregated numerical solution algorithm with a finite volume approach. By exploiting the ANSYS (Fluent 19.2) commercial CFD code, the equations of continuity, momentum and energy conservation are solved for in the steady-state regime. The 3D and double precision settings were applied when reading the mesh. The mesh was then examined on fluent and displayed no critical faults and had good quality orthogonality. For the current simulation, a laminar viscous model was chosen to demonstrate the fluid flow behavior. The discrete ordinates (DO) radiation model is utilized in regards to the radiation heat transfer present on the upper end of the module. The radiation from the sun is inputted using the ANSYS Fluent built-in solar model. A second-order upwind scheme was chosen for both the energy and momentum equations. The SIMPLE algorithm (semi-implicit method for pressure linked equations) is chosen as the scheme to link pressure and velocity. The convergence criteria of 10^{-3} for the residuals of the continuity equation, 10^{-6} for the residuals of the energy, 10^{-3} for the residuals of the velocity components and 10^{-6} for DO solar radiation are assumed. The assumptions considered for the current simulation are mentioned below:

- Flow is assumed to be laminar
- Solar radiation is not reflected by any surface and it is fully transmitted to the layer below.
- Fluid flowing is at uniform thickness of 4.5 mm along the length of PV module.

- The ambient temperature is same on all the PV faces exposed to the environment.
- Incompressible fluid flow.

3.4 SOLAR ANGLES

The photovoltaic panel inclination angle with horizontal (John and Beckman, 1982) was fixed which was calculated due to equation (3.15).

$$\beta = |\phi - \delta| \quad (3.15)$$

Where ϕ refer to the latitude, whereas Erbil latitude is 36.191° , while δ is the declination angle (John and Beckman, 1982) which was calculated by equation (3.16)

$$\delta = 23.45 \sin \left(360 \frac{284 + n_d}{365} \right) \quad (3.16)$$

Where (n) represents the day of the year. The solar angle was calculated for all the months at average day of the month, then the average tilt angle for the year was calculated which was 36° , so the panels were fixed at this angle.

3.5 ELECTRICAL MODELING

The electrical performance of the panel can be predicted by calculating the ratio of the maximum power produced to the incident irradiation over the surface area of the panel (Mahmood and Aljubury, 2023) as shown in equation (3.17). This will enable the accurate estimation of the PV's performance.

$$\eta_{elec.} = \frac{P_m}{G.A} \quad (3.17)$$

Where $\eta_{elec.}$ is the electrical efficiency of the panel, P_m is the maximum output power from the PV panel (W), G is the solar irradiation (W/m^2) and A is the area of the module (m^2).

The P_m maximum output power was calculated by multiplying maximum voltage V_m by maximum current I_m using equation (3.18) (Risdiyanto *et al.*, 2020).

$$P_m = V_m I_m \quad (3.18)$$

The panel's performance could also be evaluated by another parameter named fill factor (FF). (Risdiyanto *et al.*, 2020) the fill factor (FF) of a solar cell is a dimensionless quantity that represents the ratio of the maximum power (P_m) produced by the panel, to the product of the Open-Circuit Voltage (V_{oc}) and the Short-Circuit Current (I_{sc}), as indicated in equation (3.19).

$$FF = \frac{V_m I_m}{V_{oc} I_{sc}} \quad (3.19)$$

Different correlations were developed to calculate the power production for the simulation data of PV modules, and in the present research the correlation used to calculate the power produced from the panel (Skoplaki and Palyvos, 2008) was calculated using equation (3.20) .

$$P = G_T \tau_{pv} \eta_{T_{ref}} A [1 - 0.0045(T_c - 25)] \quad (3.20)$$

Where G_T is the incident solar radiation (John and Beckman, 1982), τ_{pv} is the transmittance of the photovoltaic panel outer layer (Tiwari and Sodha, 2006) which is value is 0.95, $\eta_{T_{ref}}$ is the panel's electrical efficiency at the reference temperature 25 °C and 1000 W/m², A is area of the panel and T_c is the cell temperature (John and Beckman, 1982).

While the electrical efficiency of PV panel can be calculated from the panel temperature by implementing equation (3.21), which is usually utilized with simulated CFD results (Ruoping *et al.*, 2020).

$$\eta_{PV} = \eta_{T_{ref}} [1 - \beta(T_c - 25)] \quad (3.21)$$

Where β is the temperature coefficient of PV efficiency and is 0.45%/°C for monocrystalline modules (Dash and Gupta, 2015). Equation (3.22) is used to calculate the percentage enhancement of panel electrical efficiency $\eta_{enh.}$ (Haidar, Orfi and Kaneesamkandi, 2021).

$$\eta_{enh.} = \frac{\eta_{PV} - \eta_{ref}}{\eta_{ref}} \times 100\% \quad (3.22)$$

η_{ref} refers to electrical efficiency of uncooled panel, while η_{PV} refers to electrical efficiency of cooled module. Additionally, temperature reduction $T_{reduction}$ of PV panel can be calculated from the equation (3.23).

$$T_{reduction} = T_{ref} - T_{pv} \quad (3.23)$$

Where T_{ref} refers to the reference PV temperature without cooling and T_{pv} is the cooled panel temperature. While the improvement in electrical power production of photovoltaic panel $P_{enh.}$ (Almuwailhi and Zeitoun, 2021), as indicated in equation (3.24).

$$P_{enh.} = P_{PV} - P_{ref} \quad (3.24)$$

The P_{PV} refers to PV power output with cooling and P_{ref} is the power output from the reference panel without cooling.

CHAPTER FOUR

(EXPERIMENTAL WORK)

4.1 INTRODUCTION

The dry, hot and dusty environment in Erbil during the summer is known to detrimentally influence the performance of photovoltaic panels, which already suffer from low efficiency. To address this challenge, two measures were implemented, the first of these was the implementation of a single-axis solar tracking system, which will lead to increase the solar radiation falling over the panel as a result power production will be increased as well. The second way is by providing a cooling and cleaning system to decrease the operating temperature of the panel and remove dust from the surface so an improvement in the power output will be observed. Within the current study spray water cooling system was provided from top, left and right side of the panel to the front surface of the panel to ensure that all the surface covered with water, additionally the water spray was controlled automatically due to the panel surface set point temperature. The lifespan and power production of the panel will be enhanced by decreasing the module temperature and increasing the radiation, also providing a clean surface. In this chapter will provide an overview about experimental installation and setup of the PV spray water cooling system.

4.2 EXPERIMENTAL SETUP

Experimental research has been conducted to assess the efficiency of a PV panel solar tracking system with a cooling system. The prototype was developed, fabricated, and installed at the Research Center/ Erbil Polytechnic University. Fig. 4-1, shows a schematic diagram of experimental setup as each sensor is connected to the Arduino individually, and Fig. 4-2 presents the system connection and description.

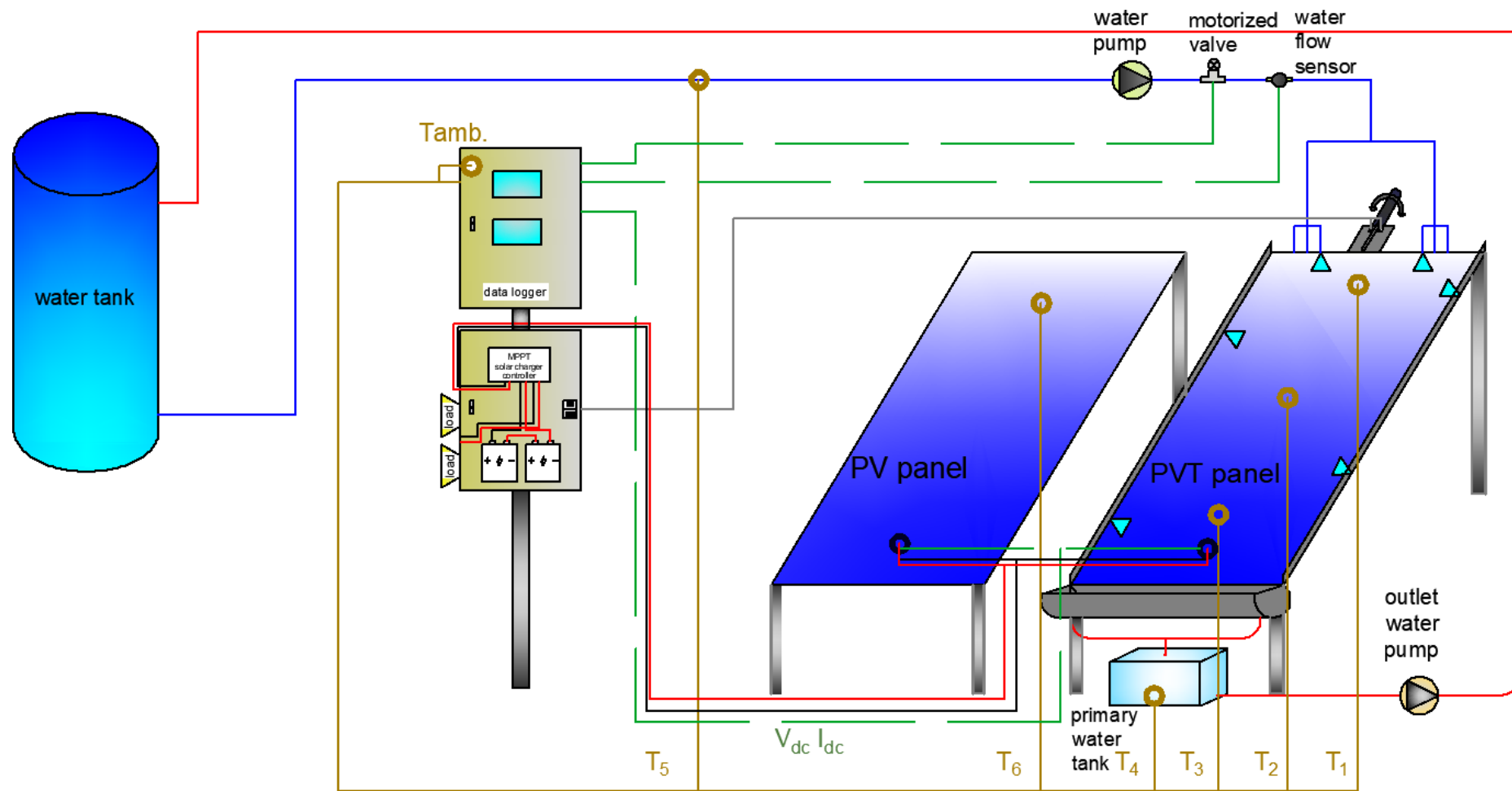


Fig. 4-1 Schematic diagram of the experimental setup

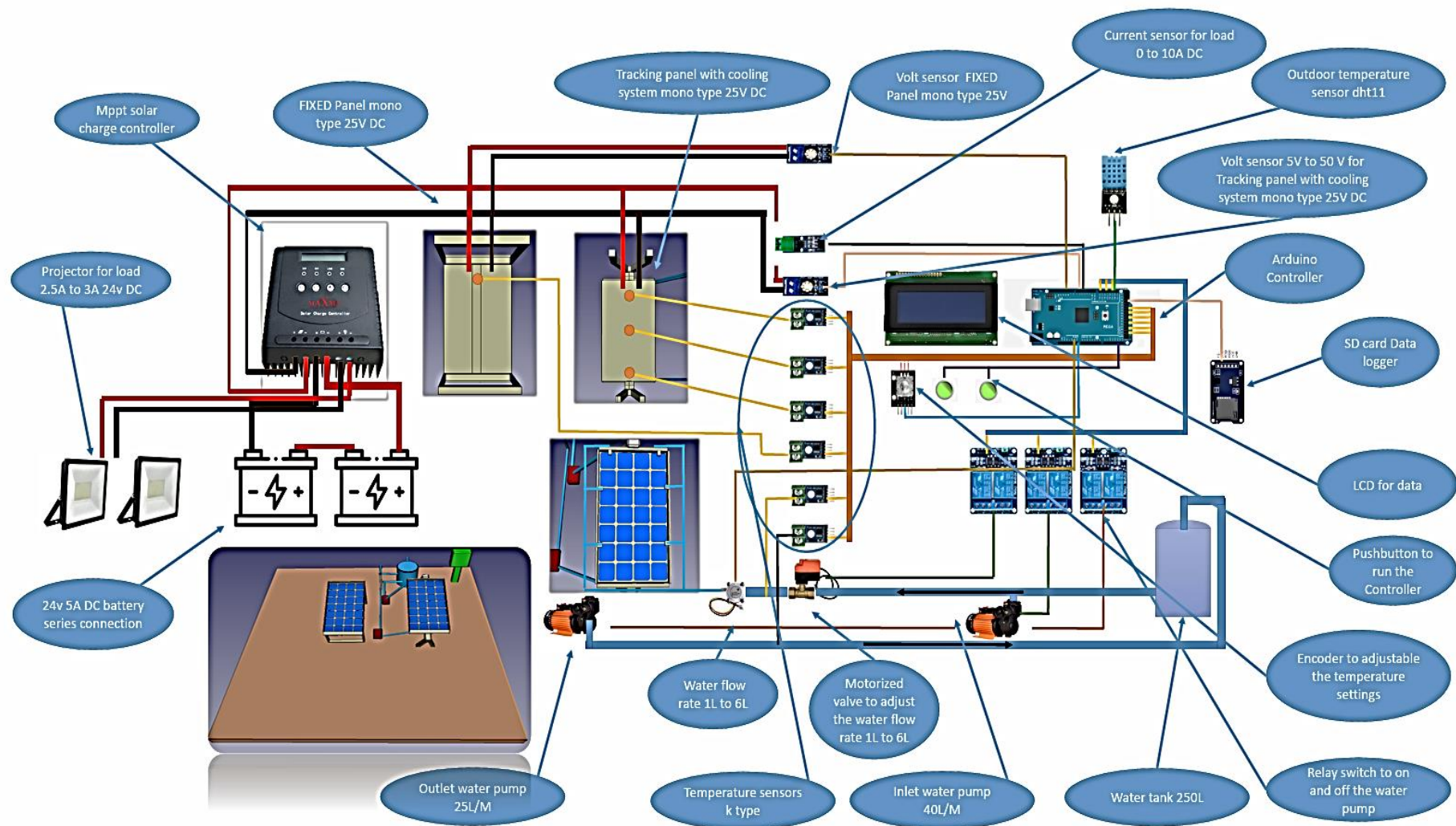


Fig. 4-2 Experimental system connection and description

While the experimental rig is presented in Fig. 4-3. In the following sections all the parts of the system will be discussed.

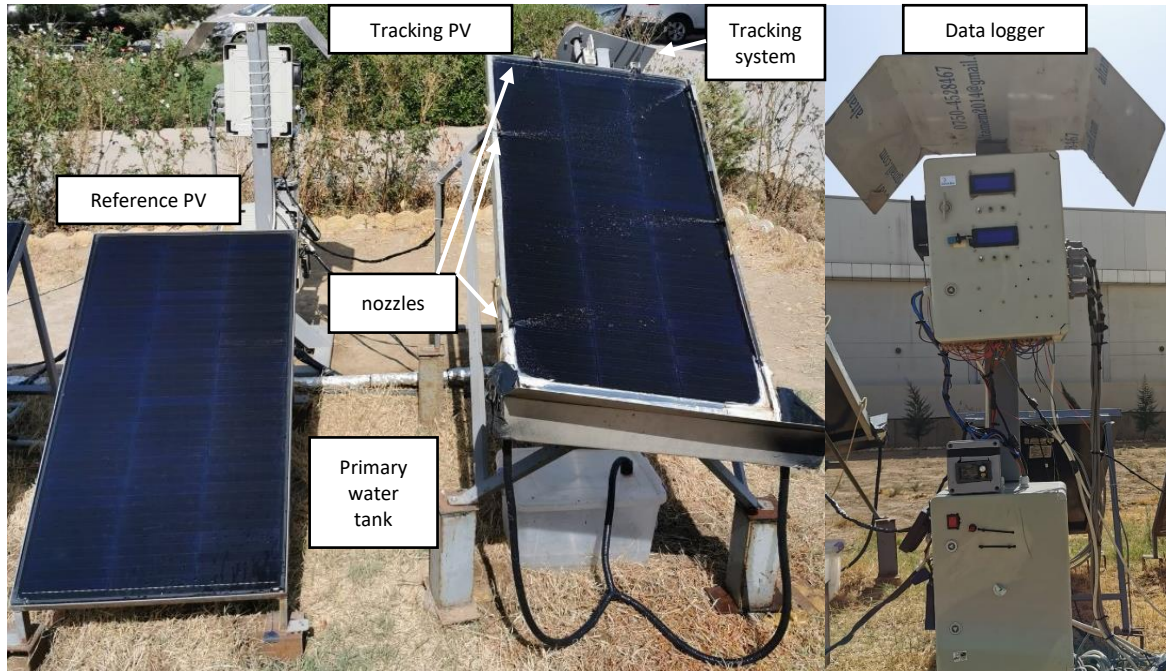


Fig. 4-3 Experimental rig

4.2.1 Photovoltaic Panel

The system consists of two monocrystalline photovoltaic panels each of 210 W with an active surface area of 0.8241 m^2 . One panel with tracking and a front surface spray water cooling system supplied from top, left and right side, was compared to another fixed reference panel without cooling. Table 4-1 presents technical features of a PV panel at nominal operating conditions of 25°C temperature and solar irradiance of 1000 W/m^2 and 1.5 m/s wind speed. The panels are mounted on an aluminum frame with an inclination angle of 36° with horizontal.

Table 4-1 Technical features of PV at nominal operating condition (25 °C, 1000 W/m², 1.5 m/s)

Parameters	PV
Module dimension	1230*670*30 mm
Module weight	9 kg
Nominal power	210 W
Cell efficiency	23%
Maximum power current (Impp)	7.68 A
Maximum power voltage (Vmpp)	27.31 V
Open circuit voltage (Voc)	31.41 V
Short circuit current (Isc)	8.2 A
Nominal operating cell temperature	25 °C
Working temperature	-40°C - +80 °C

4.2.2 Solar Tracking System

The tracking system used in this research for PV panel was a single east west solar tracker, which is an electrically driven based on the signal received from the light intensity sensor positioned on the top of the module normal to its surface. The solar tracking system was developed in some parts which are mentioned below.

4.2.2.a Frame with Rotating Shaft

The first step in designing the photovoltaic (PV) tracking system was to construct a framework with a fixed tilt angle of 36° with the ground plane. Additionally, a tilted shaft was added to enable east-west movement, as illustrated in Fig. 4-4.



Fig. 4-4 PV framework and rotating shaft

4.2.2.b Light Intensity Sensor

Two light intensity sensor types (TEMT6000X01) as shown in Fig. 4-5, were used in this study. This type of sensor is sensitive to light same as human eyes, and it has a peak sensitivity at 570 nm.



Fig. 4-5 TEMT6000X01 sensor

The tracking system operating concept is based on comparing the light intensity between two TEMT6000X01 sensors installed normal to the PV panel surface and separated by a plate as shown in Fig. 4-6, thus based on the solar ray on both sensors, when the right sensor is shaded while the left one is illuminated.



Fig. 4-6 Two light intensity sensors with a separating plate

The illuminated sensor will produce a stronger signal while the other one will produce a weaker signal, so that the difference in output voltage will indicate the rotation direction of the panel. Until the panel reaches the direction in which both of the sensors have the same output voltage then the panel will stop moving.

4.2.2.c Arduino

The output signal from the light intensity sensor will be transferred to the Arduino as shown in Fig. 4-7. Which is a physical programable circuit board (microcontroller) with a (IDE) integrated development environment, that was programmed using C++ language. Whereas the microcontroller is the brain of the solar tracking system as it manages and controls the activity of all the parts of the system. The Arduino Mega 2560 is a microcontroller board based on the ATmega2560. It has 54 digital input/output pins (of which 14 can be used as PWM outputs), 16 analog inputs, 4 UARTs (hardware serial ports), a 16

MHz crystal oscillator, a USB connection, a power jack, an ICSP header, and a reset button.

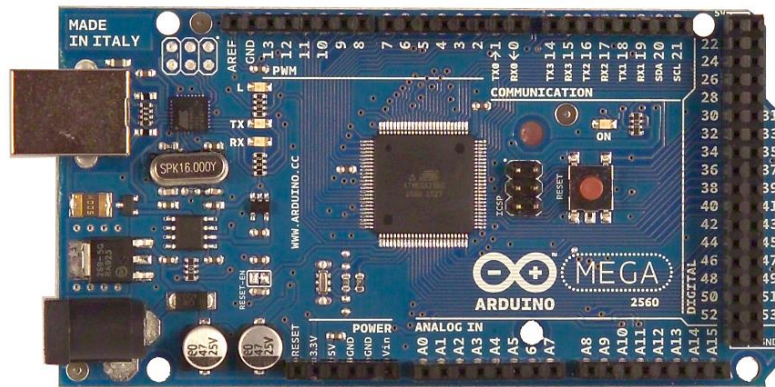


Fig. 4-7 Arduino

4.2.2.d Stepper Motor and Gearbox

The output signal from the Arduino IDE will be transferred to the stepper motor and gearbox, which drives the tilted shaft of the PV framework and results in movement of the panel in a direction perpendicular to sun's ray. Fig. 4-8 presents the gearbox and stepper motor used in this study.

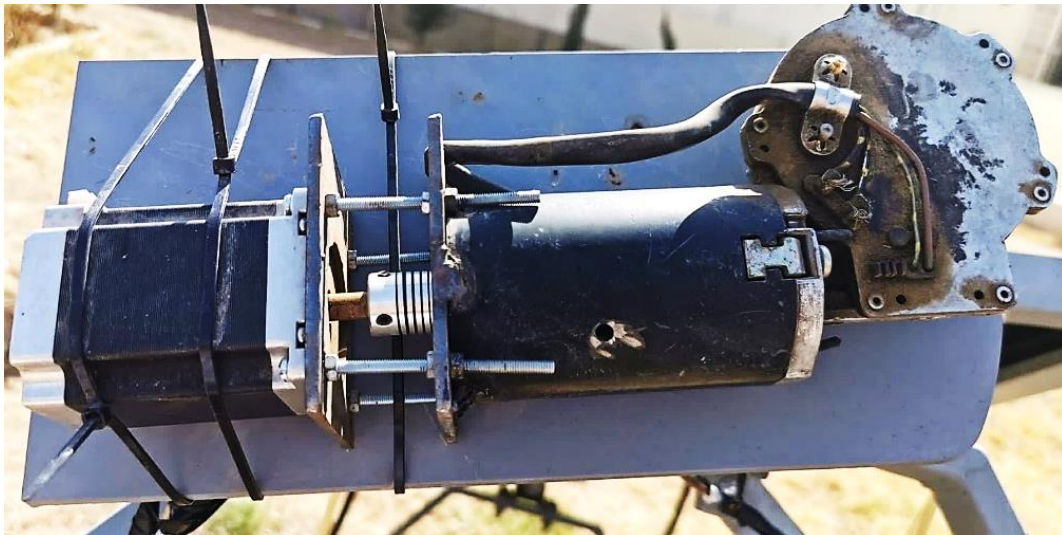


Fig. 4-8 Stepper motor and gearbox

The stepping angle of the stepper motor was set to 1.8° , so that the PV will track the sun's direction with great precision, and as a result, maximum

incident radiation falling over the PV panel all the time will be maintained, therefore converting higher portion of radiation in to electricity. To reduce energy usage within the tracking system, the power circuit can be deactivated by switching it off during nonessential times, as it consumes only 36 W DC.

4.2.2.e Working Principle

The working principle of the solar tracking system is shown in Fig. 4-9 as shown when the sun hits the light dependent resisters (LDR) on the PV module, a signal will be sent to the Arduino IDE microcontroller in the voltage produced by left sensor is bigger than the right one the panel will rotate to the left if not the panel will not move until there is a difference between the voltages of the two LDR sensors. Fig. 4-10 shows a PV module with complete tracking system at 2:00 PM facing south west.

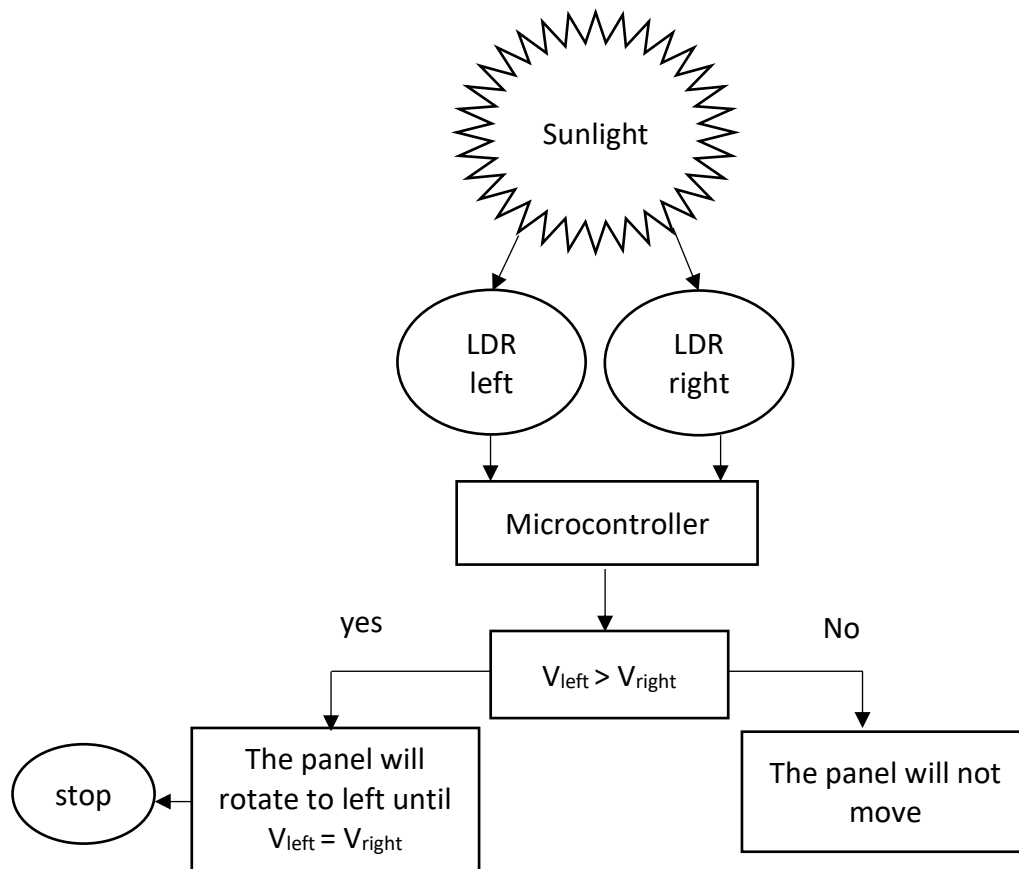


Fig. 4-9 Block diagram of solar tracking system for one iteration

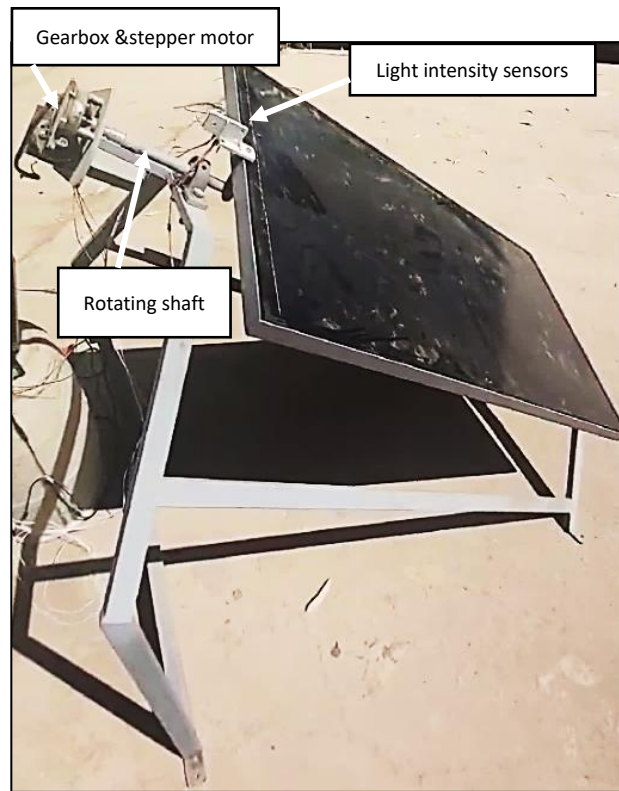


Fig. 4-10 PV module with tracking system

4.2.3 Spray Water Cooling System

In this research, a front surface spray water cooling system was implemented to regulate the temperature of the panel's front surface, by modulating the flow rate of water depending on the setpoint temperature of the module's surface. This was achieved by connecting the water flowmeter to the temperature sensor that was attached on the back side of the panel, in addition to Arduino specific coding. Upon the temperature of the panel surpassing the setpoint temperature, the system will start spraying water using the lowest flow rate possible, and if the panel does not cool down to the setpoint temperature within two minutes, the flow rate will be increased, followed by subsequent increases every two minutes until the maximum flow rate is reached and sustained until the panel temperature is minimized to the setpoint temperature. This was done by utilizing six nozzles placed on the top and sides of the panel. The components utilized for the spray water cooling system will be mentioned in the following sections.

4.2.3.a Nozzles

The spray water nozzles used in this study were windshield wiper nozzles of BMW car as shown in Fig. 4-11. As it is easy to install with a changeable spray angle with PV surface. Six water nozzles were used in this study, two on the top side, and two on each left and right side of the panel as presented in Fig. 4-12.



Fig. 4-11 Water spray nozzle

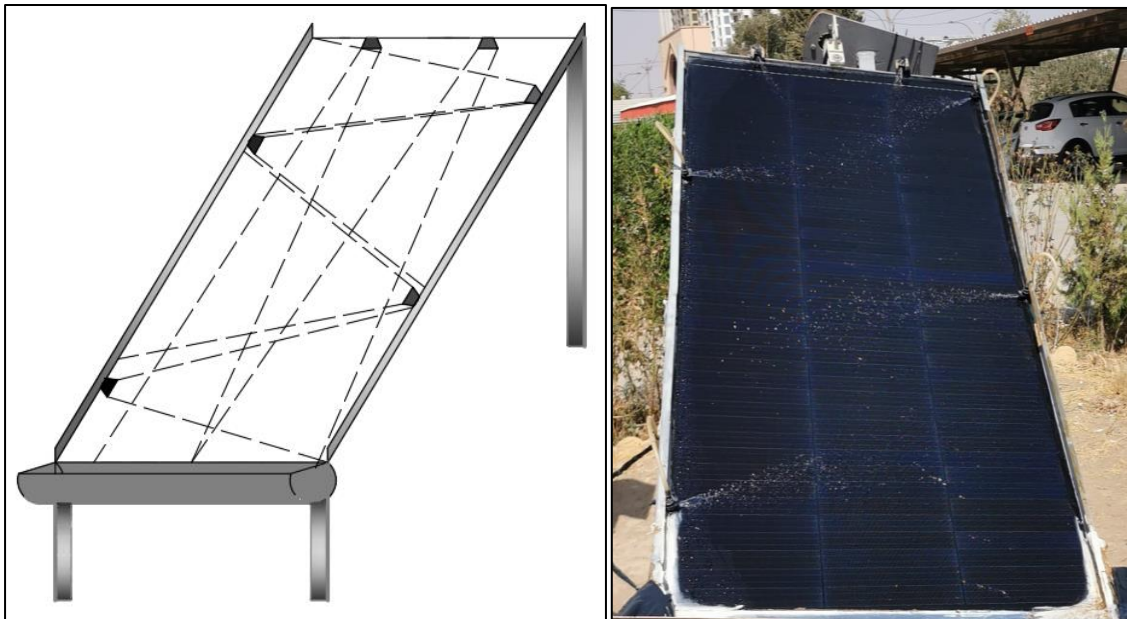


Fig. 4-12 Nozzles over the front surface

4.2.3.b Supply Water Pump

The water pump used to supply water to the spray nozzles of the PV module is shown in Fig. 4-13. The power needed to run the pump is 100 W. This type of pump has high efficiency, easy to use, energy saving and sensitive operation in addition to low operation noise.



Fig. 4-13 Supply water pump

4.2.3.c Motorized Valve

The motorized water valve used in this study was CWX model 12 V DC as shown in Fig. 4-14. This valve is a very important part of spray water system as it was placed after the supply water pump to control the water flow rate due to PV module surface temperature. As the maximum working pressure of the valve is 1 MPa with a lifetime cycle 100000 times.



Fig. 4-14 Motorized valve

4.2.3.d Return water pump

A DEVICO water pump, model W15G-15 is used to return water from the panel to the storage tank, as presented in Fig. 4-15. The pump is run when there is water to return to the tank and it is turned off when there is no water. As it consumes just 100 W of electricity power. With maximum flow rate ability 1500 l/h, and maximum head 15 m.



Fig. 4-15 Return water pump

4.2.3.e Primary Water Tank

A 10 litter capacity primary water tank was used to collect water from the photovoltaic array and it was placed before the return-water pump, thereby reducing the strain on the pump. Additionally, a filter was affixed at the water outlet point of the tank to ensure that debris was cleared before the water passed to the pump and secondary water tank. The primary water pump used is presented in Fig. 4-16.



Fig. 4-16 Primary water tank

4.2.3.f Water Softener

A water softener is a device used to soften hard water by removing minerals like calcium and magnesium, and replacing them with sodium ions. In photovoltaic (PV) cooling systems, water softener is used to reduce corrosion in the cooling water pipes and to keep the water free of mineral deposits that can clog the system. Hard water can form scale deposits on the pipes, nozzles, restricting the flow of the water and reducing the efficiency of the heat transfer. By using soft water in the system, these deposits are prevented

and a more efficient heat transfer is achieved. Additionally, the softener helps to protect the terminal components in the system from corrosion caused by the minerals in the water. The water softener used in this study is shown in Fig. 4-17.



Fig. 4-17 Water softener

4.2.3.g Secondary Water Tank

The water returning from the module will pass through a filtration system through a specialized filtration and softening process before entering the secondary storage tank. This tank, which has a volume of 250 litter, functions as a main source for supplying water to the panel and is illustrated in Fig. 4-18.



Fig. 4-18 Secondary water tank

4.2.3.h MPPT Solar Charge Controller

The MPPT (Maximum Power Point Tracking) solar charge controller is an electronics component that is used to control the charging of batteries from solar photovoltaic (PV) panels. It enables the efficient charging of solar

batteries by using supplied solar energy. It works by automatically adjusting the charging rate for the battery while tracking the maximum power as the solar panel is exposed to different levels of solar irradiance, so that the maximum amount of power is stored into the battery. By employing sophisticated algorithms and an adaptive system, the controller can even detect the type of battery being charged and fine-tune its settings to maximize the amount of energy stored when the battery limits are reached. This makes an MPPT solar charge controller an essential part of any system that uses solar energy to charge batteries. The solar charge controller used in this experimental study was power MAXMA model GSC-F2428-60A, as indicated in Fig. 4-19.



Fig. 4-19 MPPT solar charge controller

4.2.3.i Batteries

Two batteries each of 24 V, 8 A DC were used which were connected in series. The connection of MPPT with batteries, PV panel and load which wear projector are presented in Fig. 4-20.

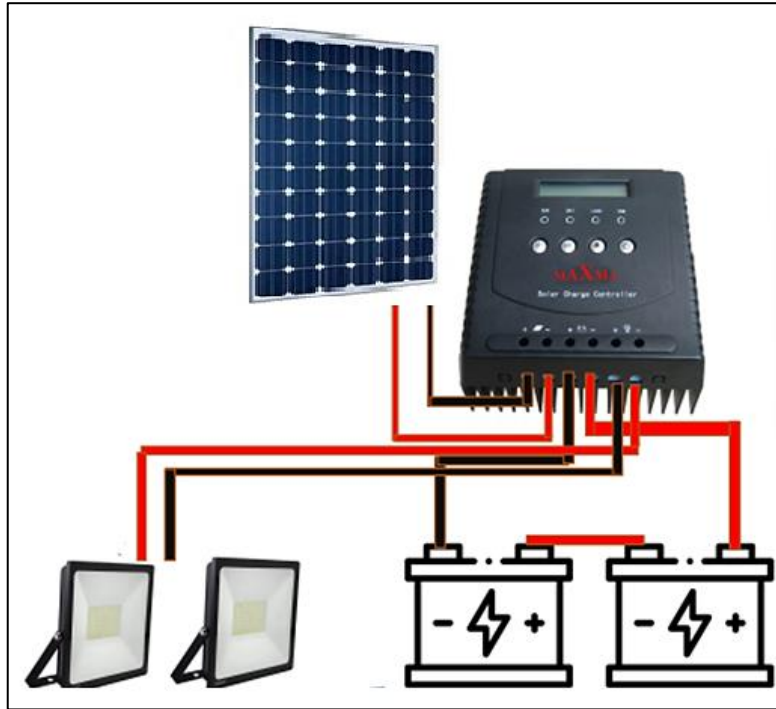


Fig. 4-20 Batteries, PV and load connection with MPPT

4.2.4 Sensors and Measuring Devices

The measuring tools and sensors are deployed to document the results of the experimental activities that will be carried out under distinct system parameters. Every device has undergone precise calibration. All the sensors and devices are connected to the data logger Arduino, which presents the data and save it on a SD card. Detailed information regarding the functions and specifications of each device and sensor will be provided in the following subsections.

4.2.4.a Water Flow Sensor

A high precision PVC water flow sensor, YF-S401 model, was used to measure the water flow rate in this study, as shown in Fig. 4-21. It consists of PVC body, water rotator and a hall-effect sensor. When the water passes through the rotor, its speed change with changing the rate of flowing water. The output from the hall effect sensor changes according to the pulse signal. This

type of sensor is especially efficient at detecting the flowrate of water in a dispenser. As the water flow measuring range is (0.3-6) l/min



Fig. 4-21 Water flow sensor YF-S401

4.2.4.b Ambient Temperature Sensor

The temperature sensor, DHT11 model, was used to measure the ambient temperature, which is presented in Fig. 4-22. This temperature sensor ensures high reliability and excellent long-term stability, by using an exclusive digital signal acquisition technique and temperature sensing technology. The ambient temperature sensor has been calibrated in the laboratory with an accuracy of ± 2 °C. with the ambient temperature measuring range (0-50) °C.

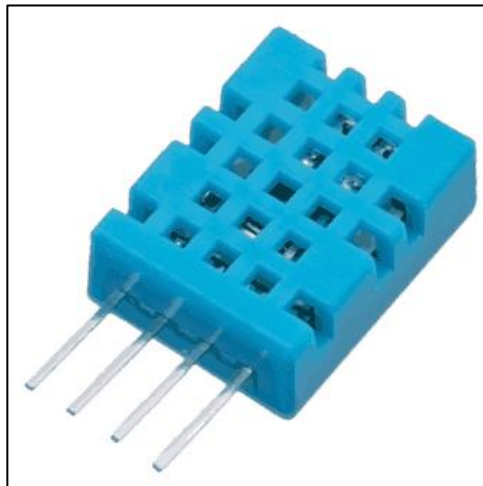


Fig. 4-22 DHT11 ambient temperature sensor

4.2.4.c PV Temperature Sensor

The type of thermocouple that is used to measure the temperatures of the PV module is a K-Thermocouple with the capability of temperature sensing measurement ranges from 0 °C to 1024 °C. Those sensors are connected to the MAX6675 amplifier, which performs cold-junction compensation and digitizes the signal from a type-K thermocouple and transfers it to the Arduino. Fig. 4-23 presents the K-type thermocouple and MAX 6675 amplifier. While Fig. 4-24 presents the connection of K type thermocouple with MAX6675 amplifier and Arduino. In this study, six temperature sensors were used, including three for the surface of the tracking PV, two for measuring water temperature at the inlet and outlet of the system, and one for measuring the surface temperature of the fixed panel.

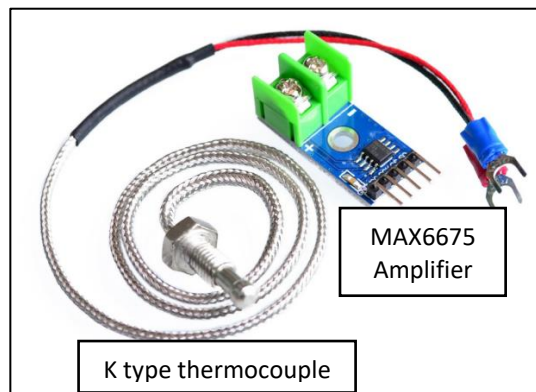


Fig. 4-23 K type thermocouple and MAX6675 Amplifier

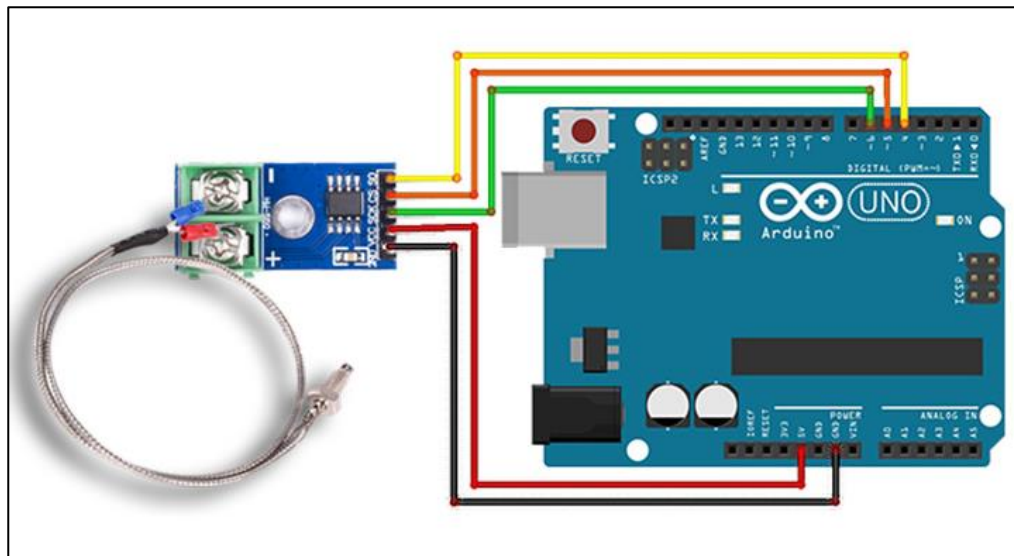


Fig. 4-24 Connection of K type thermocouple with MAX6675 and Arduino

4.2.4.d Current Sensor

The ACS712 current sensor was used to measure the output current from photovoltaic sensor, as shown in Fig. 4-25. This device features a high degree of accuracy, with a linear Hall circuit with a copper conduction path placed close to the surface of the die. The current running through this conduction path produces a magnetic field which is changed by the Hall IC into an output voltage that is proportional. With a rated current 30 Amp.

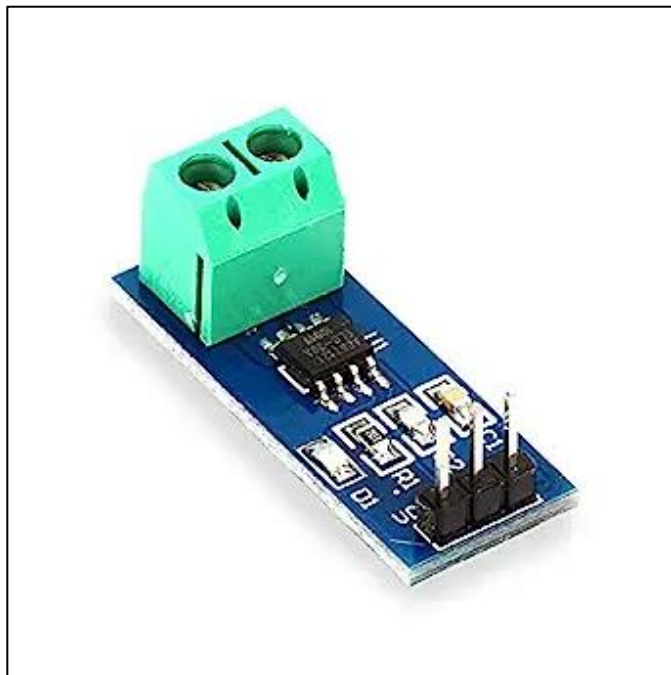


Fig. 4-25 Current sensor ACS712

4.2.4.e Voltage Sensor

The voltage sensor used in this experimental is the SEN32 REV1.1, as shown in Fig. 4-26, it is an ideal sensor for precisely measuring AC and DC voltages. This type of sensor provides high accuracy and reliable consistency in detecting various voltages up to 50 V AC or DC. Moreover, it is effortless to operate and does not require an auxiliary power source. Both the voltage and current sensors were calibrated using a DC clamp meter.

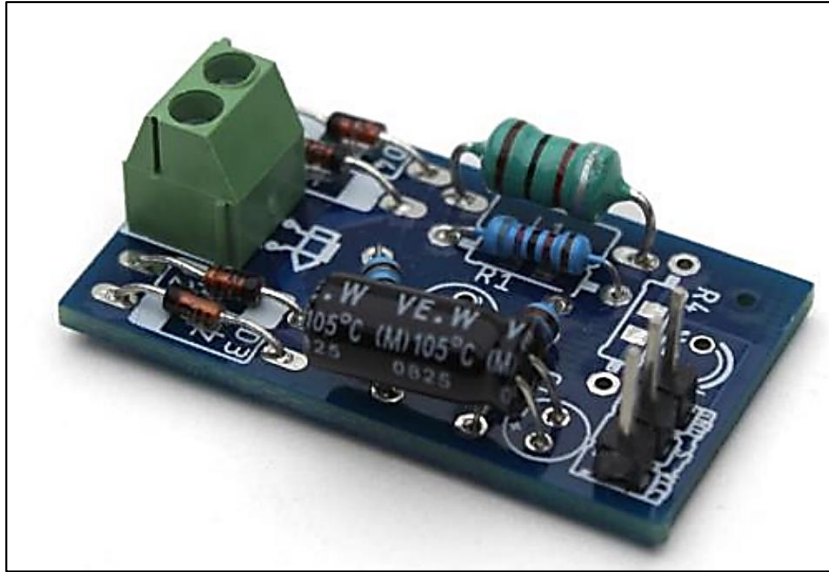


Fig. 4-26 SEN32 REV1.1 voltage sensor

4.2.4.f Solar Power Meter

A GENERAL DBTU1300 model solar power meter was utilized to measure the solar irradiance intensity in (W/m^2), which is shown in Fig. 4-27. It has a measuring range of 0 to 2000 W/m^2 . A silicon photodiode equipped with cosine angular correction is employed to accurately measure the solar energy emitted from any direction. It is not connected to the data logger as it has a 4-digit LCD display.



Fig. 4-27 GENERAL DBTU1300 solar power meter

4.2.4.g Data Logger

The data logger system was manufactured to connect the Arduino, LCD display and an SD card. The Arduino is used to read the sensor data, process the data, and store the data in the SD card. The LCD Display is used to display the readings obtained from the Arduino, and the SD card is used for storing the data. As it has 7-channels for temperature, 2-channels for voltage, 2-channels for current and 1-channel for flow rate. The data is saved every minute and recorded in the SD card. The data were displayed and recorded for both fixed and tracking with cooling panel, in addition to ambient temperature. Fig. 4-28 shows the data logger board used in this study.

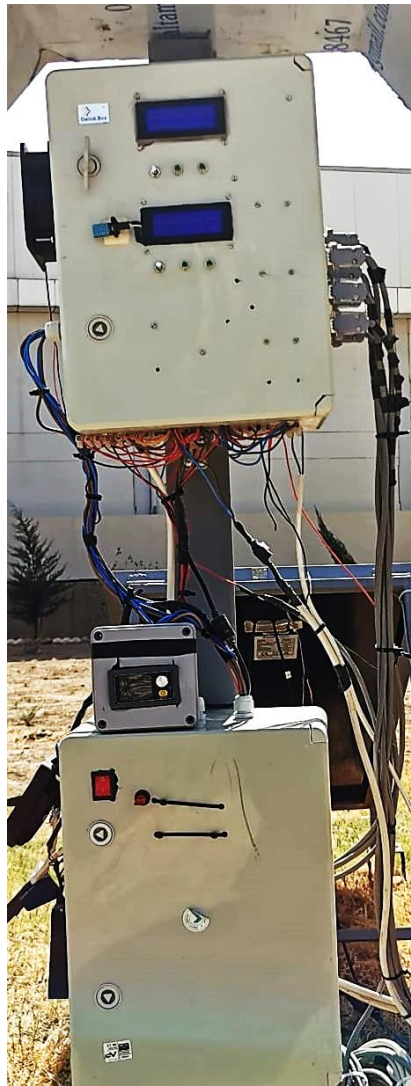


Fig. 4-28 Data logger board

4.3 EXPERIMENTAL PROCEDURE

The experiments were performed during the summer of 2022 in the Erbil Polytechnic University Research Center Garden. Five different tests were performed during this study. For all of the tests first step is turning the power on, initializing the data logger, and setting up the operating conditions.

4.3.1 Comparison between Reference and Tracking Panel

The first test was performed by activating only the single axis east-west tracking system for the PV panel and comparing it with a fixed reference panel for one day from 8:00 AM to 3:00 PM. So that to compare the panels temperatures, powers, solar radiation and electrical efficiency.

4.3.2 Comparison between Reference and Tracking with Cooling at Various Setpoint Temperature Panels

This test was done by comparing the tracking with a spray water cooling panel at three different set point temperatures (35, 40 and 45 °C) with a fixed reference panel. Each set point temperature was tested for one day.

- 1- After turning on the power switch, turn on the tracking system. The panel will track the sun's position from east to west.
- 2- Adjust the setpoint operation temperature of the PV module.
- 3- After setting the PV temperature, if the surface temperature of the panel is less than the adjusted one, then the pump will not turn on, but if it is more than the adjusted one, then the supply water pump will start pumping water from the secondary water tank to the panel.
- 4- Once the pump starts operating the motorized valve will adjust the water flow to its minimum level of 1.8 L/min.
- 5- After two minutes, if the surface temperature is less than the setpoint temperature then turn off the cooling system, if not, then the motorized valve will increase the volume flow rate of water.

- 6- Again, after two minutes, if the panel temperature does not decrease to the selected level, the motorized valve will increase the water volume flow, and so on until it reaches the maximum level of flow.
- 7- Whenever the PV temperature is equal to or less than the set point temperature, then the motorized valve will close the flow path and turn off the supply water pump.
- 8- As the PV temperature increases the motorized valve will open the water at minimum flow and the same steps will be repeated.
- 9- The output water from the panel will go through the drain pipe and then to the primary water tank. As the water reaches a specific level the return water pump will start operating, to pump the water back to the secondary water pump.
- 10- All the data will be presented on the LCD digital and recorded in the SD card every minute, from 8:00 AM until 3:00 PM.
- 11- While the solar radiation was measured every 15 minutes from 8:00 AM to 3:00 PM by a solar intensity measuring device by placing it perpendicularly over the panels.

4.3.3 Comparison between Reference and Fixed with Cooling at Various Setpoint Temperature Panels

The operating procedure of this experiment was the same as the second test except that in this test the tracking system was stopped, as the panel was fixed to the same orientation as the reference panel.

4.3.4 Comparison between Reference and Tracking with Cooling at Different Volume Flow Rates Panels

This test was done by comparing the tracking with a spray water cooling panel at four different volume flow rates (2, 3, 4 and 5 l/min) with a fixed reference panel without cooling. Each volume flow was tested for one day.

- 1- After turning on the power switch, turn on the tracking system. The panel will track the sun's position from east to west.
- 2- The temperature of the panel was set to the lowest level so that the supply water motor would operate all the time.
- 3- The water volume flow rate was adjusted manually by a ball valve.
- 4- The nozzles were spraying water at fixed flow rate throughout the day.
- 5- The output water from the panel will go through the drain pipe and then to the primary water tank as the water reaches a specific level the return water pump will start operating, and pump the water back to the secondary water pump.
- 6- All the data will be presented on the LCD digital and recorded on the SD card every minute, from 8:00 AM until 3:00 PM.
- 7- While the solar radiation was measured every 15 minutes from 8:00 AM to 3:00 PM by a solar intensity measuring device by placing it perpendicularly over the panels.

4.3.5 Comparison between Reference and Fixed with Cooling at Different Volume Flow Rates Panels

The operating procedure of this experiment was the same as the fourth test except that in this test the tracking system was stopped, as the panel was fixed to the same orientation as the reference panel.

4.3.6 PV Performance at Different Surface Temperature and Solar Irradiance

This experiment was done to test the panel efficiency at different surface panel temperatures (25, 30, 35, 40, 45, 50, 55, 60, 65 and 70 °C) at noon when the solar radiation was approximately 1000 W/m², the low surface temperature was achieved by adding ice to the secondary water tank which will supply water to the panel through the supply water pump. The water was fully opened and the set point temperature was set to the minimum so the water will be supplied

continuously. While the high surface temperatures were without using cooling system.

4.4 EQUIPMENT'S CALIBRATIONS

Calibration is an essential process for measuring and testing equipment so that it always produces the same, accurate results. Calibrations also help to identify and correct any discrepancies that may exist. Without proper calibration, these discrepancies could result in inaccurate measurements. So that different instruments used in this study have been calibrated.

4.4.1 Calibration of Water Flow Sensor

A stop watch and glass beaker were used for calibration of water flow sensor YF-S401 model, this was done by using the timer to measure the time needed to fill the glass beaker with water to the selected level. Several volume flow readings were recorded, ranging from 1 L/min to 6 L/min. The equation (4.1) was used to compute the water volume flow rate (Aldihani, 2017).

$$V_w = \frac{\text{recorded volume } (V_f)}{\text{recorded time}(t)} \quad (4.1)$$

Fig. 4-29 presents how the calibration was made, while the calibration curve is presented in Fig. 4-30.



Fig. 4-29 Calibration of flowmeter using stop watch and glass beaker

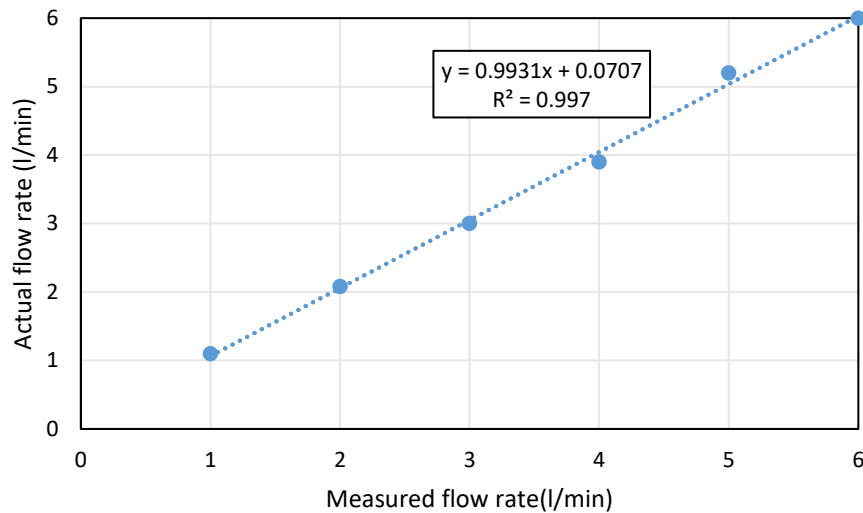


Fig. 4-30 Calibration curve between flowmeter reading and actual flow rate

4.4.2 Calibration of K-Type Thermocouple

The calibration of the K-type thermocouple was conducted by immersing both the thermocouple and the VOLTcraft thermometer in an ice bath, and recording the readings obtained, as shown in Fig. 4-31. Subsequently, both sensors were placed in a water kettle and the temperature was gradually increased from 0 °C to 100 °C. Variations in the readings taken from both sensors at varying temperatures were then analyzed and evaluated. The calibration curve is presented in Fig. 4-32.



Fig. 4-31 Calibration of K-type thermocouple with VOLTcraft thermometer

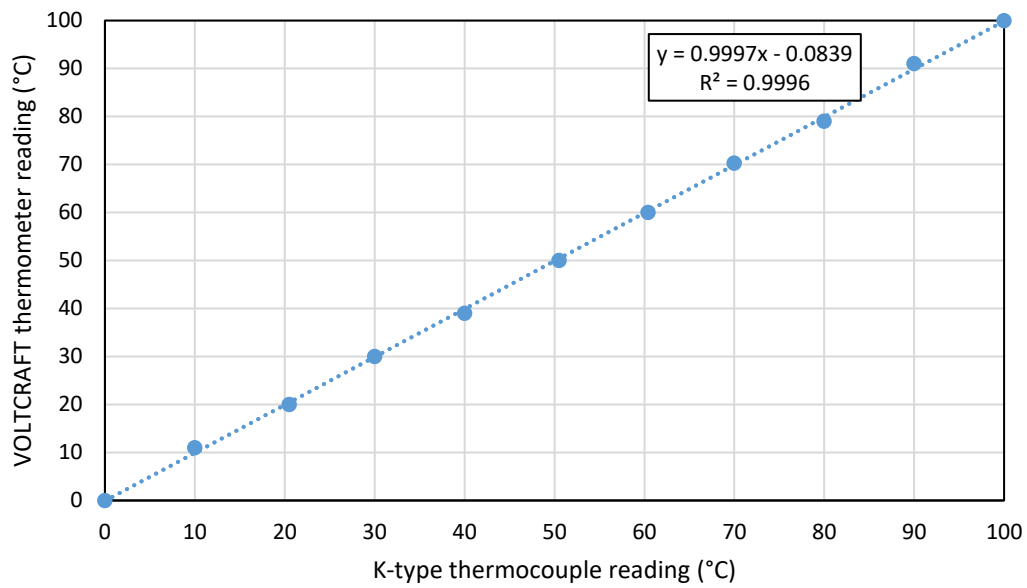


Fig. 4-32 Calibration curve of K-type thermocouple and thermometer

4.4.3 Calibration of Solar Power Meter

The solar power meter DBTU1300 model was calibrated with the SM206-SOLAR model, as shown in Fig. 4-33. Both devices were placed on the same surface with the same angle of inclination to compare their readings. The comparison of the readings is presented in Table 4-2.



Fig. 4-33 Calibration of solar power meter

Table 4-2 Calibration of solar power meter DBTU1300 with SM206-SOLAR

DBTU1300 reading (W/m ²)	SM206-SOLAR reading (W/m ²)
450	452
655	657
998	1002
1045	1046
1069	1076
1073	1078
1075	1076
1080	1083

4.5 UNCERTAINTY

Calculating uncertainty of the measuring devices is important, as it allows the researcher to assess the accuracy of the results. It provides a measure of how close the obtained values are likely to be to the true values. Without considering uncertainty, the measured values may be misleading or misinterpreted. uncertainty has the capacity to minimize random errors, whereas effective calibration procedures can eliminate systematic errors (Aldihani, 2017). The equation (4.2) has been used to calculate the uncertainty of the measuring equipment (Dieck, 1999; Ceylan *et al.*, 2019).

$$uncertainty(u) = \sqrt{\frac{\sum_{i=1}^n (x_i - \bar{x})^2}{N*(N-1)}} \quad (4.2)$$

Where N is samples number, \bar{x} is the average value of considered data for the variable x, the results of ith data is represented by x_i .

The results of uncertainty of the instrument used in this study are presented in Table 4-3.

A sample of calculation for uncertainty analysis for flowmeter is presented in Appendix A.

Table 4-3 Uncertainty of the equipment

Instrument	Uncertainty
Flow meter	± 0.013
K-type thermocouple	± 0.08
Voltage sensor	± 0.05
Power sensor	± 0.09
DHT11 ambient sensor	± 0.08

CHAPTER FIVE

(RESULT AND DISCUSSION)

5.1 INTRODUCTION

This chapter states the results of the research conducted and provides a detailed explanation of the findings, which are the outcome of the research work. It also provides evidence for the conclusions drawn by this study. The presentation of the findings is structured and organized in such a way that it clearly answers the questions raised in the research objectives. The first part of this chapter focuses on the experimental results of the photovoltaic front surface cooling with solar tracking system tests conducted during the summer season of the year 2022, at the research center- Erbil Polytechnic University. While, the second part presents the numerical validation results based on the experimental outcome. And the last part presents the ANSYS Fluent results about the effects of the different operating parameters on the cooled PV panel.

5.2 TILT ANGLE

The inclination angle for each month was calculated based on the monthly average day (John and Beckman, 1982) to determine the best tilt angle for the panels. This angle will be used to adjust the panel at an optimal angle for the year so that it will lead to optimal energy production. Based on equations (3.15) and (3.16) the results are shown in Table 5-1, where the average tilt angle calculated was 36° . So, both panels were placed at the angle of 36° with the horizontal, and in addition to that one of the panels has an east west solar tracking system.

Table 5-1 Tilt angle for the average day of the month for Erbil

Month	Date	n	δ	β
January	17	17	-20.9	56.9
February	16	47	-13	49
March	16	75	-2.4	38.4
April	15	105	9.4	26.6
May	15	135	18.8	17.2
June	11	162	23.1	12.9
July	17	198	21.2	14.8
August	16	228	13.5	22.5
September	15	258	2.2	33.8
October	15	288	-9.6	45.6
November	14	318	-18.9	54.9
December	10	344	-23	59

5.3 EXPERIMENTAL RESULTS

In order to fulfill the primary objective of this section, comprehensive analysis and comparison of the experimental findings of the PV reference panel are conducted with various scenarios, including a panel equipped with an east-west solar tracking system, tracking while cooling at different setpoint temperatures, being fixed at different flow rates, tracking with different flow rates, and being fixed at different setpoint temperatures. Additionally, the performance of the panel is evaluated under varying surface temperatures. To begin our analysis, Fig. 5-1 illustrates the average daily ambient temperature recorded over three days for both July and August. Notably, the highest ambient temperature is observed on the 2nd of August, while the lowest temperatures are recorded on the 17th of July and the 21st of August. This information sets the foundation for interpreting and understanding the subsequent experimental outcomes.

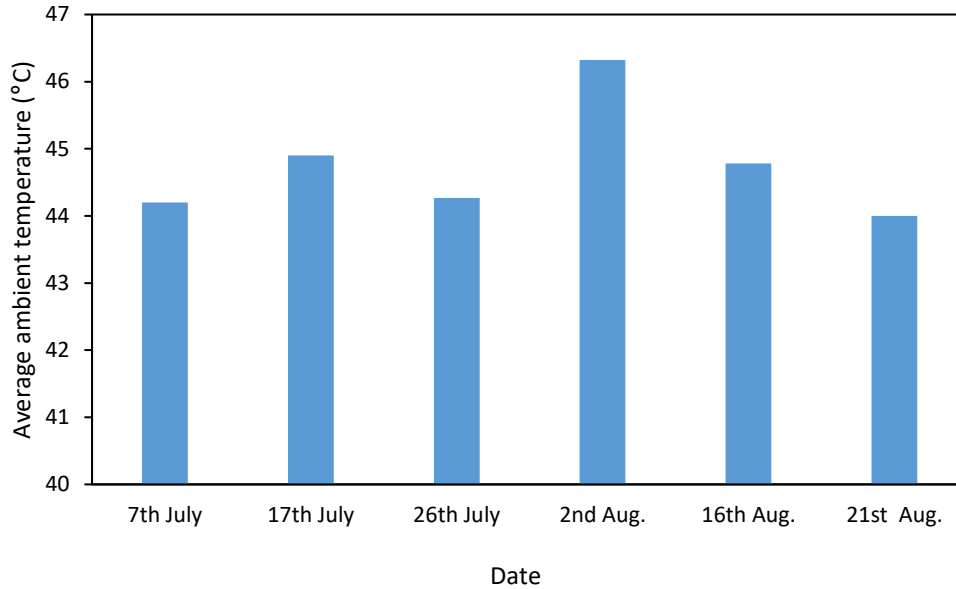


Fig. 5-1 Average daily ambient temperature during July and August

Upon Fig. 5-2, which presents the average daily solar irradiance intensity over fixed and tracking solar panels for the same days throughout July and August, it becomes evident that a significant disparity exists between the two panels. Specifically, the lowest solar intensity values were observed on the 17th of July, with the fixed panel registering 790 W/m² and the tracking panel recording 917 W/m². Conversely, on the 16th of August, the highest solar irradiance values were documented, with the tracking panel reaching 991 W/m² and the fixed panel achieving 875 W/m².

These findings shed light on the superior performance of the tracking solar panel in terms of capturing solar irradiance compared to its fixed counterpart. The substantial variance in solar intensity values between the two panel types shows the effectiveness of solar tracking systems in optimizing energy generation by aligning the panel with the sun's trajectory throughout the day. Furthermore, this disparity in performance underlines the importance of considering various factors, such as panel orientation and tilt angle, when designing and deploying solar energy systems to maximize their energy output.

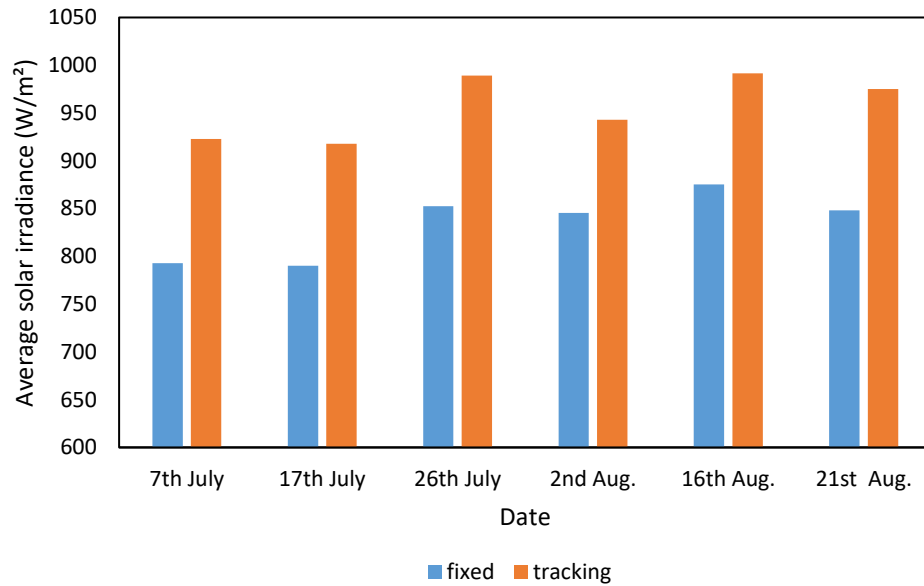


Fig. 5-2 Average daily solar intensity over fixed and tracking panel during July and August

5.3.1 Comparison between Reference, Tracking and Tracking with Cooling PV Panel at Various Setpoint Temperature

This section aims to evaluate the performance of a fixed-PV panel, with a panel having an east west solar tracking system, additionally comparing their performance together with a panel associated with solar tracking and a spray water cooling system, at various setpoint temperatures. As mentioned previously, the experiments were carried out between July and August from 8:00 to 15:00 in Erbil-Iraq. The difference in solar radiation falls over fixed and tracking PV panels on 2nd August is presented in Fig. 5-3. It is evidence that there is a marked disparity in the solar radiation of fixed and tracking panels in the morning, which is 300 W/m², this discrepancy lessens until 13:15, when the solar radiation of fixed and tracking panels is equal, as the panel orientation using the tracking system is always perpendicular to the beam solar radiation, while the fixed panel only has the beam solar radiation perpendicular to its surface at noon. The variation in solar irradiance between fixed and tracking panel for 7th, 17th and 18th July are presented in Appendix B.

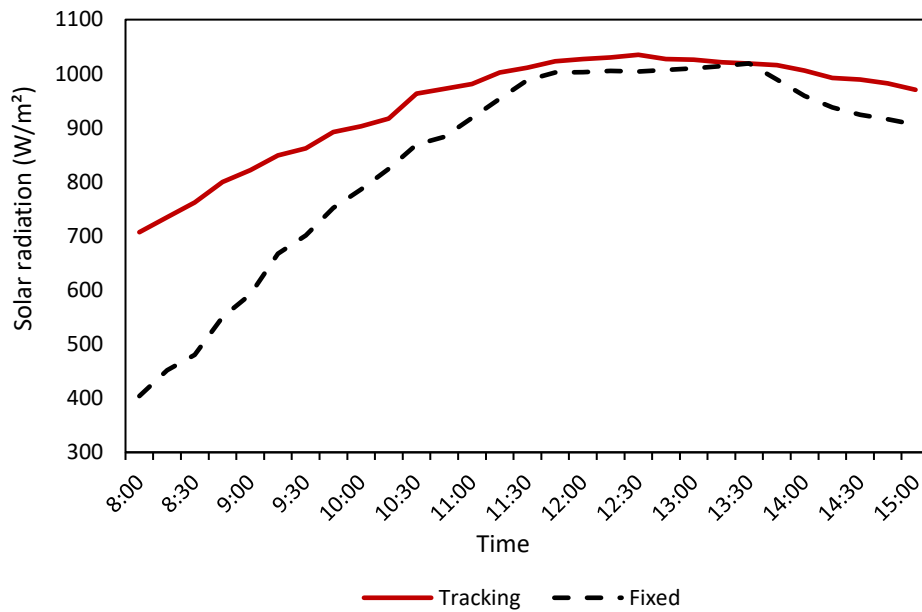


Fig. 5-3 Solar radiation intensity difference between fixed and tracking panel 2nd August

The ambient temperature variation on July 7th, 17th and 18th and August 2nd, 2022 is presented in Table 5-2, the maximum ambient temperature for Erbil city in July and August is between 13:45 to 14:15, while the minimum was at 8:00 AM. The highest recorded ambient temperature was on 2nd of August as it was 50.7 °C.

The difference between fixed and tracking panel surface temperatures without using cooling techniques on 2nd of August is illustrated in Fig. 5-4. The tracking panel displayed a higher surface temperature than the fixed panel, due to its ability to follow the sun's rays from east to west, resulting in a higher rate of thermal flux across its surface. The highest surface temperature was at 14:30 for both panels with a highest difference between both panels 7 °C, and the lowest is 1.5 °C at 8:00 were there was the lowest ambient temperature.

Table 5-2 Recorded ambient temperature on 7th, 17th & 18th July and 2nd August at Erbil City

Time	7th July	17th July	18th July	2nd August
8:00	39.7	38	39	39
8:15	40.1	38.3	39.8	39.6
8:30	41	38.7	40.9	40.4
8:45	41.5	39.2	41.4	41.8
9:00	41.7	39.5	41.8	42.5
9:15	42.2	40.9	42	42.9
9:30	42.5	41.5	42.2	43.2
9:45	43.2	42.3	43.5	43.4
10:00	43.4	43	43.8	43.9
10:15	43.5	43.5	44.3	44.6
10:30	43.6	44	44.8	44.9
10:45	43.8	44.8	45.7	45.5
11:00	44.2	45.4	46.3	46.6
11:15	44.6	45.8	46.8	47.3
11:30	44.6	46.7	47.3	47.4
11:45	44.7	46.9	47.5	47.4
12:00	44.8	47.3	47.7	47.5
12:15	44.8	47.4	47.8	48.5
12:30	45	47.4	47.8	48.7
12:45	45.2	47.9	47.9	49
13:00	45.8	47.9	47.9	49.2
13:15	46.1	48.1	48.1	49.8
13:30	46.4	48.3	48.3	50.3
13:45	47.2	48.7	48.3	50.4
14:00	47.3	48.5	48.2	50.5
14:15	47.1	48.3	48.2	50.7
14:30	46.5	48.1	47.9	50.3
14:45	45.9	48	47.2	49.9
15:00	45.5	47.9	46.4	49.5

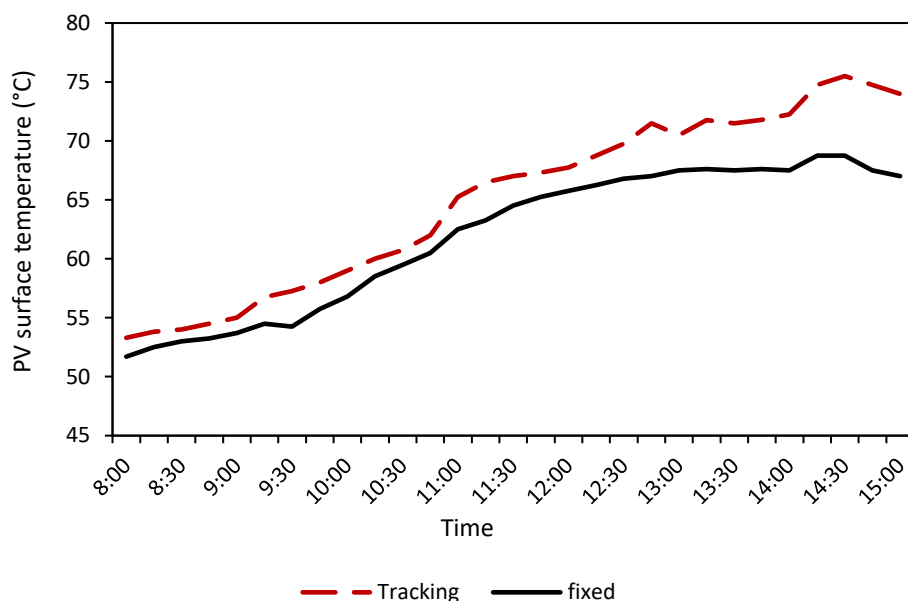


Fig. 5-4 surface temperature difference between fixed and solar tracking panel on 2nd August

The performance of the photovoltaic system was evaluated using various set temperatures, with the valve opening being controlled by a temperature sensor placed on the back of the panel, and the pump set to start pumping water at 1.8 l/min. If the surface temperature is not within the set temperature after two minutes, the flow rate will be increased by approximately 1 l/min and so on until it reaches the maximum flow rate at about 5.3 l/min. However, if the surface temperature is equal to the set temperature, then the pump will cease operation and the flow rate will register as zero. Once the surface temperature rises above the set temperature then the pump will resume spraying water over the panel.

Fig. 5-5 illustrates the water pump's behavior when the setting temperature was 45 °C, 40 °C and 35 °C. At 45 °C setpoint temperature the water is pumped over the panel until it reaches 4 or 3 l/min, and then it stops for a while before starting up again when the surface temperature exceeds the set temperature, while when the set temperature is 40 °C at the morning, the pump cycles is turning on and off with a more frequently than when set to 45 °C. by 10:22, the pump had been running continuously as the surface

temperature had not dropped below the setting temperature. On the other hand, at 35 °C the pump also runs continuously as the surface temperature remains above the set temperature. The average water flow rate for all set point temperatures is also presented in the figure, where it was 1.8, 4.2 and 5 l/min for 45, 40 and 35 °C setting temperatures, respectively.

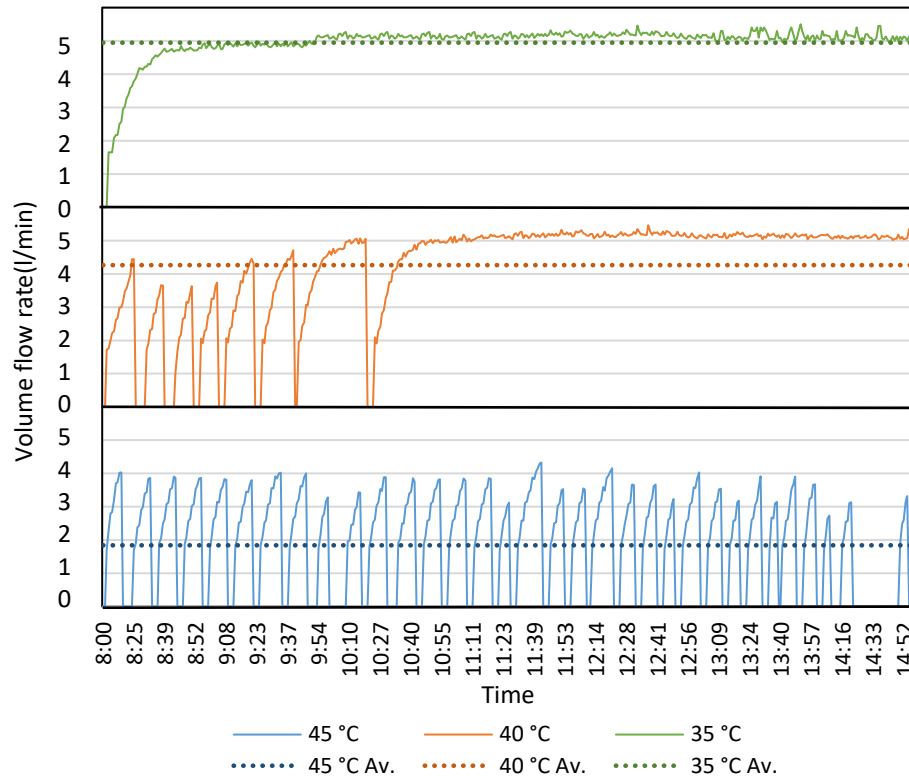


Fig. 5-5 Variation of water flow rate supply at different panel surface temperature

The variation of output power with time for fixed reference PV, solar radiation tracking PV, and tracking PV with cooling at setting temperatures of 45 °C, 40 °C, and 35 °C are presented in Fig. 5-6. Remarkably, the highest power output was observed for the tracking PV panels with cooling at 35 °C adjusted temperature, while the lowest output power was recorded for the fixed reference panel. A discernible trend from the figure is that the highest power production occurs at 12:45 for the tracking panels. Conversely, the fixed panels exhibit their highest power output at 13:30. While the lowest power output was observed in the morning. This substantial disparity between the fixed and tracking panels can be attributed to the varying solar radiation received. As

solar radiation increases, the current produced by the panels also increases, resulting in higher power production. Additionally, the PV voltage increases by decreasing the temperature, which also results in further enhancing power output. Hence, the tracking PV panels with a set point temperature of 35 °C demonstrate the highest power production.

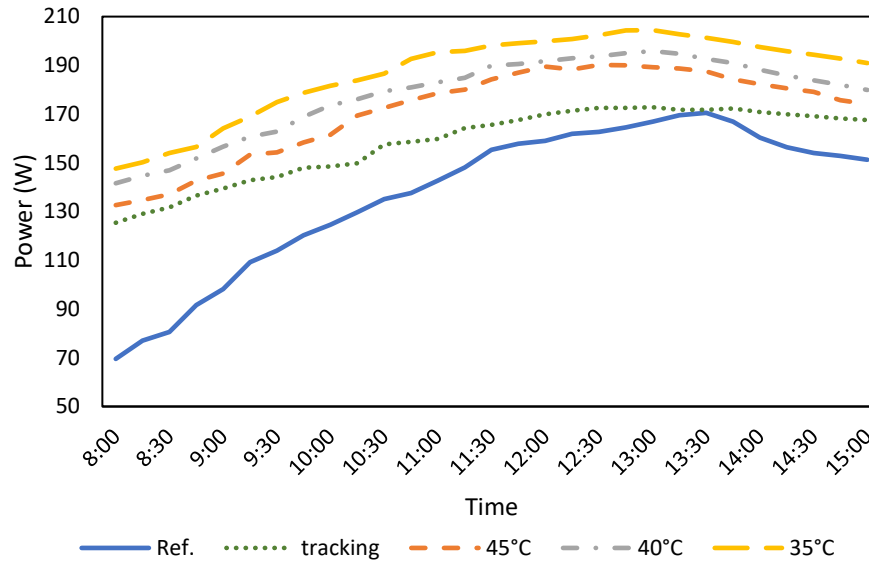


Fig. 5-6 Variation of PV power production with time using tracking and setpoint temperature

The variation in electrical efficiency with time for various modifications relative to the reference panel is visually presented in Fig. 5-7. The calculation of electrical efficiency, as per equation (3.17), highlights that the electrical efficiency is directly proportional to power and inversely proportional to solar radiation. Consequently, the fixed reference panel exhibited lower efficiency during periods of high solar radiation. In contrast, the tracking solar panel demonstrated a smaller variation in efficiency due to the continuously receiving high solar radiation. Notably, when water was utilized, efficiency increased, reaching its peak at the lowest setpoint temperature. This can be attributed to the higher voltage output achieved at lower temperatures.

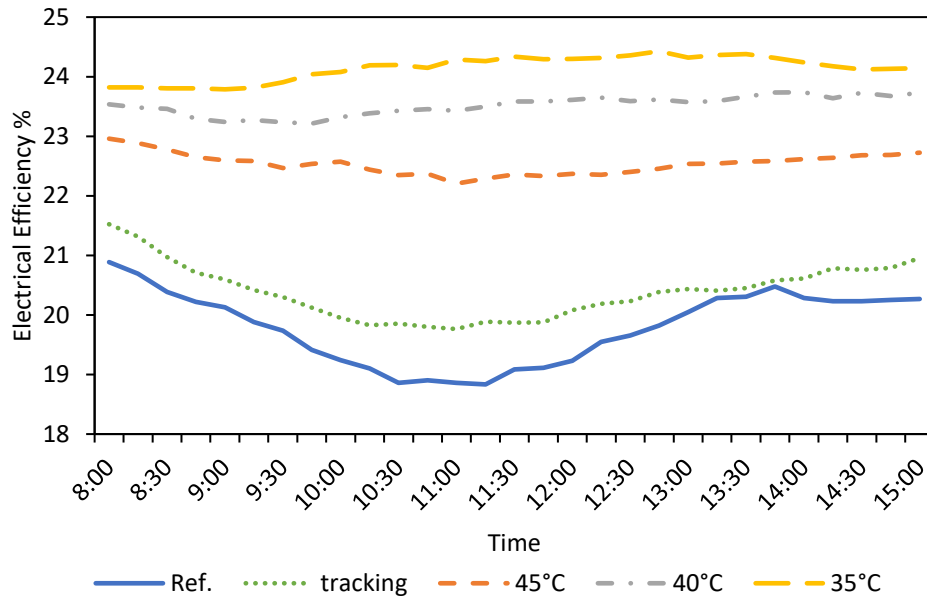


Fig. 5-7 Variation of PV electrical efficiency with time using tracking and setpoint temperature

As per equation (3.19) that was used to calculate the fill factor of the PV panel it is evidence that it is directly proportional to the power and inversely proportional to both open circuit voltage and short current, which is presented in Fig. 5-8. So that its variation is related to the power produced as the other two factors are constant.

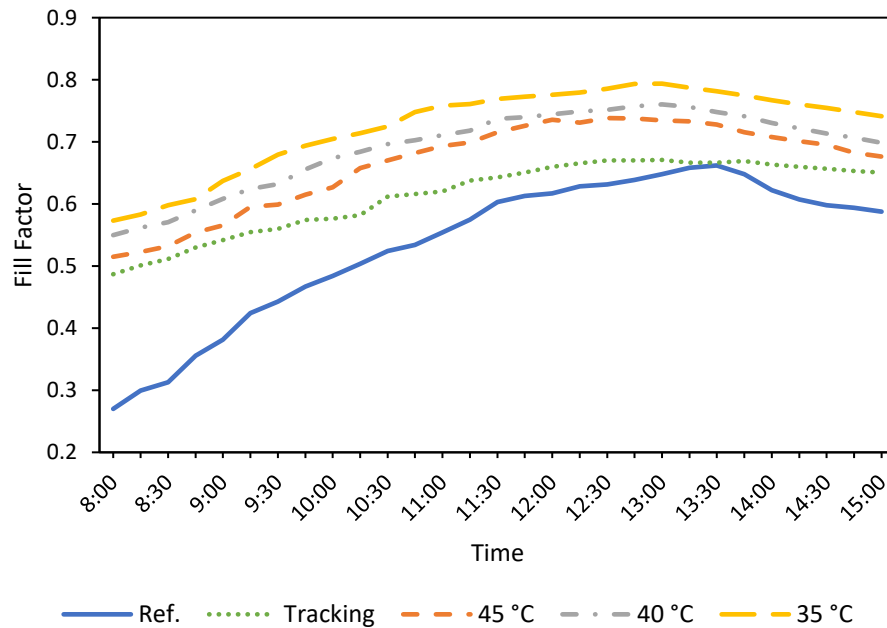


Fig. 5-8 Variation of fill factor with time using tracking and setpoint temperature

Fig. 5-9 clearly showcases the remarkable advancements made in enhancing the performance of PV panel, by comparing the electrical efficiency of fixed reference panel with tracking and tracking with cooling at 45,40 and 35 °C. Each modification's maximum performance is presented, offering valuable insights into the potential improvements achieved. By just applying an east-west tracking system the maximum PV electrical efficiency enhancement was 9.9%, on the other hand by cooling the panel at 45 °C yielded a 7.5% improvement in efficiency compared to tracking alone, while the maximum enhancement was achieved at 35 °C which was 25.11 %.

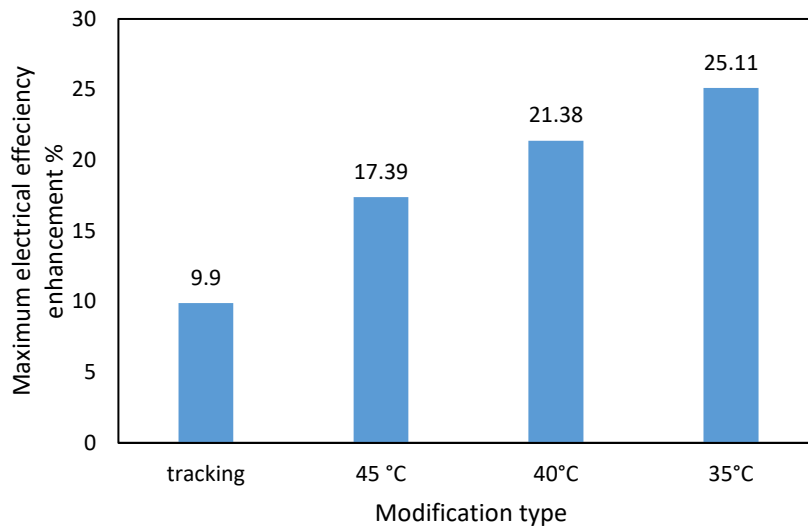


Fig. 5-9 Maximum electrical efficiency improvement at different modifications

The water consumption rate for one day and the average electrical efficiency for each set point temperature is presented in Fig. 5-10. The results observed that there is a substantial difference in water consumption between 40 °C and 45 °C, while the variation between 35 °C and 40 °C is slighter. Additionally, the electrical efficiency difference is also slighter between 35 °C and 40 °C, relative to the disparity between 40 °C and 45 °C.

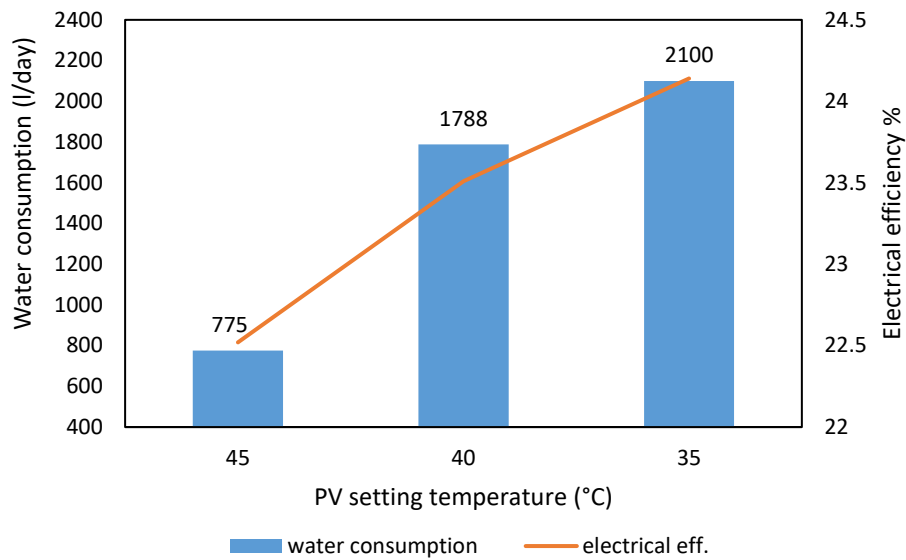


Fig. 5-10 Water consumption rate and average electrical efficiency at different PV set temperature

5.3.2 Comparison between Reference and Fixed Equipped with Cooling at Various Setpoint Temperature PV Panel

The performance of a fixed reference solar panels with fixed panels equipped with cooling mechanisms at various setpoint temperatures of 35 °C, 40 °C and 45 °C has been compared. The difference between this section and the previous one is that the tracking system was not utilized with the cooling system, as panel was fixed exactly the same as the reference panel. The test days were 19th, 21st and 24th of July, the variation in ambient temperature and solar irradiance with time during these days are presented in Table 5-3. The highest ambient temperature was 48.8 on 19th July at 14:30, while due to other two days the highest ambient temperature was at 13:30. On the other hand, the highest solar irradiance for all three days was at 12:45 with maximum irradiance recorded being on 24th July for fixed panel which was 1088 W/m².

Fig. 5-11 illustrates the behavior of the water pump under varying setting temperatures: 45 °C, 40 °C, and 35 °C. At a setting temperature of 45 °C, the pump operated for approximately 9-10 minutes before turning off for 5 minutes at early hours of the day. It then had a longer operating period of around 15-18

minutes at noon due to the elevated surface temperature, related to the higher ambient temperature and solar rays being perpendicular to the panel surface.

Table 5-3 Ambient temperature and solar irradiance on 19th, 21st and 24th of July

Time	19 th July		21 st July		24 th July	
	T _{amb.} (°C)	Irradiance (W/m ²)	T _{amb.} (°C)	Irradiance (W/m ²)	T _{amb.} (°C)	Irradiance (W/m ²)
8:00	41.5	435	40.6	455	40	430
8:15	42	465	40.9	495	40.5	478
8:30	42.4	515	41	525	41.7	519
8:45	43	550	41.2	587	42.5	560
9:00	43.6	600	41.4	629	42.8	605
9:15	44.7	691	41.5	695	43.6	690
9:30	45	729	42.2	746	44.1	738
9:45	44.5	776	42.7	798	45	800
10:00	44.7	800	43	834	45.3	837
10:15	44.9	864	43.8	875	45.4	883
10:30	45	908	44.4	920	45.6	930
10:45	45.2	953	44.7	970	45.8	962
11:00	45.5	990	45.5	1008	46	1000
11:15	45.7	1010	45.9	1022	46.2	1029
11:30	45.7	1035	46.4	1038	46.4	1035
11:45	45.9	1055	47.2	1045	46.6	1050
12:00	46.1	1074	47.2	1060	46.9	1068
12:15	46.3	1077	47	1062	47.1	1078
12:30	46.9	1082	47.4	1070	47.1	1084
12:45	47.3	1084	47.8	1077	47.2	1088
13:00	47.6	1079	48.4	1075	47.4	1084
13:15	47.7	1052	48.3	1058	47.5	1067
13:30	47.9	1024	48.3	1038	47.7	1036
13:45	47.9	1009	48	1013	47.4	1013
14:00	48.4	962	48	955	47.3	955
14:15	48.4	906	47.7	915	47.2	919
14:30	48.8	852	47.2	855	46.5	855
14:45	47.5	788	46.7	798	46	803
15:00	46.7	750	46.2	756	45.3	755

When the surface temperature was adjusted to 40 °C, the pump turned on and off until 9:42, with a longer operating period compared to 45 °C. After that time, it began operating continuously as it was unable to decrease the surface temperature of the panel below the setpoint temperature.

On the other hand, when the setpoint temperature was lowered to 35 °C, the pump operated continuously until 9:48. The spray water employed effectively reduced the water temperature below 35 °C, causing a brief 2-minute halt in operation. The pump then resumed its operation, with longer periods compared to the other setpoint temperatures. In total, the pump turned off only five times at the 35 °C setpoint temperature.

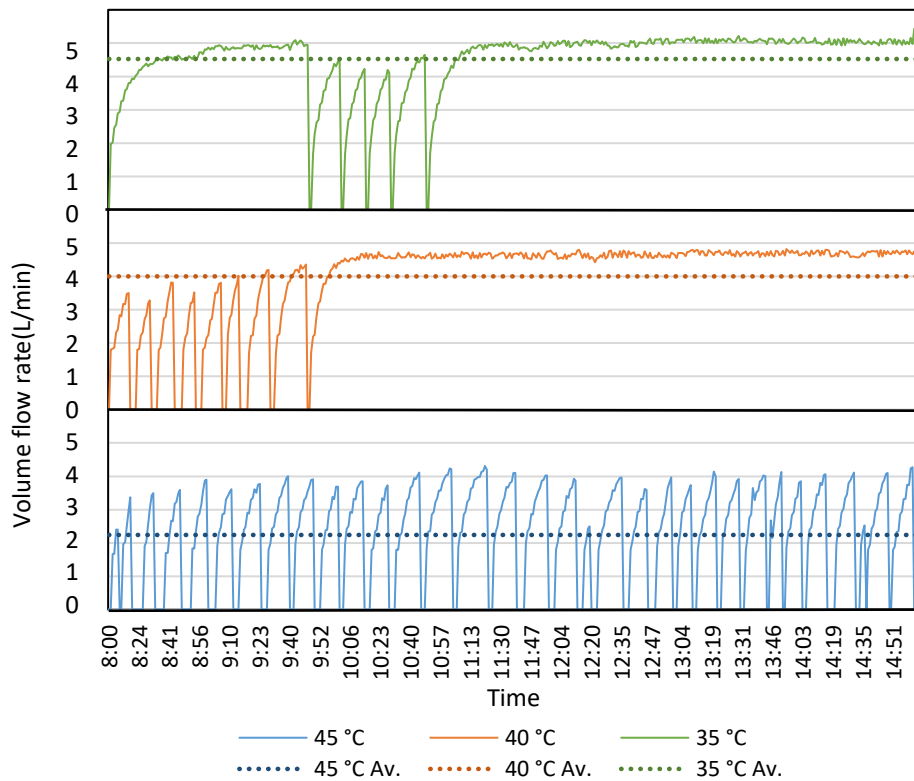


Fig. 5-11 Variation of water volume flow rate at various panel setpoint temperature

The power production variation with time for the photovoltaic panel at all three setpoint temperatures, as well as the reference temperature, is depicted in Fig. 5-12. It is evident that across all cases, the greatest power production occurred between the hours of 11:30 and 13:30, coinciding with the period of

highest solar radiation. This correlation suggests that the panel's current is maximized during this time frame, consequently leading to higher power outputs. Specifically, the power production was found to be highest when the setpoint temperature was set at 35 °C. There was only a marginal difference between the panels at different setpoint temperatures. However, when comparing the cooled panels with the reference panel, the rate of power production was notably higher.

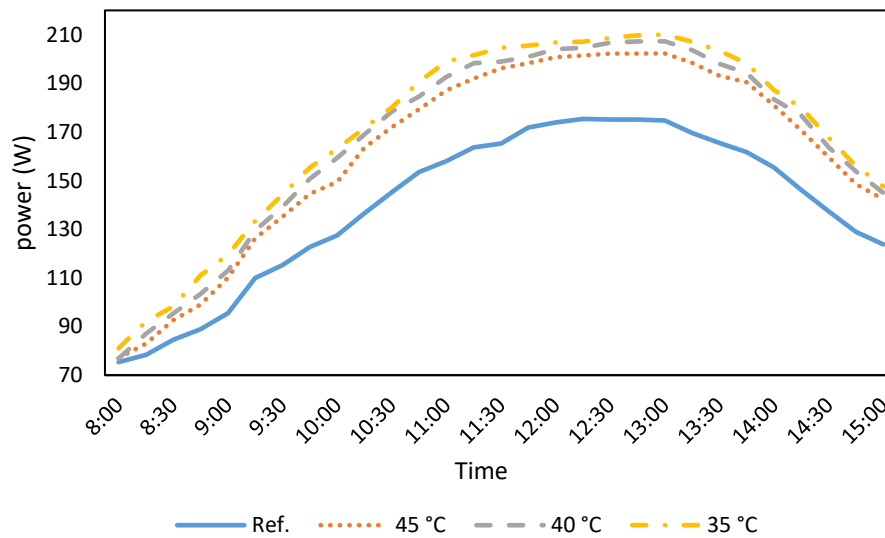


Fig. 5-12 Variation of power with time at various panel set point temperature

Fig. 5-13 shows the variation of electrical efficiency with time. The highest electrical efficiency produced by the reference panel is at 8:00 AM due to the low ambient temperature which led to higher voltage, but when the panel is cooled by spraying water and the panel temperature is reduced by about 25 to 40 °C, the electrical efficiency is higher throughout the operating hours, the efficiency is higher at a lower set point. At the hour range from 11:30 to 13:30 the electrical efficiency for all the set temperatures has a slight decrease due to the high solar radiation at that period as it is conversely proportional with the electrical efficiency, also due to high temperature as the solar ray was roughly perpendicular to the panel surface that the spray water's ability to minimize surface temperature was lower; resulting in lower voltage production.

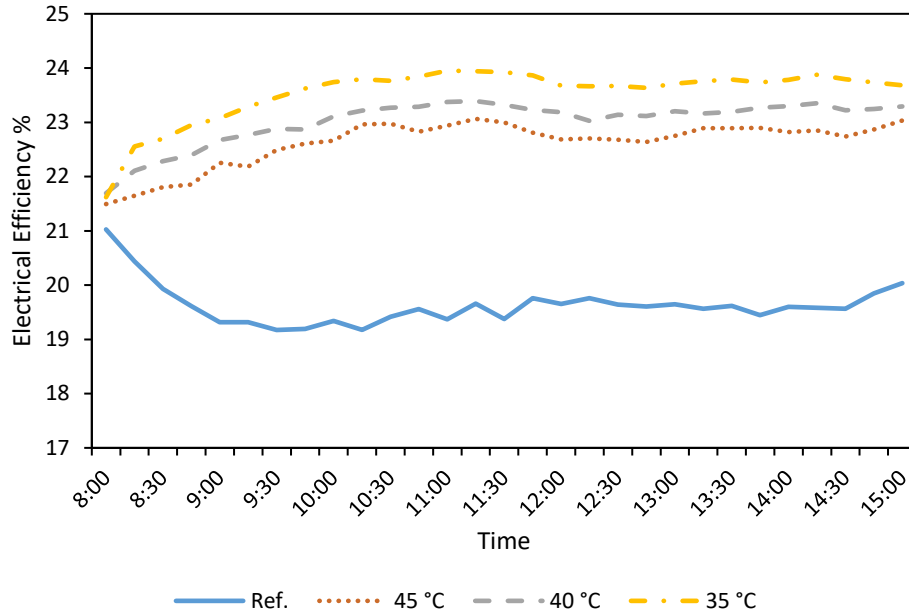


Fig. 5-13 Variation of electrical efficiency with time at various panel set point temperature

The fill factor variation with time is indicated in Fig. 5-14. The variation of fill factor is related to variation of power produce by the panel, as it is directly proportional to it. So that the fill factor trend is same as power production over time.

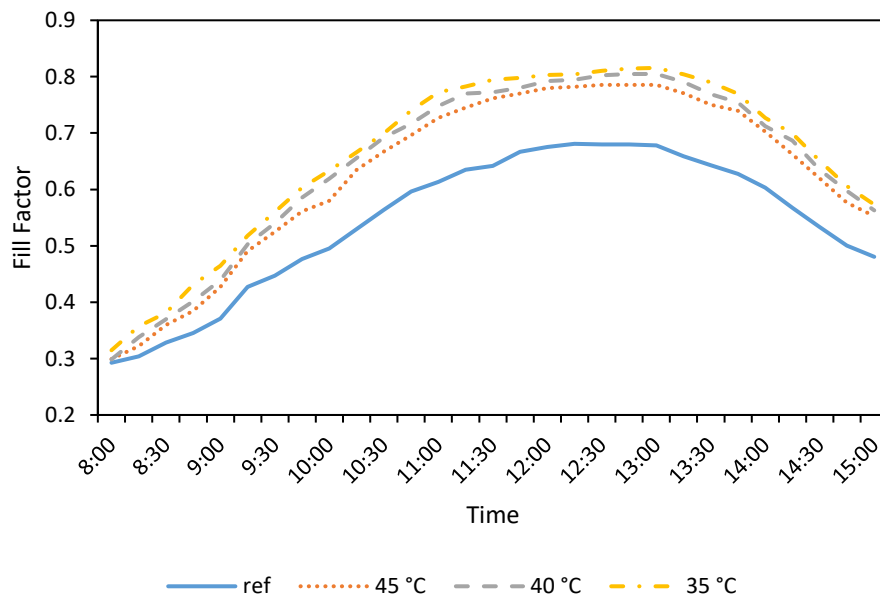


Fig. 5-14 Variation of fill factor with time at various panel set point temperature

The maximum electrical efficiency enhancement rate at different set point temperatures compared to the reference one is presented Fig. 5-15. As

depicted in the figure, the greatest improvement was observed at a set point temperature of 35 °C, which resulted in a 2.88% increase compared to the 40 °C set point. Additionally, the difference in percentage between the 40 °C and 45 °C set points was approximately 1.69.

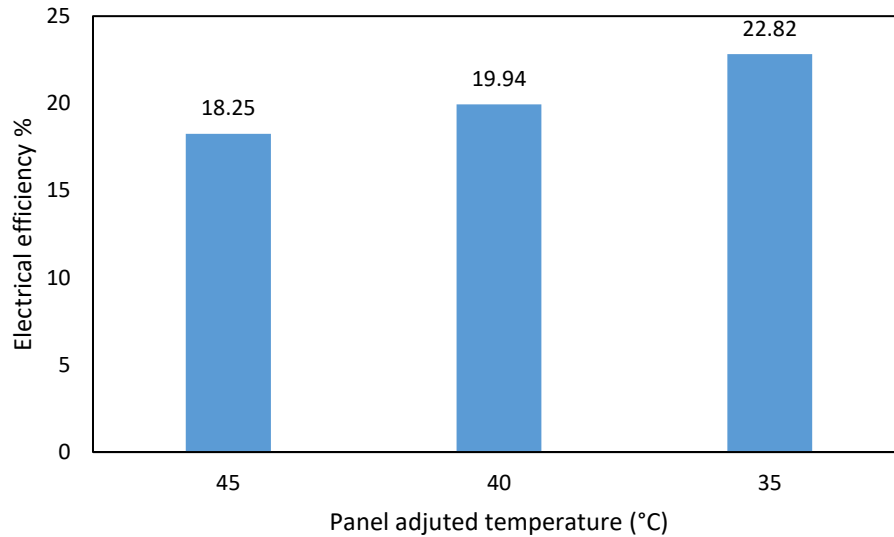


Fig. 5-15 Maximum electrical efficiency enhancement at different set point temperature

The water consumption rate for one day and the average electrical efficiency for each set point temperature is shown in Fig. 5-16 the difference in water consumption between 40 °C and 45 °C set point temperatures was approximately 740 l/day which is too high if we compare it with the difference range between 35 °C and 40 °C, as it was only 220 l/day. And this is due to the higher rate of pump operation at both setpoint temperatures of 35 °C and 40 °C as compared to 45 °C.

By comparing the rate of water consumed per day for fixed and tracking at various setpoint temperatures, it's clear from Fig. 5-10 and Fig. 5-16 that the water consumed for tracking is more than for fixed and this is due to higher surface temperature of panel tracking the solar ray. Except at 45 °C the water consumption was lower with tracking than for the fixed one, which is due to ambient temperature and solar radiation being much higher during the fixed

one compared to the tracking panel with cooling at the same setpoint temperature.

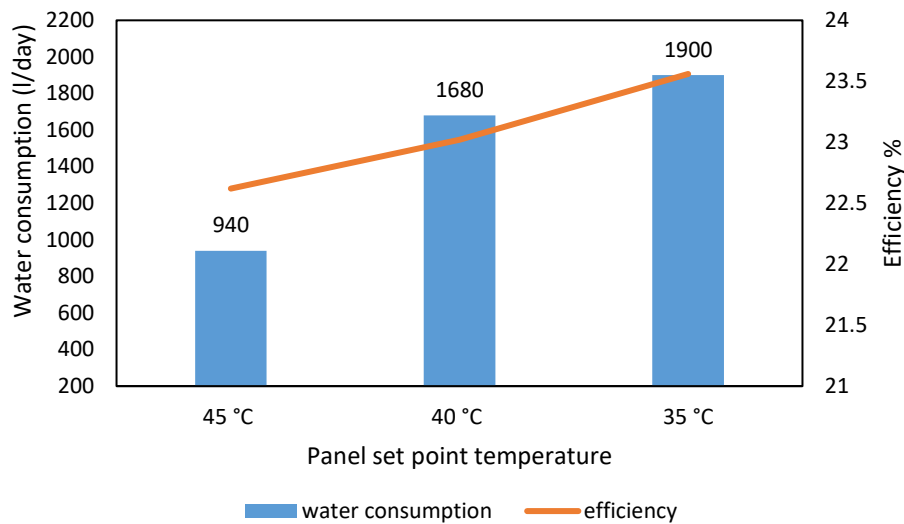


Fig. 5-16 Water consumption rate and average electrical efficiency at different PV set temperature

5.3.3 Comparison between Reference and Tracking PV Panel Equipped with Cooling at Different Volume Flow Rate

The objective of this section is to compare the performance of fixed reference panel with the panel being modified by implementing an east-west tracking system as well as a cooling system at different volume flow rate (2, 3, 4 and 5) l/min being fixed throughout the day. The test was hold on the 26th, 27th, 28th and 31st of July; the ambient temperature variation with time for these days are indicated in Table 5-4. The maximum ambient temperature was on 31st July as its minimum was at 8:00 which was 41.3 °C, while the maximum temperature was 49 °C at 14:15. The maximum ambient temperature on the 26th and 27th of July was 47 °C, but it was 47.9 °C on the 28th of July.

The difference in solar irradiance over fixed and tracking panels throughout the day from 8:00 to 15:00 on 26th July is presented in Fig. 5-17. The solar irradiance of fixed and tracking panels is approximately equal from 11:15 to 12:30. Before and after this period a huge difference exists as the tracking panel follow suns ray from east to west, so having the largest

discrepancy at the hours 8:00 and 15:00. The highest solar irradiance being recorded for a tracking system on 26th July was 1078 W/m² at 13:15. The variation in solar irradiance between fixed and tracking panel for 27th, 28th and 31st July are presented in Appendix B.

Table 5-4 Variation in ambient temperature with time on 26th, 27th, 28th and 31st of July

Time	26 th July	27 th July	28 th July	31 st July
8:00	38.7	38	38.2	41.3
8:15	39.5	38.5	38.8	42
8:30	40	39.2	39.6	42.5
8:45	40.9	39.8	40.5	42.6
9:00	41.2	41.5	41.2	43
9:15	41.6	41.8	41.7	43.8
9:30	41.9	42.3	42.5	44.3
9:45	42.5	42.5	42.5	44.2
10:00	43.2	42.6	43.4	44.7
10:15	43.5	43.7	44.2	44.9
10:30	44.2	44.2	44.5	45.2
10:45	45	44.3	44.8	45.4
11:00	45.4	44.7	45	45.5
11:15	45.4	44.9	45.3	46.3
11:30	45.5	44.9	45.9	46.7
11:45	45.5	45.3	46.5	47.3
12:00	46	45.3	46.8	47.8
12:15	46.9	45.5	46.9	48.2
12:30	46.9	46.2	46.9	48.3
12:45	47	46.9	47	48.7
13:00	46.9	47	47	48.8
13:15	46.9	47	47.2	49.2
13:30	46.8	46.5	47.2	48.8
13:45	46.3	46.4	47.9	48.9
14:00	45.5	45.4	47.7	48.9
14:15	45	46.3	47.4	49
14:30	44.9	46.2	46.7	48.7
14:45	44.8	45.7	46.4	48.3
15:00	44.6	45.7	46.3	48

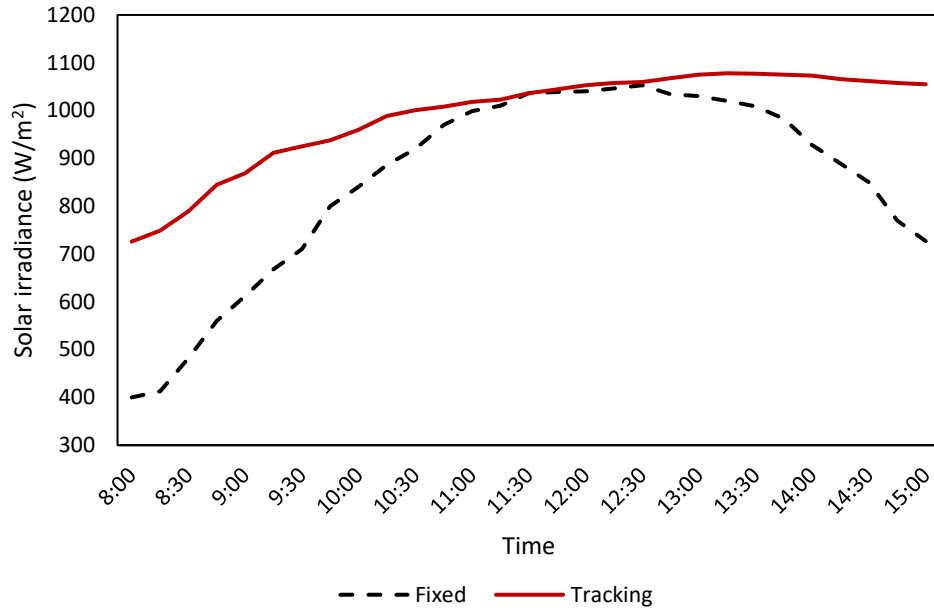


Fig. 5-17 Variation of fixed and tracking solar irradiance with time on 26th July

The variation in panel surface temperature at different water volume flow rates and at no flow rate for the fixed one with time is presented in Fig. 5-18. By setting the flow to 5 l/min the PV surface temperature was decreased by approximately 30 °C which was the highest temperature reduction while the lowest temperature reduction was at 2 l/min where the panel temperature was minimized by 23 °C.

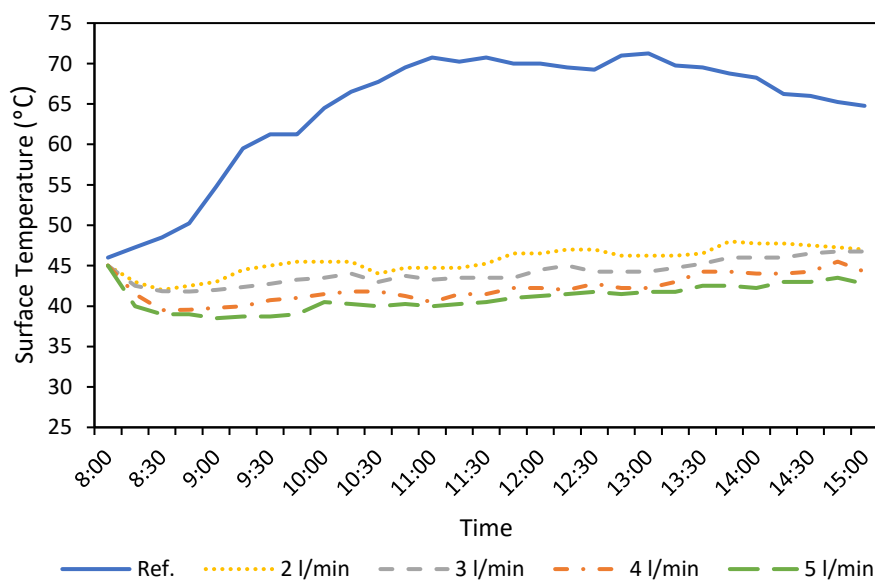


Fig. 5-18 Variation in panel surface temperature at different volume flow rate

The graph in Fig. 5-19 demonstrates the variations in power production for panels with different spray water volume flow rates, along with the implementation of a solar east-west tracking system. It is evident that there is a significant disparity in power production between the reference fixed panel and the panels equipped with tracking and cooling systems, particularly during the early and late hours of the day. This discrepancy can be attributed to the higher current generated by the tracking panel, as a result of the greater solar radiation it receives, approximately double that of the fixed panel. Furthermore, increasing the water flow rate by 1 l/min resulted in a 5 W increase in power production. For example, the power produced was 195 W at a flow rate of 2 l/min and increased to 205 W at a flow rate of 4 l/min.

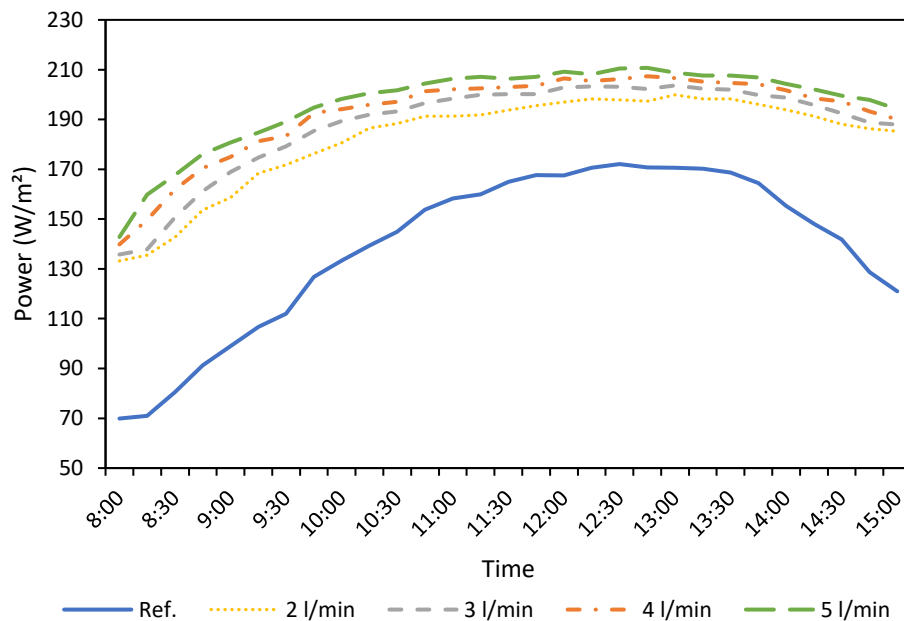


Fig. 5-19 PV power production at various water flow with solar tracking system

The variation in fill factor at different flow rates in addition to tracking system is indicated in Fig. 5-20. Also, the trend is the same as power as mentioned in the last section. The fixed panel curve is sharp while tracking with cooling has almost a straight curve. With a maximum fill factor of 0.82 being at 12:45 with a flow of 5 l/min, while it was 0.76 for the 2 l/min at the same time.

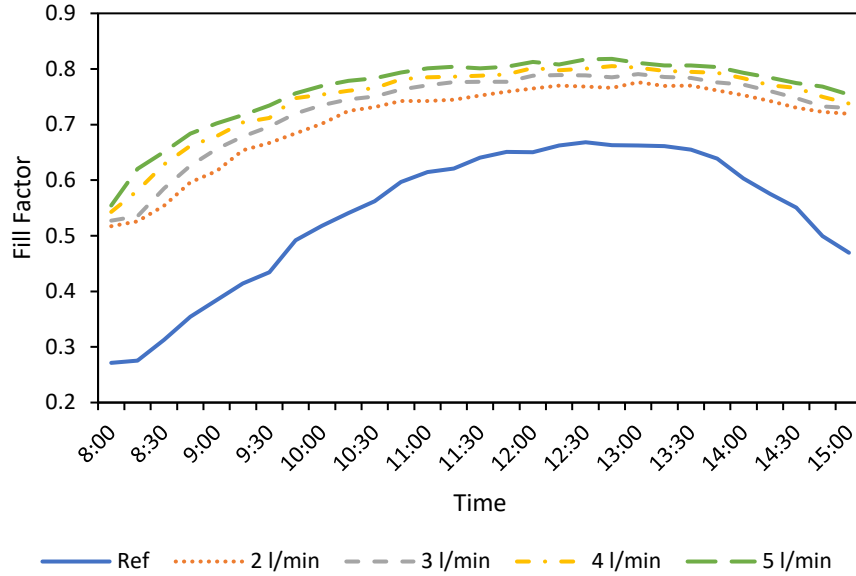


Fig. 5-20 Variation in fill factor of the panel at various water flow

The graphical representation in Fig. 5-21 demonstrates the variation in electrical efficiency at various water flow rates, in addition to the solar tracking system compared to the reference panel without tracking system. It is evident that the electrical efficiency of the tracking system, when combined with cooling, surpasses that of the fixed system. However, there is a slight decline in electrical efficiency for all cases when there is a high solar irradiation falling over the panels, for the tracking panel after 11:00 when the solar radiation is over 1030 W/m^2 , and also due to a high ambient temperature. Conversely, the fixed panel exhibits its lowest electrical efficiency during periods when the sun's rays align perpendicularly to the panel's surface.

The variation in average daily electrical efficiency and power production at 2, 3, 4 and 5 l/min is presented in Fig. 5-22. The lowest power produced was for fixed panel which was 138 W, while by using tracking with only 2 l/min spray water cooling the panel power production was 182.31 W. and by increasing the volume flow by 1 l/min the power was increased by approximately 5 W each time. On the other hand, the electrical efficiency for the fixed panel was 19.82 while by using tracking with cooling at 5 l/min the electrical efficiency was maximized to 23.49%.

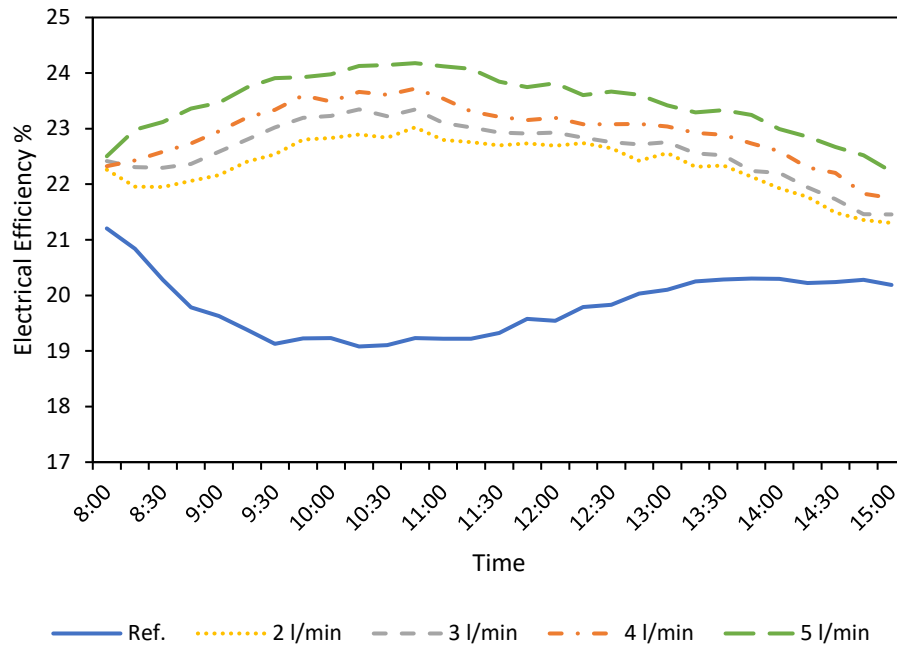


Fig. 5-21 Variation in electrical efficiency of the panel at various water flow

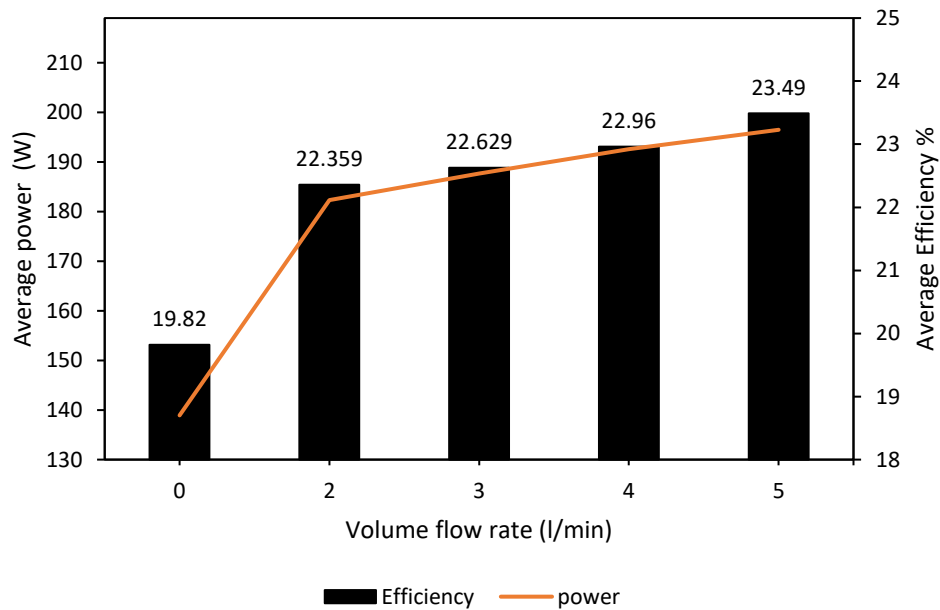


Fig. 5-22 Average daily efficiency and power production at different water flow rate with a tracking system

5.3.4 Comparison between Reference and Fixed PV Panel Equipped with Cooling at Different Volume Flow Rate

The objective of this section is to evaluate the effect of different water volume flow rates (2, 3, 4, and 5 l/min) on cooling a fixed panel, as compared

to a reference panel without a cooling system. The experimental tests were conducted on the 7th, 9th, 10th, and 11th of August 2022.

To provide a comprehensive understanding of the experimental conditions, the ambient temperature and solar irradiance levels were monitored throughout the duration of the experiments. Table 5-5 presents the variation in ambient temperature and solar irradiance recorded over the fixed panel during the experimental days. The highest ambient temperature recorded during the experimental period was 48 °C on 7th of August at 13:00. Conversely, the lowest ambient temperature was 36 °C on the 11th of August at 8:00. Regarding solar irradiance, the lowest recorded value was 400 W/m² at 8:00 on the 9th of August. In contrast, the highest solar intensity recorded during the experiments was 1050 W/m² on the same day at 12:45. Moreover, it was observed that the solar irradiance consistently exceeded 1000 W/m² approximately at 11:30 throughout all experimental days.

The reference panel surface temperature compared to the surface temperature of the PV module equipped with a spray water cooling system at various volume flow rates fixed throughout the experimental day is indicated in Fig. 5-23. The fixed panel temperature is increasing with time as its lowest temperature was 50 °C at 8:00. After that, it starts to increase as it reaches its maximum value of 71.5 °C at 12:30, after that, it starts to decrease reaching its minimum 64.75 °C at 15:00. While due to the cooled panel the surface temperature curve was almost straight at all the adjusted flows, the highest surface temperature was at 8:00 when the system started cooling and the temperature started to decrease. The lowest surface temperature was with the highest volume flow of 5 l/min, whereas the highest surface temperature was at 2 l/min. Additionally, by maximizing the flow by 1 l/min the surface temperature was minimized by 3-4 °C.

Table 5-5 Variation in ambient temperature and solar irradiance on 7th, 9th, 10th and 11th August

Time	7/8/2022		9/8/2022		10/8/2022		11/8/2022	
	T _{amb.} (°C)	I (watt/m ²)	T _{amb.} (°C)	I (watt/m ²)	T _{amb.} (°C)	I (watt/m ²)	T _{amb.} (°C)	I (watt/m ²)
8:00	39	415	38	400	36.8	440	36	425
8:15	39.7	470	38.5	457	37	504	36.2	507
8:30	40.2	530	39.2	521	37.2	539	36.7	547
8:45	41.9	605	39.8	610	38	606	37.6	604
9:00	42.3	665	40.5	645	38.6	670	38.4	672
9:15	43.3	730	41.4	739	39.7	740	39.5	733
9:30	43.6	775	42.3	786	39.2	786	39.5	784
9:45	43.7	828	42.5	823	40.5	835	39.6	828
10:00	43.8	865	42.6	870	39.8	865	39.7	865
10:15	44	895	43.7	900	41.6	897	40.5	898
10:30	44.6	936	44.2	930	43.4	926	41.8	924
10:45	44.6	965	44.3	960	44.1	955	42.2	958
11:00	44.6	993	44.7	993	44.8	981	42.7	998
11:15	45	1008	44.9	1016	45.2	998	43.5	1000
11:30	45.3	1016	44.9	1024	45.4	1004	43.5	1012
11:45	46.3	1022	45.3	1033	45.5	1012	43.9	1018
12:00	47.5	1029	45.3	1039	45.5	1020	44.5	1020
12:15	47.5	1033	45.5	1041	46.2	1022	44.8	1022
12:30	47.8	1036	46.2	1048	46.3	1026	44.9	1027
12:45	48.2	1033	46.9	1050	46.5	1023	45	1025
13:00	48	1018	47	1030	46.5	1015	45.5	1020
13:15	47.9	1015	47	1022	46.7	998	45.9	1009
13:30	47	995	46.5	1009	46.7	984	45	992
13:45	46.7	979	46.4	992	46.8	963	44.9	962
14:00	46.7	940	46.3	950	46.8	935	44.8	930
14:15	46.7	919	46.3	925	46.8	902	44.8	913
14:30	47	892	46.2	910	47.4	888	44.7	892
14:45	46.9	859	45.7	870	47.3	863	44.7	859
15:00	45.8	820	45.7	828	46.2	823	44.7	832

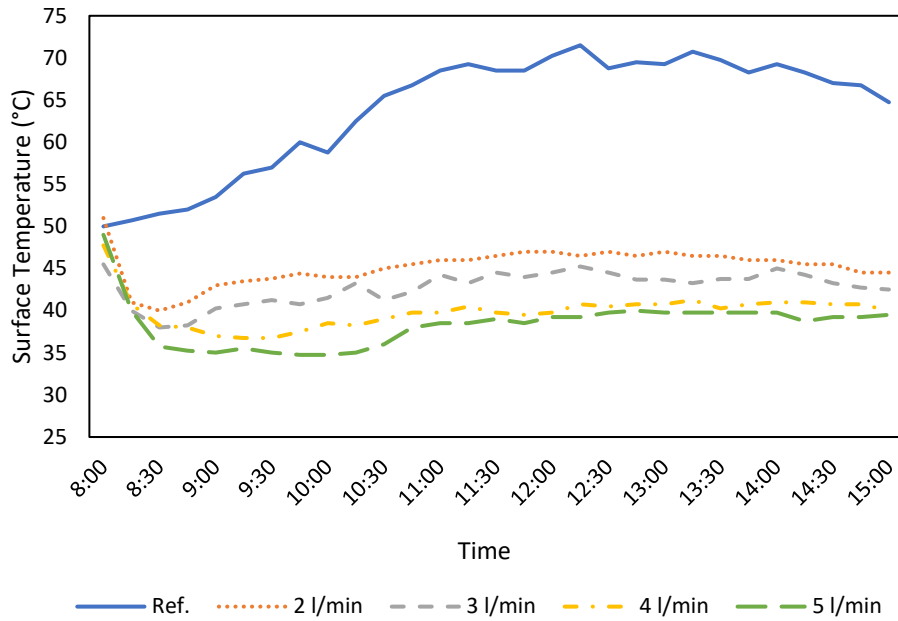


Fig. 5-23 Variation in fixed panel surface temperature at various flow

The variation in power and fill factor with time at different fixed volume flow rates are presented in Fig. 5-24 and Fig. 5-25, respectively. It is evident that there is a significant disparity in power production between the reference fixed panel and the panels equipped with cooling systems at different volume flow rate, at the beginning of the day the power and fill factors are equal as the system starts working. As the cooling continues in operation, the power production increases due to the increasing in voltage related to rate of cooling being added to the panel so the fill factor will also increase. The maximum solar radiation received by a fixed panel facing south is at noon, as this discrepancy can be attributed to the higher current generated by the panel, as a result of the greater solar radiation it receives at that time, approximately double that of the morning.

Furthermore, the power produced by fixed panel compared to the cooled one at 2 l/min is 20 W less. Increasing the water flow rate by 1 l/min resulted in a 2.4 W increase in power production. The highest power produced by the panels was 202.95 at 12:30 with the 5 l/min water volume flow rate.

On the other hand, the fill factor has the same trend of the power as it is directly proportional to it. The highest fill factor was 0.78 at 12:30 for 5 l/min flow, while the lowest value at the same time was 0.67 for fixed reference panel.

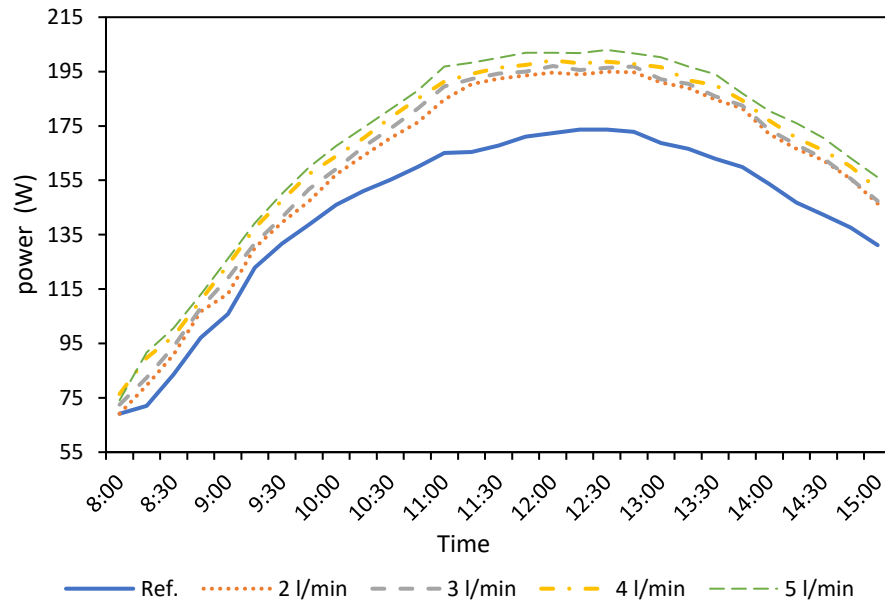


Fig. 5-24 Variation in fixed panel Power production at various flow

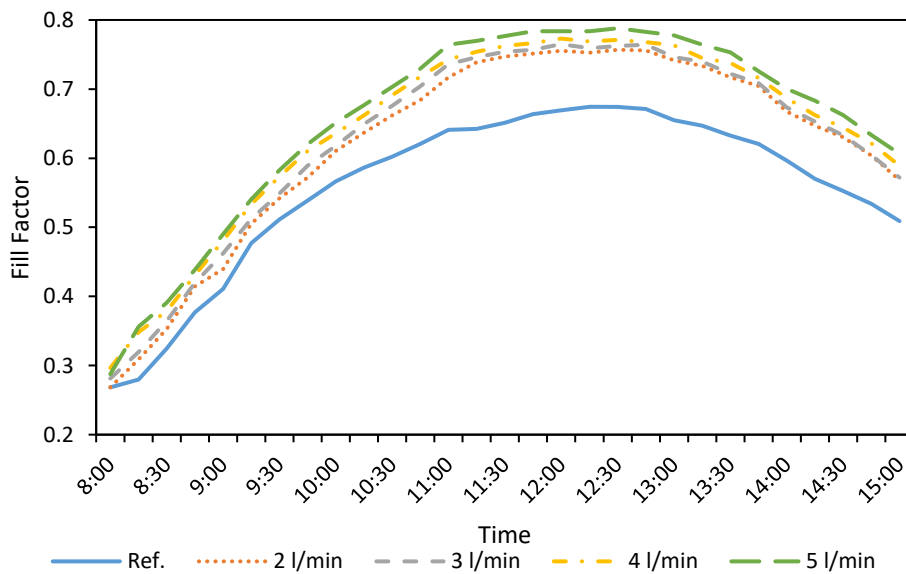


Fig. 5-25 Variation in fixed panel fill factor at various flow

The electrical efficiency at different volume flow rate variation with time is presented in Fig. 5-26. The trend of electrical efficiency with a fixed panel

differs from tracking as the solar intensity with the fixed one is lower as compared to the tracking one specifically at the beginning and the end of the day. In this case when fixed panel was cooled at fixed flow rate as the surface temperature is approximately at fixed temperature while the current increased with increasing solar radiation so the maximum electrical efficiency was recorded between 11:30 and 13:00 for the cooled panel. On the other hand, the higher electrical efficiency for reference panel was at the early morning due to lower ambient temperature. Additionally, the maximum electrical efficiency recorded was 23.97% for 5 l/min flow, while at the same time for the fixed on the efficiency was 19%.

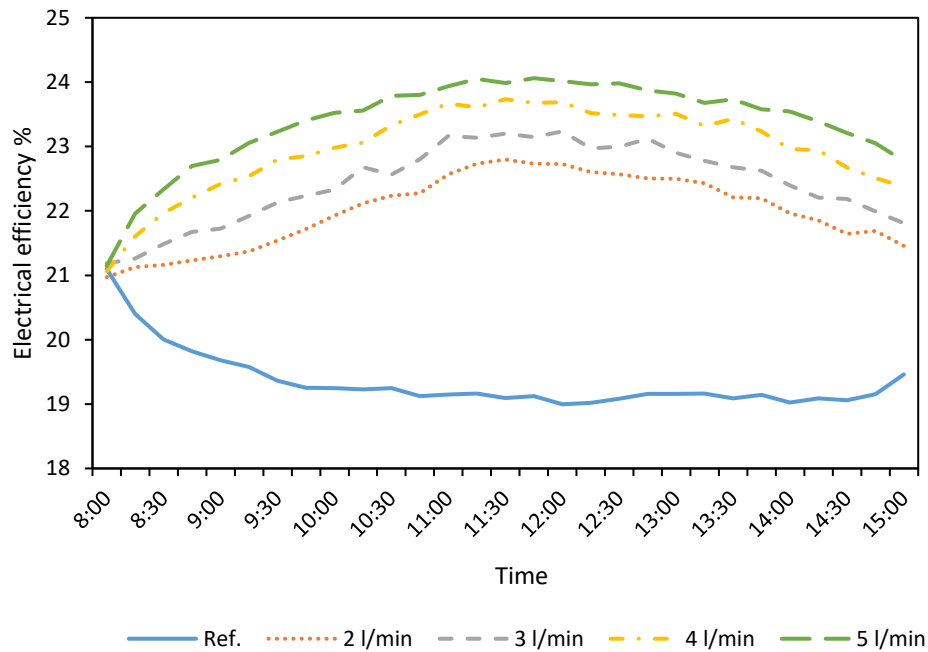


Fig. 5-26 Variation in fixed panel electrical efficiency at various flow

The average daily power and electrical efficiency for fixed panel and cooled fixed panel at different adjusted flows of 2, 3, 4 and 5 l/min is presented in Fig. 5-27. Just by spraying water at 2 l/min, the average electrical efficiency and power were increased by 3% and 21.73 W, respectively. Additionally, at the highest volume flow, the average electrical efficiency and power produced were 23.37 and 168 W, respectively.

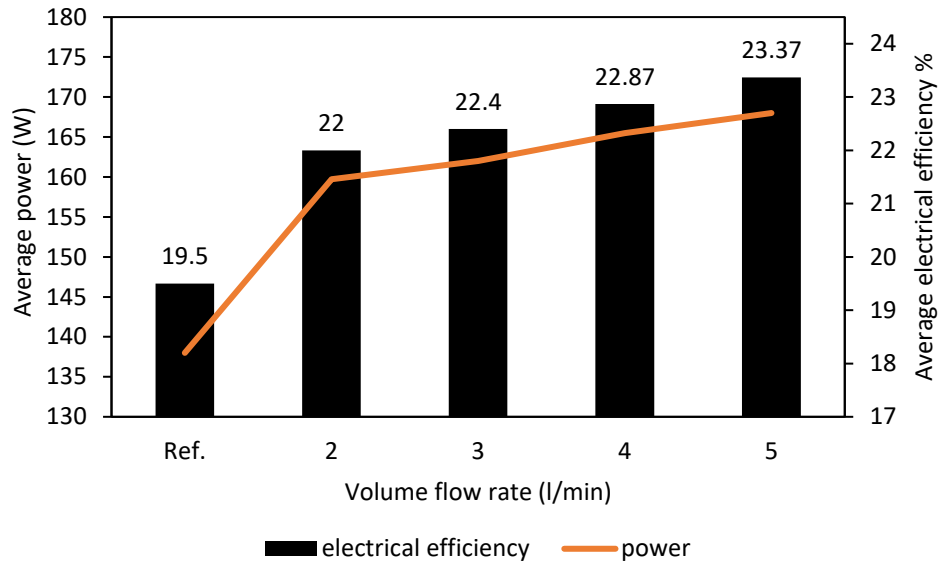


Fig. 5-27 Average daily power and electrical efficiency of fixed panel at various flow

5.3.5 PV Performance at Different Surface Temperature and Solar Intensity

This section evaluated the performance of PV panels at different surface operating temperatures and solar radiation intensities. Fig. 5-28 presents the output power and electrical efficiency of the PV panel at varying panel surface temperatures under 1000 W/m^2 solar radiation intensity. The power production sharply descended when the panel temperature exceeded 40°C . The data reveals a slight decrease in electrical efficiency when the panel temperatures ranges from 25 to 40°C , whereas by a 5°C increase in PV surface temperature was resulted in a reduction of electrical efficiency by $0.2\text{-}0.3\%$, moreover when the panel temperature exceeded 40°C , each 1°C increase in temperature was associated with 0.2% decrease in panel efficiency, this is due to the decrease in the voltage production of the panel whereas the maximum operating temperature of the panel is 80°C so that as the temperature of the panel approaches that range its ability to convert sun light to electricity decreases, as the temperature rises the electrons of the photovoltaic cell become more energetic and more likely to escape, reducing the efficiency of the panel. While Tan *et al.* (2017) observed that when the temperature on the panel exceeded 25

°C the efficiency decreased by 0.5% with each 1 °C increase in panel temperature.

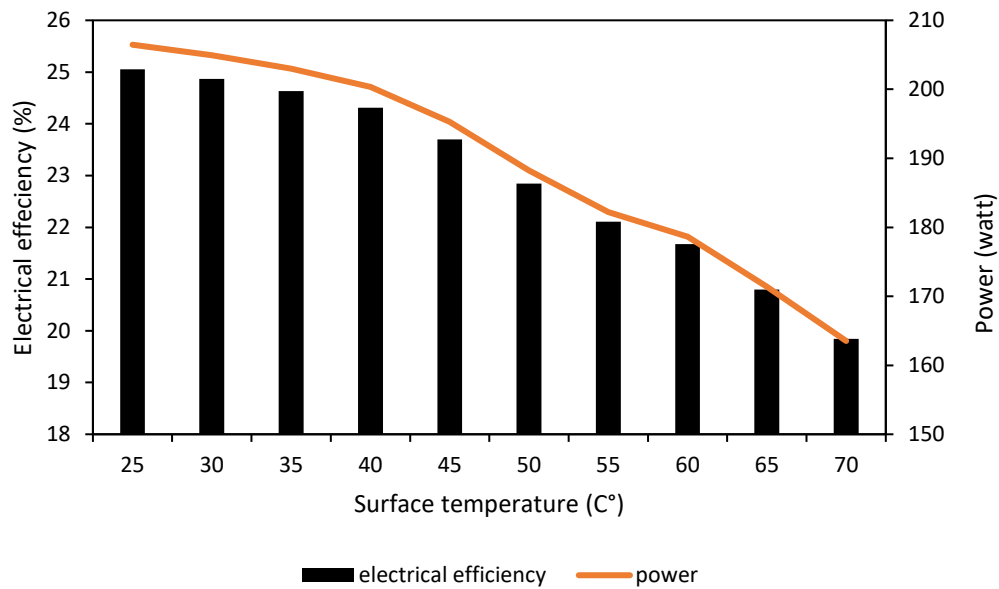


Fig. 5-28 Variation of output power and electrical efficiency with panel temperature at 1000 w/m² solar radiation

The power production of PV panels is greatly influenced by the amount of solar radiation they receive. This relationship is demonstrated in Fig. 5-29, which clearly illustrates that as the solar radiation increases from 800 to 1000 W/m², the power production of the PV panel increases by 24 watts.

Furthermore, when cooling was employed with varying setting temperatures, the power production increased farther as at 45 °C and 40 °C setpoint temperatures when the radiation increased by from 800 W/m² to 1000 W/m² the power output increased by 36 W and 41 W respectively. The most significant improvement in power production was observed at a setpoint temperature of 35 °C, resulting in a difference of 44 watts.

These findings highlight the significant effect that solar radiation and cooling systems can have on the power production of PV panels. It is crucial for researchers and industry professionals to carefully consider these factors when designing and implementing new solar energy systems.

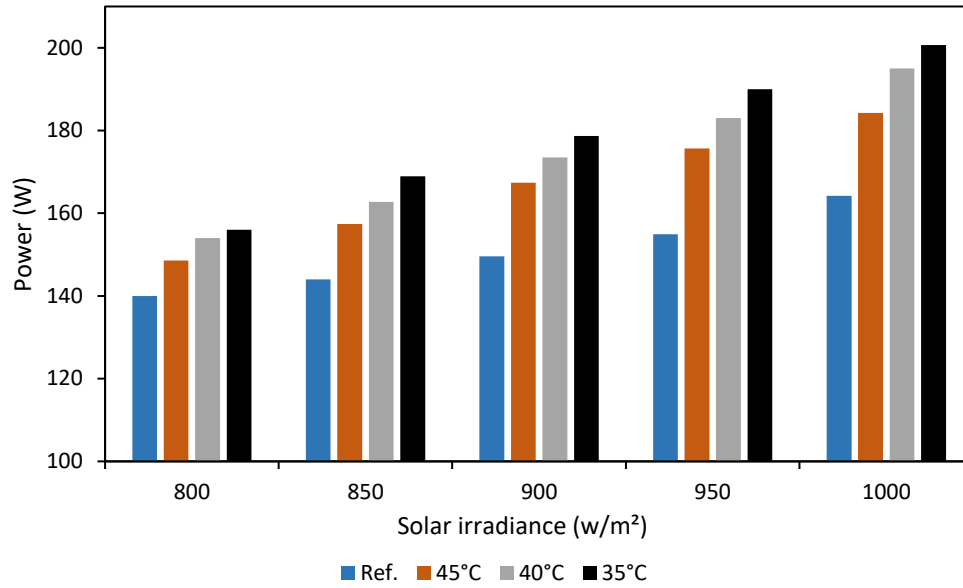


Fig. 5-29 Variation of output power with solar irradiance at different set point temperature

5.3.6 Comparative Study with Previous Literature

Throughout this study, the main focus was on maximizing the electrical efficiency of photovoltaic panels. In order to evaluate the results, a comparison the maximum improvement outcomes throughout current experiments and the previous literature. Fig. 5-30 presents the maximum electrical efficiency improvement achieved through various techniques compared to the current study.

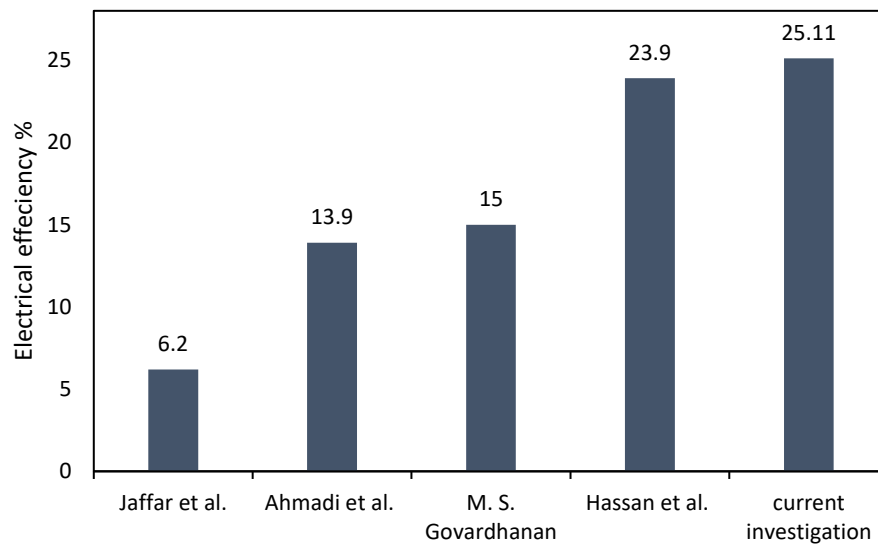


Fig. 5-30 Comparative study of maximum electrical efficiency improvement

Jaffar, Mohammad and Ahmed (2022) aimed to enhance photovoltaic panel electrical efficiency through air cooling, which resulted in a 6.20% improvement in electrical efficiency. In another study done by Ahmadi, Monadinia and Maleki (2021) PCM paraffin wax was utilized yielding an enhancement rate of 13.9%. While (Govardhanan *et al.*, 2020) tested uniform water flow over the PV panel and accomplished a 15% improvement in electrical efficiency.

In contrast, Hassan *et al.* (2020) implemented the use of nano particles with PCM and achieved an impressive electrical efficiency of 23.90%. However, the experimental results surpassed all these previous studies, by employing the water spray technique at a PV setting temperature of 35 °C, along with a solar east-west tracking mechanism. This combination led to a significant enhancement in electrical efficiency.

Therefore, this study not only provides an extensive improvement in electrical efficiency, but also offers a contribution when compared to other research works. By achieving a high percentage of electrical efficiency through this experimental approach, which sets this study apart from previous studies in this field.

5.4 VALIDATION RESULTS

The verification of simulation results is a critical step in ensuring the accuracy and reliability of computational fluid dynamics (CFD) simulations. One popular software used for such simulations is ANSYS Fluent, which is widely used in various engineering industries. In this particular case, the verification of simulation results is carried out using ANSYS Fluent for the cooling of the front surface of a photovoltaic panel using various water flow rates.

To verify the simulation results, it is essential to compare them with experimental data. This comparison not only validates the accuracy of the

simulation models but also helps in identifying any discrepancies and improving the simulation setup. In this case, experimental data was obtained by conducting a physical test at the Erbil Polytechnic University research center during the summer season, where water at different flow rates was used to cool the PV panel, and measurements of various parameters, such as surface temperature, ambient temperature, water inlet and outlet temperature, solar irradiance and flow rate, were recorded. The current simulation boundary conditions were based on the Erbil location due to its latitude and longitude. The operating conditions of verification for both experimental and ANSYS fluent data were 40 °C ambient temperature and 1000 W/m² solar irradiance.

A comparison of the two revealed that the simulation outcomes were in close accordance with the experimental ones. The simulation results were within 1.08% of the experimental results, indicating that the model was valid and reliable for forecasting the performance of solar cells.

The comparison between the surface temperature of photovoltaic (PV) panels obtained through ANSYS simulations and experimental measurements at various volume flow rates is illustrated in Fig. 5-31. The figure highlights that a slight discrepancy exists between the surface temperature values obtained from ANSYS simulations and experimental data for PV panels subjected to a volume flow rate of 2 and 3 l/min, which amounts to only 0.5 °C. This difference further decreases to 0.38 °C and 0.43 °C for PV panels subjected to volume flow rates of 4 and 5 l/min, respectively.

On the other hand, a comparison between the experimental and ANSYS Fluent outlet water temperatures at various volume flow rates is presented in Fig. 5-32. The largest observed deviation between the two datasets occurred at a volume flow rate of 2 l/min, with a magnitude of 0.6 °C. However, this disparity decreased to 0.39 °C and 0.3 °C, at volume flow rates of 3 l/min and

4 l/min, respectively. At a volume flow rate of 5 l/min, the variation between the experimental and simulation results was measured to be 0.45 °C.

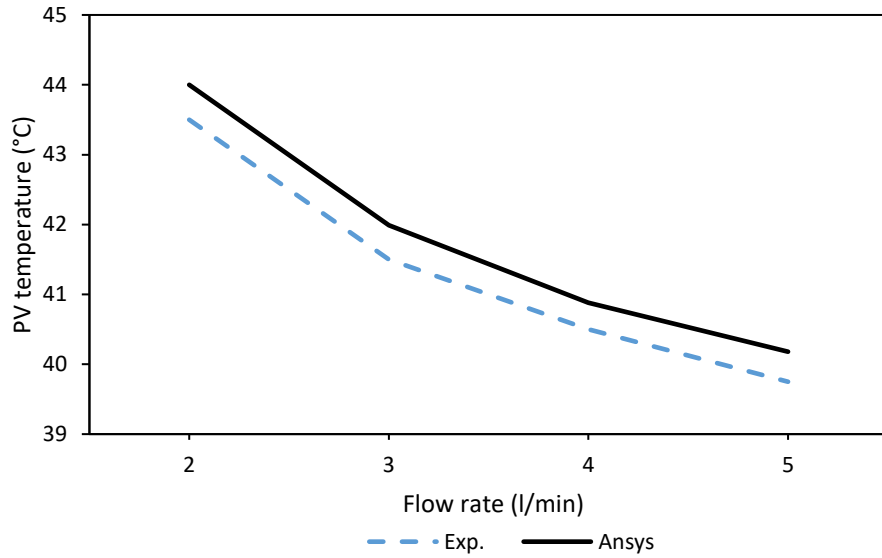


Fig. 5-31 Verification of experimental and ANSYS Fluent PV surface Temperature at various water flow rate

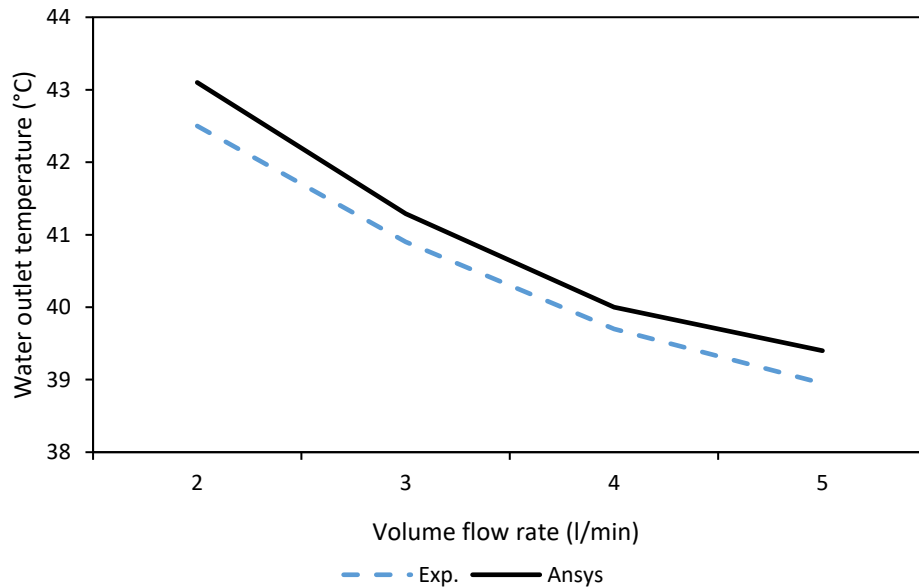


Fig. 5-32 Verification of experimental and ANSYS Fluent PV water outlet temperature at various water flow rate

The presented comparison is of great significance as it sheds light on the accuracy and reliability of ANSYS simulations in predicting the surface temperature and outlet water temperature of PV panels. It is evident from the figures that the deviation between the ANSYS simulations and experimental

measurements is minimal, which indicates that ANSYS is the most suitable simulation tool for effectively predicting the surface temperature and water outlet temperature of PV panels at various volume flow rates.

These results hold crucial implications for the field of PV panel research and development. Researchers and engineers can now make informed decisions regarding the design and optimization of cooling systems for these panels.

5.5 ANSYS FLUENT RESULTS

Computational fluid dynamics (CFD) simulations were conducted to investigate the influence of various parameters, including ambient temperature, water inlet temperature, and solar intensity, on the temperature and performance of cooled photovoltaic (PV) panels. The aim of this study was to comprehensively evaluate the behavior of cooled PV modules under varying operating conditions.

CFD is a powerful tool used to simulate and analyze fluid flow, heat transfer, and other related phenomena. In this study, CFD simulations were employed to model the behavior of water flowing over the PV panels and to calculate the resulting temperature distribution and performance of the panels.

5.5.1 Influence of Variation in Ambient Temperature

The influence of ambient temperature on the performance of cooled PV panels was investigated by varying the temperature of the surrounding environment. The ambient temperatures tested within this simulation were (35, 40, 45 and 50 °C), the water inlet temperature was fixed at 35 °C and the solar radiation at 1000 W/m². The variation in PV surface temperature at various flow rate (2, 3, 4 and 5 l/min) by varying ambient temperature are illustrated in Fig. 5-33. The figure highlights that when the ambient temperature is 50 °C, the water volume flow rate set at 2 l/min with 1000 W/m² solar irradiance and 35 °C water inlet temperature the PV surface temperature recorded is 46.6 °C,

Subsequently, when the flow rate was increased to 5 l/min under the same operating conditions, the PV surface temperature decreased by an additional 4.5 °C compared to the 2 l/min flow rate. Furthermore, at an ambient temperature of 45 °C, the minimum and maximum surface temperatures observed were 45.31 °C and 40.94 °C, respectively, with flow rates of 2 l/min and 5 l/min. Conversely, when the ambient temperature was reduced to 35 °C, and all other parameters remained constant, the PV surface temperature was lowered by 3.42 °C by increasing the water flow rate from 2 l/min to 5 l/min.

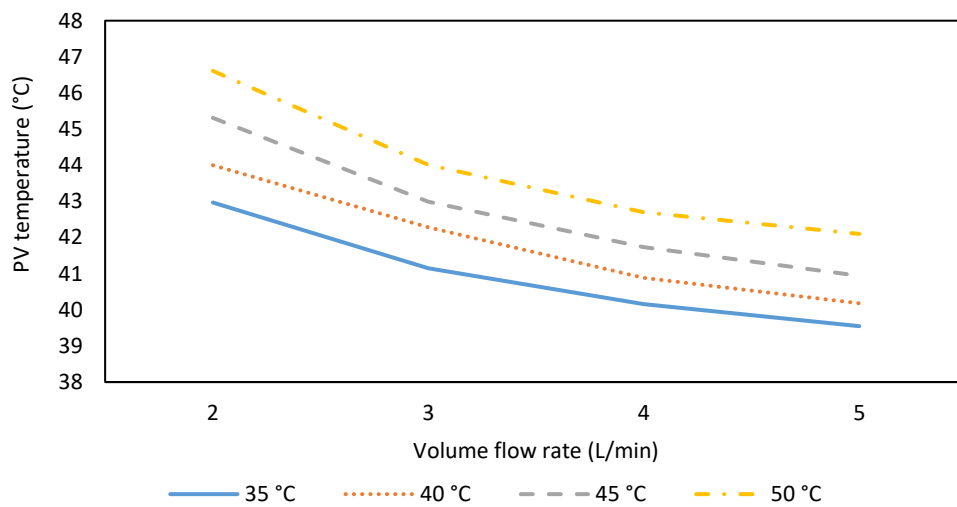


Fig. 5-33 Variation of PV temperature with flow rate at various ambient temperature

It is evident from the graph that at higher ambient temperatures, the deviation in PV surface temperature between different flow rates is bigger. This indicates that as the ambient temperature increases, the effect of increasing the water volume flow rate on the PV surface temperature becomes more significant. On the other hand, at lower ambient temperatures, the impact of increasing the water flow rate on the PV surface temperature is relatively smaller.

The power production of the PV panel was analyzed in relation to the flow rate and ambient temperature, as illustrated in Fig. 5-34. The lowest power output recorded was 176.69 W at 50 °C ambient temperature and 2 l/min volume flow rate, subsequently, when the ambient temperature was reduced to

35 °C while maintaining the same flow rate the PV power output enhanced by just 3.2 W.

In contrast, at a volume flow rate of 5 L/min, the panel was able to produce 180.66 W at an ambient temperature of 50 °C and 182.91 W at an ambient temperature of 35 °C. This graph clearly demonstrates that the impact of high ambient temperatures on the power output of a cooled PV panel is minimal, particularly when the panel is cooled at a high-volume flow rate of 5 L/min. Increasing the ambient temperature by 5 °C resulted in a decrease in power production of only 0.56 W to 0.98 W in the range of 35 °C to 50 °C ambient temperatures.

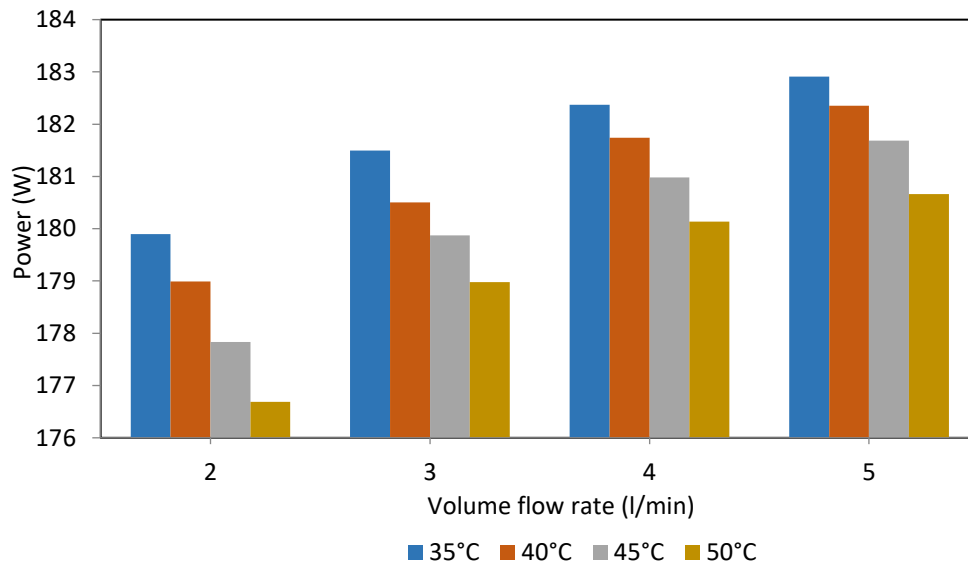


Fig. 5-34 Variation in PV power with flow rate at various ambient temperature

In Fig. 5-35 the electrical efficiency was analyzed in relation to water volume flow rate and ambient temperature, whereas the lowest panel electrical efficiency recorded was 22.56 % at 50 °C ambient temperature and 2 l/min flow rate but when the ambient temperature was minimized by 15 °C, while maintaining the flow rate, the electrical efficiency was enhanced by only 0.41%.

On the other hand, the highest efficiency recorded was 23.36 at 35 °C ambient temperature and 5 l/min volume flow, subsequently, when the ambient

temperature was maximized to 50 °C at the same flow rate, the electrical efficiency was minimized by just 0.29%.

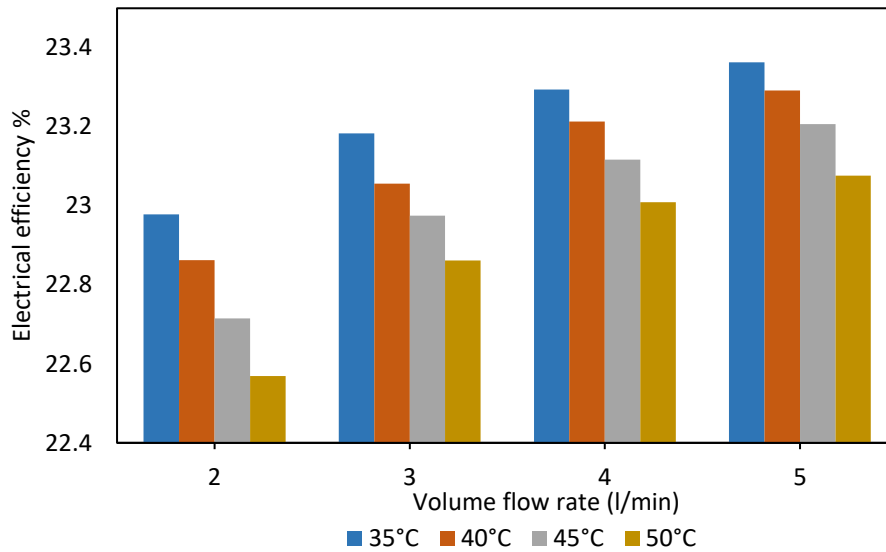


Fig. 5-35 Variation of PV efficiency with flow rate at various ambient temperature

The contour of temperature distribution of water over the panel surface at 35 °C ambient temperature, 1000 W/m² solar irradiance and 35 °C water inlet temperature at volume flow rates (2, 3, 4 and 5 l/min) are shown in Fig. 5-36. The figure shows how the temperature distribution of water change by varying its volume flow rate, as the water flow increases the variation in temperature decreases, due to the reducing surface temperature of the panel.

The variation in surface temperature of uncooled photovoltaic panel at different ambient temperatures when solar radiation was fixed at 1000 W/m² is illustrated in Fig. 5-37. The graph clearly shows that at the effect of ambient temperature on uncooled panels is very high as at 35 °C ambient temperature the PV panel surface temperature was 64.24, additionally when the ambient temperature was increased to 50 °C the PV temperature was maximized as well to 76.91 °C.

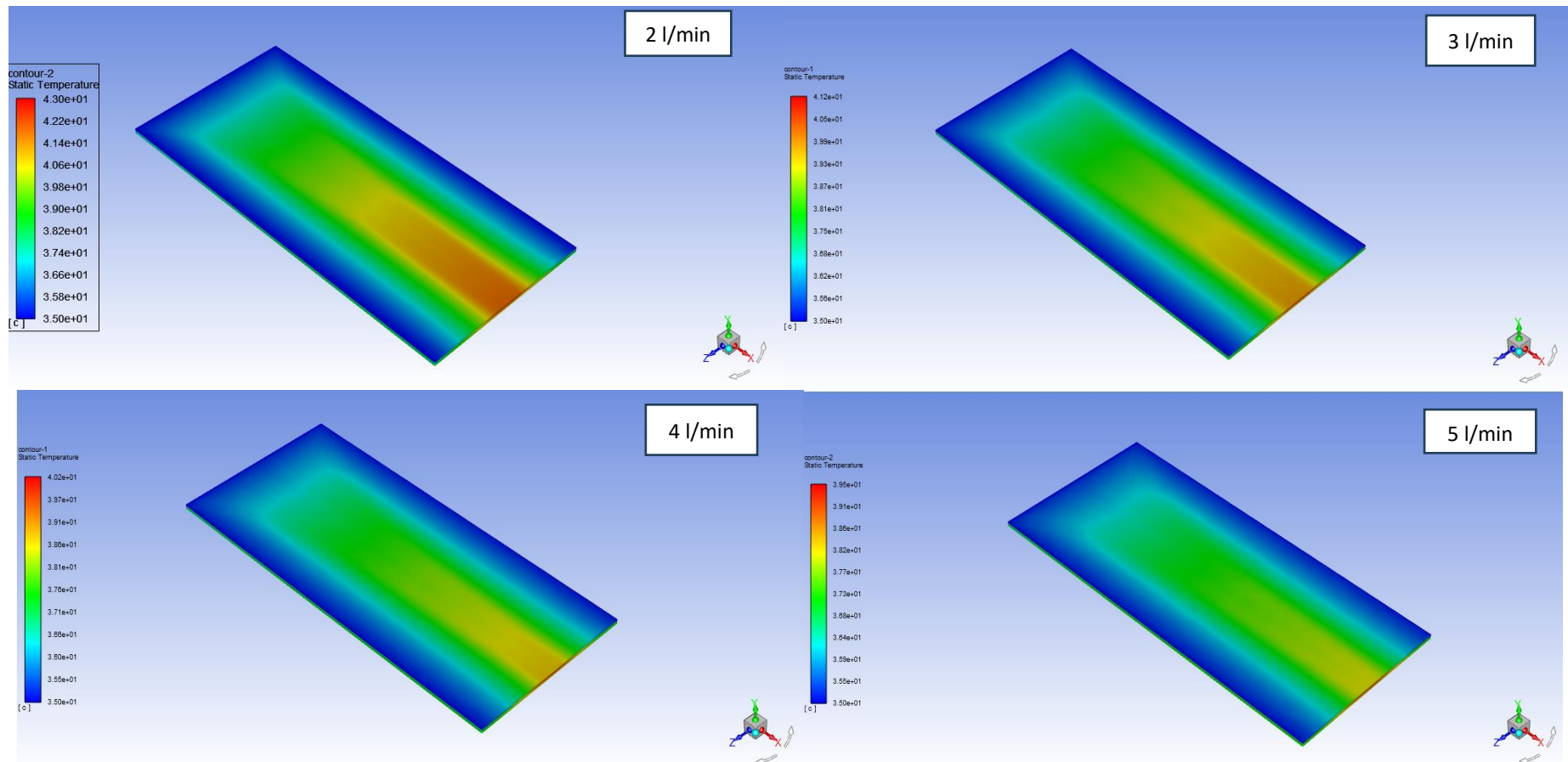


Fig. 5-36 Variation in water temperature distribution at 35 °C ambient temperature at various flow rates

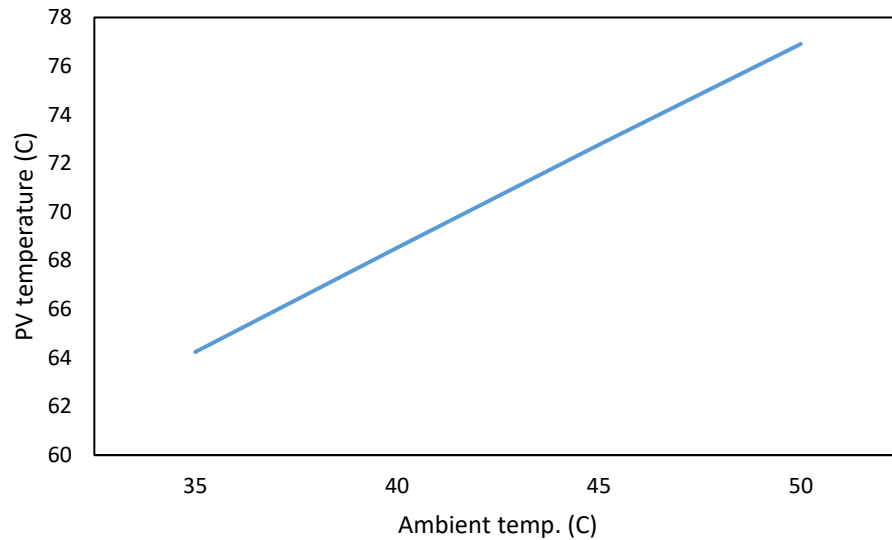


Fig. 5-37 Variation in surface temperature of uncooled PV with ambient temperature at 1000 W/m²

The variation in electrical efficiency and power production of uncooled solar panel in relation to various ambient temperatures at 1000 W/m² is presented in Fig. 5-38. It is clear from the figure that both power and electrical efficiency are hugely influenced by increasing ambient temperature when the cooling is not exist, whereas by maximizing the ambient temperature from 35 °C to 50 °C the power production and electrical efficiency decreased by 11.16 W and 1.48%, respectively.

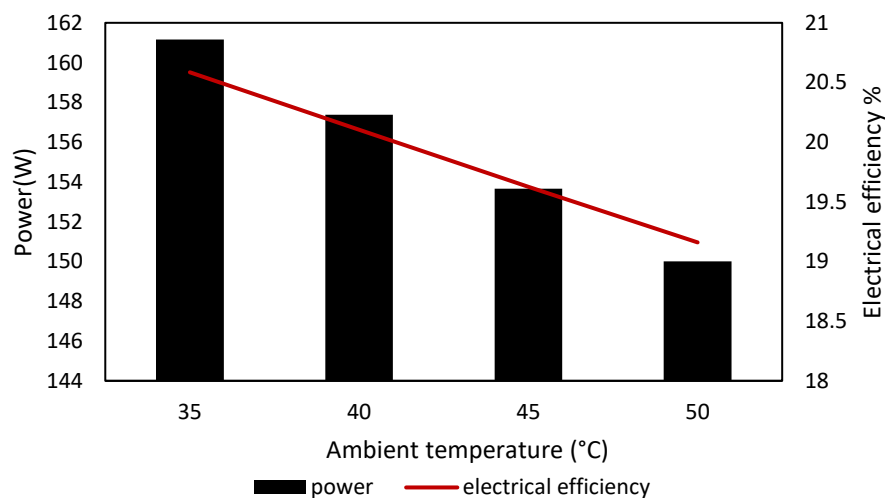


Fig. 5-38 Variation in power and electrical efficiency of uncooled PV with ambient temperature at 1000 W/m²

5.5.2 Influence of Variation in Solar Irradiance

This section presents and discusses the effect of variation in solar irradiance on the PV panel surface temperature at various volume flow rates when the ambient temperature and water inlet temperature were fixed at 40 °C and 35 °C, respectively as presented in Fig. 5-39. At a water volume flow rate of 2 l/min and a solar irradiance of 600 W/m², the PV surface temperature was measured at 40.49 °C. In comparison, when the solar irradiance was increased to its maximum value of 1000 W/m² at the same volume flow rate, the surface temperature only increased by 3.51 °C.

Furthermore, at a volume flow rate of 5 l/min and a solar irradiance of 1000 W/m², the PV surface temperature was found to be 40.18 °C. By reducing the solar irradiance to 600 W/m² while maintaining the other operating conditions, the panel temperature decreased by 2.1 °C.

Its evidence from the graph that at high solar radiation, however, the ambient and water inlet temperatures were fixed at a constant value, the impact of increasing the volume flow rate exhibits a more significant influence on reducing the panel temperature in comparison to low solar irradiance.

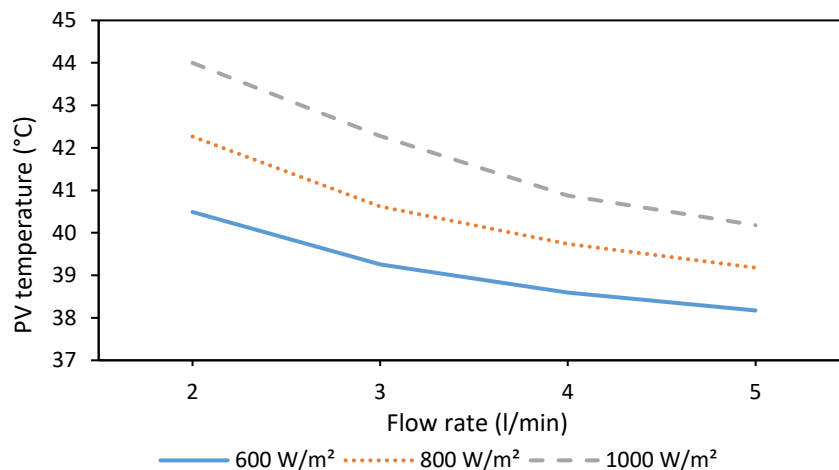


Fig. 5-39 Variation in PV temperature with flow at different solar irradiance

The variation in power production with different flow rates at various solar irradiance is illustrated in Fig. 5-40. The graph highlights that there is a broad influence of increasing solar irradiance on power production at any water

volume flow rate, whereas when the water volume flow rate is 2 l/min at solar irradiance 600 W/m² the output power was 109.2 W while at 800 W/m² and 1000 W/m² solar irradiance the PV power output was maximized to 144.4 W and 178.9 W, respectively. On the other hand, when the solar irradiance is maintained at 1000 W/m² and just water flow rate is maximized the enhancement in power production by increasing 1 l/min flow rate is in the range of (1.6 to 0.6) W.

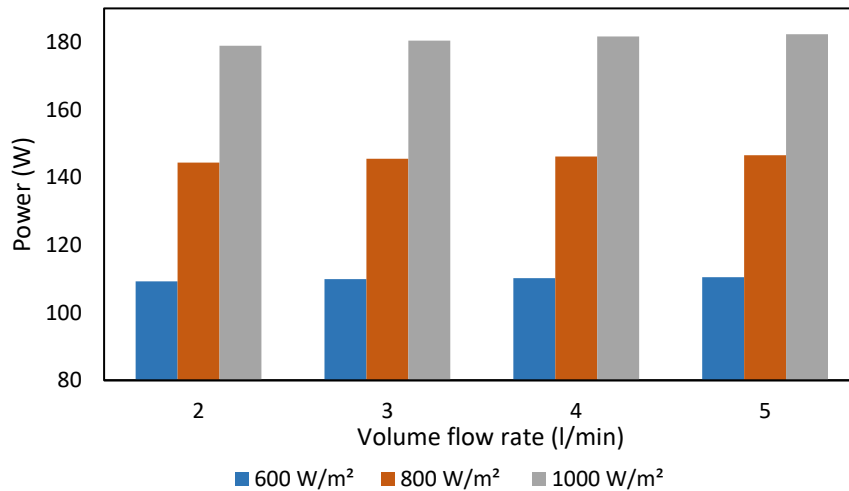


Fig. 5-40 Variation in PV power production with flow at various solar irradiance

The electrical efficiency analyzed in relation to volume flow rate and solar irradiance is presented in Fig. 5-41, as shown in the figure when the ambient temperature and water inlet temperature are fixed by increasing the solar irradiance there is a slight decrease in electrical efficiency at all the flow rates and this discrepancy decrease as the water volume flow rate is maximized, with the minimum disparity exist at 5 l/min water volume flow rate as by increasing the solar irradiance from 800 W/m² to 1000 W/m² the electrical efficiency was decreased by only 0.11%. Subsequently, at a flow rate of 2 l/min the electrical efficiency was reduced by 0.19% when the solar irradiance was increased from 800 W/m² to 1000 W/m².

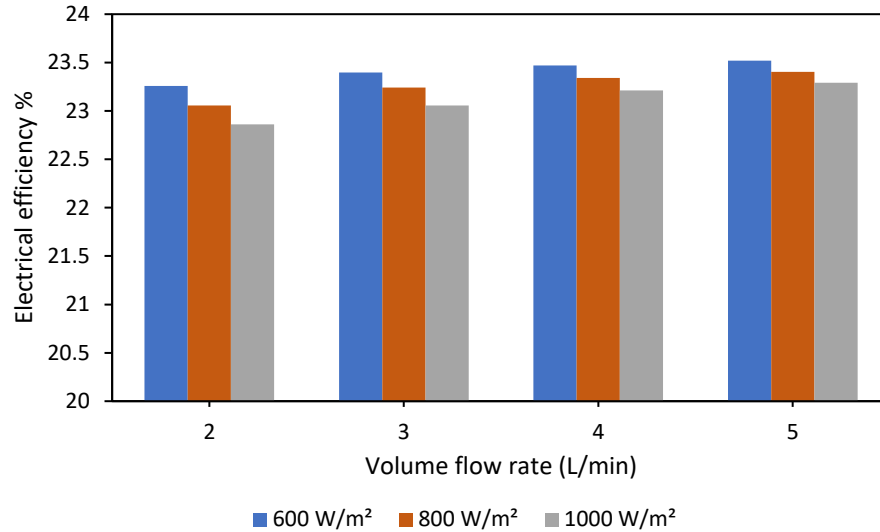


Fig. 5-41 variation in PV electrical efficiency with flow at various solar irradiance

The contour of temperature distribution of water over the panel surface at 800 W/m² solar irradiance, 40 °C ambient temperature and 35 °C water inlet temperature, at various water volume flow rate (2, 3, 4 and 5 l/min) is shown in Fig. 5-42. As shown in the figure the variation range in PV surface temperature at low flow rates is much higher than that of high-volume flow rates with the smallest variation being at 5 l/min volume flow.

The variation in PV surface temperature without cooling at different solar irradiance is presented in Fig. 5-43. Its significant from the graph that solar irradiance has a huge influence on PV surface temperature even at the times when ambient temperature is fixed, whereas the panel surface temperature rises from 55.4 °C to 68.53 °C by increasing the solar irradiance from 600 W/m² to 1000 W/m², this clearly shows why the PV with tracking system has a higher surface temperature compared to a fixed panel operating at the same ambient temperature.

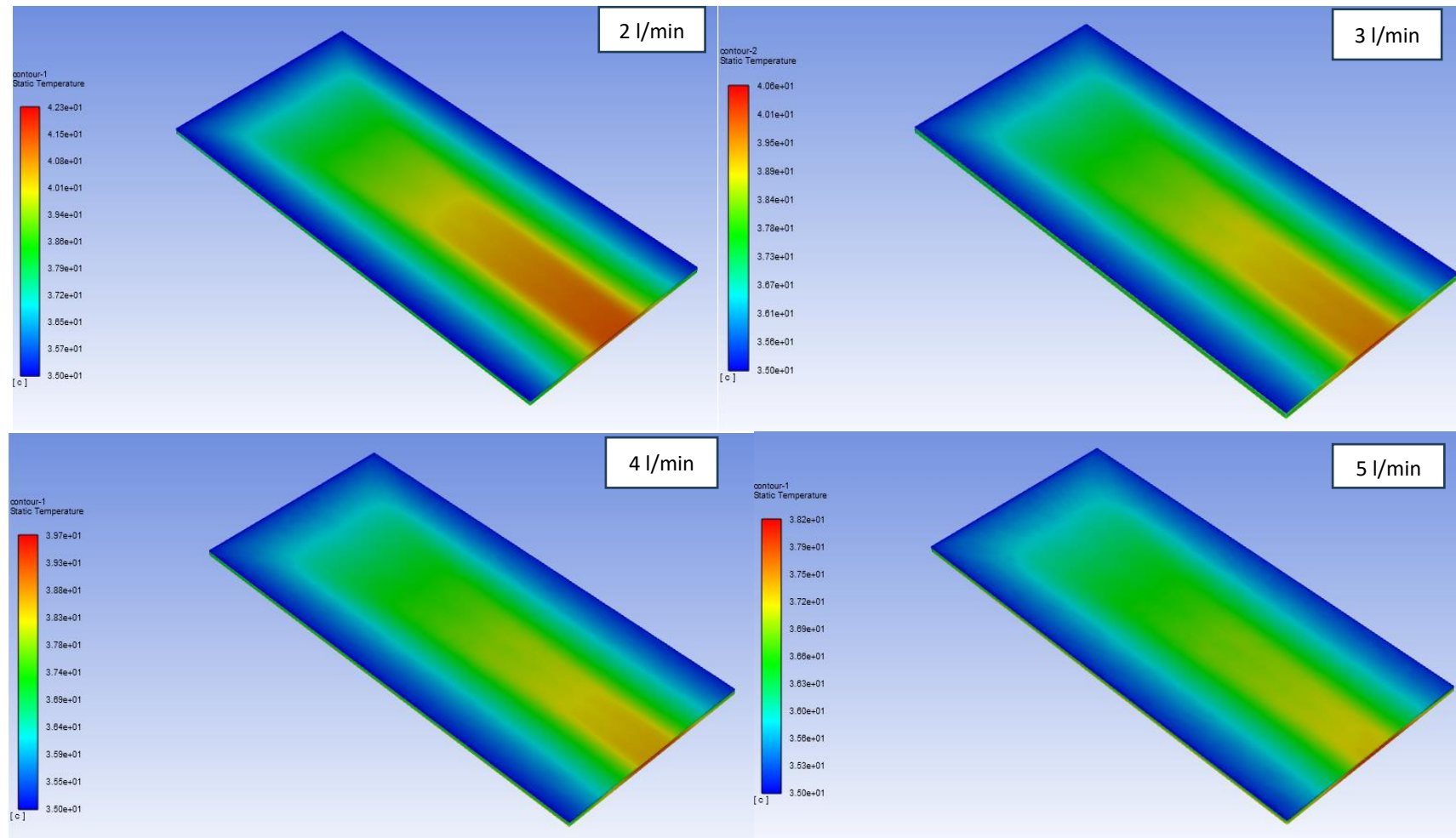


Fig. 5-42 Variation in water temperature distribution at 800 W/m^2 solar irradiance at various flow rates

The variation in electrical and power production at various solar radiation for PV panel without cooling when the ambient temperature was fixed at 40 °C is illustrated at Fig. 5-44. The highlighted from the figure is that the electrical efficiency inversely proportional to the solar irradiance while the power is directly proportional to it. Whereas the highest electrical efficiency was 21.58% at 600 W/m², subsequently, the highest power was 157.38 W at 1000 W/m².

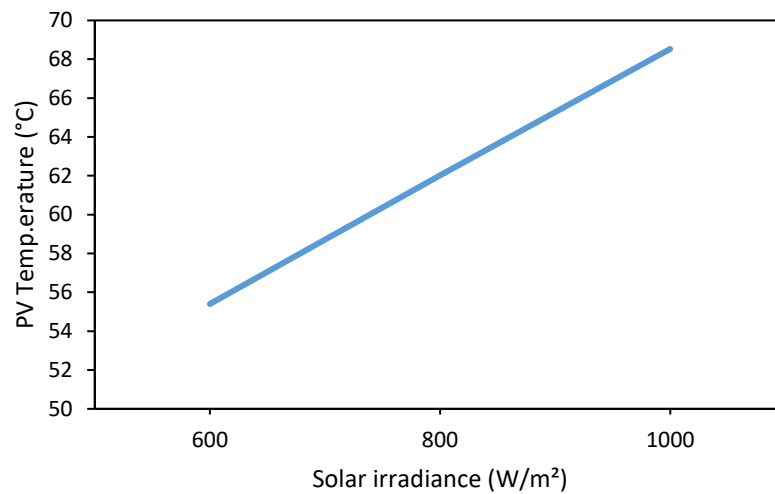


Fig. 5-43 Variation in PV surface Temperature at various solar irradiance

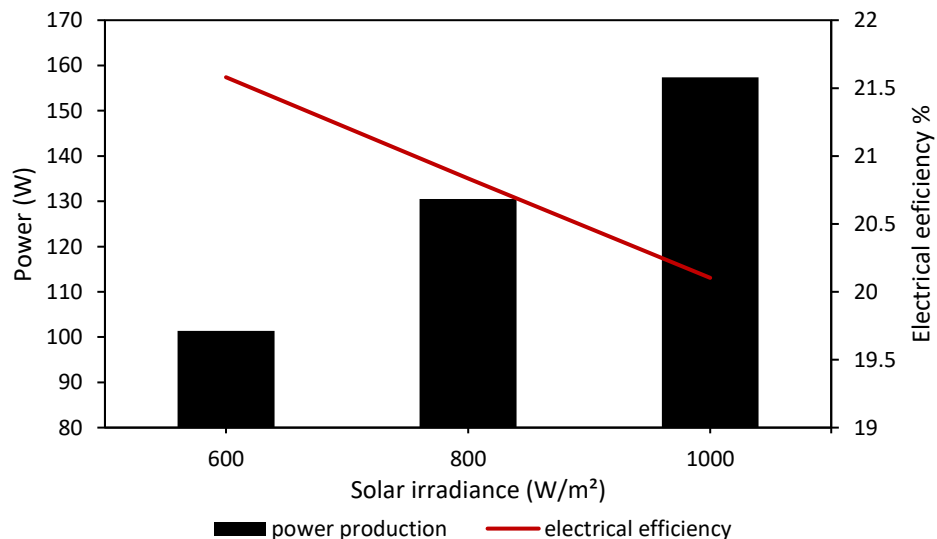


Fig. 5-44 Variation in PV power production and electrical efficiency at various solar irradiance

5.5.3 Influence of Variation in Water Inlet Temperature

This section presents the effect of various water inlet temperatures (20, 25, 30, 35 and 40 °C) at various volume flow rate (2, 3, 4 and 5 l/min) with fixed solar radiation and ambient temperature. Fig. 5-45, Fig. 5-46 and Fig. 5-47 present the PV panel surface temperature in relation to various water inlet temperatures and volume flow rates, at 1000 W/m², 800 W/m² and 600 W/m², respectively.

It's clear from the figures that the water inlet temperature highly influences the PV surface temperature at any volume flow rate of water. Also, the lowest panel temperature was recorded at the lowest solar irradiance for all water inlet temperature while the ambient temperature was fixed at 40 °C.

At 1000 W/m² solar irradiance when the water inlet temperature decreases from 40 °C to 35 °C, at volume flow rate 5 l/min, the PV temperature decreases from 44.5 °C to 40.18 °C, while when the water temperature was minimized to 20 °C the PV surface temperature is 28.44 °C.

On the other hand, at low solar irradiance 600 W/m² the minimum surface temperature recorded was 26.97 °C, at water inlet temperature of 20 °C and 5 l/min volume flow, additionally the maximum surface temperature at same solar irradiance was 44.23 °C at 2 l/min water flow rate and 40 °C water inlet temperature.

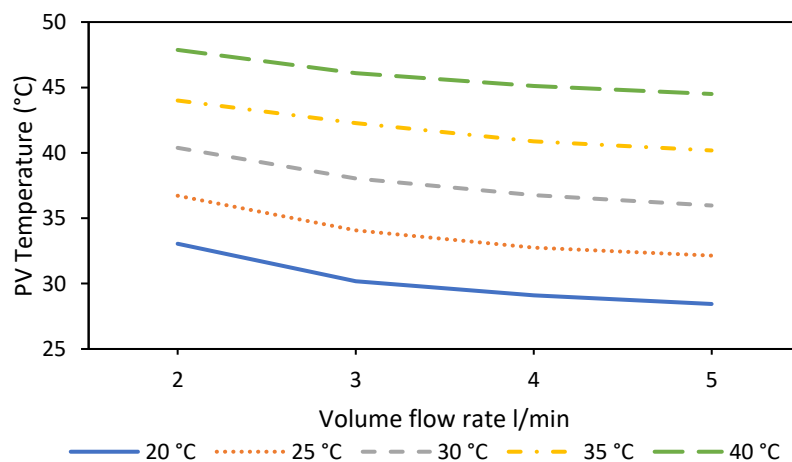


Fig. 5-45 Variation in PV temperature with flow at various water inlet temperature & 1000 W/m²

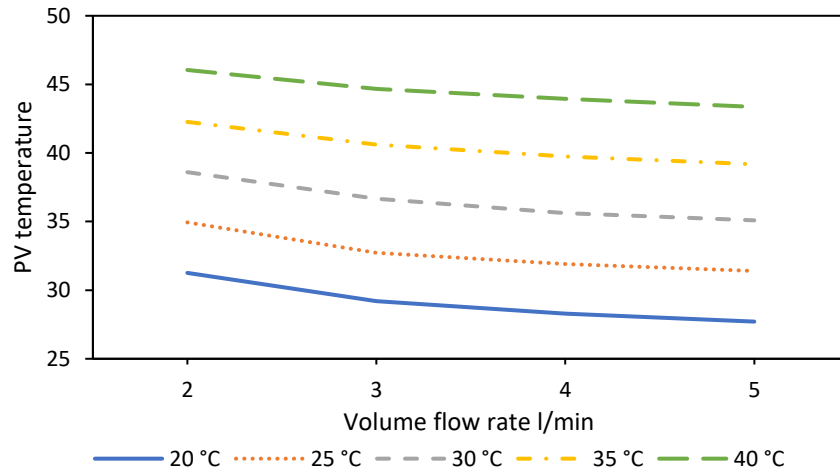


Fig. 5-46 Variation in PV temperature with flow at various water inlet temperature & 800 W/m^2

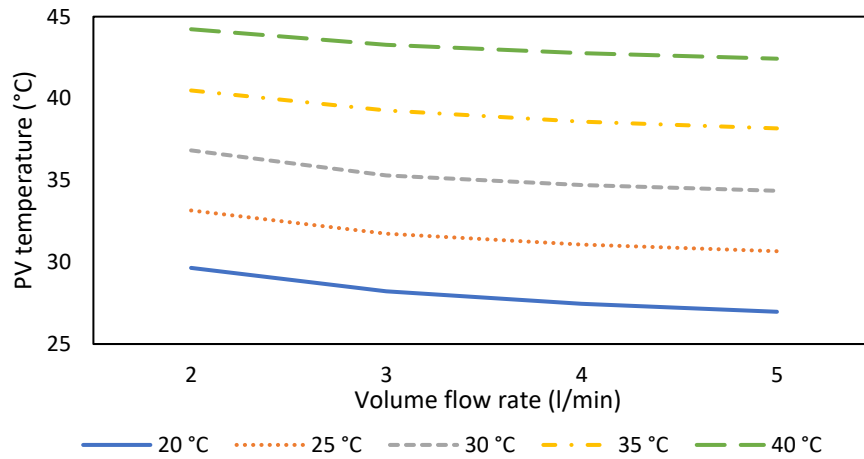


Fig. 5-47 Variation in PV temperature with flow at various water inlet temperature & 600 W/m^2

Furthermore, the impact of water inlet temperature on the power output of photovoltaic (PV) panels was investigated. The variation in power output of the PV panels was analyzed at different water inlet temperatures and water flow rates under three different solar radiation intensities: 1000 W/m^2 , 800 W/m^2 , and 600 W/m^2 . The results are depicted in Fig. 5-48, Fig. 5-49 and Fig. 5-50 respectively.

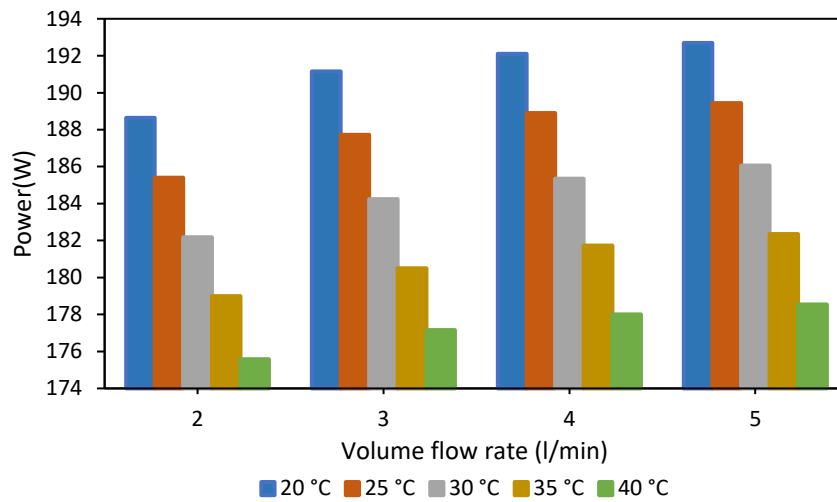


Fig. 5-48 Variation in PV power with flow at various water inlet temperature & 1000 W/m²

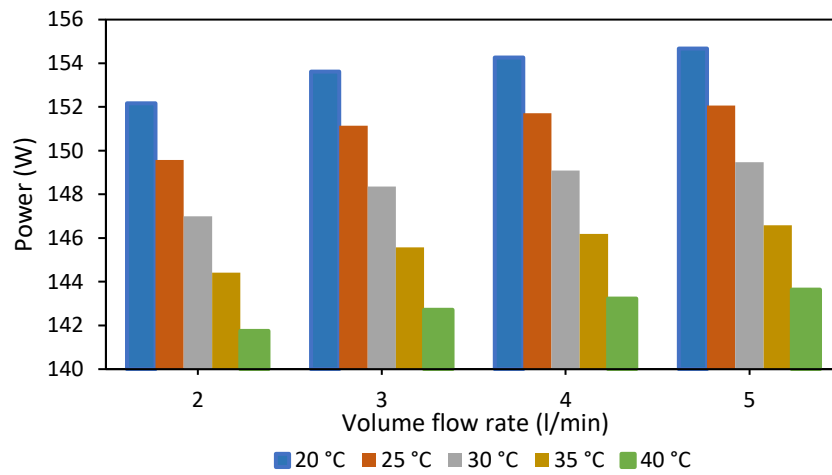


Fig. 5-49 Variation in PV power with flow at various water inlet temperature & 800 W/m²

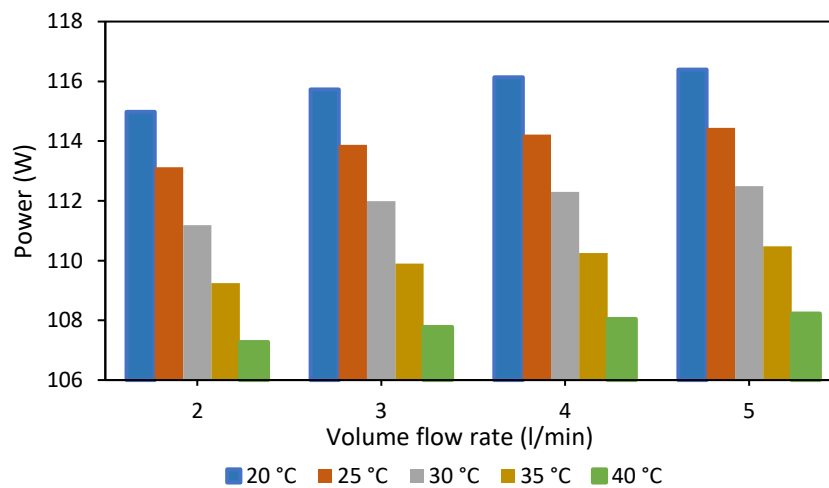


Fig. 5-50 Variation in PV power with flow at various water inlet temperature & 600 W/m²

The figures clearly demonstrate that the most influential factor in enhancing the power output of a cooled panel is the water inlet temperature, regardless of the water volume flow rate. It was observed that the power output significantly decreased as the solar radiation intensity was decreased.

The highest recorded power production was 192.69 W, achieved at 5 l/min water volume flow rate and solar intensity of 1000 W/m², when the water inlet temperature was maintained at its lowest level of 20 °C. Conversely, when the flow rate was minimized to the lowest level and the water inlet temperature was maximized to its highest level under the same operating conditions the PV power production was minimized to 175.5 W.

One of the key findings depicted in the figures is the notable improvement in PV power production achieved by reducing the water inlet temperature by 5 °C. Throughout all observed water inlet temperatures and solar irradiance levels, the PV power production witnessed a noteworthy increase ranging from 3.26 W to 3.81 W. Furthermore, the graphs highlight another significant result in which the PV power production experienced a reduction of 38 W when the solar irradiance was lowered by 200 W/m², while keeping the water flow rate and inlet temperature constant at 5 l/min and 20 °C, respectively.

These outcomes demonstrate the direct impact of water inlet temperature and solar irradiance on the efficiency of PV power production. By manipulating these variables, it becomes evident that a lower water inlet temperature and a higher solar irradiance contribute to enhanced PV power production. The implications of these findings highlight the importance of optimizing these parameters for improved performance and efficiency in PV power generation systems.

The electrical efficiency was also analyzed in relation to various water inlet temperatures and volume flow rates, at different solar irradiance 1000

W/m^2 , $800 W/m^2$ and $600 W/m^2$ as illustrated at Fig. 5-51, Fig. 5-52 and Fig. 5-53 respectively.

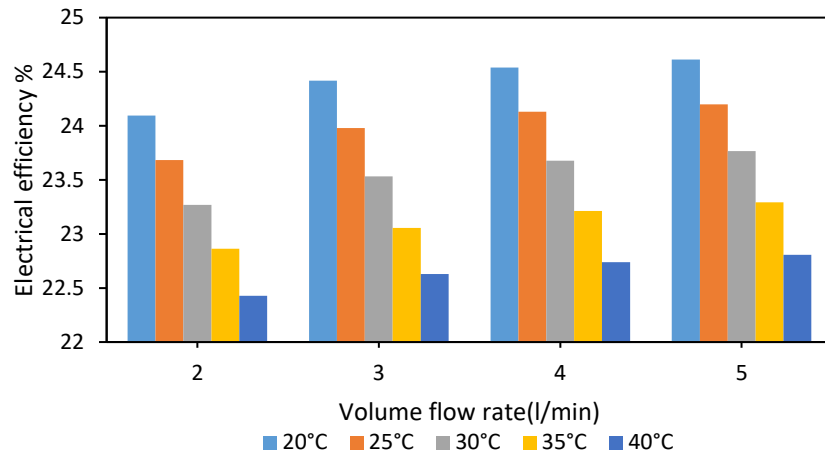


Fig. 5-51 Variation in PV efficiency with flow at various water inlet temperature & $1000 W/m^2$

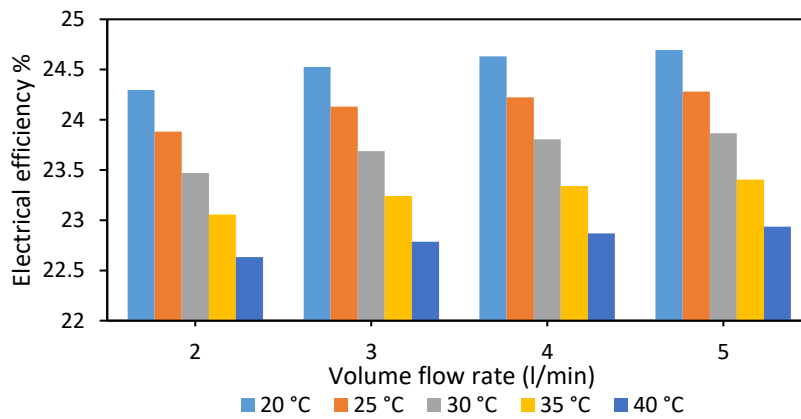


Fig. 5-52 Variation in PV efficiency with flow at various water inlet temperature & $800 W/m^2$

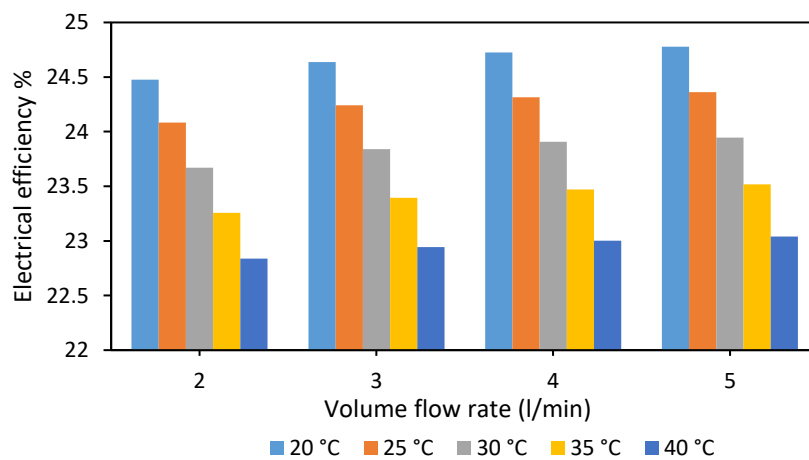


Fig. 5-53 Variation in PV efficiency with flow at various water inlet temperature & $600 W/m^2$

The figures presented clearly demonstrate the influence of water inlet temperature on the electrical efficiency of the panel. It was observed that by reducing the water inlet temperature by 5 °C, while maintaining the water flow rate, the electrical efficiency was enhanced by a range of 0.41% to 0.49%.

Another significant outcome from the figures is that by cooling the panel at a high-water flow rate of 5 l/min and the lowest water inlet temperature of 20 °C while reducing the solar irradiance from 1000 W/m² to 800 W/m² the electrical efficiency was reduced by only 0.08%. This suggests that efficient cooling of the photovoltaic panel can mitigate the detrimental effects of high ambient temperature and solar irradiance. This contributed to that an efficient cooling of the photovoltaic panel can lead to high electrical performance by almost vanishing the effect of high ambient temperature and solar irradiance.

Overall, these findings emphasize the significance of proper cooling mechanisms in optimizing the electrical efficiency of photovoltaic panels. By carefully controlling the water inlet temperature and ensuring efficient cooling of the panel, it is possible to enhance its performance and maximize its electrical output. This is particularly important in regions with high ambient temperatures and intense solar irradiance, as these conditions can have a negative impact on the efficiency of the panel.

The temperature distribution contour of water over the panel surface at 20 °C water inlet temperature and 1000 W/m² solar irradiance at various water volume flow rates (2, 3, 4 and 5 l/min) are shown in Fig. 5-54 , as shown in the figure by increasing the water volume flow rate while the water temperature was constant the water temperature deviation decreased.

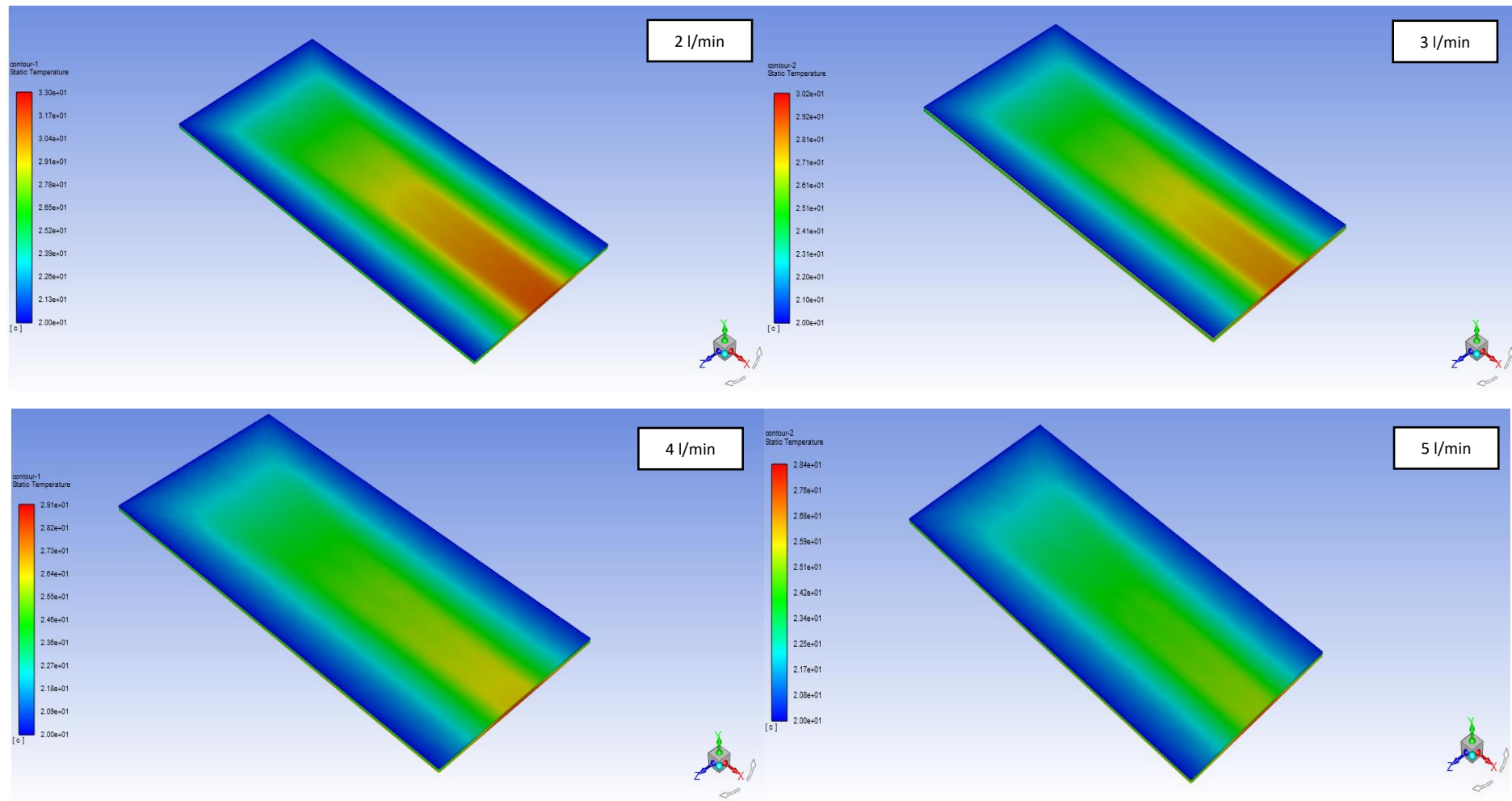


Fig. 5-54 Variation in water distribution temperature at various flow and 20 °C water inlet temperature & 1000 W/m² solar irradiance

Overall, the results of this simulation study highlight the importance of considering various parameters, such as ambient temperature, water inlet temperature, and solar intensity, when assessing the behavior of PV modules. By understanding the influence of these parameters on the temperature and performance of the panels, and which region is most suitable to install solar panel in, finally appropriate measures can be taken to improve their efficiency and overall performance.

CHAPTER SIX

(CONCLUSIONS AND RECOMMENDATIONS)

6.1 INTRODUCTION

This chapter presents the conclusions and recommendations of the study, which was conducted experimentally and theoretically at the Erbil Polytechnic University Research Center. The purpose of the study was to evaluate the effectiveness of a one-axis tracking system in combination with a front surface spray water cooling system that was placed on top and both left and right sides of the front surface to cover the surface of a photovoltaic (PV) panel.

The experimental setup involved comparing the performance of the cooled panel with and without the solar tracking system to a fixed reference panel without tracking. Additionally, ANSYS Fluent software was utilized to study the influence of various parameters that were not studied during the experimental.

The most prominent findings to emerge from the experimental and ANSYS Fluent study of the front surface water cooling system in combination with single axis solar tracking system are elaborated upon the subsequent section.

6.2 CONCLUSIONS

The following conclusions have been drawn from the research conducted:

- The water flow rate has been significantly reduced by regulating the flow rate according to the panel surface temperature. This reduction will reduce the electric power required for pump operation. The lowest water consumption is achieved at 45 °C, while the highest water consumption is observed at 35 °C as long as the pump's maximum flow rate is maintained.

- The maximum electrical efficiency enhancement recorded by using solar east west tracking system was 9.9% compared to the fixed reference panel.
- A notable disparity in the solar radiation intensity between fixed and tracking panels has been noted, up to 300 W/m^2 specifically during the morning.
- The tracking PV panels with cooling exhibited the highest power output recorded, reaching 204.438 W, when adjusted to a lower test temperature of 35°C .
- A fixed reference panel showed lower efficiency during periods of high solar radiation. In contrast, the tracking solar panel demonstrated a smaller variation in efficiency, benefiting from its continuous exposure to high solar radiation.
- The highest electrical efficiency achieved was 24.32 % at 13:00 by performing solar tracking with a water-cooling system at a 35°C setpoint temperature.
- The fill factor recorded its lowest level in the morning for fixed and tracking panel at 0.269 and 0.486, respectively. While the highest recorded fill factor was 0.79 for the panel with tracking and cooling system at a setpoint temperature of 35°C .
- By implementing an east-west tracking system with a cooling system at setpoint temperatures of 45°C , 40°C , and 35°C , the maximum enhancements in PV electrical efficiency recorded were 17.39%, 21.38%, and 25.11% respectively, as compared to the fixed reference panel without cooling.
- Through the implementation of a solar tracking system, the best temperature for cooling was found to be 40°C . This resulted in a significant reduction in water consumption, when compared to the consumption at 35°C by 312 l/day. Additionally, the system demonstrated a high electrical

efficiency of 23.51%, which only marginally deviated by 0.63% from the setpoint at 35 °C.

- Increasing the volume flow rate of water resulted in a greater reduction in panel surface temperature. The highest reduction of 30 °C was recorded when the water volume flow was set at 5 L/min for panels equipped with a solar tracking system. Conversely, the lowest temperature reduction of 23 °C was observed when the water volume flow rate was at 2 l/min.
- The power output of PV panels is greatly influenced by solar irradiance. When solar radiation reached 1083 W/m² and the panel was cooled with a water volume flow rate of 5 l/min, the produced power reached 210 W.
- Implementing a solar tracking system with cooling at a water volume flow rate of 2 l/min resulted in double the power production compared to a fixed panel cooled at the same flow rate. Specifically, the maximum enhancement in power output achieved with the tracking system and cooling at 2 l/min was 44.31 W or 32%. In contrast, the maximum enhancement in power output with a fixed panel cooled at 2 l/min was only 21.73 W or 15.74%.
- The daily average power production of a fixed panel with a water volume flow rate of 5 l/min was measured to be 168 W. However, when a tracking system was added to the panel with the same flow rate, the power production increased to 196.48 W.
- The output power and electrical efficiency of PV panels are optimal when operating at temperatures below 40 °C.
- Another contribution in this study confirmed that increasing the monocrystalline PV surface temperature by 5 °C within the temperature range of below 40 °C, had a minimal effect on electrical efficiency, reducing it by only 0.2-0.3%, which is significantly lower than has previously been reported.

- When the panel temperature exceeded 40 °C, each 1 °C increase in temperature led to a 0.2% decrease in panel efficiency.
- The results of the ANSYS Fluent simulation closely matched the experimental data, with a discrepancy of only 1.08%. This indicates that the model used in the simulation was valid and reliable for predicting the performance of solar cells. Therefore, this model can be used to optimize the performance of conventional photovoltaic systems.
- The simulation results demonstrated that ambient temperature had a minimal impact on the performance of the cooled PV panels. When the ambient temperature was increased from 35 °C to 50 °C, while maintaining a water volume flow rate of 5 l/min and other parameters constant, the power production and electrical efficiency of the photovoltaic panels only decreased by 2.3 W and 0.29% respectively.
- The effect of ambient temperature on the performance of uncooled PV panels was much more significant, leading to a decrease in power production of 11 W.
- Additionally, it is observed that an increase of 100 W/m² in solar radiation at a volume flow rate of 5 l/min led to a significant increase in power production of 16.6% with the PV surface temperature only increasing by 0.5 °C. Furthermore, decreasing the water inlet temperature by 5 °C at 5 l/min volume flow rate resulted in a 2.25% increase in power production.
- The contribution from the ANSYS Fluent simulation was that the most influential parameter on power production from cooled PV is the solar intensity, so this study suggests using PV panels in region with high solar intensity and providing a cooling system with a low water inlet temperature, no matter how hot is their climate.

6.3 RECOMMENDATIONS

In this section, several recommendations are provided for improving photovoltaic performance. These recommendations focus on enhancing the efficiency and reliability of PV systems, ultimately leading to increased energy generation and cost-effectiveness.

- The implementation of underground cooling technology involves an innovative approach that includes the utilization of an underground water tank in conjunction with a pump mechanism to facilitate the cooling process within the heat exchanger.
- The backside cooling spray water cooling system technology can be implemented in conjunction with tracking and front surface cooling system.
- Implementing two axis solar tracking system to the panel.
- A thermal analysis of the panel can be conducted to optimize the utilization of the hot water.
- Testing the electrical efficiency of PV panels at higher water volume flow rate.
- Using different type of PV panel for example polycrystalline and implement cooling and tracking system to it.

REFERENCES

- Abdolzadeh, M. and Ameri, M. (2009) 'Improving the effectiveness of a photovoltaic water pumping system by spraying water over the front of photovoltaic cells', *Renewable Energy*, 34(1), pp. 91–96. Available at: <https://doi.org/10.1016/j.renene.2008.03.024>.
- Abdulazeez, M.K. (2018) 'Experimental investigation of the effect of dust on monocrystalline photovoltaic module performance in Kirkuk, Iraq', *Kirkuk University Journal-Scientific Studies*, 13(2), pp. 127–138. Available at: <https://doi.org/10.32894/kujss.2018.145723>.
- Abdullah, A. et al. (2019) 'Hybrid photovoltaic thermal PVT solar systems simulation via Simulink/Matlab', *CFD Letters*, 11(4), pp. 64–78.
- Abed, A.F., Hachim, D.M. and Najim, S.E. (2021) 'Numerical simulation of heat transfer from PV panel with a wetted porous wick', *Basrah Journal for Engineering Sciences*, 21(2), pp. 29–38. Available at: <https://doi.org/10.33971/bjes.21.2.5>.
- Ahmad, A. et al. (2021) 'Evaluation of new PCM/PV configurations for electrical energy efficiency improvement through thermal management of pv systems', *Energies*, 14(14). Available at: <https://doi.org/10.3390/en14144130>.
- Ahmadi, R., Monadinia, F. and Maleki, M. (2021) 'Passive/active photovoltaic-thermal (PVT) system implementing infiltrated phase change material (PCM) in PS-CNT foam', *Solar Energy Materials and Solar Cells*, 222(December 2020), p. 110942. Available at: <https://doi.org/10.1016/j.solmat.2020.110942>.
- Al-Damook, M. et al. (2022) 'Photovoltaic module efficiency evaluation: The case of Iraq', *Alexandria Engineering Journal*, 61(8), pp. 6151–6168. Available at: <https://doi.org/10.1016/j.aej.2021.11.046>.

Al-Ghezi, M.K.S., Ahmed, R.T. and Chaichan, M.T. (2022) ‘The influence of temperature and irradiance on performance of the photovoltaic panel in the middle of iraq’, *International Journal of Renewable Energy Development*, 11(2), pp. 501–513. Available at: <https://doi.org/10.14710/ijred.2022.43713>.

Al-Hasan, A.Y. (1998) ‘A new correlation for direct beam solar radiation received by photovoltaic panel with sand dust accumulated on its surface’, *Solar Energy*, 63(5), pp. 323–333. Available at: [https://doi.org/10.1016/S0038-092X\(98\)00060-7](https://doi.org/10.1016/S0038-092X(98)00060-7).

AL-Rousan, N., Mat Isa, N.A. and Mat Desa, M.K. (2021) ‘Correlation analysis and MLP/CMLP for optimum variables to predict orientation and tilt angles in intelligent solar tracking systems’, *International Journal of Energy Research*, 45(1), pp. 453–477. Available at: <https://doi.org/10.1002/er.5676>.

Al-Saffa, F. Salim, S. Sallam, S. Jamal, M. (2021) *Iraqi Electricity Sector Overview*.

Al-Waeli, A.H. *et al.* (2016) ‘Photovoltaic solar thermal (PV/T) collectors past, present and future: A review’, *International Journal of Applied Engineering Research*, 11(22), pp. 10757–10765.

Al-Waeli, A.H.A. *et al.* (2017) ‘An experimental investigation of SiC nanofluid as a base-fluid for a photovoltaic thermal PV/T system’, *Energy Conversion and Management*, 142, pp. 547–558. Available at: <https://doi.org/10.1016/j.enconman.2017.03.076>.

Aldihani, A. (2017) *Enhancing the performance of PV system in dusty environment*. University of Birmingham.

Alexandru, C. and Pozna, C. (2008) ‘Different tracking strategies for optimizing the energetic efficiency of a photovoltaic system’, *2008 IEEE International Conference on Automation, Quality and Testing, Robotics, AQTR 2008 - THETA 16th Edition - Proceedings*, 3, pp. 434–439. Available at: <https://doi.org/10.1109/AQTR.2008.4588958>.

Almuwailhi, A. and Zeitoun, O. (2021) ‘Investigating the cooling of solar photovoltaic modules under the conditions of Riyadh’, *Journal of King Saud University - Engineering Sciences*, 35(2), pp. 123–136. Available at: <https://doi.org/10.1016/j.jksues.2021.03.007>.

ANSYS Inc. (1999) ‘ANSYS Manual’, *Theory Reference*, pp. 1–1286. Available at: <http://research.me.udel.edu/~lwang/teaching/MEx81/ansys56manual.pdf>.

Arefin, M.A. (2019) ‘Analysis of an integrated photovoltaic thermal system by top surface natural circulation of water’, *Frontiers in Energy Research*, 7. Available at: <https://doi.org/10.3389/fenrg.2019.00097>.

Ayadi, O. *et al.* (2022) ‘Experimental comparison between Monocrystalline, Polycrystalline, and Thin-film solar systems under sunny climatic conditions’, *Energy Reports*, 8(July), pp. 218–230. Available at: <https://doi.org/10.1016/j.egyr.2022.06.121>.

Bagher, A.M., Mahmoud, A.V.M. and Mirhabibi Mohsen (2015) ‘Types of solar cells and application’, *American Journal of Optics and Photonics*, 3(5), pp. 94–113. Available at: <https://doi.org/10.11648/j.ajop.20150305.17>.

Baouche, F.Z. *et al.* (2022) ‘Design and simulation of a solar tracking system for PV’, *Applied Sciences (Switzerland)*, 12(19), pp. 1–22. Available at: <https://doi.org/10.3390/app12199682>.

Barsoum, N. and Vasant, P. (2010) ‘Simplified solar tracking prototype’, *Global Journal on Technology & Optimization*, 1(June), pp. 38–45. Available at: www.pcoglobal.com/gjto.htm.

Bayrak, F., Oztop, H.F. and Selimefendigil, F. (2019) ‘Effects of different fin parameters on temperature and efficiency for cooling of photovoltaic panels under natural convection’, *Solar Energy*, 188, pp. 484–494. Available at: <https://doi.org/10.1016/j.solener.2019.06.036>.

Benato, A. *et al.* (2021) ‘Spraying cooling system for pv modules: Experimental measurements for temperature trends assessment and system design feasibility’, *Designs*, 5(2), pp. 1–28. Available at: <https://doi.org/10.3390/designs5020025>.

Benda, V. and Černá, L. (2020) ‘PV cells and modules – State of the art, limits and trends’, *Heliyon*, 6(12). Available at: <https://doi.org/10.1016/j.heliyon.2020.e05666>.

Bevilacqua, P. *et al.* (2021) ‘Efficiency improvement of photovoltaic modules via back surface cooling’, *Energies*, 14(4). Available at: <https://doi.org/10.3390/en14040895>.

Bonkaney, A.L., Madougou, S. and Adamou, R. (2017) ‘Impact of climatic parameters on the performance of solar photovoltaic (PV) module in niamey’, *Smart Grid and Renewable Energy*, 08(12), pp. 379–393. Available at: <https://doi.org/10.4236/sgre.2017.812025>.

Buonomano, A., Calise, F. and Vicidomini, M. (2016) ‘Design, simulation and experimental investigation of a solar system based on PV panels and PVT collectors’, *Energies*, 9(7), pp. 1–17. Available at: <https://doi.org/10.3390/en9070497>.

Ceylan, İ. *et al.* (2019) ‘Determination of the heat transfer coefficient of PV panels’, *Energy*, 175, pp. 978–985. Available at: <https://doi.org/10.1016/j.energy.2019.03.152>.

Chaichan, M.T. *et al.* (2023) ‘Sand and dust storms’ impact on the efficiency of the photovoltaic modules installed in Baghdad: A review study with an empirical investigation’, *Energies*, 16(3938). Available at: <https://doi.org/10.3390/en16093938>.

Chaichan, M.T. and Kazem, H.A. (2020) ‘Experimental evaluation of dust composition impact on photovoltaic performance in Iraq’, *Energy Sources, Part A: Recovery, Utilization and Environmental Effects*, 00(00), pp. 1–22. Available at: <https://doi.org/10.1080/15567036.2020.1746444>.

Chapin, D. N., Fuller, C. S. and Pearson, G.L. (1954) ‘A new silicon p-n junction photocell for converting solar radiation into electrical power’, *Letters To The Editor*, 18(1), pp. 676–677.

Chong, K.K. and Wong, C.W. (2009) ‘General formula for on-axis sun-tracking system and its application in improving tracking accuracy of solar collector’, *Solar Energy*, 83(3), pp. 298–305. Available at: <https://doi.org/10.1016/j.solener.2008.08.003>.

Choubey, P.C., Oudhia, A. and Dewangan, R. (2012) ‘Solar cell current scenario and future trends’, *Progress in Photovoltaics: Research and Applications*, 4(8), pp. 99–101.

Corio, R.P. (2008) ‘Single axis solar tracking system’. United States: United States publisher.

Dash, P.K. and Gupta, N.C. (2015) ‘Effect of temperature on power output from different commercially available photovoltaic modules’, *Journal of Engineering Research and Applications*, 5(1), pp. 1–4. Available at: www.ijera.com.

Dieck, R.H. et al. (1999) *The measurement, instrumentation, and sensors handbook*. Edited by J.G. Webster. CRC Press LLC. Available at: <https://doi.org/10.1201/b15474>.

Dobriyal, R. et al. (2020) ‘A brief review on solar flat plate collector by incorporating the effect of nanofluid’, *Materials Today: Proceedings*, 21(3), pp. 1653–1658. Available at: <https://doi.org/10.1016/j.matpr.2019.11.294>.

Doulati, F. et al. (2011) ‘Application of computational fluid dynamics (CFD) for simulation of acid mine drainage generation and subsequent pollutants transportation through groundwater flow systems and rivers’, *Computational Fluid Dynamics Technologies and Applications*, (May), pp. 124–160. Available at: <https://doi.org/10.5772/16927>.

Eicker, U. et al. (2014) ‘Economic evaluation of solar thermal and photovoltaic cooling systems through simulation in different climatic conditions: An analysis in three different cities in Europe’, *Energy and Buildings*, 70, pp. 207–223. Available at: <https://doi.org/10.1016/j.enbuild.2013.11.061>.

Fumo, N., Bortone, V. and Zambrano, J.C. (2013) ‘Comparative analysis of solar thermal cooling and solar photovoltaic cooling systems’, *Journal of Solar Energy Engineering, Transactions of the ASME*, 135(2). Available at: <https://doi.org/10.1115/1.4007935>.

Gomaa, M.R., Ahmed, M. and Rezk, H. (2022) ‘Temperature distribution modeling of PV and cooling water PV/T collectors through thin and thick cooling cross-fined channel box’, *Energy Reports*, 8(November), pp. 1144–1153. Available at: <https://doi.org/10.1016/j.egyr.2021.11.061>.

Gómez-Uceda, F.J. *et al.* (2020) ‘Analysis of the influence of terrain orientation on the design of pv facilities with single-axis trackers’, *Applied Sciences (Switzerland)*, 10(23), pp. 1–16. Available at: <https://doi.org/10.3390/app10238531>.

Govardhanan, M.S. *et al.* (2020) ‘Photovoltaic module with uniform water flow on top surface’, *International Journal of Photoenergy*, 2020, pp. 1–9. Available at: <https://doi.org/10.1155/2020/8473253>.

Grant, C.D. *et al.* (2002) ‘Characterization of nanocrystalline and thin film TiO₂ solar cells with poly(3-undecyl-2,2’-bithiophene) as a sensitizer and hole conductor’, *Journal of Electroanalytical Chemistry*, 522(1), pp. 40–48. Available at: [https://doi.org/10.1016/S0022-0728\(01\)00715-X](https://doi.org/10.1016/S0022-0728(01)00715-X).

Grubišić-Čabo, F. *et al.* (2018) ‘Experimental investigation of the passive cooled free-standing photovoltaic panel with fixed aluminum fins on the backside surface’, *Journal of Cleaner Production*, 176, pp. 119–129. Available at: <https://doi.org/10.1016/j.jclepro.2017.12.149>.

Haidar, Z.A., Orfi, J. and Kaneesamkandi, Z. (2021) ‘Photovoltaic panels temperature regulation using evaporative cooling principle: Detailed theoretical and real operating conditions experimental approaches’, *Energies*, 14(145). Available at: <https://doi.org/10.3390/en14010145>.

Hannah, E. Murdock, D. and Gibb, T.A. (2019) *Renewables 2019 global status report*. REN21 Renewable Now. Available at: http://www.ren21.net/Portals/97/documents/GSR/REN21_GSR2011.pdf.

Hasan, A. *et al.* (2017) ‘Yearly energy performance of a photovoltaic-phase change material (PV-PCM) system in hot climate’, *Solar Energy*, 146, pp. 417–429. Available at: <https://doi.org/10.1016/j.solener.2017.01.070>.

Hasan, H.A. *et al.* (2017) ‘Experimental investigation of jet array nanofluids impingement in photovoltaic/thermal collector’, *Solar Energy*, 144, pp. 321–334. Available at: <https://doi.org/10.1016/j.solener.2017.01.036>.

Hassan, A. *et al.* (2020) ‘Thermal management and uniform temperature regulation of photovoltaic modules using hybrid phase change materials-nanofluids system’, *Renewable Energy*, 145, pp. 282–293. Available at: <https://doi.org/10.1016/j.renene.2019.05.130>.

Hernandez-Perez, J.G. *et al.* (2020) ‘A new passive PV heatsink design to reduce efficiency losses: A computational and experimental evaluation’, *Renewable Energy*, 147, pp. 1209–1220. Available at: <https://doi.org/10.1016/j.renene.2019.09.088>.

Holman, J.P. (1986) *Heat transfer*. London: MacGraw-Hill Book Company.

Hua, Z. *et al.* (2019) ‘Optimal capacity allocation of multiple solar trackers and storage capacity for utility-scale photovoltaic plants considering output characteristics and complementary demand’, *Applied Energy*, 238(May 2018), pp. 721–733. Available at: <https://doi.org/10.1016/j.apenergy.2019.01.099>.

Husain, A.A.F. *et al.* (2018) ‘A review of transparent solar photovoltaic technologies’, *Renewable and Sustainable Energy Reviews*, 94(June), pp. 779–791. Available at: <https://doi.org/10.1016/j.rser.2018.06.031>.

Hussein, H.A., Numan, A.H. and Abdulmunem, A.R. (2017) ‘An experimental investigation on the performance enhancement of photovoltaic/thermal panel using a tracking system and nanofluid (Al₂O₃)’, *Engineering and Technology Journal*, 35(5), pp. 493–508. Available at: <https://doi.org/10.30684/etj.35.5a.9>.

Ibrahim, A. *et al.* (2010) ‘Thermal theoretical study on PV/T water based collectors’, *Recent Advances in Applied Mathematics*, (January), pp. 545–551.

Ibrahim, A. *et al.* (2023) ‘A comprehensive study for Al₂O₃ nanofluid cooling effect on the electrical and thermal properties of polycrystalline solar panels in outdoor conditions’, *Environmental Science and Pollution Research* [Preprint]. Available at: <https://doi.org/10.1007/s11356-023-25928-3>.

Jaffar, M.F., Mohammad, A.T. and Ahmed, A.Q. (2022) ‘An experimental study for enhancing the performance of the photovoltaic module using forced air’, *Journal of Techniques*, 4(2), pp. 1–9. Available at: <http://journal.mtu.edu.iq>.

Jailany, A.T., Abd El-Al, A. and Rashwan, M.A. (2016) ‘Effect of water cooling on photovoltaic performance’, *Misr Journal of Agricultural Engineering*, 33(1), pp. 257–268. Available at: <https://doi.org/10.21608/mjae.2016.98185>.

Jiyuan, T., Guan-Heng, Y. and Chaoqun, L. (2018) *Computational fluid dynamics a practical approach*, Butterworth- Heinemann. Available at: <https://doi.org/10.1016/b978-0-08-098243-4.09986-8>.

John, D. and Beckman, W. (1982) *Solar engineering of thermal processes, Design Studies*. Available at: [https://doi.org/10.1016/0142-694x\(82\)90016-3](https://doi.org/10.1016/0142-694x(82)90016-3).

Jose, J.P.A. *et al.* (2023) ‘An analysis of the effects of nanofluid-based serpentine tube cooling enhancement in solar photovoltaic cells for green cities’, *Journal of Nanomaterials*, 2023. Available at: <https://doi.org/10.1155/2023/3456536>.

Joshi, A.S. *et al.* (2009) ‘Performance evaluation of a hybrid photovoltaic thermal (PV/T) (glass-to-glass) system’, *International Journal of Thermal Sciences*, 48(1), pp. 154–164. Available at: <https://doi.org/10.1016/j.ijthermalsci.2008.05.001>.

Jumrusprasert, P., Smith, G. and Kirkup, L. (2007) ‘Comparing the efficiency of fixed solar cell panels in a tropical location’, *ISES Solar World Congress 2007, ISES 2007*, 2, pp. 1478–1483. Available at: https://doi.org/10.1007/978-3-540-75997-3_300.

Kasim, N.K. and Atwan, A.F. (2017) *Improvement of PV/thermal solar system via a water cooling*. Al-Mustansiriyah University College.

Khalil, A., Abdelgaied, M. and Hamdy, M. (2019) ‘Performance improvement of PV panel using water cooling technology under Egyptian conditions’, *Journal of Engineering Research*, 2, pp. 42–47. Available at: <https://doi.org/10.21608/ERJENG.2019.125503>.

Krauter, S. (2004) ‘Increased electrical yield via water flow over the front of photovoltaic panels’, *Solar Energy Materials and Solar Cells*, 82(1–2), pp. 131–137. Available at: <https://doi.org/10.1016/j.solmat.2004.01.011>.

Kumar, M.S. and Annappa, C.M. (2013) ‘Use of heat pump along with multi utilities for domestic and light commercial market’, *International Journal of Application or Innovation in Engineering & Management (IJAIEM)*, 2(1), pp. 294–304.

Kumar, R. and Rosen, M.A. (2011) ‘Performance evaluation of a double pass PV/T solar air heater with and without fins’, *Applied Thermal Engineering*, 31(8–9), pp. 1402–1410. Available at: <https://doi.org/10.1016/j.applthermaleng.2010.12.037>.

Kumar, S. (2018) *Modelling and simulation of solar PV/T hybrid systems*. Anna University.

Li, B. *et al.* (2006) ‘Review of recent progress in solid-state dye-sensitized solar cells’, *Solar Energy Materials and Solar Cells*, 90(5), pp. 549–573. Available at: <https://doi.org/10.1016/j.solmat.2005.04.039>.

Luo, W. *et al.* (2017) ‘Potential-induced degradation in photovoltaic modules: A critical review’, *Energy and Environmental Science*, 10(1), pp. 43–68. Available at: <https://doi.org/10.1039/c6ee02271e>.

Mahmood, D.M.N. and Aljubury, I.M.A. (2023) ‘Experimental evaluation of PV panel efficiency using evaporative cooling integrated with water spraying’, *Journal of Engineering*, 29(5), pp. 29–48. Available at: <https://digital-library.theiet.org/content/journals/10.1049/joe.2018.8601>.

Matias, C.A. *et al.* (2017) ‘Increasing photovoltaic panel power through water cooling technique’, *Transactions on Environment and Electrical Engineering*, 2(1). Available at: <https://doi.org/10.22149/teee.v2i1.90>.

El Mays, A. *et al.* (2017) ‘Improving photovoltaic panel using finned plate of aluminum’, *Energy Procedia*, 119, pp. 812–817. Available at: <https://doi.org/10.1016/j.egypro.2017.07.103>.

Mazón-Hernández, R. *et al.* (2013) ‘Improving the electrical parameters of a photovoltaic panel by means of an induced or forced air stream’, *International Journal of Photoenergy*, 2013. Available at: <https://doi.org/10.1155/2013/830968>.

Metwally, H. (2022) ‘Comprehensive analysis of PCM container construction effects PV panels thermal management’, *Advance in Environmental Waste Management & Recycling*, 5(3). Available at: <https://doi.org/10.33140/aewmr.05.03.010>.

Mohammed, F.M., Mohammed, J.A.-K. and Sanad, M.A.-S. (2019) ‘Performance enhancement of photovoltaic panel using double-sides water glazing chambers cooling technique’, *Al-Nahrain Journal for Engineering Sciences*, 22(1), pp. 22–30. Available at: <https://doi.org/10.29194/njes.22010022>.

Moharram, K.A. *et al.* (2013) ‘Enhancing the performance of photovoltaic panels by water cooling’, *Ain Shams Engineering Journal*, 4(4), pp. 869–877. Available at: <https://doi.org/10.1016/j.asej.2013.03.005>.

Mohsin, A.T. and Abdulbaqi, I.M. (2018) ‘Analysis of an irrigation pump driver fed by solar PV panel’, *1st International Scientific Conference of Engineering Sciences - 3rd Scientific Conference of Engineering Science, ISCES 2018 - Proceedings*, 2018-Janua(April), pp. 92–97. Available at: <https://doi.org/10.1109/ISCES.2018.8340534>.

Muiruri, P.I. and Motsamai, O.S. (2018) ‘Three dimensional CFD simulations of a wind turbine blade section; validation’, *Journal of Engineering Science and Technology Review*, 11(1), pp. 138–145. Available at: <https://doi.org/10.25103/jestr.111.16>.

Muslim, N.H., Ghadhban, S.A. and Hilal, K.H. (2020) ‘Enhancement of solar photovoltaic module performance by using a water-cooling chamber for climatic conditions of Iraq’, *International Journal of Renewable Energy Research*, 10(3), pp. 1103–1110. Available at: <https://doi.org/10.20508/ijrer.v10i3.10937.g7984>.

Natarajan, S.K. *et al.* (2019) ‘Experimental analysis of a two-axis tracking system for solar parabolic dish collector’, *International Journal of Energy Research*, 43(2), pp. 1012–1018. Available at: <https://doi.org/10.1002/er.4300>.

Nateqi, M., Zargarabadi, M.R. and Rafee, R. (2021) ‘Experimental investigations of spray flow rate and angle in enhancing the performance of PV panels by steady and pulsating water spray system’, *SN Applied Sciences*, 3(1), pp. 1–13. Available at: <https://doi.org/10.1007/s42452-021-04169-4>.

Nižetić, S. *et al.* (2016) ‘Water spray cooling technique applied on a photovoltaic panel: The performance response’, *Energy Conversion and Management*, 108, pp. 287–296. Available at: <https://doi.org/10.1016/j.enconman.2015.10.079>.

Parida, B., Iniyar, S. and Goic, R. (2011) ‘A review of solar photovoltaic technologies’, *Renewable and Sustainable Energy Reviews*, 15(3), pp. 1625–1636. Available at: <https://doi.org/10.1016/j.rser.2010.11.032>.

Peng, Z., Herfatmanesh, M.R. and Liu, Y. (2017) ‘Cooled solar PV panels for output energy efficiency optimisation’, *Energy Conversion and Management*, 150, pp. 949–955.

Qi, C. *et al.* (2019) ‘Experimental study on the flow and heat transfer characteristics of nanofluids in double-tube heat exchangers based on thermal efficiency assessment’, *Energy Conversion and Management*, 197(May), p. 111877. Available at: <https://doi.org/10.1016/j.enconman.2019.111877>.

Racharla, S. and Rajan, K. (2017) ‘Solar tracking system—a review’, *International Journal of Sustainable Engineering*, 10(2), pp. 72–81. Available at: <https://doi.org/10.1080/19397038.2016.1267816>.

Radwan, A., Ahmed, M. and Ookawara, S. (2016) ‘Performance enhancement of concentrated photovoltaic systems using a microchannel heat sink with nanofluids’, *Energy Conversion and Management*, 119, pp. 289–303. Available at: <https://doi.org/10.1016/j.enconman.2016.04.045>.

Risdiyanto, A. *et al.* (2020) ‘Implementation of photovoltaic water spray cooling system and its feasibility analysis’, *2020 International Conference on Sustainable Energy Engineering and Application (ICSEEA)*, pp. 88–93. Available at: <https://doi.org/10.1109/ICSEEA50711.2020.9306133>.

Robert, C. (2010) *solar panel processing*. Philadelphia: old city publication inc.

Rosli, M.A.M. *et al.* (2022) ‘The effect of variation in mass flow rate and solar irradiance on temperature uniformity and thermal performance of photovoltaic thermal: a simulated CFD study’, *Journal of Advanced Research in Fluid Mechanics and Thermal Sciences*, 91(2), pp. 106–119. Available at: <https://doi.org/10.37934/arfmts.91.2.106119>.

Ruoping, Y. *et al.* (2020) ‘Study of operation performance for a solar photovoltaic system assisted cooling by ground heat exchangers in arid climate, China’, *Renewable Energy*, 155, pp. 102–110. Available at: <https://doi.org/10.1016/j.renene.2020.03.109>.

Sainthiya, H. and Beniwal, N.S. (2019) ‘Comparative analysis of electrical performance parameters under combined water cooling technique of photovoltaic module: An experimental investigation’, *Energy Sources, Part A: Recovery, Utilization and Environmental Effects*, 42(15), pp. 1902–1913. Available at: <https://doi.org/10.1080/15567036.2019.1604894>.

Sajjad, U. *et al.* (2019) ‘Cost effective cooling of photovoltaic modules to improve efficiency’, *Case Studies in Thermal Engineering*, 14, p. 100420. Available at: <https://doi.org/10.1016/j.csite.2019.100420>.

Savvakis, N., Dialyna, E. and Tsoutsos, T. (2020) ‘Investigation of the operational performance and efficiency of an alternative PV + PCM concept’, *Solar Energy*, 211(November), pp. 1283–1300. Available at: <https://doi.org/10.1016/j.solener.2020.10.053>.

Sharaf, M., Yousef, M.S. and Huzayyin, A.S. (2022) ‘Review of cooling techniques used to enhance the efficiency of photovoltaic power systems’, *Environmental Science and Pollution Research*, 29(18), pp. 26131–26159. Available at: <https://doi.org/10.1007/s11356-022-18719-9>.

Sharma, S., Jain, K.K. and Sharma, A. (2015) ‘Solar cells: in research and applications—a review’, *Materials Sciences and Applications*, 06(12), pp. 1145–1155. Available at: <https://doi.org/10.4236/msa.2015.612113>.

Skoplaki, E. and Palyvos, J.A. (2008) ‘On the temperature dependence of photovoltaic module electrical performance: A review of efficiency/power correlations’, *Solar Energy*, 83(5), pp. 614–624. Available at: <https://doi.org/10.1016/j.solener.2008.10.008>.

Solanki, C.S. (2011) *solar photovoltaic and technology and applications*. 2nd edn. Prentice Hall of India.

Sorrell, S. (2015) ‘Reducing energy demand: A review of issues, challenges and approaches’, *Renewable and Sustainable Energy Reviews*, 47, pp. 74–82. Available at: <https://doi.org/10.1016/j.rser.2015.03.002>.

Stambouli, A.B. and Koinuma, H. (2012) ‘A primary study on a long-term vision and strategy for the realisation and the development of the Sahara Solar Breeder project in Algeria’, *Renewable and Sustainable Energy Reviews*, pp. 591–598. Available at: <https://doi.org/10.1016/j.rser.2011.08.025>.

Sugianto, S. (2020) ‘Comparative Analysis of Solar Cell Efficiency between Monocrystalline and Polycrystalline’, *INTEK: Jurnal Penelitian*, 7(2), p. 92. Available at: <https://doi.org/10.31963/intek.v7i2.2625>.

Sultan, T.N., Farhan, M.S. and Salim Alrikabi, H.T.H. (2021) ‘Using cooling system for increasing the efficiency of solar cell’, in *Journal of Physics: Conference Series*, pp. 1–7. Available at: <https://doi.org/10.1088/1742-6596/1973/1/012129>.

Syafiqah, Z. *et al.* (2017) ‘Analysis of photovoltaic with water pump cooling by using ANSYS’, *Journal of Physics: Conference Series*, 908(1). Available at: <https://doi.org/10.1088/1742-6596/908/1/012083>.

T. D. Canonsburg (2013) ‘ANSYS Fluent Theory Guide’, *ANSYS Inc., USA*, 15317(November), p. 814. Available at: http://www.afs.enea.it/project/neptunius/docs/fluent/html/th/main_pre.htm.

Tan, L. *et al.* (2017) ‘Efficiency gains of photovoltaic system using latent heat thermal energy storage’, *Energy Procedia*, 110(2017), pp. 83–88. Available at: <https://doi.org/10.1016/j.egypro.2017.03.110>.

Teo, H.G., Lee, P.S. and Hawlader, M.N.A. (2012) ‘An active cooling system for photovoltaic modules’, *Applied Energy*, 90(1), pp. 309–315. Available at: <https://doi.org/10.1016/j.apenergy.2011.01.017>.

Tiwari, A. and Sodha, M.S. (2006) ‘Performance evaluation of solar PV/T system: An experimental validation’, *Solar Energy*, 80(7), pp. 751–759. Available at: <https://doi.org/10.1016/j.solener.2005.07.006>.

Tripanagnostopoulos, Y. Nousia, T. and S.M. (2001) ‘Test results of air cooled modified PV modules’, *Advanced Solar Vacuum Collectors & Systems*, (October), pp. 2519–2522.

Tripanagnostopoulos, Y. and Themelis, P. (2010) ‘Natural flow air cooled photovoltaics’, in *7th International Conference of the Balkan Physical Union*, pp. 1013–1018. Available at: <https://doi.org/10.1063/1.3322300>.

Tudorache, T., Oancea, C.D. and Kreindler, L. (2012) ‘Performance evaluation of a solar tracking PV panel’, *U.P.B. Sci. Bull., Series C*, 74(1), pp. 1–10.

Waqas, A., Jie, J. and Xu, L. (2017) ‘Thermal behavior of a PV panel integrated with PCM-filled metallic tubes: An experimental study’, *Journal of Renewable and Sustainable Energy*, 9(5). Available at: <https://doi.org/10.1063/1.4995022>.

Wongwuttanasatian, T., Sarikarin, T. and Suksri, A. (2020) ‘Performance enhancement of a photovoltaic module by passive cooling using phase change material in a finned container heat sink’, *Solar Energy*, 195(October 2019), pp. 47–53. Available at: <https://doi.org/10.1016/j.solener.2019.11.053>.

Wu, S. and Xiong, C. (2014) ‘Passive cooling technology for photovoltaic panels for domestic houses’, *International Journal of Low-Carbon Technologies*, 9(2), pp. 118–126. Available at: <https://doi.org/10.1093/ijlct/ctu013>.

Xu, L. *et al.* (2021) ‘A hybrid PV thermal (water or air) wall system integrated with double air channel and phase change material: A continuous full-day seasonal experimental research’, *Renewable Energy*, 173, pp. 596–613. Available at: <https://doi.org/10.1016/j.renene.2021.04.008>.

Xu, Z. and Kleinstreuer, C. (2014) ‘Computational analysis of nanofluid cooling of high concentration photovoltaic cells’, *Journal of Thermal Science and Engineering Applications*, 6(3), pp. 1–9. Available at: <https://doi.org/10.1115/1.4026355>.

Yadav, A. and Kumar, P. (2015) ‘Enhancement in efficiency of PV cell through p&o algorithm’, *International Journal For Technological Research In Engineering*, 2(11), pp. 2347–4718. Available at: www.ijtre.com.

Yousef, M.S., Sharaf, M. and Huzayyin, A.S. (2022) ‘Energy, exergy, economic, and enviroeconomic assessment of a photovoltaic module incorporated with a paraffin-metal foam composite: An experimental study’, *Energy*, 238, p. 121807. Available at: <https://doi.org/10.1016/j.energy.2021.121807>.

Zhe, L.W. *et al.* (2019) ‘Effect of water cooling temperature on photovoltaic panel performance by using computational fluid dynamics (CFD)’, *Journal of Advanced Research in Fluid Mechanics and Thermal Sciences*, 56(1), pp. 133–146.

APPENDIX A

UNCERTAINTY ANALYSIS

The uncertainty analysis was made for all the measuring equipment used in the current study the sample of calculation for flowmeter uncertainty analysis is presented below.

Table A-1 Flowmeter uncertainty calculation sample

Flowmeter measurement (L/min)	$(x_i - \bar{x})$	$(x_i - \bar{x})^2$
x_i		
1.98	-0.02	0.0004
1.93	-0.07	0.0049
1.98	-0.02	0.0004
1.97	-0.03	0.0009
1.98	-0.02	0.0004
1.92	-0.08	0.0016
1.95	-0.05	0.0025
1.95	-0.05	0.0025
1.96	-0.04	0.0016
1.96	-0.04	0.0016

Where $\bar{x} = 2$

number of reading (N)=10

$$uncertainty (u) = \sqrt{\frac{\sum_{i=1}^n (x_i - \bar{x})^2}{N*(N-1)}}$$

$$uncertainty (u) = \sqrt{\frac{0.0168}{10*(10-1)}}$$

$$uncertainty(u) = \sqrt{\frac{0.0168}{10*(10-1)}}$$

$$uncertainty(u) = \pm 0.013$$

APPENDIX B

VARIATION BETWEEN FIXED AND TRACKING SOLAR IRRADIANCE

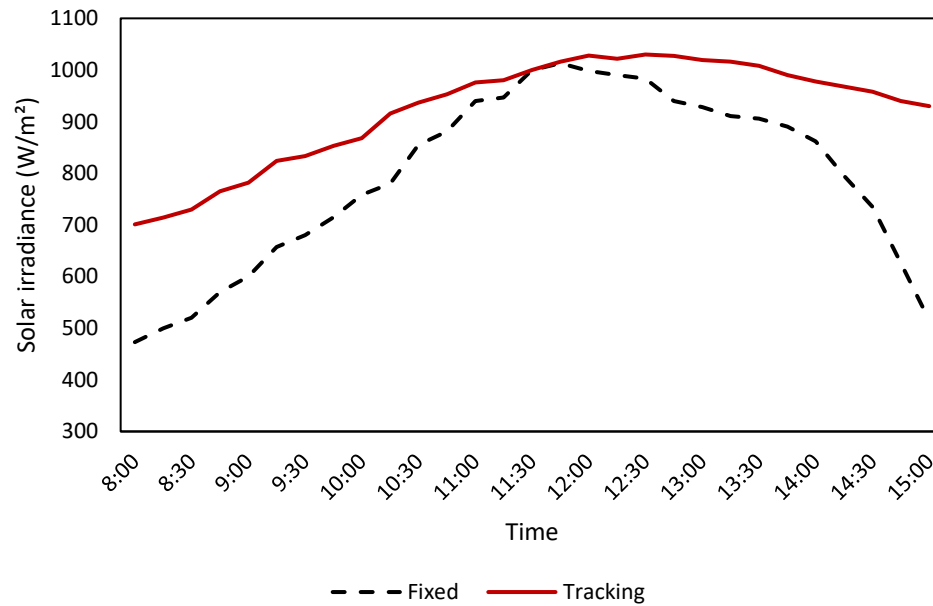


Fig. B-1 Variation between fixed and tracking panel solar irradiance 7th July

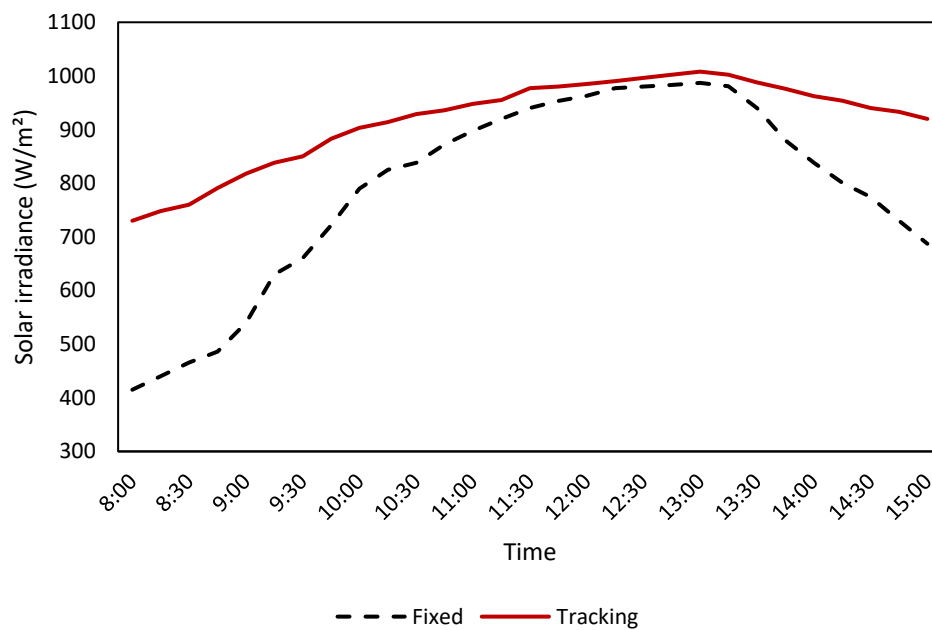


Fig. B-2 Variation between fixed and tracking panel solar irradiance 17th July

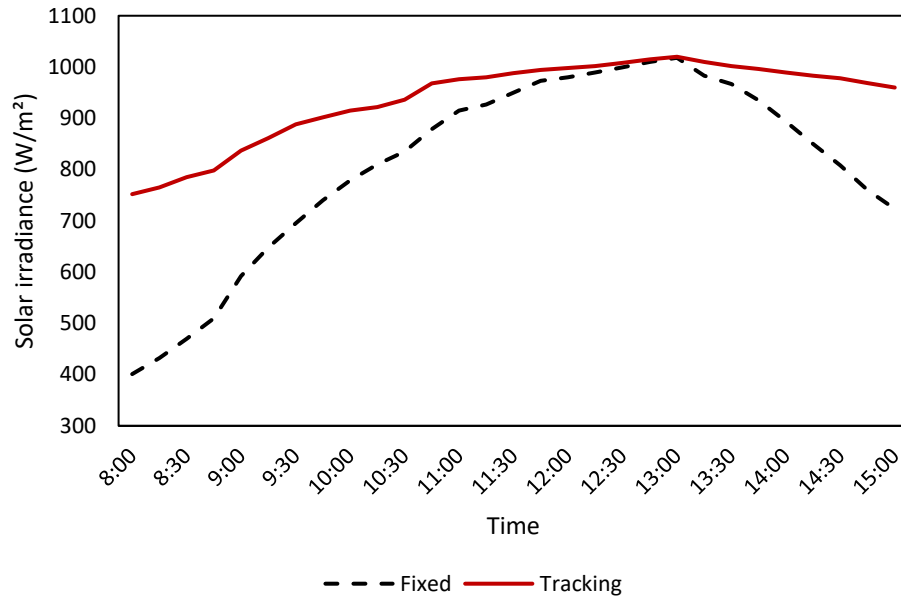


Fig. B-3 Variation between fixed and tracking panel solar irradiance 18th July

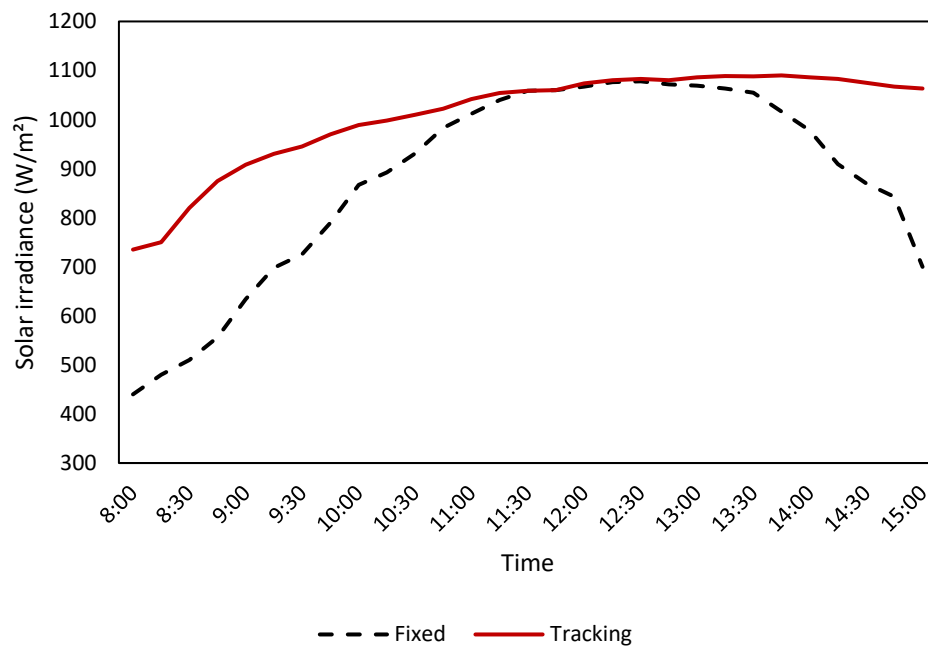


Fig. B-4 Variation between fixed and tracking panel solar irradiance 27th July

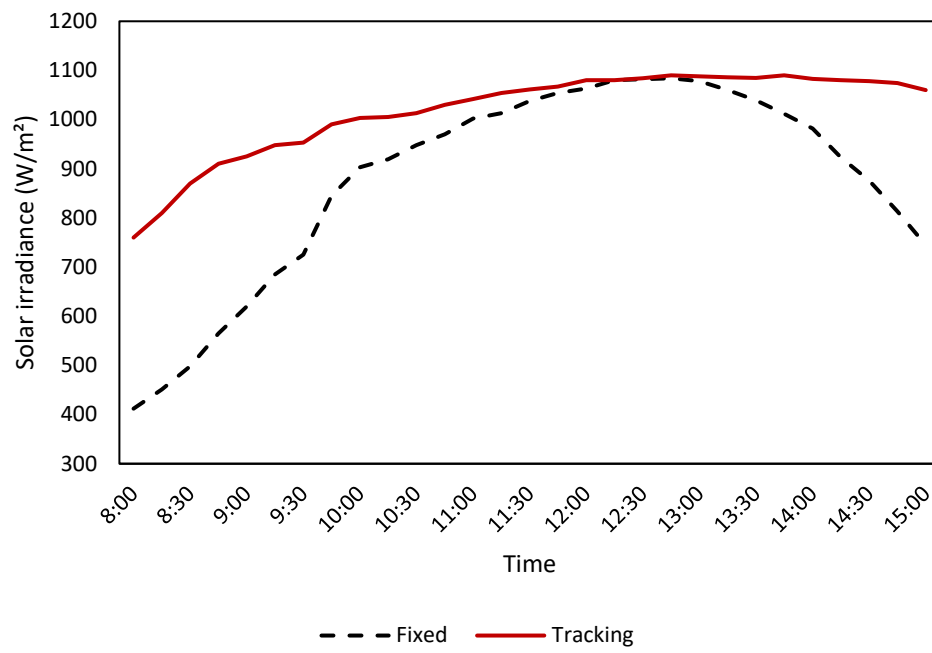


Fig. B-5 Variation between fixed and tracking panel solar irradiance 28th July

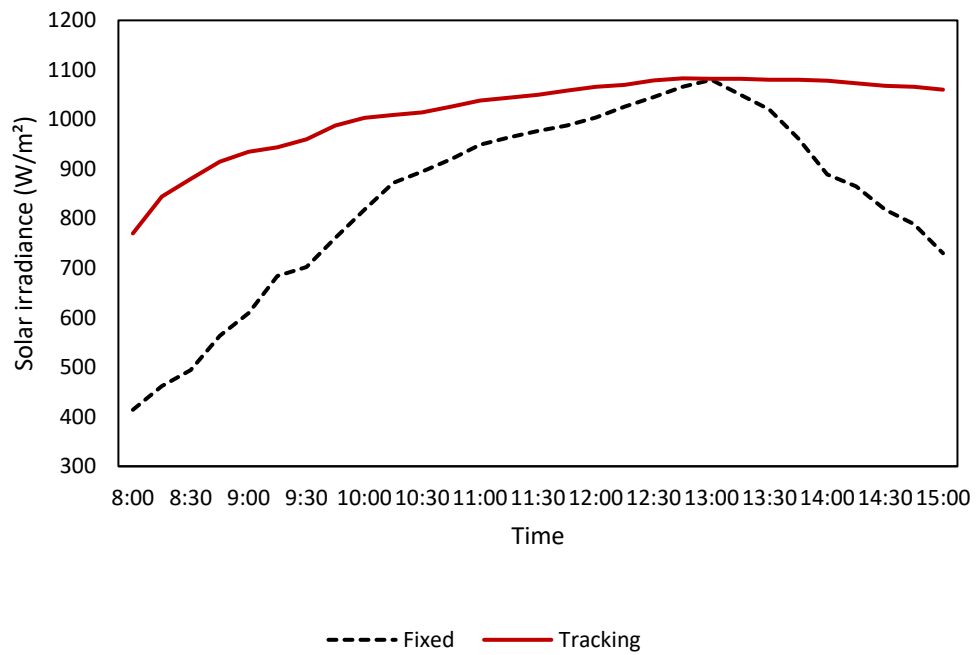


Fig. B-6 Variation between fixed and tracking panel solar irradiance 31st July

LIST OF PUBLICATIONS

PUBLISHED:

S. A. Polus and R. S. Abdullah, “Experimental performance evaluation of tracking photovoltaic system based on variable water flow rate with surface temperature” *Energy Sources, Part A: Recovery, Utilization, and Environmental Effects*, vol. 45, no. 2, pp. 5297-5309, 2023, doi:10.1080/15567036.2023.2209533.

ENERGY SOURCES, PART A: RECOVERY, UTILIZATION, AND ENVIRONMENTAL EFFECTS
2023, VOL. 45, NO. 2, 5297–5309
<https://doi.org/10.1080/15567036.2023.2209533>



Experimental performance evaluation of tracking photovoltaic system based on variable water flow rate with surface temperature

Sally Afram Polus and Ranj Sirwan Abdullah

Department of Technical Mechanical and Energy Engineering, Erbil Technical Engineering College, Erbil Polytechnic University, Erbil, Kurdistan Region, Iraq

ABSTRACT

A solar tracking system with an effective cooling technique is developed and implemented. Due to the solar radiation, high ambient temperature and dusty climate condition affected photovoltaic panel power production. A single east–west solar tracking system incorporating monocrystalline panel and a front surface spray water cooling system was conducted and compared to a fixed reference panel. The water flow rate is adjustable according to the set point temperature of the panel surface. The experiment was conducted during the summer season in north of Iraq (latitude 36.191° and longitude 44.009°). The study revealed that the implementation of the tracking system results in 4.19% increase in power production, while tracking with a cooling system has resulted in an improvement of up to 25.11% in Photovoltaic efficiency. The water consumption has been optimized, and the optimal cooling setting temperature was determined to be 40°C. Additionally, this model demonstrates that the performance of photovoltaic panel was decreased by only 0.2%–0.3%, when the surface temperature increased by 5°C within a range of 25–40°C.

ARTICLE HISTORY

Received 2 March 2023
Revised 24 April 2023
Accepted 27 April 2023

KEYWORDS

Photovoltaic panel; tracking system; flow rate; water cooling; electrical performance

SUBMITTED:

S. A. Polus and R. S. Abdullah, “Enhancing Photovoltaic Efficiency Through Water Cooling System Design and Analysis”. Under review at Journal of the Brazilian Society of Mechanical Sciences and Engineering.

پوخته

سیستمیکی به‌دو‌اد‌چوونی تیشکی خۆر به ته‌کنیکی کاریگەر بۆ ساردکردن‌ه‌وه له‌م لیکۆلینه‌وه‌یه‌دا پهری پندراوه و جیه‌جی کراوه، چونکه تیشکی خۆر، پله‌ی گهرمی و بارودۆخی که‌شو‌ه‌وای تۆز‌وای کاریگهری له‌سه‌ر به‌ره‌مه‌ینانی پانیلی فۆتۆفۆلتایک هه‌یه. سیستمیکی تاکه میحوه‌ری به‌دو‌اد‌چوونی تیشکی خۆری رۆژه‌لات-رۆژ‌ئاوا که پانیلی تاک بلوری و سیستمی ساردکردن‌ه‌وه‌ی ئاوی سپرای پرووی پێشه‌وه‌ی له‌خۆ‌گرتبوو ئه‌نجام‌درا و به‌راورد‌کرا به پانیلیکی ئاماژه‌ی جیگیر. سیستمیکی ساردکردن‌ه‌وه‌ی گونجاو پهری پندرا به شەش نۆژ که له سه‌ره‌وه و هه‌ردوو ته‌نیشته‌کانی پرووی پێشه‌وه‌ی پانیله‌که دانه‌بوو، بۆ دانه‌بوون له‌وه‌ی که پرووی پێشه‌وه‌ی پانیله‌که به ئاو له هه‌موو ئاراسته‌که‌وه‌ دا‌پۆش‌راوه. دوو جۆری جیا‌واز له ساردکردن‌ه‌وه‌ی ئاوی سپرا ئه‌نجام‌درا؛ یه‌که‌م به ریک‌خستنی پله‌ی گهرمی پرووی پانیله‌که ۳۵، ۴۰ و ۴۵ پله‌ی سه‌دی، له ریک‌گه‌ی ریک‌خستنی ریزه‌ی رۆیشتنی ئاو، و دوو‌ه‌مین جیگیرکردنی ریزه‌ی لێشاوی قه‌باره‌ی ئاو بوو له ۲، ۳، ۴ و ۵ ل/ده‌قه. تاقیکردن‌ه‌وه‌که له وهرزی هاویندا له شاری هه‌ولێری عێراق (پانی 36.191° و دریزی 44.009°) ئه‌نجام‌دراوه. هه‌روه‌ها لیکۆلینه‌وه‌یه‌کی تیوری به‌ه‌کاره‌ینانی ANSYS Fluent R19.2 ئه‌نجام‌درا. توێژینه‌وه‌ ئه‌زمۆنییه‌که دهریخستوه که زۆرت‌رین باشت‌ربوونی به‌ره‌مه‌ینانی کاره‌بایی به ریزه‌ی ۹.۹% و هه‌ک به‌رز‌بوونه‌وه‌یه‌ک تۆمار‌کراوه به به‌راورد به پانیلی ئاماژه‌ی جیگیر به به‌کاره‌ینانی سیستمی به‌دو‌اد‌چوونی خۆر رۆژه‌لاتی رۆژ‌ئاوا. له کاتی‌که‌دا به به‌کاره‌ینانی سیستمی به‌دو‌اد‌چوونی خۆر له‌گه‌ڵ سیستمی ساردکردن‌ه‌وه‌ به دیاری کردنی پله‌ی گهرمی پرووی پانیل له ۳۵ پله‌ی سه‌دی بووه‌ته هۆی باشت‌ربوونی کارایی تا ۲۵.۱۱%. پارامیته‌ریکی دیکه که باشت‌ر کراوه بریتیه له ریزه‌ی به‌کاره‌ینانی ئاو بۆ ساردکردن‌ه‌وه. گونجاوت‌رین پله‌ی گهرمی بۆ ساردکردن‌ه‌وه‌ی پرووی پانیله‌که به ۴۰ پله‌ی سه‌دی دیاری‌کرا. له لایه‌کی دیکه‌وه، له‌گه‌ڵ یه‌ک‌خستنی سیستمی ساردکردن‌ه‌وه‌ بۆ پانیلی فۆتۆفۆلتایک له پله‌ی گهرمی خاله دیاری‌کراوه‌کانی ۴۵، ۴۰ و ۳۵ پله‌ی سه‌دی، به‌جی یه‌ک‌خستنی سیستمی به‌دو‌اد‌چوونی خۆر، باشت‌ربوونی ۱۸.۲۵%، ۱۹.۹۴% و ۲۲.۸۲% له به‌ره‌مه‌ینانی کاره‌بادا به ریک‌که‌وت به‌ده‌ست هاتوون. کاتی‌که تیشکی خۆر له بارودۆخی کارکردنی ستانداردا هیزه‌که‌ی تپه‌راندا، ته‌نانه‌ت ئه‌گه‌ر پله‌ی گهرمی پانیله‌که زیات‌ر بێت له پله‌ی گهرمی تاقیکردن‌ه‌وه‌ی ستانداردا، پانیل توانای به‌ره‌مه‌ینانی هه‌مان هیزی تاقیکردن‌ه‌وه‌ی ستانداردی ۲۱۰ واتی هه‌یه سه‌ره‌رای ئه‌وه‌ش، یه‌ک‌خستنی سیستمی به‌دو‌اد‌چوونی خۆر له‌گه‌ڵ ساردکردن‌ه‌وه‌ به ریزه‌ی لێشاوی قه‌باره‌ی ئاو ۲ ل/ده‌قه بووه هۆی دوو هینده به‌ره‌مه‌ینانی کاره‌با به به‌راورد به پانیلیکی جیگیر که به هه‌مان ریزه‌ی لێشاوی ساردکرایه‌وه. ئه‌م مۆدیه‌ ئه‌وه نیشان ده‌دا که به‌ره‌مه‌ینانی پانیلی فۆتۆفۆلتایک ته‌نها به ریزه‌ی ۰.۲-۰.۳% که‌می کردوه، کاتی‌که پله‌ی

گەرمى پرووى پانئېلەكە بە رېژەى ۵ پلەى سەدى زىاد بوو لە مەوداى ۲۵ بۆ ۴۰ پلەى سەدى. ئەنجامەكانى ANSYS ئاماژەيان بەوە كرد كە كارىگەرىي پارامېتەرەكانى جياواز لەسەر بەرھەمھەنانە و پلەى گەرمى دەتوانرېت بە وردى پېشبینى بکرىت و پلەى گەرمى پانئېلى فۆتوئۆلتايىك بە شىوهمەكى بەرچا و كەم بېتەو، ئەمەش بووئە ھۆى زىادبوونى بەرھەمھەنانى كارەبا. بەشداریکردن لە ھاوشىوهمکردنى رواوھى ANSYS ئەوە بوو كە چرى تېشىكى خۆر كارىگەرتريين فاکتەرە لەسەر بەرھەمھەنانى كارەبا لە مۆدیۆلى ساردکراو، چونكە بە زىادکردنى تېشىكى خۆر بە رېژەى ۱۰۰ وات/م^۲، بەرھەمھەنانى كارەبا بە رېژەى ۱۶.۶% زىاد دەكرېت. لە كاتىكدا زىادکردنى رېژەى لىشاوى ئاو لە نزمترین پلەى گەرمى ھاتنە ژوورمەوى ئاودا بەرھەمھەنانى پانئېلى فۆتوئۆلتايىكى باشتەر كرد. ئەم توئېزىنەوهمە تېروانېنەكانى پىوېست بۆ دىزاین و جېيەجىکردنى فۆتوئۆلتايىكى كارا لەگەل ساردکردنەوھى پرووى پېشەوە دەخاتە روو.



زانکۆی پۆلیتیه کنيکی ههولير
ERBIL POLYTECHNIC UNIVERSITY

**بهرزکردنهوهی توانای پانيلی فوؤقوؤلتايک به بهکارهينانی
سیستهمی بهدواداچوونی تاکه میحوهر و سیستهمی پرشاندنی ئاو**

تیزیکه

**پیشکەشی ئەنجومەنی کۆلیژی تەکنیکی ئەنداز یاری ههولیر کراوه له زانکۆی
پۆلیتیه کنيکی ههولير وهک بهشیکی جییهجیکردنی مهرجهکان بۆ بهدهست
هينانی پروانامهی دکتورا له ئەنداز یاری میکانیک و ووزه**

له لایهن

سالی افرام بولس

**بهکالتوریۆس له ئەنداز یاری ساردکردنهوهو ههواسازی
ماستر له ئەنداز یاری میکانیک و ووزه**

به سهرپرشتیاری

پ. ی. د. رهنج سیروان عبدالله

ههولير - کوردستان

تشرینی یهكهم ٢٠٢٣